Simulation of natural circulation in an air-cooled Reactor Cavity Cooling System using Flownex

KA Sehoana

24768200

Dissertation submitted in partial fulfilment of the requirements for the degree *Magister* in Nuclear Engineering at the Potchefstroom Campus of the North-West University

Supervisor: Prof. P.G Rousseau

Co-supervisor: Prof. C.G Du Toit

November 2014

Abstract

Nuclear reactors with improved safety concepts are currently being studied within the nuclear engineering community, with a focus on passive safety features. One of these reactor concepts is the Very High Temperature gas-cooled Reactor (VHTR) of which the Reactor Cavity Cooling Systems (RCCS) is seen as an integral and crucial part of the passive safety concept. Considerable validation and development of the necessary software tools is required to perform analysis and designs of these future reactor concepts.

The primary objective of this study is to establish a methodology for the creation of an integrated system level process model of a typical air-cooled RCCS in Flownex®, and to illustrate its applicability by simulating different scenarios that illustrate the operational characteristics of such a system. For this purpose, the existing RCCS conceptual design that is being studied by the KAERI was used as the case study.

As a start, selected case studies were performed to verify that the Flownex® models were set up correctly to perform natural circulation flows, both in steady and transient conditions, and with radiation, convection and conduction taking part. These are the major typical physical phenomena in the RCCS. The models were compared with EES (Engineering Equation Solver) models of the same geometries and specifications. There was a good agreement between Flownex® and EES model results.

After this verification, a simulation model of the integrated RCCS system was developed. The Flownex® models were applied to model selected possible operational scenarios. The major observations from the results are that:

- The RCCS carries with it enough heat to the ambient such that the concrete wall temperature is maintained below the benchmark value of 65°C for the different boundary conditions imposed.

- The RCCS maintains its functionality even with three quarters of the risers blocked or in the event that there is a break in one of the chimney pipes.

Keywords: VHTR, RCCS, Passive safety, Simulation, Flownex®.

Declaration

I, the undersigned, hereby declare that the work contained in this project is my own original work.

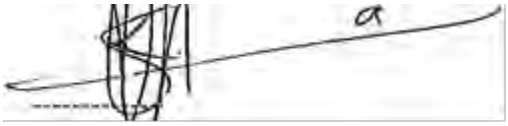

Date: November 2014

Potchefstroom

Acknowledgements

Firstly, I want to thank my Heavenly Father and Jesus Christ for giving me the strength, knowledge and ability to do a research study at the North West University (NWU).

I want to thank my supervisor Prof. Pieter Rousseau and co-supervisor Prof. C.G Du Toit for their interesting discussions and their immense support throughout the project. Thank you for the guidance and insight. By far the most intelligent people I have ever met.

Thank you to M-Tech Industrial (Pty) Ltd for the licence to use their software package Flownex®.

Thank you to my family who have supported and motivated me the whole time throughout my project.

Lastly, I want to thank the North-West University (Potchefstroom Campus), the (Department of Science and Technology) DST and (National Research Foundation) NRF for their financial support. Without your help this project would not be able to be done.

This work is based upon research supported by the South African Research Chairs Initiative of the Department of Science and Technology and National Research Foundation.

Table of Contents

List of figures

List of tables

Nomenclature

Variables

Variable	Description	Units
A	Area	m^2
A_i	Area of surface i	m^2
A'	Effective area of the throat	m^2
A_{back}	Area of the riser duct back wall	m^2
A_{front}	Area of the riser duct front wall	m^2
A_{ff}	Flow area	m^2
$A_{insulation}$	Area of the insulation surface	m^2
A_{side}	Area of the riser duct side wall	m^2
Bo	Buoyancy parameter	
C_c	Ratio of orifice area to vena contracta	
C_l	Loss coefficient	
C_l^*	Pseudo-Loss coefficient	
c_p	Heat capacity of the fluid	kJ/kg
dA_i	Elemental area of surface	m^2
dA_j	Elemental area of surface	m^2
D	Diameter	m
D_H	Hydraulic diameter	m
E_{bi}	Black body emissive power of surface i	W/m^2
G_i	Irradiation rate of surface i	W/m^2
Gr	Grashof number	
h	Heat transfer coefficient	W/m^2—K
h_0	Total enthalpy in the control volume	kJ/kg
h_{0i}	Total enthalpy in the inlet of the control volume	kJ/kg
h_{0e}	Total enthalpy in the outlet of the control volume	kJ/kg
h_{0s}	Enthalpy addition via a source	kJ/kg
J_i	Radiosity of surface i	W/m^2
J_j	Radiosity of surface j	W/m^2
$\sum K$	Sum of secondary loss-coefficients	
L	Length of pipe	m
$\dot{m}$	Mass flow rate through the channel	kg/s

$\dot{m}_e$	Mass flow that exits the control volume	kg/s
$\sum \dot{m}_e$	Sum of all mass flow exiting the node	kg/s
$\dot{m}_i$	Mass flow that enters the control volume	kg/s
$\sum \dot{m}_i$	Sum of all mass flow entering the node	kg/s
$\dot{m}_s$	Mass source	kg/s
Nu	Nusselt Number	
p	Static pressure in the control volume	kPa
p_{0e}	Total pressure at exit of the control volume	kPa
p_{0i}	Total pressure at inlet of the control volume	kPa
ΔP_{0L}	Total pressure loss through the control volume	kPa
Pr	Prandtl Number	
P_w	Wetted perimeter	m
$\dot{Q}$	Total rate of heat transfer to the fluid	kW
Q	Volume flow	m^3/s
$\dot{Q}_i$	Total heat transfer rate at surface	kW
Q_{ij}	Net heat transfer between surface i and j	W/m^2—K
q_x	Heat transfer rate in the x-direction	kW
Re	Reynolds number	
R_T	Temperature factor	
R_i	Surface resistance	
R_{ij}	Space resistance	
S_c	Continuity source term	
S_e	Energy source term	
S_m	Momentum source term	
T_f	Fluid temperature ()	°C
T_C	Temperature of the cold plate	°C
T_H	Temperature of the heated plate	°C
T_i	Temperature of surface i	°C
T_j	Temperature of surface j	°C
T_s	Temperature of the surface	°C
V	Mean velocity	m/s
$\dot{W}$	Total rate of work done on the fluid	kJ
z_e	Elevation at the exit of control volume	m
z_i	Elevation at the inlet of control volume	m
$1-D$	One-dimensional	

$3-D$	Three-dimensional	

Symbols

Symbols	Description	Units
α	Pressure constant	
α_c	Weighing factor for continuity	
α_e	Weighing factor for energy conservation	
α_m	Weighing factor for momentum conservation	
β	Pressure constant	
C_k	Constant	
Δx	Width of medium	m
ρ	Density of the fluid	kg/m^3
$\bar{\rho}$	Average density inside the element	kg/m^3
ε_i	Emissivity of surface i	
ε	Surface roughness	m
f	Darcy-Weisbach friction factor or fluid	
ff	Free flow area	
g	Gravitational acceleration	m/s^2
k	Thermal conductivity	W/m—K
0	Total	
∂	Rate of change	
s	Source or surface	
$\sum$	Sum	
t	Time	s
μ	Fluid viscosity	kg/m—s
$\forall$	1-D control volume	m^3

Subscripts

Subscript	Definition
b	Black body
c	Cold or continuity
e	Exit or energy conservation
f	Fluid
H	Hot or hydraulic diameter
i	Inlet or surface i

j	Surface j
m	Momentum conservation
s	Source or surface
w	Wetted
x	x-direction

List of abbreviations

ANL	–	Argonne National Laboratory
CFD	–	Computational Fluid Dynamics
CV	–	Control Volume
DC	–	Downcomer
DOE	–	Department of Energy
DPCC	–	Depressurized Conduction Cooldown
DPLOFC	–	Depressurized Loss of Forced Coolant
DST	–	Department of Science and Technology
EES	–	Engineering Equation Solver
GCR	–	Gas Cooled Reactor
GFR	–	Gas-Cooled Fast Reactor System
GIF	–	Generation IV International Forum
GT-MHR	–	Gas Turbine – Modular Helium Reactor
HS	–	Heat Surfaces
HTGR	–	High Temperature Gas-cooled Reactor
HTR-10	-	High Temperature Reactor with 10 MW_{th} power
HTTF	–	High Temperature Test Facility
HTTR	–	High Temperature Test Reactor
IAEA	–	International Atomic Energy Agency

JAERI	–	Japan Atomic Energy Agency Institute
KAERI	–	Korean Atomic Energy Agency Institute
LFR	–	Lead-Cooled Fast Reactor System
LWR	–	Light Water Reactor
MHTGR	–	Modular High Temperature Gas-cooled Reactor
MSR	–	Molten Salt Reactor System
NHDD	–	Nuclear Hydrogen Development and Demonstration
NGNP	–	Next Generation Nuclear Plant
NRF	–	National Research Foundation
NSTF	–	Natural Convection Shutdown Heat Removal Facility
NWU	–	North-West University
PBMR	–	Pebble Bed Modular Reactor
PCC	–	Pressurized Conduction Cooldown
PCU	–	Power Conversion System
PCS	–	Power Conversion System
PLOFC	–	Pressurized Loss of Forced Coolant
PMR	–	Prismatic Modular Reactor
PWR	–	Pressurized Water Reactor
RCCS	–	Reactor Cavity Cooling System
RPV	–	Reactor Pressure Vessel

SCS	–	Shutdown Cooling System
SCWR	–	Supercritical-Water-Cooled Reactor System
SNU	–	Seoul National University
SFR	–	Sodium-Cooled Fast Reactor System
TAMU	–	Texas A&M University
TMI	–	Three Mile Island
TRISO	–	Tri-Isotropic
UW	–	University of Wisconsin Madison
VHTR	–	Very High Temperature Reactor

Chapter 1

1 Introduction

Nuclear reactor technology requires safe and reliable heat removal systems. Currently, around the world, active decay heat removal systems fulfil this requirement. In the event of failure of these systems, core meltdown can occur and dangerous fission products can escape to the environment (Kugeler, 1992). The accidents at Three Mile Island (TMI) in 1979, Chernobyl in 1986 and most recently at Fukushima Daichi power station in 2011 are very good examples of accidents where the active cooling systems failed.

It is estimated that the world's population will increase by as much as 40% from six billion to 10 billion people by 2050 (GIF, 2002). Thus, there is a need to ensure energy security while at the same time limiting the CO_2 problem. To this end, nuclear energy is expected to take on a vital role in world energy. However, special attention needs to be given to safety, waste, proliferation, and public perception concerns. New developments worldwide are especially discussed towards the question of how to improve the reliability in decay heat removal.

In 2002, the Generation IV International Forum (GIF) was formed to develop reactor concepts with more advanced safety and reliability than their current counterparts. Six reactor concepts were selected and are shown in Figure 1-1 together with their mission and focus.

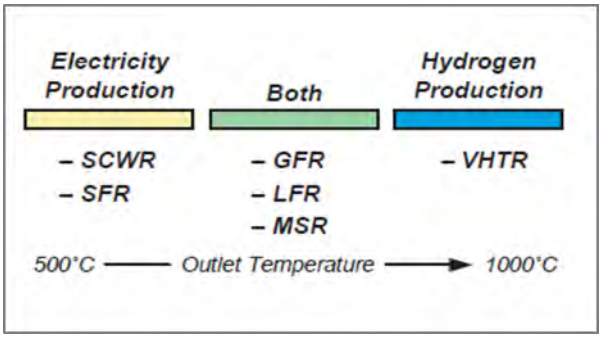

Figure 1-1: Generation IV reactor concepts and mission focus (GIF, 2002).

The Very High Temperature gas-cooled Reactor (VHTR) is a leading candidate for the Next Generation Nuclear Plant (NGNP). As can be seen in Figure 1-1, higher coolant exit temperatures can be realized with this reactor concept, immediately creating interest in broader applications such as hydrogen and process heat generation, although it can still be used to produce electricity.

The VHTR concept forms the core background of this study.

1.1 Gas-cooled reactors

From as early as the 1950's, development work was started between the United States and the Federal Government of Germany (Mears & GoodJohn, 1989) in an effort to improve on the Gas-Cooled Reactors (GCR's) already in operation, predominantly in the United Kingdom from 1953 onwards. It was realized that utilizing ceramic fuel particles surrounded by coatings, dispersed in a graphite matrix along with a graphite moderator allows the reactors to be operated at high coolant temperatures. Helium could be used as a coolant, due to its chemical inertness. Brey (2000) and Chang et al. (2006) followed the development of High Temperature Gas-cooled Reactors (HTGR's) from the early research reactors (Dragon reactor experiments and Peach Bottom no 1) to the present focus.

Presently, the most likely VHTR candidates are the prismatic block and pebble-bed designs with a thermal neutron spectrum. One of the mission focuses of the VHTR is to produce hydrogen combined with a power plant. This system is preferred over the current Pressurized Water Reactor (PWR) systems because it could have efficiencies as high as 50% compared to a typical value of 33% in the PWR's.

1.1.1 Similarities between the pebble bed and prismatic block reactor

Some of the characteristics common to both VHTR configurations are listed below;

- The working fluid is helium.
- The moderator for both configurations is graphite.
- The fuel design consists of Tri-isotropic (TRISO) fuel-particles dispersed in a matrix.
- Both designs rely on forced flow, provided by blowers, of the helium coolant during operation.

- Both designs rely on passive cooling during any loss of power or loss of coolant scenarios.

- The ultimate heat sink is the environment. Heat is transported via conduction and radiation to the vessel walls, then via a combination of radiation and natural circulation transport using some form of Reactor Cavity Cooling System (RCCS).

- The cavity is filled with air, such that if the reactor depressurizes due to a leak in the pipe, the air will ultimately enter the vessel by diffusion.

- The balance of plant is virtually identical with the heated helium collected from the core and mixed in the lower plenum and then flows out of the vessel to the Power Conversion Unit (PCU).

1.1.2 Fundamental differences between the pebble bed and prismatic block reactor

Some of the fundamental differences between the two configurations are listed below;

1) Core configuration

- According to Hicks (2011), the prismatic core consists of an inner reflector region surrounded by an annulus of fuel blocks which is in turn surrounded by an annulus of outer reflector elements. The fuel blocks are composed of hexagonal columns of graphite with circular holes that run the full length of the column. The fuelled holes contain fuel compacts that contain TRISO particles, while the coolant holes align axially to form coolant channels.

- The pebble bed core consists of fuel pebbles that are stacked in a graphite reflector structure. Figure 1-2 shows the configuration of the prismatic and pebble bed cores.

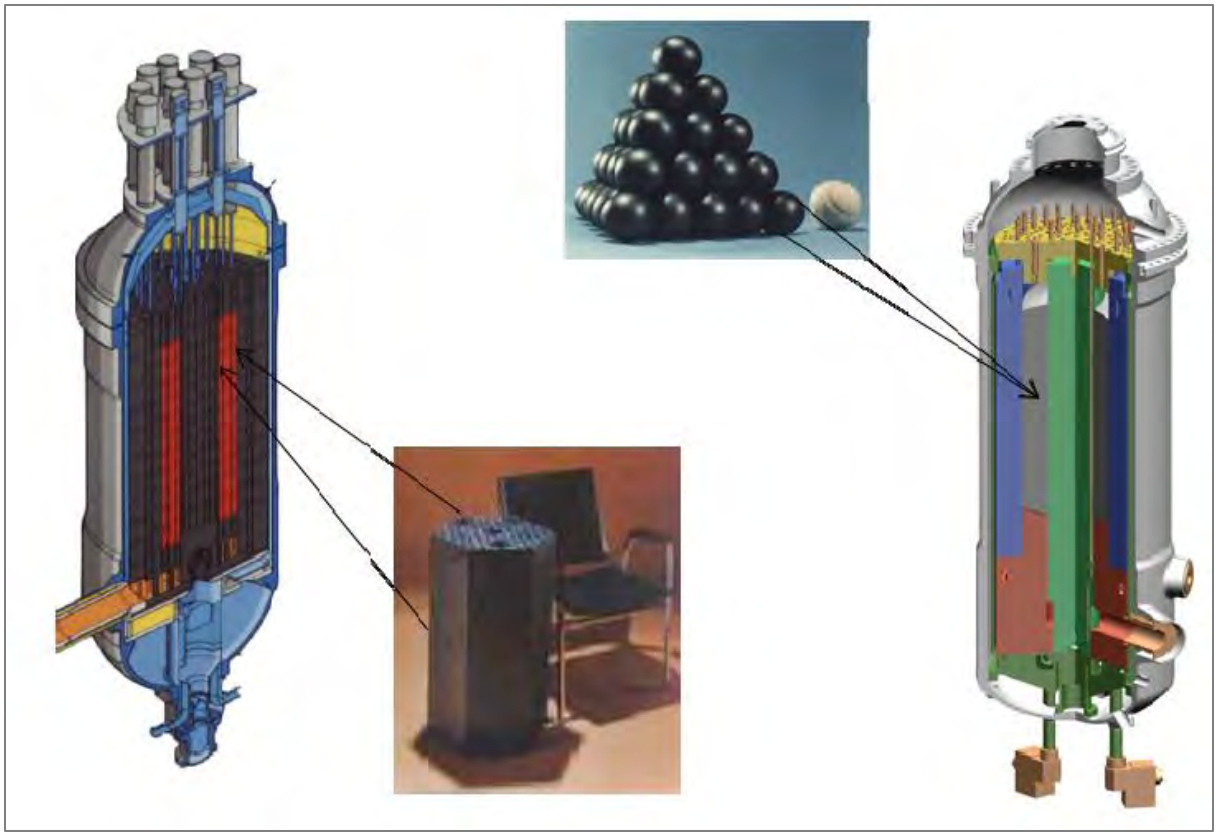

Figure 1-2: Prismatic block and Pebble Bed Reactor (Gougar & Schultz, 2010).

2) Helium coolant flow

- In the prismatic core, the helium coolant follows a well-defined path through the coolant channels or ducts between the core barrel and the vessel wall. Helium is collected in the upper plenum and flows downwards into the core. In the prismatic design, there is an undefined quantity of by-pass flow as the flow moves between the blocks (Hicks, 2011).

- In the pebble bed, helium flows upward through the riser which consists of circular channels inside the outer reflector. Helium is collected in the upper plenum and flows downwards into the core. In the pebble bed, the helium coolant follows a multi-dimensional path defined by the voids between the pebbles (Hicks, 2011).

3) Refuelling

- The pebbles are continuously refuelled during plant operation and spent pebbles are removed from the system, therefore, the pebble bed core has a wider spectrum of

depletion than the prismatic block reactor. The prismatic block reactor is refuelled at the end of the burn up cycle.

4) Passive cooling medium

- The envisaged prismatic block reactor designs use natural circulating air while the pebble bed reactor concepts typically use water natural circulation.

1.2 Heat removal systems

During normal operation of the reactor, heat is generated by the fission reactions in the reactor core and is removed by forced circulation of helium as it flows within the core. However, a portion of this heat is not removed and penetrates the structures into the reactor building. The reactor building is surrounded by a wall of concrete which is reported to become brittle at temperatures above 65° (Dilling *et al.*, 1982). Therefore, it becomes imperative to remove this heat to protect the concrete citadel from overheating.

During accident scenarios after the reactor shutdown, decay heat (approximately 6% of reactor power) is produced by the radioactive fission products and fission energy from the delayed neutron emission. The decay heat decreases exponentially to 1% after one hour and even after 100 hours the decay heat is approximately 2 per thousand of the reactor power (Kugeler, 1992). Although the decay heat is small in relation to the full thermal power, failing to cool the reactor after shutdown could result in core heat up and possible damage.

There are various ways in which heat is rejected. The circulation of helium through the reactor core to the steam generators is the primary mode of removing heat from the reactor. In the event of an accident such as a loss-of-forced-coolant accident, heat must be removed from the core by other means. The first of these modes is the shutdown heat exchanger and shutdown circulator located at the bottom of the reactor pressure vessel. This is known as the Shutdown Cooling System (SCS) which is a forced cooling system actuated when the main cooling loop is unavailable. The SCS is arranged in line with the shutdown circulator and shutdown valves as can be seen in Figure 1-3.

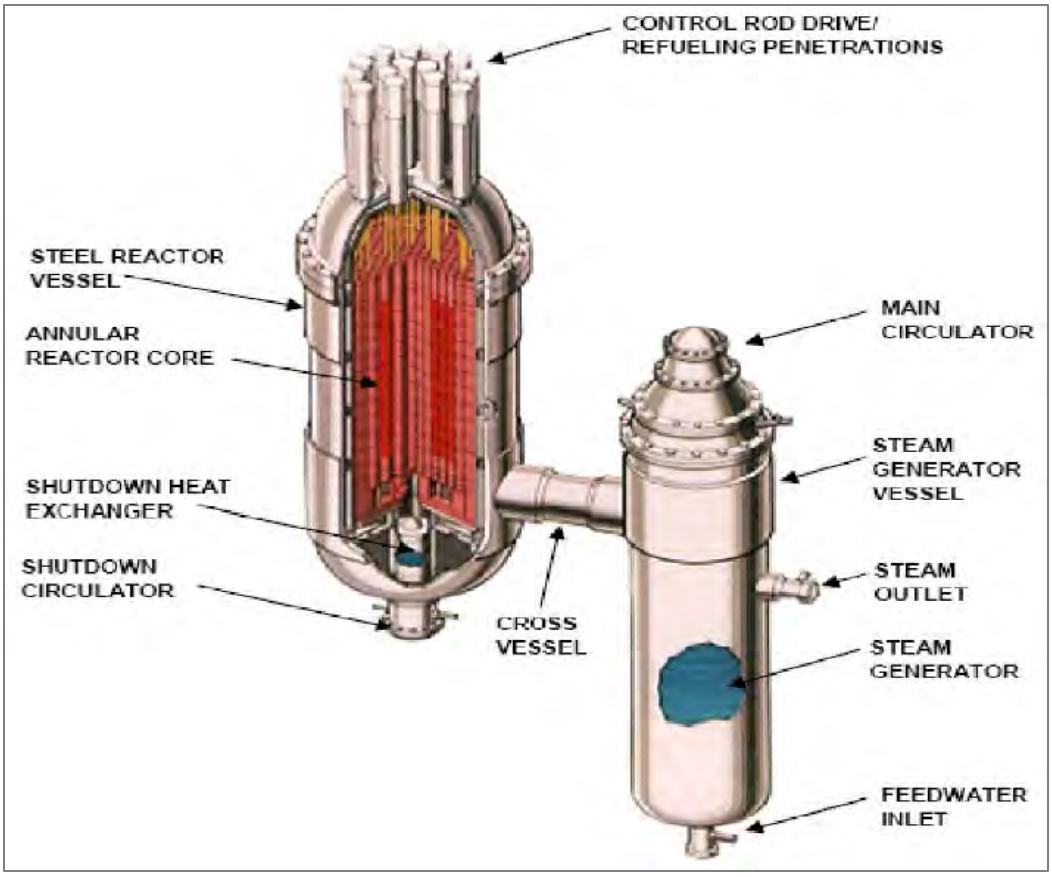

Figure 1-3: Steam Cycle – Modular Helium Reactor (SC-MHR) reactor system (Hicks, 2011).

In the absence of the primary cooling system, hot helium flows into the pipes and into the water cooled heat exchanger from where the cooled helium flows through the shutdown circulator and then to the core inlet plenum to flow back into the reactor (Hicks, 2011). The hot water then flows to the plant service water system. This is an active cooling system.

In the event that all the active cooling systems are unavailable, there is an independent cooling system known as the RCCS. This system relies on natural circulation of a fluid to effect heat removal. The RCCS is a passive cooling system.

As a last resort, heat can be directly dumped to the underground containment by radiation and conduction.

Passive heat removal systems provide the opportunity to remove decay heat from the Reactor Pressure Vessel (RPV) to an ultimate heat sink without the need to actuate any components. The heat is rejected by conduction and radiation through the vessel structures to the reactor

cavity. The RCCS can take advantage of the high temperature at the vessel wall through radiation heat transfer to remove this heat to the environment. There are two types of RCCS currently under consideration for the VHTR; an air-cooled RCCS and a water-cooled RCCS.

It has been reported by Chang et al. (2006) and shown by Frisani (2010) that the water-cooled RCCS has higher heat removal capability than an air-cooled option of comparable size. However, to provide the same level of reliability compared to the air option, the water-cooled RCCS needs to be provided with very complex features which include a secondary loop and a water purification system (CRP, 2000). Moreover, Dilling et al. (1982) reported that there is significant uncertainty and complexity associated with the two phase phenomena in the boiling mode for the water cooling scheme. Kumar et al. (2012) demonstrated using RELAP5/MOD 3.2 that flow instabilities may occur at low and high qualities due to phase change. Flow oscillations greater than 30% of the average flow rate are possible in two phase natural circulation, which these researchers considered to be unstable.

The air cooling scheme is reported to be more passive, has fewer failure modes and is more economical (Dilling *et al.*, 1982). However, due to the poor cooling capability of air, a very high chimney is required to supply enough air flow to remove the after-heat. The choice between the water-cooled and the air-cooled RCCS is subject to a great deal of debate within the nuclear community. Both modes are currently being investigated given the pros and cons of each cooling scheme. This study is devoted to the air-cooled RCCS.

1.3 Motivation for the study

The PMR200 (Prismatic Modular Reactor with 200 MW thermal power) is a candidate High Temperature Gas-cooled Reactor (HTGR) being investigated by the Korean Atomic Energy Research Institute (KAERI) for the Nuclear Hydrogen Development and Demonstration (NHDD) project (Tak *et al.*, 2011). The design is based on the concept of the Gas Turbine – Modular Helium Reactor (GT-MHR) with virtually the same fuel element design. The PMR200 adopts the air-cooled RCCS option and was selected as the object for further study and as part of a formal collaboration project between the North-West University (NWU) and the KAERI.

Various design and analysis tools are needed to calculate the behaviour of the RCCS both under normal and accident conditions. Presently, the state-of-the-art software and advanced detailed methods are not ready to perform design and analysis to the standard required by the

VHTR development. Considerable validation and development of the necessary software tools is required (Gougar & Schultz, 2010).

The thermal hydraulic behaviour of the VHTR can be analysed with Computational Fluid Dynamics (CFD) codes, system codes or other codes that can model severe accidents (Zhen, 2008). CFD has advantages in that these codes can model the presence of localized hot spots and areas where greater detail about thermal interactions is required. The downside is the computational requirements related to the size of the problem. Systems codes can also be used to analyse fluid dynamics using one-dimensional analysis. In general, both types of codes are based on the conservation laws and empirical modes but differ in the level of problem definition required. The other disadvantage to using CFD is that separate effects experiments need to be performed to validate the code, while integral experiments which can take into account more than one phenomena are sufficient to validate systems codes (Frisani, 2010). Systems codes typically use equations that have been simplified by not including the viscous stress terms in the momentum equation. The problem is subdivided into a macroscopic structure that does not model phenomena such as turbulent eddies.

The choice between CFD and systems code depends on the level of detail required and the size of the problem. For problems where global effects are of importance and the system can be approximated without modelling the detailed local effects, systems codes can be applied. There are currently projects underway at the KAERI to develop a one-dimensional systems code that can capture the major phenomena and demonstrate the behaviour of the air-cooled RCCS. The existing South African code Flownex® is just such a tool and therefore it can serve as a good platform for inter-code comparison in order to build confidence in the respective codes. For such code comparison, various scenarios can be postulated in an effort to highlight the interplay between the major physical phenomena and to gain an understanding of the operational characteristics of such an air cooled RCCS. The focus of this project is the development of a modelling methodology in Flownex® that can be applied to simulate and analyse various operational scenarios that may be encountered in such an RCCS.

1.4 Objectives of the study

The primary objective of this study is to establish a methodology for the creation of an integrated system level process model of a typical air cooled RCCS in Flownex®, and to illustrate its applicability by simulating different scenarios that will illustrate the operational characteristics of such a system. For this purpose, the existing RCCS conceptual design that is being studied by the KAERI will be used as the case study.

The enabling objectives of the study are to:

- Conduct a literature review on the different RCCS concepts, experimental and numerical techniques used to create models of the RCCS.
- Identify the major physical phenomena that need to be taken into account in the model in order to simulate the operational characteristics.
- Identify, obtain or generate suitable input data for the Flownex® model.
- Develop a Flownex model of the existing RCCS concept design that captures the major physical phenomena.
- Apply the model to simulate selected steady-state and transient scenarios that will illustrate the operational characteristics of the system.
- Evaluate the results of the simulations and put forward insights gained that may be useful in the future design of a real-life air cooled RCCS.

1.5 Thesis outline

The first chapter provided an overview of the Generation IV reactor concepts and associated heat removal systems. The motivation and objectives of this study were also given. In order to achieve the above mentioned goals, a literature study was conducted into the use of passive system in nuclear reactors. This is discussed in ***Chapter 2.*** The different RCCS design considerations are discussed, as well as the emergency situations which are of importance to this study. A literature study regarding natural convection as well as experimental and numerical studies in the RCCS was done to provide a sound understanding of the current or previous engagements in this field.

Chapter 3 is devoted to the theoretical background that is relevant to the study. The mathematical theory used to create the theoretical model of heat transfer and natural circulation in the RCCS is discussed. Basic information pertaining to the software code Flownex® is given.

Chapter 4 describes the particular RCCS that will be simulated in this study. The geometries of the various components are also described.

Chapter 5 deals with the verification of the Flownex® software. Different steady state and transient simulations are conducted to verify the capability of Flownex® in modelling natural circulation flows. Simulations are also developed in Engineering Equation Solver (EES) and compared with Flownex® simulations for different boundary conditions.

In ***Chapter 6***, a typical layout diagram of the RCCS systems modelling is given with a description of each component. The method of how the model was set up is given together with the simplifying assumptions. Finally, the Flownex® models of the RCCS are presented.

Chapter 7 presents a discussion of the results from ***Chapter 6***.

Chapter 8 provides a discussion on the selected case studies that were imposed. Comparisons and interpretations of the results are made in this chapter.

In ***Chapter 9*** the thesis is summarized as a whole based on the objectives of the study. Finally, the thesis is concluded.

Finally in ***Chapter 10***, the contributions of this study are presented together with proposals for future work that can be undertaken.

Chapter 2

2 Literature study

2.1 Introduction

This part of the study will familiarize the reader with various proposed designs for safety and the use of passive cooling systems to create an inherently safe nuclear reactor. First, the various RCCS design considerations are discussed, including the functionality and basic requirements of the RCCS both under normal and abnormal conditions. It must be mentioned at the onset that presently no VHTR's have been commissioned to full scale as the concept is still in the development phase. Therefore, the majority of the work done is aimed at contributing to the understanding of the heat transfer and natural circulation processes associated with the VHTR. Secondly, natural convection will be discussed. The different modes of convection are described and the research narrows down to the turbulent mixed convection regime, under which the envisioned PMR200 RCCS operates.

Finally, focus is placed on experimental and numerical studies that have been invested in the RCCS. This is done to get more insight into the different components and physical phenomena that are important and required to model such a system.

2.2 Reactor cavity cooling system design considerations

The passive cooling concept using the RCCS was introduced in the HTR-Module design in 1979 and extended to other recent designs. Golovo et al. (1992) and Dilling et al. (1982) discuss the RCCS design selections, flow schemes and design features of residual heat removal systems. In general, these options include using air or water in the primary loop with an air/water heat exchanger to remove heat to the environment. Table 2-1 shows the types and characteristics of the most recent designs under development.

Table 2-1 : Type and characteristics of RCCS in the HTGRs.

Reactor	RCCS Coolant/Type	Secondary Coolant/Type
HTTR	Water Forced Convection	Water Forced Convection
HTR-10	Water Natural Convection	Air Natural Convection
PBMR	Water Natural Convection	Air Natural Convection
GT-MHR	Air Natural Convection	No Secondary Cooling
MHTGR	Air Natural Convection	No Secondary Cooling

The High Temperature Test Reactor (HTTR) was built in Japan by the Japanese Atomic Energy Research Institute (JAERI) and became operational in 1998 (Hicks, 2011). It is a 30 MWth engineering test reactor that uses helium coolant and a prismatic core. The HTTR has a RCCS design that relies on forced convection cooling with water through a set of standpipes and radiation fins. When forced circulation of helium is disrupted, this residual heat removal system is used as a redundant cooling system.

Experimental data from the HTTR experiments were selected as benchmark problems by the International Atomic Energy Agency (IAEA). Six benchmark problems were presented by JAERI with various experimental conditions. Each condition with a different power, type of coolant (helium, nitrogen), and operating pressures as well as different cooling panels, i.e. water or air-cooled. The results were compared with analytical results obtained from France (CASTEM2000 code), China (THERMIX and CCRCC codes), Russia (SMI and DUPT codes), USA (MORECA and FIDAP codes) and Japan (THANPACT2 code). It was found that the vessel temperature during cooldown conditions exceed the benchmark limit of 400°C and the radiative heat transfer accounts for more than 86% of the heat transfer. The general result is that, although radiation is the dominant mechanism for heat transfer from the reactor to the RCCS (50 – 98%), natural convection plays a significant role in producing localized temperature distributions which are essential for confirming cooling system performance, particularly close to the RPV wall. Therefore, the applicability of empirical correlations is very limited and experiments become necessary to validate the models. They concluded that as long as the geometric view factors are computed properly, the calculations tend to be robust (CRP, 2000).

In China, the High Temperature Reactor with a 10 MW power (HTR-10) was built in INET achieving criticality in December 2002 (Hicks, 2011). The HTR-10 as it is known, has inherent safety features envisioned for the HTGRs such as a negative reactivity coefficient, and passive

afterheat removal system. The passive removal system adopts two independent water and air RCCS loops. Both loops rely on natural circulation as can be seen in Table 2-1. The working fluid is water and the exchange to the environment is by means of air. Gao et al. (1992) analysed the heat removal characteristics of the water-cooled and air-cooled RCCS under accident conditions. Using the THERMIX code, a computer program used for two-dimensional thermal hydraulics of a pebble bed HTGR, they showed that the system is able to remove the afterheat. Furthermore, they showed that all peak temperatures of the components are within the design limits even in the event of a Depressurized Loss of Forced Coolant (DPLOFC) and Pressurized Loss of Forced Coolant (PLOFC). The researchers note the weak heat transfer ability of air compared to water. The peak temperature of the core, side reflector and reactor vessel with the air RCCS are higher than those with the water RCCS under the same reactor power.

The Pebble Bed Modular Reactor (PBMR) was identified by ESKOM in 1993 as an option for expansion of the electrical generating capacity. The original design was a 265 MWth HTGR which adopted a similar RCCS to the HTR-10 in that it relies on external water to air heat exchange to reject heat. In Figure 2-1, a conceptual layout of the PBMR RCCS design is shown.

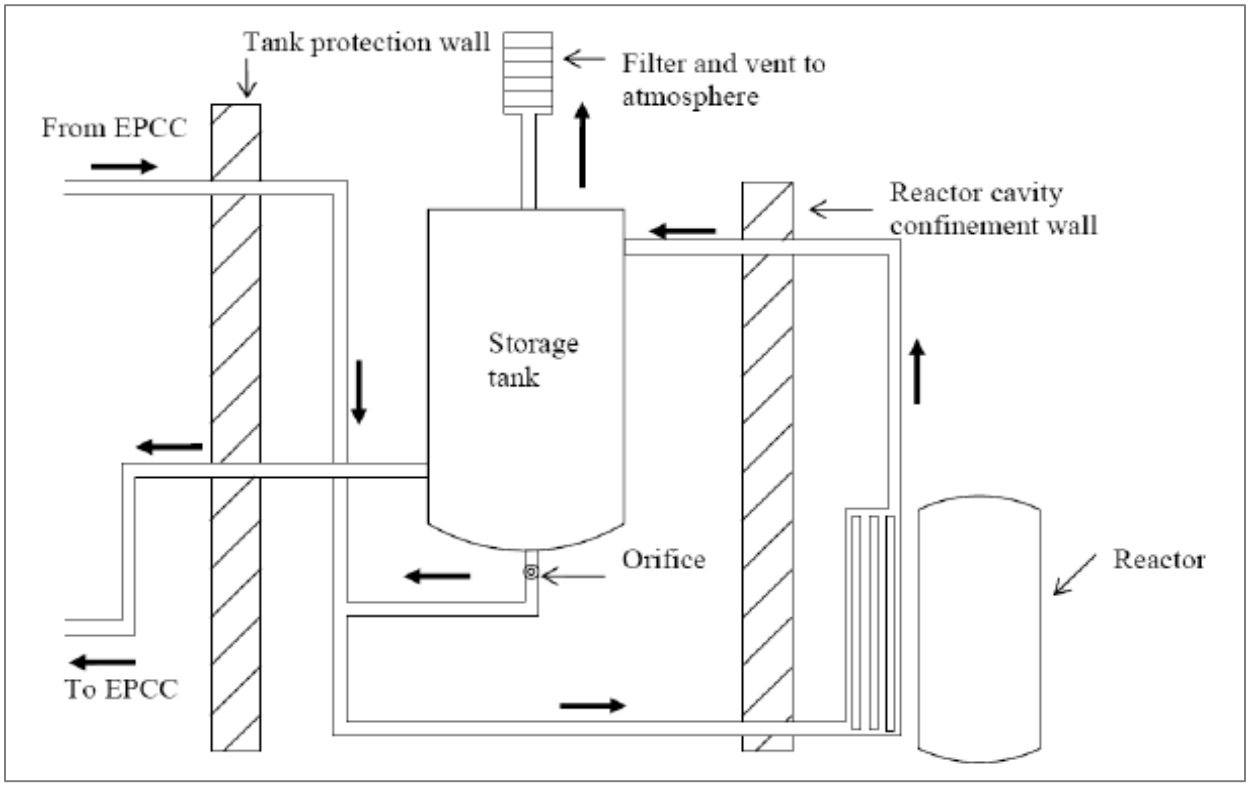

Figure 2-1: Conceptual layout of the original PBMR design (Verwey, 2010).

During emergency operations, the Equipment Protection Cooling Circuit (EPCC) which is normally active during normal operations is off. The cooling water in the standpipes is heated by the decay heat generated in the reactor. The water begins to flow upwards because of the density changes in the storage tanks. Cold water will subsequently be drawn out of the tank through the orifice. The water in the storage tank will evaporate and pass through the filter to the environment. It is understood that there are 18 storage tanks each connected to four standpipes (Verwey, 2010). The major drawback to this setup is that the entire contents of the tanks could evaporate before the decay heat is ultimately removed. As an improvement, it was envisioned to incorporate the air heat exchange loop as a secondary coolant. Unfortunately, this project has since been terminated.

The 600 MWth Russian GT-MHR and the 450 MWth American Modular High Temperature Gas-cooled Reactor (MHTGR) both utilize the air cooled RCCS. There is no secondary coolant. The vessel conducts heat from the fuel elements to a set of cooling panels by radiation and convection and is subsequently removed by natural convection to the atmosphere. In the air-cooled RCCS design, heat is radiated from the RPV wall to a series of pipes arranged in a circle a few meters from the RPV. Air flowing through these pipes is heated and carries the heat to the environment (CRP, 2000). A conceptual overview of the air-cooled RCCS is shown Figure 2-2.

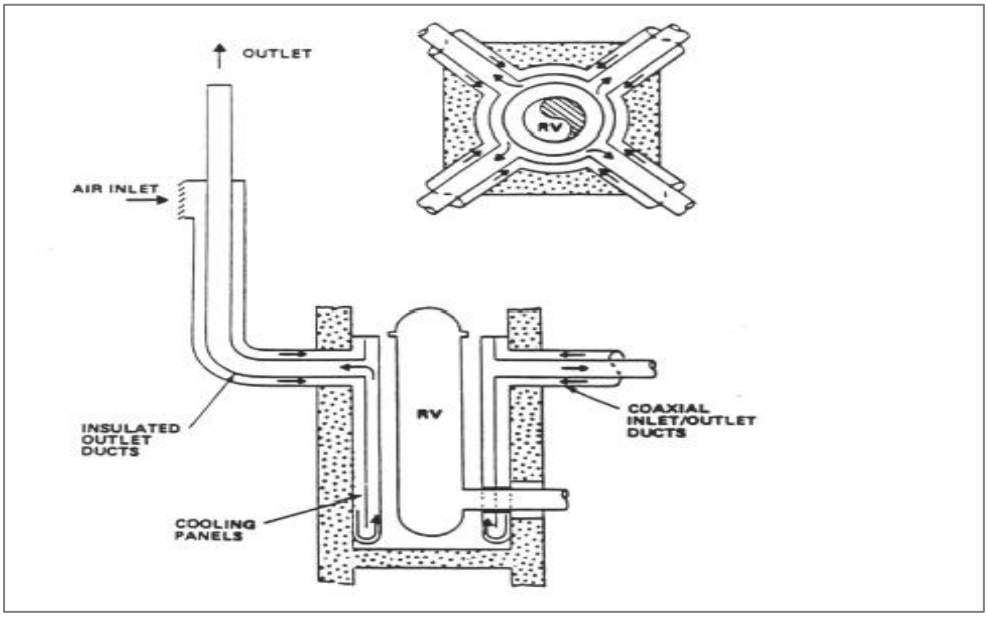

Figure 2-2: Conceptual overview of the air cooled RCCS option (Lommers, 2010).

Different codes have been used to analyse heat transport from the reactor to the RCCS for loss of forced coolant accidents. IN France, the CASTEM finite element code which allows for developing 3D thermal, structural and fluid mechanics models including 3D radiative heat transfer. In the Netherlands, CFX-F3D flow modelling software which solves (partial differential) conservation equations for mass, momentum (Navier-Stokes equations) and energy with their boundary conditions was used. The software uses the finite volume method to discretize these conservation equations. Radiation heat transfer is taken into account via a Monte Carlo method. China used the THERMIX code. In the US the MORECA code, a 3D special purpose code for hexagonal geometry core flow channels was used. (CRP, 2000)

They found that the maximum fuel and reactor vessel temperatures are realised in the accident with a depressurization of the primary circuit, and their values do not exceed the prescribed benchmark conditions of 1600°C and 420°C, respectively. The researchers conclude that the use of a finite-element technique holds great promise for simulation of problems such as the RCCS. However, fine-tuning of the models might be necessary to obtain optimum performance and to achieve validation prior to construction of a full-scale prototype.

As has been mentioned this project will focus on the air-cooled RCCS.

2.3 Air-cooled RCCS system description and functional requirements

The functions and basic requirements of the RCCS are summarized below:

- The RCCS must provide investment protection by keeping the structures and reactor building wall from exceeding their design limits.

- The RCCS must remove residual heat from the reactor cavity during normal operation, thereby maintaining the concrete surfaces of the cavity below the specified design temperatures of below 80°C for normal conditions (CRP, 2000) and below 100 °C during postulated accident conditions. A value specified by Dilling et al. (1982) of 65°C will be used in this analysis.

- The RCCS must remove all decay heat and residual heat transferred to the reactor cavity during a pressurized or depressurized loss of forced coolant incident.

- The transition from active to passive mode must take place with no mechanical, electrical or human intervention.

- The RCCS must maintain availability under external impacts such as flooding, earthquake, air crash and blasts.

2.4 RCCS heat load during emergency situations

Two emergency situations are of importance within the nuclear engineering community as they have the potential to result in the vessel wall and fuel exceeding maximum temperatures:

- Pressurized Loss of Forced Coolant (PLOFC).

- Depressurized Loss of Forced Coolant (DPLOFC).

2.4.1 PLOFC

The PLOFC, often referred to as the Pressurized Conduction Cooldown (PCC) relates to an event where the forced circulation of helium stops abruptly while the reactor is at 100% power. The reactor should trip immediately. The decay heat will start heating the helium in the channels within the core. During this heating, a natural circulation of pressurized helium is initiated within the core and tends to equalize the core temperature. The vessel structure temperatures, however, will increase as well as parts of the core that are not in contact with the circulating helium. Heat will also be removed from the RPV vessel by conduction and radiation to the reactor cavity. It is reported by Frisani (2010) that the core heat-up slows down due to the heat removal by conduction and radiation and the system attains a safe shutdown. .

2.4.2 DPLOFC

The DLOFC or Depressurized Conduction Cooldown (DPCC) scenario is initiated by a helium leakage in the primary cooling circuit. Helium inventory is discharged into the cavity causing a loss of pressure in the helium circuit. The reactor trips immediately to decay heat power levels. There is very little circulation of helium at low pressure and therefore the core temperature increases (Frisani, 2010). The air molecules in the cavity are replaced by the helium inventory and can subsequently be vented to the atmosphere. Helium will continue to be discharged into the containment until the pressure of the helium is equal to the pressure of the containment (Frisani, 2010). The system peak temperatures are governed by the power level and the

subsequent heat transfer from the core, through the structures to the cavity. If the amount of heat removed from the vessel is greater than the decay heat, the core heat-up slows down.

The air in the cavity continuously enters the RPV by molecular diffusion which subsequently initiates a natural circulation because of the differences in the density of the gas mixture. There is also an element of graphite oxidation which generates a large amount of heat and continues until the air inventory in the RPV is depleted (Frisani, 2010). From there, the temperature decreases as heat is removed from the cavity to the environment.

In light of the scenarios described, it becomes evident that residual and decay heat removal systems are key to ensuring the integrity of the concrete structure, maintaining the vessel and fuel temperatures to below their design limits. Here, the important need for a cavity cooling system both under normal and abnormal operations is illustrated. Without such a system, adequate removal of heat from the cavity might not be possible which could lead to possible core heat up and eventual damage to the reactor system.

2.5 Natural convection in the RCCS

Removal of heat from the RPV to the environment takes place ultimately through a process of natural convection. This will be discussed in section 3.2.1; however, a brief introduction will be presented here regarding its contribution in the RCCS.

Convection can be divided into three regimes; forced, free and mixed convection. Forced convection is the flow that is driven by an external mode that imposes a pressure difference in the system. In this mode of heat transfer, the heat transfer coefficient depends largely on the Reynolds and Prandtl numbers (Lee, 2005). However, if there is a large enough buoyancy head, due to a density gradient induced by a temperature difference between the hot and cold media, forced convection can still be achieved, even without the presence of a pump or blower, or any such medium that would otherwise impose a pressure difference. This is to say that even in a natural circulating flow; heat may be removed by forced convection if the globally induced flow is so large that the local buoyancy forces which affect the velocity are small. Care must therefore be taken when characterizing the flow regime as this depends more on the local effects rather than the global system behaviour.

Natural or free convection is defined as the flow that is driven by the local buoyancy force induced by a temperature difference between the wall or surface and the bulk fluid temperature

(Incropera & DeWitt, 2002:534-536). It is understood that the density variations caused by the temperature difference between the fluid and the contacting surfaces causes this fluid motion. When heat is added, the fluid become less dense and rises. Therefore, it would be intuitive to assume that for natural convection to occur there should be a solid medium and a fluid. The heat transfer is governed by non-dimensional parameters namely the Grashof and Prandtl numbers (Lee, 2005). Due to the fact that there is no externally imposed pressure difference, the velocity depends on the local density gradient caused by the temperature field. In other words, if the local forces which affect the velocity are large due to the temperature field in relation to the global effects, the flow can be said to be driven by free convection.

There is a third effect, namely that which the temperature and the flow interact and affect one other. Therefore all the terms in the momentum and energy equations become significant and cannot easily be neglected (Lee, 2005). This effect is called the mixed convection heat transfer regime and is used to describe the flow condition where both the external forces and the gravitational body force have effects on the velocity and temperature profiles of the flow (Jackson *et al.*, 1989). The typical governing non-dimensional numbers are the Reynolds, Grashof and Prandtl numbers (Lee, 2005). There are other non-dimensional numbers in various literature sources but most of these can be expressed as a combination of the aforementioned non-dimensional numbers.

Further, the convective regimes can be divided into two regions: laminar and turbulent flow. There is another region (i.e. transitional region) which is a region where the flow develops from laminar to the turbulent regime. Laminar flow is the more stable and streamlined, while turbulent flow is unstable and unstructured. It is widely known that in laminar flow, heat and momentum is transferred by viscous shear and molecular diffusion while the unstable nature of the flow enhances transport of momentum and heat in the turbulent regime.

In this literature review particular focus will be given to the mixed convection regime. It has been reported that the MHTGR RCCS design on which the PMR200 is based operates well into the turbulent mixed convection regime (Gang, 1991). Mixed Convection heat transfer is further divided into aided flow (heated upward or cooled downward) and opposing flow (heated downward or cooled upward flow). This discussion is to identify the hydraulic components which are needed to characterise the buoyancy aided flow.

2.5.1 Turbulent mixed convection

There has been a vast amount of interest invested in various literature publications on this subject. Jackson et al. (1989) and Galanis & Behzadmehr (2008) give a good review on all the work done both numerically and experimentally in this field from 1960 to 2008. In general, the researchers investigated the effects of buoyancy forces on the heat transfer and pressure drop in mixed convection flow, compared to their forced convection values.

The general result is that in turbulent aiding flow; buoyancy first decreases the heat transfer rate by 50% from the forced convection value, and then increases, even past the forced convection value. Jackson et al. (1989) and You et al. (2002) provide an explanation for this behaviour as follows: as the heating increases, there are three mechanisms which decrease the heat transfer; (1) the local buoyancy effect decreases the generation of turbulence within the boundary layer due to shear stress redistribution; (2) acceleration of the bulk flow due to bulk density decreases and (3) variation of fluid properties such as thermal conductivity, viscosity and so forth. Subsequently the turbulence production in the boundary layer diminishes and the flow begins to behave more or less like laminar flow. This point is called “laminarization”. Further increase in the buoyancy effect enhances the heat transfer above the laminarization zone. This behaviour is depicted in Figure 2-3.

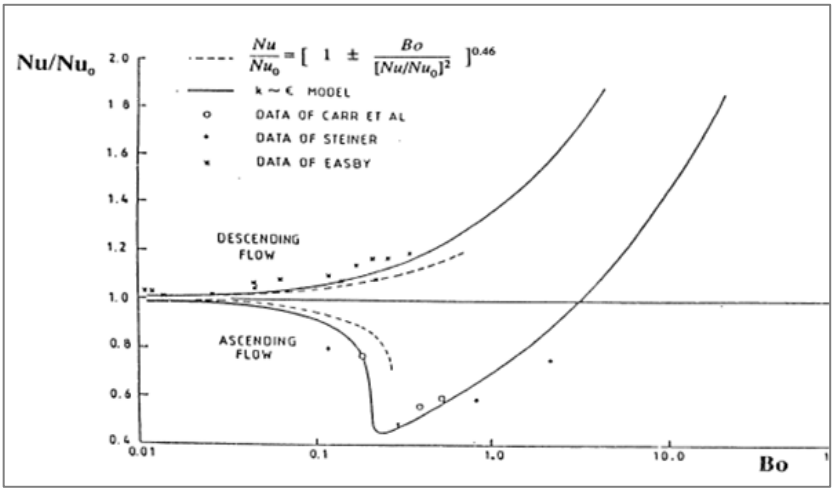

Figure 2-3: Theoretical prediction of mixed convection features in vertical tubes (Gang, 1991).

The parameter Bo along the x-axis is the buoyancy parameter which is used to show the buoyancy effects in this case on the heat transfer. This parameter takes the form:

$$Bo = \frac{8x10^4 Gr}{\mathrm{Re}^{3.425}\,\mathrm{Pr}^{0.8}}$$ Equation 2-1

Gang (1991) calculated the values for these parameters to be 0.0113 and 0.011 for the PCC and DPCC scenarios respectively. For calculation purposes, these results suggest that one can use a Nusselt number for forced convection without introducing a significant overestimation of the heat transfer coefficient.

This well-known Dittus-Boelter correlation was used by Lomperski et al. (2011), Frisani (2010) and Bae et al. (2012) to develop scaling laws for the respective experimental setups from the reference MHTGR and GT-MHR RCCS designs. In these studies, the researchers note that for benchmark studies where the global effects are of importance and where the bulk flow is significantly high in relation to the local effects, the well-known Dittus-Boelter correlation can be used without introducing too much error to the results.

Gang (1991) reported that little work has been done to characterize the friction factor in vertical heated pipes because of the difficulty in measuring the friction factor experimentally. However, since the friction factor is a function of the wall shear stress, which is in turn a function of the velocity gradient, the latter will show an increase as the buoyancy effect increases. Recent work was conducted by You et al. (2002) to study this effect numerically. They found that for upward heated flow with increasing heat flux, the peak velocity shifts from the tube centre towards the wall, causing the velocity gradients at the wall to be steeper and more pronounced, resulting in the increase in the skin friction. As can be seen in Figure 2-4, the skin friction exhibits the same trend as the heat transfer coefficient. Thus with the same reasoning, pressure drop in the RCCS standpipes can be calculated by using a friction factor for forced convection flows. The trends observed by You et al. (2002) are consistent with other work in literature as can be seen in Figure 2-4. Gang (1991) calculated Grashof numbers of 3.66 x 10^7 and 3.53 x 10^7 for the PCC and DPCC respectively. For Re > 10,000 which is the situation in the RCCS; Figure 2-5 also suggests that a friction factor for forced convection can be used for calculation purposes.

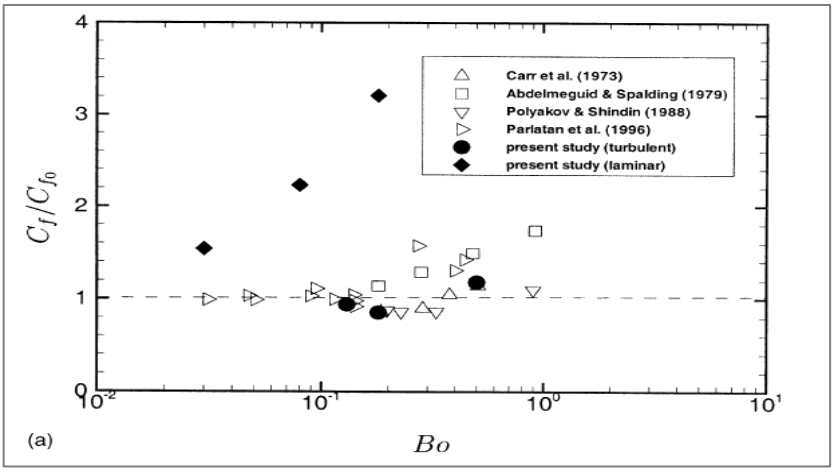

Figure 2-4: Skin friction ratio (You* et al.*, 2002).

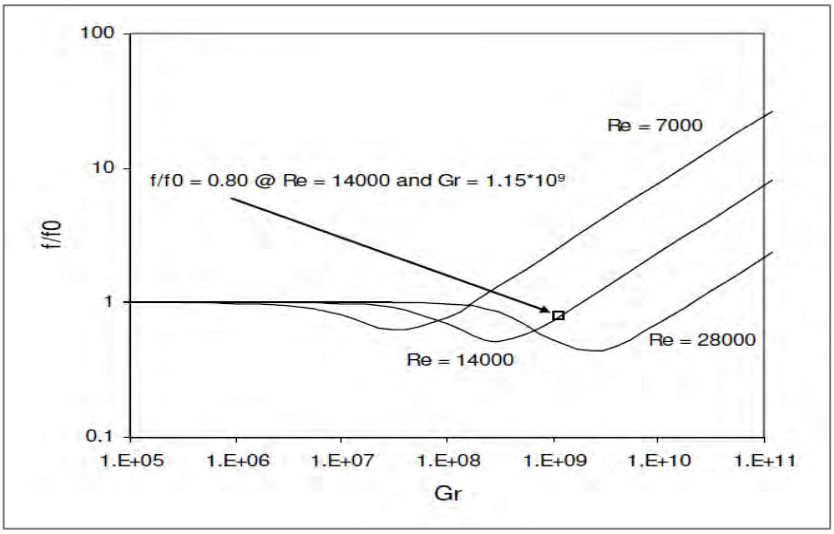

Figure 2-5: Ratio of friction factor in vertical up flow heated pipe (Vilim* et al.*, 2004).

The heat transfer coefficient and the friction factor are important tools that are required to resolve the heat transport in mixed convection. Given these two parameters, the heat transfer inside the risers can be easily determined by solving the continuity, momentum and energy equations. In their investigations, (Vilim *et al.*, 2004) have suggested that the 1-D system codes used for accident analysis must have appropriate correlations for heat transfer and pressure drop. The correlations should include Re, Pr, Gr and the dependency on geometry.

This phenomenon of mixed convection is a topic of continuing interest in recent years, particularly as it can be applied in nuclear reactors. An understanding of the fluid flow and heat exchange processes enables efficient designs of these devises. An intense amount of work has

been conducted by researchers to understand the velocity and temperature profiles in turbulent mixed convection, both numerically and experimentally. To this end, these studies can be summarized by the following expression between two parallel plates;

$$R_T = \frac{T_C - T_f}{T_H - T_f} \qquad \text{Equation 2-2}$$

where

R_T - Temperature factor

T_H - Temperature of the heated plate (°C)

T_C - Temperature of the cold plate (°C)

T_f - Fluid temperature (°C)

For R_T equals unity infers that both plates are symmetrically heated. In this event the general findings are that a velocity and temperature profile with a minimum at the centre will emerge. Experiments with R_T < 0 representing the event where the colder wall is cooled below the fluid temperature have been conducted. The findings from these types of studies are not relevant to the air-cooled RCCS. When R_T is equal to zero is an event where the temperature of one wall is equal to the fluid temperature. Federov & Viskanta (1997) and Terekhov & Ekaid (2012) mention that the up flow may become significantly weaker and the velocity profile becomes diagonally linear. However, due to the coupling between natural convection and radiation effects between the walls at high emissivity, the colder wall temperature will peak above the fluid temperature (Cheng & Muller, 1998; Cheng et al, 2000; Yilmaz & Frazer, 2007). A likely scenario in the RCCS is a situation for R_T > 1, that is, the temperature of the walls will be greater than the fluid temperature. The velocity and temperature profiles are reported to have a minimum at the centre and peak at the respective walls. Lisowski et al. (2013) tested asymmetrical heating of the RCCS at the University of Wisconsin (UW) and found to have a smaller effect on the flow distribution. This was attributed to the smoothing effects of both convection in the cavity and conduction in the riser walls. This is particularly encouraging since

it implies that despite real-world asymmetry, the full scale design will have a stable flow distribution and evenly cool the RPV during accident scenarios.

The following sections deal with experimental and numerical studies of the heat transfer and natural circulation in the RCCS.

2.6 Experimental studies on the RCCS

An approach to understand the heat transfer and thermal hydraulics in the RCCS is to construct an experimental testing facility. This is the most reliable technique to obtain information about a physical system. A full replica of the system can be created and investigated under exact operating conditions. It must be mentioned that experimental set-ups can be an expensive way of recreating a subsystem, especially if the full scale physical system is in itself large. Nonetheless, to overcome this shortcoming, various systems or small scale models can be created and the results extrapolated to full scale. This approach is somewhat subject to inaccuracies as the exact operating conditions are not simulated. Therefore, instruments need to be tested, calibrated and results modified accordingly.

A number of experiments have been conducted on a small scale to investigate various phenomena that occur during passive natural circulation in the RCCS, both during normal and abnormal operating conditions.

The US Department of Energy (DOE) is supporting the testing of passive heat removal systems and concepts at the following institutions:

- Argonne National Laboratory;
- Texas A&M University;
- University of Wisconsin – Madison;
- Oregon State University, and
- University of Idaho.

These experimental set-ups at these facilities are briefly discussed below;

2.6.1 Argonne National Laboratory (ANL)

At the Argonne National Laboratory (ANL) in Idaho, an experimental facility, the Natural Convection Shutdown Heat Removal Test Facility (NSTF) was built to acquire data for natural convection and radiation heat transfer in the reactor cavity and RCCS. This is a state-of-the-art facility for evaluating performance capabilities of decay heat removal systems. The purpose of the NSTF is to;

- Examine the passive safety nature for future nuclear reactors.
- Generate bench marking data to validate advanced computer simulations.

The facility was built in 2010 and is expected to commence with experimental testing by early 2014 (DOE, 2014). The NSTF will be used as an experimental simulator and provide the data for development and assessment of applicable CFD and systems codes (DOE, 2014).

At the Oregon State University a HTTF (High Temperature Testing Facility) was built which will use the NSTF as a boundary condition to model depressurized conduction cooldown transients and examine different core types (DOE, 2014).

2.6.2 Texas A&M University RCCS facility

At the Texas A&M University, a simple test facility was constructed to obtain more comprehensive data for code validation of the air flow and temperature distributions in the reactor cavity (Capone *et al.*, 2011). It is understood that the system is designed to study both air and water as the cooling fluids without much adjustments needed to be done on the set-up (Capone *et al.*, 2011).

2.6.3 University of Wisconsin (UW)-Madison Air Cooled RCCS Facility

The RCCS at UW-Madison contains all aspects common to typical water driven natural circulation loop; a downcomer to provide the driving head, heated section, adiabatic chimney and a bulk mixing tank as a heat sink. The three riser tube section represents 5° radial sector of the full scale GT-MHR RCCS (Lisowski *et al.*, 2013).

It is understood that both water and air as a cooling fluid can be used. There are currently tests being conducted to generate data and further develop predictive capabilities of both the 1D system codes and CFD computer codes (Lisowski *et al.*, 2013).

2.6.4 Seoul National University (SNU) RCCS

At the Seoul National University (SNU) an experimental facility was built to study the water-cooled RCCS option (Frisani, 2010). This facility is different to the common water cooled scheme in that it contains an air cavity fitted within the water pool. This system may be preferred since its heat removal capacity has been proven to be larger than the air-cooled option. The data provided by these experiments are basis for validation CFD calculations specific to the behaviour of water-cooled RCCS (Frisani, 2010).

Park et al. (2006) used the MARS-GCR code to study the natural convection inside the water pool and the cooling pipe. They found that the results predicts well for the convection inside the water pool but shows discrepancies from the experimental data when the built in Dittus-Boelter correlation was implemented.

Thus, further investigations are currently being conducted to simulate the forced convection in the multiple U-bend pipes. Also in the future analysis, the authors plan to demonstrate the capability of the MARS-GCR code to model the radiation and natural convection heat transfer in the cavity (Park *et al.*, 2006).

2.7 Studies on different numerical models

2.7.1 Heat transfer and fluid flow in the reactor cavity

A thermal hydraulics code TAC-NC was used to analyse temperature transients during the heat up experiment designed for the HTR-10 reactor (CRP, 2000). This code calculates natural circulation by a one-dimensional flow network model. The basic flow network equations that are solved are the; one-dimensional momentum and continuity equation for each path, the equation of state and the energy equation for each plenum which connects each path. It was found that the radiation heat transfer is approximately 80% of the heat transfer in the annulus between the RPV and the water cooling panel.

Kim et al. (2006) and Tadaka et al. (1997) performed studies of the heat transfer characteristics inside the reactor cavity. Using a CFD code CFX-5, and a developed simplified model, Kim et al. (2006) modelled a 1/8 (45° domain) of a reference GT-MHR after considering symmetry. A cosine temperature profile was imposed at the RPV wall with a peak temperature of 550°C and an average temperature of 450°C. They found that the RCCS outer wall is heated by radiation

and its temperature is about 200°C. Also, when the temperature at the RPV wall was increased, the portion of heat transfer attributed to radiation increased, reaching values of above 80%.

Tadaka et al. (1997) reported a value of 74.4% for the radiation portion. This value is lower because they used a boundary value of 210°C on the RPV compared to 450°C in Kim et al. (2006). CFX-5 was used to simulate the same boundary condition and found the portion of radiation heat transfer to be 73.9% which showed good agreement.

Lisowski et al. (2013) used the University of Wisconsin's (UW's) one-quarter-scale model of the full General Atomics-Modular High Temperature Gas-cooled Reactors (GA-MHTGR), to study different heating conditions. The working fluid was water in the riser tubes. The experimental results were compared with a RELAP5 and FLUENT model of the facility. Over a range of heat flux levels, radiation was found to be the dominant mode of heat transfer resulting in 60% to 80% of the heat transferred to the RCCS. Capone et al. (2011) conducted an experimental characterization of the Texas A&M University (TAMU) RCCS of the heat transferred to the RCCS and reported a value of 80%. Frisani (2010) and Lomperski et al. (2011) reported a value as high as 87.8% and 88% that is attributed to radiation heat transfer for studies conducted at the NSTF facility.

From the studies it emerged that radiation and convection are the two modes of heat transfer in the RCCS cavity with the portion by radiation ranging between 60 – 90% of the total heat transfer.

Frisani (2010) and Capone et al. (2011) characterized the flow regime in the cavity. The tendency of a system to operate in a certain convective regime is characterized by the ratio of $\frac{Gr}{Re^2}$.This number indicates the relevance of buoyancy forces with respect to the inertia forces. For large $\frac{Gr}{Re^2} >> 1$, buoyancy forces prevail over the inertia forces and the flow is said to be in the free convection. Vice versa, if $\frac{Gr}{Re^2} << 1$, the inertia forces prevail over the boundary forces and the flow is said to be in the forced convection regime. For $\frac{Gr}{Re^2} = 1$, then mixed convection is present. Frisani (2010) and Capone et al. (2011) calculated values for this ratio to be 13.35

and 250 depending on their experimental conditions. These findings showed that free convection prevails in the cavity.

2.7.2 Heat transfer in the RCCS standpipes

Gang (1991) conducted a detailed calculation of the overall heat transfer from the reactor vessel to the air. In his work, he described the radiation between the different surfaces in the RCCS, the inside-cavity convection as well as the heat transfer in the riser tubes. In particular, an in-depth review was done on two key governing parameters; the friction and Nusselt numbers. The fluid flow in the riser tube is presented as a balance between the buoyancy gain and the frictional losses, as both ends are open to atmosphere and the acceleration loss was neglected. A computer code, RECENT was written for this system. The boundary conditions are the heat flux at the vessel wall, air temperature at the riser inlet, which is equal to the ambient temperature. The conservation equations related to the RCCS have also been covered in the works by Frisani (2010), Lomperski et al. (2011) and Bae et al. (2012). The methodology in these works will be very valuable in this project.

Tzanos (2005) used Star-CD to simulate the GT-MHR RCCS in its operating conditions under constant wall temperature of 480°C and 560°C and specifying an inlet temperature of 43°C. He demonstrated the heat removal capability of the RCCS. It was shown that the Reynolds number decreases along the vertical height with heating because the air viscosity increases, unlike in liquids. It was also shown that the Nusselt number decreases along the height as the buoyancy parameter increases. These findings are consistent with the explanations given by Jackson et al. (1989).

Park et al. (2006) performed a two-dimensional and three-dimensional analysis of the RCCS heat transfer characteristics. Their particular focus was to characterize the heat transfer at the element walls. A computer code *RadRec* was developed and incorporated into a CFD code CFX-5 for the heat transfer between the RPV and the elements. In the work by Kim et al. (2006) only two interacting surfaces were modelled. In reality however, the standpipes are located inches from the back wall and it is possible therefore that there will be interactions between the RPV and the back wall and to the sides of the standpipes. Heat flux profiles along the different sides of the standpipes are given. The main finding was that two-dimensional analysis can be used to find the basic heat transfer characteristics.

The works done by Kim et al. (2006) and Park et al. (2006) formed the basis of the study by Sim et al. (2007) to set up an analysis method for the performance of various RCCS designs. A radiation ray interface of the RCCS was developed and reduced to an electrical network analogy. The simplified electrical network illustrates the different heat transfer paths in the RCCS. It was incorporated into a CFD code, CFX and compared with an algebraic method to check performance of some practical RCCSs.

The general findings from these works were that convection heat transfer dominates the lateral region. Radiation heat transfer dominates the front surface of the standpipes. The researchers note that heat transfer to the rear surface attributes 4% of the total heat transfer. This immediately suggests the possibility of ignoring its contribution in simpler approaches such as 1-D analysis.

Zhen (2008) approached this problem quite differently. A MELCOR model was developed which uses a set of Control Volumes (CV's) and Heat Surfaces (HS's) that represent the air flow and sides of the standpipes, lateral support plates and downcomer. This model uses the fact that air moves upwards along the RPV and heat is removed by colder air in a CV in contact with the hot air. The air then moves downwards forming a natural circulation loop. The heat removal rate compared well with a similar RCCS in a normal plant operation.

Lomperski et al. (2011) used three *RELAP-5* (systems code) models: Full scale GA-MHTGR, half-scale GA-MHTGR and the NSTF experimental configuration at certain heat flux boundary conditions at the RPV wall. These models are valuable to this research in the way they are created. The riser leg is treated as a leg from the cold chimney inlet to the hot chimney outlet. Further tests were also done for a two channel grouping where the cavity risers are divided into two groups connected to a common chimney. It is assumed that the two group channel is a representative of the effect on both halves and the heat load is therefore symmetric. The NSTF configuration was conducted as a riser, vessel and cavity. Calculations were performed for the inside cavity radiation and natural convection. Unlike the work by Sim et al. (2007) inside riser duct radiation between the four internal surfaces of the hot duct was considered. It was shown that heat transfer was enhanced when the inside riser duct radiation was included in the assessments and therefore this phenomenon is probably important to take into account.

Frisani et al. (2011) performed a study to analyse heat exchange in the RCCS using CFD code Star-CCM+. They used a 180°C section of the TAMU RCCS test facility after considering

symmetry in the cavity. Two cooling fluids were used in the standpipes; water and air with a uniform heat source imposed on the inside of the RPV. They found that the air-cooled configuration gives a higher air temperature in the cavity. Further, it was found that for the water cooled option; the maximum concrete wall temperature remained below 100°C for the range of tests performed. This demonstrated the better performance of the water-cooled RCCS configuration compared to the air-cooled option.

2.8 Summary of the literature study

This literature review was a valuable exercise to gain a better understanding of passive cooling systems. In section 2.2 a brief overview was given for the theoretical work, relating to RCCSs of the most recent designs. It emerged that researches have successfully demonstrated the heat removal capabilities of the RCCS experimentally and theoretically using CFD and system codes. In Section 2.3, the heat load on the RCCS during normal and emergency situations were described. The DPLOFC and the PLOFC emerged as important scenarios within the nuclear community.

The RCCS operates in the mixed convection flow regime. It was shown in Section 2.5.1, however, that for calculation purposes the forced convection correlations for the heat transfer coefficient and friction factors can be used.

There are experiments invested worldwide to further improve the understanding of the heat transfer phenomena in the RCCS. These are described in Section 2.6 and section gives an overview on the numerical simulations of the RCCS. Different CFD and System codes have been considered for this purpose. It is clear that the RCCS performance can be demonstrated using CFD or System codes depending on the amount and nature of the detail required. The models used in literature appear to have similar traits. Firstly, they represent the radiation and convection in the cavity and secondly, different techniques are used to resolve the conservation equations in the standpipes.

Certain simplifications have been done by the various researchers:

- Heat transfer in the rear wall could be neglected. It accounts for (3-4%) of the total heat transfer (Sim *et al.*, 2007).

- Forced convection heat transfer coefficients and friction factor correlations may be used.

- On the reactor vessel, either a temperature or heat flux boundary condition was specified.

- Ambient temperature and pressure are given as constant.

- Radiation accounts for 50 – 98% of the total heat transfer in the cavity depending on the conditions.

- All the risers can be lumped into one group connected to a single chimney (Lomperski *et al.*, 2011).

The theoretical models of other researchers have provided insight regarding how a model of the RCCS will look. This research has provided all the building blocks and can now be implemented to create a theoretical model of the RCCS.

Chapter 3

3 Theory

3.1 Introduction

A literature study was conducted in ***Chapter 2*** pertaining in part to the numerical simulation of the heat removal in the air-cooled RCCS. It was found that the overall heat transfer from the RPV to the ambient air involves several heat transfer modes. From the RPV to the riser tubes, radiation is dominant although cavity convection makes a contribution. Radiation from the cavity wall and adjacent risers is re-radiated heat received from the RPV wall. Conduction transports this energy, received as radiation, from the outer surface of the riser to its inner surface. The heat is finally transferred to the air by convective heat transfer from the inner riser surface to the flowing air. After absorbing the energy, the air transports the energy to the atmosphere.

The different modes of heat transfer work concurrently to remove heat; therefore, the model that is used to simulate the RCCS must be able to represent these different modes of heat transfer. This will include adequately representing the view factors (space resistances) between the different surfaces in the cavity, the radiation surface resistances due to non-blackbody behaviour, conduction through the solid parts and convection between a fluid and a solid.

The calculations to determine the fluid flow in the riser, downcomer and chimney involve resolving the conservation equations of mass, momentum and energy. To this end, applicable heat transfer and pressure drop correlations have been sourced. The basic principles of the conservation equations and heat transfer are explained. The literature study showed that, inside the riser tubes and the downcomer, radiation heat transfer occurs between the walls and will be taken into account.

Flownex® was used for this study and the basic principles of the software code are discussed.

3.2 Heat transfer theory

Heat transfer is defined as; the transport of thermal energy due to spatial temperature differences (Incropera & DeWitt, 2002:2). There are three types of heat transfer, namely conduction, radiation and convection which will be described in the following section.

3.2.1 Convection heat transfer

Convection heat transfer can be described as energy transfer occurring within the fluid due to molecules moving from one place to another (Incropera & DeWitt, 2002:6-8). It is a form of heat transfer that is particularly different to conduction and radiation heat transfer in that it requires the presence of a fluid motion to occur. It is this motion that enhances the heat transfer by bringing the hotter molecules of the fluid into contact, thus initiating greater heat transfer at more sites in the fluid.

Regardless of the nature of the convection heat transfer process, the rate equation for the transfer of heat between a surface with temperature T_s and fluid with temperature T_f can be expressed as follows:

$$q_x = hA(T_s - T_f) \qquad \text{Equation 3-1}$$

where

h - Heat transfer coefficient (W/m^2—K)

A - Area of the heat transfer medium (m^2)

T_s - Temperature of the surface (°C)

The heat transfer coefficient depends on the surface geometry, conditions of the boundary layer and the nature of the fluid motion amongst other factors (Incropera & DeWitt, 2002:8).This mode of heat transfer contributes to the heat transfer between a solid and a fluid.

In this study, convection heat transfer will be used to determine the heat transfer between the solid parts and the fluid, both in the reactor cavity and the RCCS standpipes. The heat transfer coefficient is discussed in section 3.4.5

3.2.2 Conduction heat transfer theory

Conduction is the transfer of energy from particles which are more energetic to less energetic particles due to interactions between the particles (Incropera & DeWitt, 2002:3-6). This is due to the temperature gradient which exists between the particles. In the RCCS, conduction heat transfer occurs in all solid parts (i.e. riser walls, insulation, reflective surface and concrete wall).

To calculate the conduction heat transfer in a simulation model, *Fourier's Law* is used (Incropera & DeWitt, 2002:4). If conduction heat transfer is calculated for a one-dimensional plane wall, in steady state where the temperature distribution is linear, the rate equation is expressed as:

$$q_x = kA\frac{T_H - T_C}{\Delta x} \qquad \text{Equation 3-2}$$

where

k - Thermal conductivity (W/m-K)

A - Area of the medium (m^2)

Δx - Width of the medium (m)

T_C - Temperature of colder boundary (°C)

T_H - Temperature of hotter boundary (°C)

3.2.3 Radiative heat transfer

Radiation is described as an energy transfer across a system boundary due to a temperature gradient by the mechanism of photon or electromagnetic wave emission. Due to the fact that the mechanism of transmission is through photon emission, unlike conduction and convection, there is no need for intermediate matter for radiation to occur (Incropera & DeWitt, 2002:9). The intensity of the radiation flux depends on the temperature of the body and the nature of the interacting surfaces. If a solid particle is at a higher temperature than its surroundings, it is expected that the solid will come to a thermal equilibrium with the surroundings. This is a direct

result of emission of thermal radiation from the surface to the surroundings and in turn absorption of radiation from the surroundings.

In order to analyse radiation heat transfer for a number of surfaces, a number of assumptions have to be made, particularly since not all surfaces are blackbodies (i.e. absorb all incident radiation). The calculations in this analysis will be performed under the assumptions that all surfaces are **opaque, gray, diffuse and isothermal** (Incropera & DeWitt, 2002:10). The assumption of gray surface is reasonable if the emitted radiation and incident radiation are confined to the same wavelength which is the case in this analysis. For a diffuse, isothermal surface, all incident radiation upon a surface must be reflected with uniform intensity regardless of direction.

For non-black surfaces, the energy emitted from any surface along with the energy reflected is the total energy leaving the surface. This is called the radiosity and is expressed as follows;

$$J_i = \varepsilon_i E_{bi} + \left(1-\varepsilon_i\right) G_i \qquad \text{Equation 3-3}$$

The net rate at which radiation leaves surface i is proportional to the difference between the radiosity and irradiation of the surface. The heat transfer rate can be represented by;

$$\dot{Q}_i = A_i \left(J_i - G_i\right) \qquad \text{Equation 3-4}$$

Substituting Equation 3-3 into Equation 3-4, an expression for the net radiation rate can be obtained;

$$\dot{Q}_i = \frac{A_i \varepsilon_i}{1-\varepsilon_i}\left(E_{bi} - J_i\right) \qquad \text{Equation 3-5}$$

where

$\dot{Q}_i$ - Total heat transfer rate at surface i (kW)

J_i - Radiosity of surface i (W/m)

A_i - Area of surface i (m^2)

E_{bi} - Total emissive power of surface if it were a blackbody (W/m)

G_i - Irradiation rate of surface i (W/m)

ε_i - Emissivity of surface i

For an enclosure with multiple surfaces, the term "view factor" is introduced. This will be explained in section 3.3. The total rate at which radiation leaves surface i towards all surfaces including i if it can view itself, is

$$\dot{Q}_i = \sum_{j=1}^{N} A_j F_{i\to j} \left(J_i - J_j \right) \qquad \text{Equation 3-6}$$

In Equation 3-6, N is the total number of surfaces.

Combining Equation 3-5 and Equation 3-6 gives;

$$\frac{A_i \varepsilon_i \left(E_{bi} - J_i \right)}{1-\varepsilon_i} = \sum_{j=1}^{N} \frac{J_i - J_j}{R_{i\to j}} \qquad \text{Equation 3-7}$$

$$R_{i\to j} = \frac{1}{A_i F_{i\to j}} \qquad \text{Equation 3-8}$$

The term $J_i - J_j$ on the RHS of Equation 3-7 is the driving potential of this exchange, whilst $\left(A_i F_{i\to j} \right)^{-1}$ is the space resistance. Therefore in short, Equation 3-7 says that the rate of radiation transfer through its surface resistance must be equal to the net rate of radiation transfer from i to all the other surfaces through the spatial resistances (Cegnel *et al.*, 2008:912). In the RCCS, it is this space resistance, or rather the view factor that was used to characterize the radiation heat transfer between different solid parts.

The mathematical evaluation of radiation heat transfer in an enclosure involves the resolution of Equation 3-7. Firstly, it must be mentioned that Equation 3-7 is useful when the surface temperature is known. Secondly, there are N linear algebraic equations to determine N

unknown radiosities. Once the radiosities have been obtained, the heat transfer rates can be determined from either Equation 3-5 or Equation 3-6. This approach is suitable for use in equation solvers such as EES, Mathcad and Matlab and is known as the direct method (Cegnel *et al.*, 2008:913).

The direct method is described below and is based on the electrical network analogy. It has been reported by Cegnel et al. (2008:913) that this method has found worldwide acceptance because of its simplicity and emphasis on the physics of the problem. For this method, a surface resistance is drawn associated with each surface of an enclosure and then connected to the space resistances. The radiation network is solved by treating it as an electrical network where the radiation heat transfer replaces the current and the radiosity replaces the potential.

Consider a simple five surface enclosure and radiation network given below.

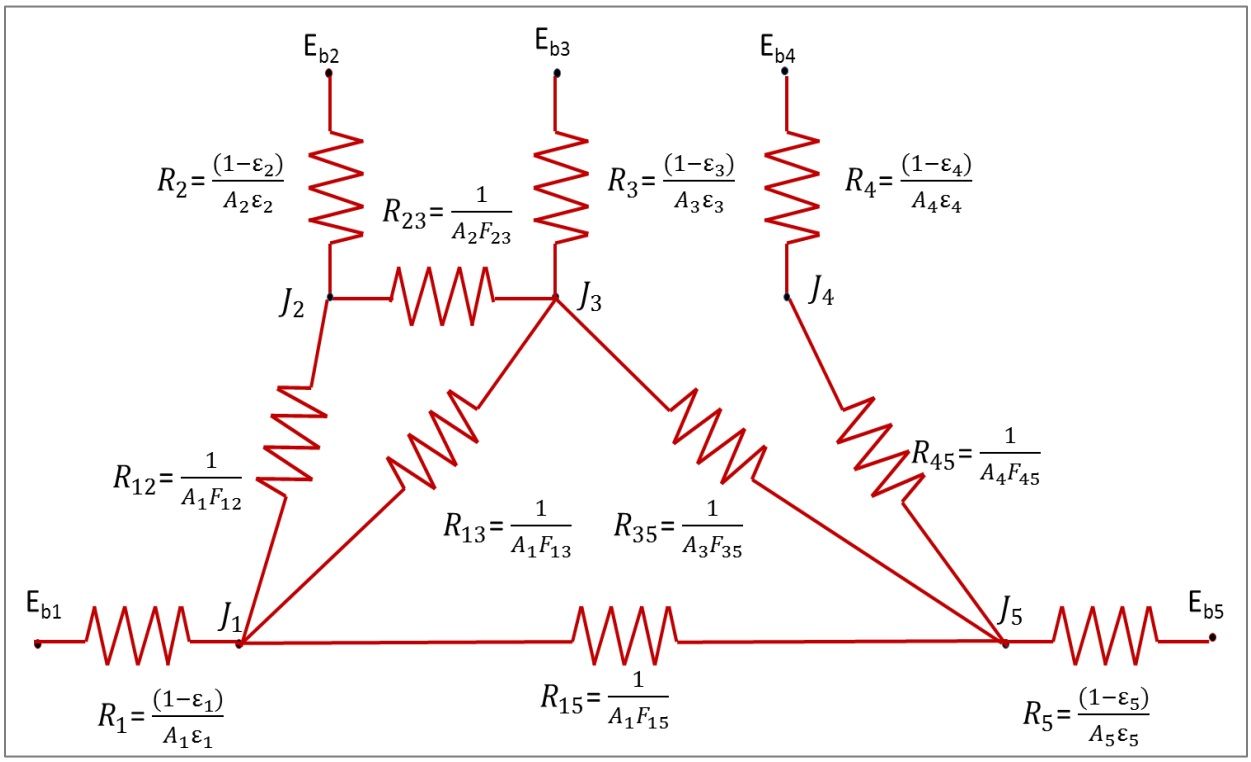

Figure 3-1: Schematic of a five surface enclosure and the radiation network associated with it.

In Figure 3-1 the potentials, E_{bN} are known since the surface temperatures are specified. The symbols R_1 to R_5 represent the surface resistances at the five walls whilst the symbols $R_{i\to j}$

represent the space resistances between the interacting surfaces. The radiosities $J_1 \quad \cdots \quad J_5$ are found by expanding Equation 3-7 as follows;

$$\frac{Eb_1 - J_1}{R_1} + \frac{J_2 - J_1}{R_{1\to 2}} + \frac{J_3 - J_1}{R_{1\to 3}} + \frac{J_4 - J_1}{R_{1\to 4}} + \frac{J_5 - J_1}{R_{1\to 5}} = 0 \qquad \text{Equation 3-9}$$

$$\frac{J_1 - J_2}{R_{1\to 2}} + \frac{Eb_2 - J_2}{R_2} + \frac{J_3 - J_2}{R_{3\to 2}} + \frac{J_4 - J_2}{R_{4\to 2}} + \frac{J_5 - J_2}{R_{5\to 2}} = 0 \qquad \text{Equation 3-10}$$

$$\frac{J_1 - J_3}{R_{1\to 3}} + \frac{J_2 - J_3}{R_{2\to 3}} + \frac{Eb_3 - J_3}{R_3} + \frac{J_4 - J_3}{R_{4\to 3}} + \frac{J_5 - J_3}{R_{5\to 3}} = 0 \qquad \text{Equation 3-11}$$

$$\frac{J_1 - J_4}{R_{1\to 4}} + \frac{J_2 - J_4}{R_{2\to 4}} + \frac{J_3 - J_4}{R_{3\to 4}} + \frac{Eb_4 - J_4}{R_4} + \frac{J_5 - J_4}{R_{5\to 4}} = 0 \qquad \text{Equation 3-12}$$

$$\frac{J_1 - J_5}{R_{1\to 5}} + \frac{J_2 - J_5}{R_{2\to 5}} + \frac{J_3 - J_5}{R_{3\to 5}} + \frac{J_4 - J_5}{R_{4\to 5}} + \frac{Eb_5 - J_5}{R_5} = 0 \qquad \text{Equation 3-13}$$

There are five equations which can be solved simultaneously for five unknown radiosities and subsequently the heat transfer at each surface. The view factors need to be specified for all $R_{i\to j}$ and the emissivity for all surfaces R_j. The next section gives an overview on the view factor.

3.3 Radiation view factors

The view factor is the fraction of the total radiation leaving one surface in all directions, which is intercepted directly by the other surfaces in an enclosure. By an enclosure is meant that the space is enclosed completely by the surfaces such that no heat escapes. From this description, it is clear that the limiting values for the view factor are zero and unity.

To derive a general expression for the view factor, consider two bodies as shown in Figure 3-2.

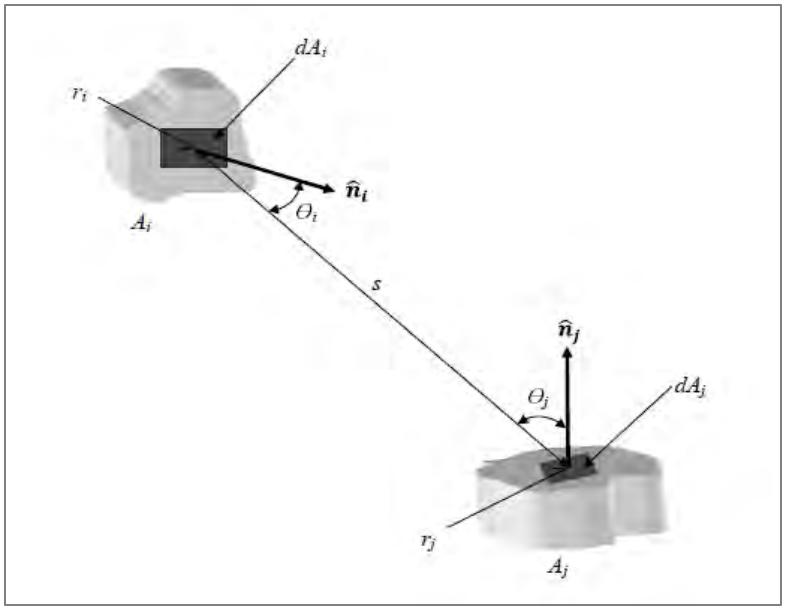

Figure 3-2: Arbitrary bodies used to determine the view factor (Verwey, 2010).

In Figure 3-2, s is an imaginary line joining the midpoints and the normal while θ_i and θ_j are the angles between the imaginary line and the normals on the respective surfaces. Radiation is considered between the elemental areas dA_i and dA_j. The calculation of the radiation view factor between any two surfaces requires the solution of the double integral (Incropera & DeWitt, 2002:791); (Coulson & Richardson, 1999:448).

$$F_{Ai \to Aj} = \frac{1}{A_i} \int_{A_i} \int_{A_j} \frac{cos\theta_i cos\theta_j}{\pi s^2} dA_i dA_j \qquad \text{Equation 3-14}$$

Two important rules applicable to view factors in an enclosure which must be conserved;

1. Reciprocity Rule

$$A_i F_{i \to j} = A_j F_{j \to i} \qquad \text{Equation 3-15}$$

2. Summation Rule

$$\sum_{j=1}^{N}\left(F_{i\to j}\right)=1 \qquad \text{Equation 3-16}$$

It has been reported that the integrals in Equation 3-14 can be considerably complex and often computer software is required; especially if the geometry of the two areas is complex (Coulson & Richardson, 1999:449). Alternatively, experiments can be conducted to determine the view factors. There are also typical data in Incropera and De Witt (2002:793-797) and Coulson and Richardson (1999:450-453) for different geometries. View factors are also easily accessible on the internet and various other journals in heat transfer literature. Furthermore, view factors can also be obtained using computational methods such as implemented in STAR-CCM+ and other CFD codes.

For this project, the view factors for the radiation in the cavity and inside the risers have been provided by the KAERI. It was not the aim of the project to calculate the view factors in the cavity. However, it will be a shortcoming for this work not to verify the appropriateness of the view factors provided, especially since it is not known how they were calculated. To this end, as will be shown in section 7.5, view factors for the RCCS were calculated using STAR-CCM+ and compared with those provided by the KAERI.

3.4 Heat transfer and fluid flow in pipe networks

Considering a fluid flowing through a control volume with boundaries at the inlet and outlet, there would be a change in the mass, momentum and energy due to different factors that have an effect on the fluid. These changes in the mass, momentum and energy are represented by the conservation laws discussed below.

Figure 3-3 presents a schematic of an infinitesimal one dimensional control volume that was used to derive the conservation laws. Only the final conservation equations will be described together with the meaning of each term. The derivations of these equations will not be repeated.

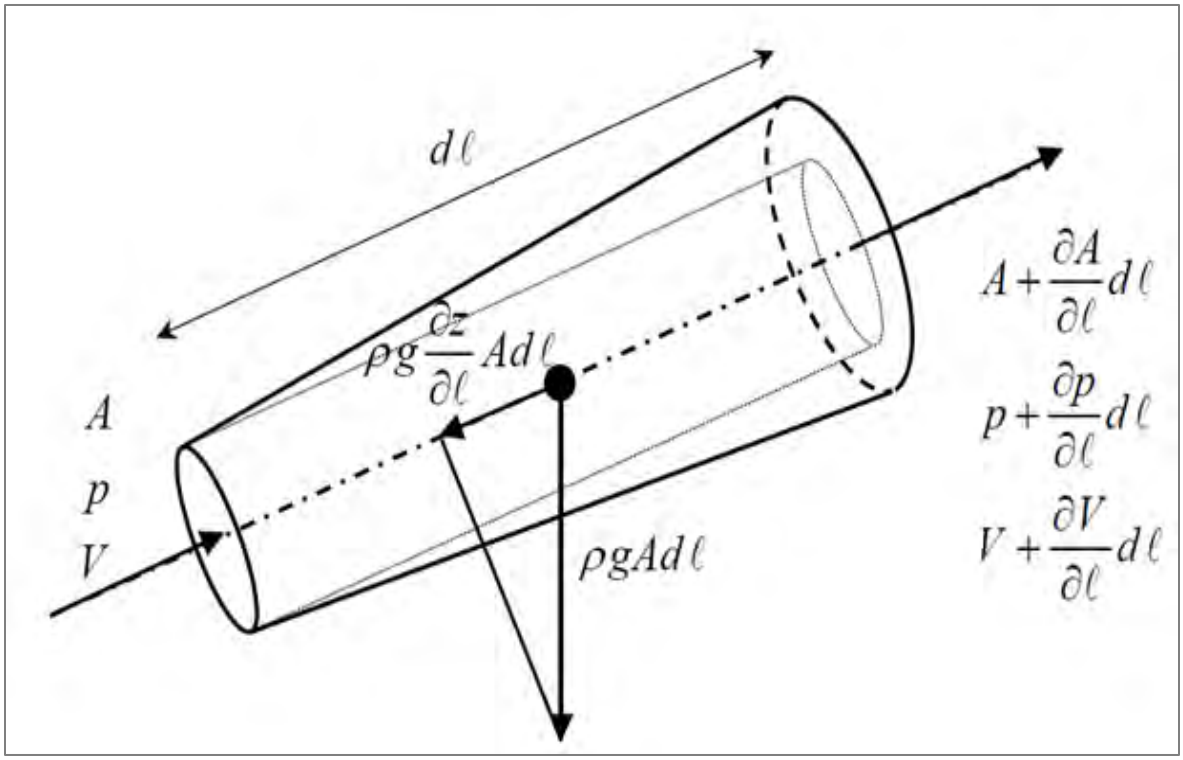

Figure 3-3: Schematic of an infinitesimal one dimensional control volume (Rousseau & Van Eldik, 2013).

3.4.1 Conservation of mass

The conservation of mass is also known as the continuity equation. The rate of change of mass through a one-dimensional control volume is derived from Figure 3-3. The derived equation is given by Equation 3-17.

$$\forall \frac{\partial \rho}{\partial t} + \dot{m}_e - \dot{m}_i = 0 \qquad \text{Equation 3-17}$$

where

$\forall$ - 1-D control volume (m^3)

ρ - Density of the fluid (kg/m^3)

t - Time

$\dot{m}_i$ - Mass flow entering the control volume (kg/s)

$\dot{m}_e$ - Mass flow exiting the control volume (kg/s)

The first term of Equation 3-17 refers to the rate of change of mass within the control volume over time, the second term is the rate at which mass flow exiting the control volume and the last term is the rate at which mass flow entering the control volume (Rousseau & Van Eldik, 2013).

3.4.2 Conservation of momentum

The conservation of momentum is derived for compressible and incompressible flow from the well-known Navier-Stokes equations. For this study, only incompressible flow was used since the velocities involved are low enough to ignore the compressibility effects. The conservation of momentum for incompressible flow through a one-dimensional control volume is given by Equation 3-18.

$$\rho L \frac{\partial V}{\partial t} + (p_{0e} - p_{0i}) + \rho g (z_e - z_i) + \Delta P_{0L} = 0 \qquad \text{Equation 3-18}$$

where

V - Mean velocity (m/s) in the flow channel

L - Length of the pipe (m)

p_{0i} - Total pressure at the inlet of control volume (kPa)

p_{0e} - Total pressure at the outlet of control volume (kPa)

z_i - Elevation at the inlet of control volume (m)

z_e - Elevation at the exit of control volume (m)

g - Gravitational acceleration (m/s^2)

ΔP_{0L} - Total pressure loss through the control volume (kPa)

The first term of Equation 3-18 represents the rate of change of momentum within the control volume over time. The second term is the difference in the total pressure between the inlet and outlet of the control volume and the third term represents the gravitational force. The last term is the total pressure loss through the control volume (Rousseau & Van Eldik, 2013). This will be discussed in section 3.4.4

3.4.3 Conservation of energy

The conservation of energy, also known as the first law of thermodynamics (Rousseau & Van Eldik, 2013), describes the rate of change of energy within the control volume. The conservation of energy for a one-dimensional control volume is given by Equation 3-19.

$$\dot{Q}+\dot{W}=\forall\frac{\partial}{\partial t}(\rho h_0-p)+\dot{m}_e h_{0e}-\dot{m}_i h_{0i}+\dot{m}_e g z_e-\dot{m}_i g z_i \qquad \text{Equation 3-19}$$

where

$\dot{Q}$ - Total rate of heat transfer to the fluid (kW)

$\dot{W}$ - Total rate of work done on the fluid (kJ)

h_{0i} - Total enthalpy at the inlet of the control volume (kJ/kg)

h_{0e} - Total enthalpy at the outlet of the control volume (kJ/kg)

h_0 - Total enthalpy in the control volume (kJ/kg)

p - Static pressure in the control volume (kPa)

The first term on the RHS of Equation 3-19 is the change of energy in the control volume over time while the rest of the terms are the net inflow and outflow of energy from the control volume (Rousseau & Van Eldik, 2013).

3.4.4 Pressure drop calculations

Pressure losses are always present in any normal flow channel due to frictional drag on a surface and secondary losses in the control volume (Rousseau & Van Eldik, 2013). It emerged

from the literature review that for the current analysis, a pressure drop for forced convection may be used. The Flownex® Library User Manual 2013 gives the so-called Darcy-Weisbach friction factor correlation for pressure drop (Anon., 2013).

$$\Delta P_{0L} = \left(\frac{fL}{D_H} + \sum K \right) \frac{1}{2} \rho V |V| \qquad \text{Equation 3-20}$$

where

f - Darcy-Weisbach friction factor

D_H - Hydraulic diameter (m)

$\sum K$ - Sum of the secondary loss-coefficients

The mean velocity in Equation 3-20 can be solved with the following equation:

$$V = \frac{\dot{m}}{\rho A} \qquad \text{Equation 3-21}$$

where

A - Mean flow area of the pipe (m^2)

$\dot{m}$ - Mass flow rate through the channel (kg/s)

By substituting Equation 3-21 into Equation 3-20, the pressure drop through a flow channel is given by the following equation (Rousseau & Van Eldik, 2013) and (Anon., 2013).

$$\Delta P_{0L} = \left(\frac{fL}{D_H} + \sum K \right) \frac{\dot{m}|\dot{m}|}{2\rho A_{ff}^{\ 2}} \qquad \text{Equation 3-22}$$

The friction factor may be calculated for laminar flow, $Re < 2 \times 10^3$ from (Rousseau & Van Eldik, 2013).

$$f = \frac{C}{\mathrm{Re}}$$ Equation 3-23

where

- $C = 64$ for round ducts and pipes.
- $C = 57$ for square ducts.
- $C \approx 64$ for very flat rectangular-shaped ducts.

For turbulent flow ($5 \times 10^3 \leq Re < 10^8$) with ($10^{-6} \leq \frac{\varepsilon}{\mathrm{D}} < 10^{-2}$) it can be calculated from (Rousseau & Van Eldik, 2013).

$$f = 0.25\left(\log\left(0.27\frac{\varepsilon}{\mathrm{D_H}} + \frac{5.74}{\mathrm{Re}^{0.9}}\right)\right)$$ Equation 3-24

where

ε - Pipe roughness (m)

3.4.5 Heat transfer coefficient calculation

To determine the heat transfer coefficient, the literature study revealed that a forced convection correlations such as the Dittus-Boelter correlation for turbulent flow may be used. The Dittus-Boelter equation is given by Equation 3-25.

$$Nu = 0.023 Re^{0.8} Pr^{0.4}$$ Equation 3-25

In Equation 3-25, Nu is the Nusselt number, Re the Reynolds and Pr is the Prandtl number. The Reynolds number Re can be calculated with Equation 3-26.

$$Re = \frac{\rho V D_H}{\mu} = \left|\frac{\dot{m} D_H}{\mu A_{ff}}\right|$$ Equation 3-26

In Equation 3-26, μ is the viscosity of the fluid. The Prandtl number is calculated with Equation 3-27.

$$Pr = \frac{c_P \mu}{k} \qquad \text{Equation 3-27}$$

In Equation 3-27, c_P is the specific heat of the fluid. The convection heat transfer coefficient is then calculated with Equation 3-28.

$$Nu = \frac{hD_H}{k} \qquad \text{Equation 3-28}$$

In short, the Nusselt number Nu is the ratio of convective to conductive heat transfer across a boundary. The Reynolds number Re is the ratio of the inertia forces (forces exerted by a fluid by virtue of its motion) over the viscous forces (forces between a body and a fluid particle moving past it, in a direction so as to oppose the flow). The Prandtl number Pr is a dimensionless ratio of momentum transport via diffusion to energy transport via diffusion.

3.5 CFD vs. SCFD

There are various ways in which the solution of the conservation equations can be obtained. Two of these are the Computational Fluid Dynamics (CFD) and the Systems Computational Fluid Dynamics (SCFD) approaches which are described below.

3.5.1 CFD

This approach involves the solution of the differential equations for the mass, momentum and energy equations on a per volume basis (Rousseau & Van Eldik, 2013).

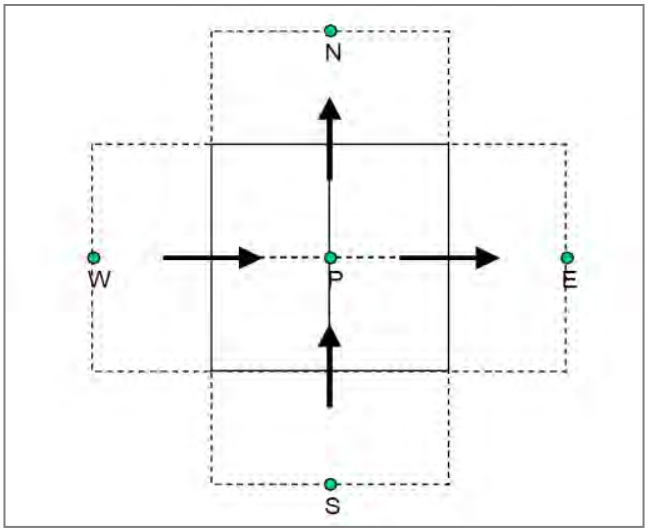

Figure 3-4: Typical control volume for a CFD approach (Rousseau & Van Eldik, 2013).

Figure 3-4 shows a typical two-dimensional control volume in the CFD approach. It is assumed that the pressure, temperature and velocity vary smoothly over the control volume. Averaged values situated at the nodal point P in the middle of the control volume can be used to represent the property values of the control volume. The properties such as temperature, velocity and pressure may be written in relation to their nearest neighbours (N, E, W, and S). The mass, momentum and energy are written across the boundaries of the control volumes.

In the staggered grid CFD approach, the mass and energy are written around the focal point P while the momentum equation is written for flows over the boundary at the interfaces (dashed lines in Figure 3-4) of the control volume (Rousseau & Van Eldik, 2013).

3.5.2 SCFD

The SCFD approach, on which Flownex® is based, makes use of one-dimensional elements that are connected to nodes in any unstructured manner (Rousseau & Van Eldik, 2013).

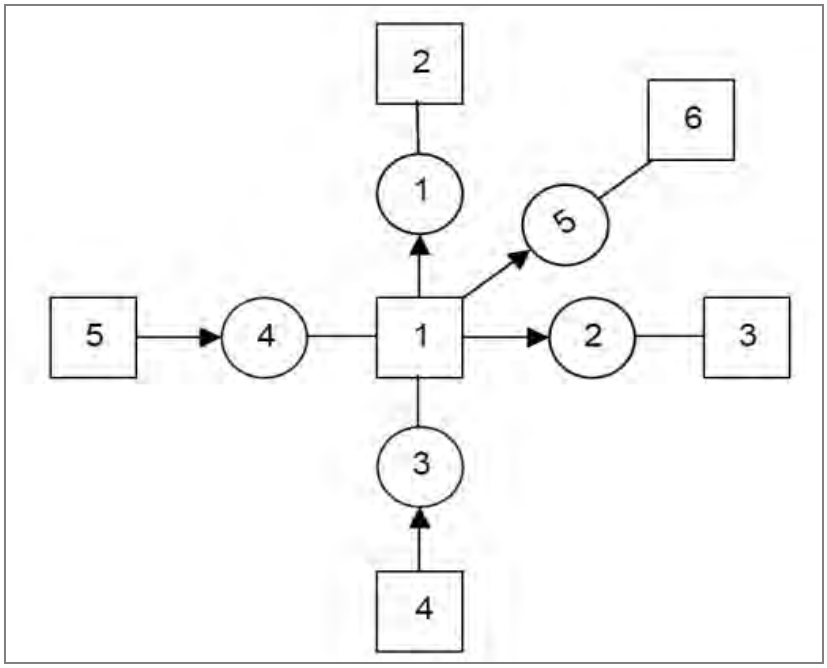

Figure 3-5: Node element of SCFD approach method (Rousseau & Van Eldik, 2013).

In Figure 3-5, the circles represent the elements, which can be any type of thermal fluid component such as pumps, pipes, fans, compressors, turbines or heat exchangers. The blocks represent the nodes, which can be used for the connection between the elements or to specify a boundary condition. The blocks can also have a volume to represent a tank of reservoir (Rousseau & Van Eldik, 2013).

One of the similarities of the CFD and SCFD approach is that the node represents the average fluid properties. Another similarity is that the conservation of mass and energy are also written in terms of a node and the conservation of momentum equations are written in terms of the elements (Rousseau & Van Eldik, 2013).

Although it is assumed that only one-dimensional flow can be solved with this approach; two-or three-dimensional flow fields can be built up from the one-dimensional case with the correct combinations of elements and nodes. The network can be built for the different directions on the coordinate system (Rousseau & Van Eldik, 2013). Normally when this is done, the diffusion term is assumed to be negligible.

The model of the RCCS will focus on the SCFD approach rather than the CFD approach.

3.6 Transient modeling of pipe networks

The transient case refers to a situation where the boundary values change over time resulting in accumulation of mass and energy at any point in the system. Consider an example of a network of elements and nodes (SCFD) representing a pipe as shown in Figure 3-6. The network consists of four nodes and three elements. The elements represent the pipe while the nodes as has been mentioned before can have no physical significance but to connect the elements or they can have a volume to represent a tank or reservoir.

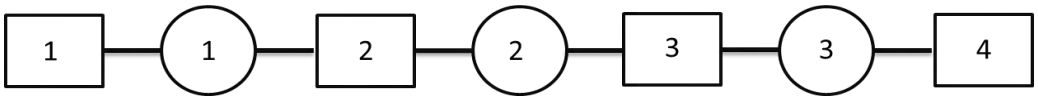

Figure 3-6: Node and element representation of a pipe network.

In Figure 3-7, the mass conservation control volumes (red) are shown. Each control volume consists of the volume of the actual node (zero in this case), together with half of the volume of the elements connected to the node (Rousseau & Van Eldik, 2013).

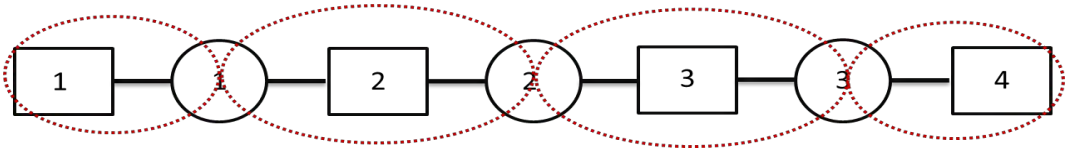

Figure 3-7: Control volume definition for mass conservation (red).

The equations governing transient flow through a duct are the continuity, momentum and energy equations. These can be written from Equation 3-17 to Equation 3-19 as

$$\frac{\partial \rho}{\partial t} = \frac{1}{\forall}(\sum \dot{m}_i - \sum \dot{m}_e + \dot{m}_s) \qquad \text{Equation 3-29}$$

$$\rho L \frac{\partial V}{\partial t} = p_{0\mathrm{i}} - p_{0\mathrm{e}} + \rho \mathrm{g}(\mathrm{z}_i - z_e) - \Delta P_{0L} \qquad \text{Equation 3-30}$$

$$\forall \frac{\partial}{\partial t}(\rho h_0 - p) = \sum \dot{m}_i (h_{0i} + g z_i) - \sum \dot{m}_e (h_{0e} + g z_e) + \dot{m}_s h_{0s} + \dot{Q} + \dot{W} \qquad \text{Equation 3-31}$$

where

$\dot{m}_s$ - Total mass flow rate addition via a source (kg/s)

h_{0s} - Enthalpy addition via a source (kJ/kg)

The subscript i in all of the equations refers to the upstream side while e refers to the downstream side of the element or node. The subscript s is the rate of mass or energy addition via a source, which may be either positive or negative. Also the subscript 0 refers to the total pressure or enthalpy.

Using the fundamental relationship given in Equation 3-21, Equation 3-30 can be written in terms of the change in mass rather than velocity to arrive at the following expression for the momentum conservation.

$$\frac{\partial \dot{m}}{\partial t} = \frac{A}{L}\left(p_{0\mathrm{i}} - p_{0\mathrm{e}} + \rho \mathrm{g}\left(\mathrm{z_i} - \mathrm{z_e}\right) - \Delta P_{0L} + LV\frac{\partial \rho}{\partial t}\right) \qquad \text{Equation 3-32}$$

Equation 3-31 can be expanded to Equation 3-33

$$\frac{\partial h_0}{\partial t} = \frac{1}{\rho \forall}\left(\sum \dot{m}_i \left(h_{0i} + \mathrm{gz_i}\right) - \sum \dot{m}_e \left(h_{0e} + \mathrm{gz_e}\right) + \dot{m}_\mathrm{s} h_{0\mathrm{s}} + \dot{Q} + \dot{W} + \forall\left(\frac{\partial p}{\partial t} - h_0 \frac{\partial \rho}{\partial t}\right)\right) \qquad \text{Equation 3-33}$$

Equation 3-29, Equation 3-32 and Equation 3-33 are solved by the so called time-wise integration (Rousseau & Van Eldik, 2013). This includes separating the variables and integrating over a time step with length Δt between the previous time t^0 and the current time t.

From Equation 3-29, an expression for a time step can be written by

$$\forall \frac{\left(\rho - \rho^0\right)}{\Delta t} = \alpha_c \left(\dot{m}_i - \dot{m}_e + \dot{m}_s\right) + \left(1 - \alpha_c\right)\left(\dot{m}_i^{\,0} - \dot{m}_e^{\,0} + \dot{m}_s^{\,0}\right) \qquad \text{Equation 3-34}$$

The first term in Equation 3-34 refers to the current time while the last term refers to a previous time. Therefore, defining the source terms

$$S_c = \left(\dot{m}_i - \dot{m}_e + \dot{m}_s\right) \qquad \text{Equation 3-35}$$

$$S_c^{\,0} = \left(\dot{m}_i^{\,0} - \dot{m}_e^{\,0} + \dot{m}_s^{\,0}\right) \qquad \text{Equation 3-36}$$

Equation 3-34 can be written as;

$$\frac{\rho - \rho^0}{\Delta t} = \alpha_c S_c + \left(1 - \alpha_c\right) S_c^{\,0} \qquad \text{Equation 3-37}$$

where

ρ^0 - Fluid density at the previous time (kg/m^3)

Δt - Time step length (s)

α_c - weighing factor for continuity equation

S_c - Source term at the current time

$S_c^{\,0}$ - Source term at a previous time

The same methodology is followed for Equation 3-32 and Equation 3-33 to arrive at the following expressions for the momentum and energy equations;

$$\frac{\dot{m} - \dot{m}^0}{\Delta t} = \alpha_m S_m + \left(1 - \alpha_m\right) S_m^{\,0} \qquad \text{Equation 3-38}$$

where

$\dot{m}$ - Mass flow rate at the current time (kg/s)

$\dot{m}^0$ - Mass flow rate at a previous time (kg/s)

α_m - weighing factor for momentum conservation equation

S_m - Momentum source term at the current time

$S_m^{\,0}$ - Momentum source term at a previous time

$$\frac{h_0 - h_0^{\,0}}{\Delta t} = \alpha_e S_e + \left(1 - \alpha_e\right) S_e^{\,0} \qquad \text{Equation 3-39}$$

where

h_0 - Fluid enthalpy at the current time (kJ/kg)

$h_0^{\,0}$ - Fluid enthalpy at a previous time (kJ/kg)

α_e - weighing factor for energy conservation equation

S_e - Energy source term at the current time

$S_e^{\,0}$ - Energy source term at a previous time

The variable α_c, α_m and α_e are the weighing factors between the previous and present time step. Their values can be anything between zero and unity. For $\alpha = 0$ gives and explicit solution; this is to say that the source term remains at the old source term S^0 between t^0 and t thereafter jumps instantaneously to the new source terms S at time t. For $\alpha = 1$ gives and implicit solution, that is, the source term jumps to the new S instantaneously at time is t^0 and remains constant for the duration of time. For a smooth linear change in the source term between two time steps $\alpha = 0.5$ (the source term is maintained at an average S^0 between S for the full time step). This is known as the Crank-Nicholson method. The variation of the source term over the integration step is shown in Figure 3-8. (Rousseau & Van Eldik, 2013).

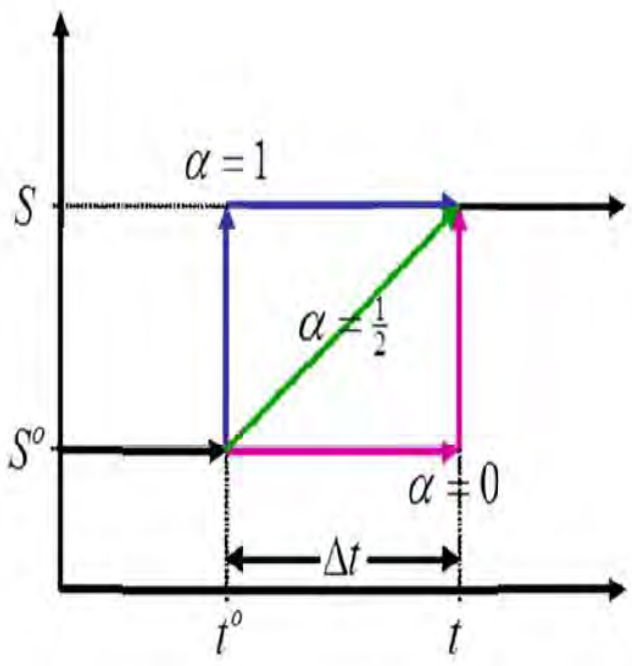

Figure 3-8: Illustration of the source term over the time step (Rousseau and Van Eldik, 2013).

It has been reported by Greyvenstein (2001) that implicit and explicit methods depend of the size of the time increment. They are second order accurate while the Crank-Nicholson method is first order accurate but numerically unstable at large time steps. Semi-implicit methods are conditionally stable. Furthermore, it has been reported that a value of α = 0.6 gives a good compromise between accuracy and stability (Greyvenstein, 2001).

The transient simulation involves solving Equation 3–(37–39) together with the fluid property relationships using EES, Matlab etc. for pressure, mass flow rate, enthalpy and density of each node iteratively and with time. The simulation methodology starts with known values of ρ^0, T^0, $p^0, h_0{}^0, P_0^0$, Sc^0 and Se^0 at the nodes as well as $\dot{m}^0$, ρ^0 and Sm^0 at the elements. Then the properties p_{0i}, p_{0e} h_{0i} and h_{0e} are calculated taking into account if the mass flow is greater, equal to or less than zero, average properties are also calculated. In Figure 3-8, Δt is the time step which is defined as the previous time t^0 to the current time t and these equations are iterated until sufficient convergence is obtained for ρ, h_0 and pressure at each node and mass flow rate at each element. The full methodology for simulating transient scenarios in pipe networks is detailed in Rousseau and Van Eldik (2013: 159-162).

A case study will be performed to model a transient case in EES and Flownex® to verify that the software is setup correctly to model the transient scenarios in pipe networks and also to show that the theory related to modelling transient conditions is understood and can be applied to a practical case. This is dealt with in section 5.2.3.

3.7 Flownex®

For this project the software Flownex® was used to set up a simulation of natural circulation in an air-cooled RCCS. Flownex® is based on an Implicit Pressure Correction Method (IPCM) that solves the momentum equation in each element and the continuity and energy equation at each node in large structured networks for both steady-state and dynamic situations (Anon., 2013). This gives the software a pseudo-CFD capability and allows Flownex® to analyze complex scenarios such as temperature and pressure gradient through pipes and buoyancy effects (Anon., 2013).

The governing equations in Flownex® are the same as those presented in sections 3.4 and 3.6. A detailed description of the Flownex® library and nodalization is given in **Appendix A.** Further, an explanation of all the elements that were used in this study can also be found in **Appendix A**.

3.8 Summary of the theory chapter

In this chapter, the theory related to the thermal-hydraulic calculations in pipe networks was introduced. This was done in particular because it is relevant to the simulation of heat transfer in the RCCS. The different modes of heat transfer have been described including the equations resolved to solve for the total heat transfer and associated temperatures. Finally, the calculation methodology for calculating transient conditions was explained that accounts for the event where there are changes in the boundary values.

Flownex® is a systems code that will be used in this assessment and the software capability was introduced. Further information on the software can be found in **Appendix A.**

The theory detailed in this chapter will now be used to create a model that will simulate the performance of the RCCS.

Chapter 4

4 RCCS geometry description

4.1 Basic information about the air-cooled RCCS

A schematic diagram of the RCCS under consideration is shown in Figure 4-1. It consists of an intake/exhaust structure which forms the chimney. In the chimney, there are a series of rectangular ducts to provide passage for motion of air. The hot fluid flows upwards in the inner ducts while the cold fluid flows downwards in the outer ducts. The chimney structure is approximately 27 – 30 m in height above the core to provide additional driving force to maximize the natural convection circulation effect. Furthermore, the cross connection between the inner ducts and the cross connection between the outer ducts is to ensure that in the event that one duct is blocked, the ability of the RCCS to remove heat is not compromised.

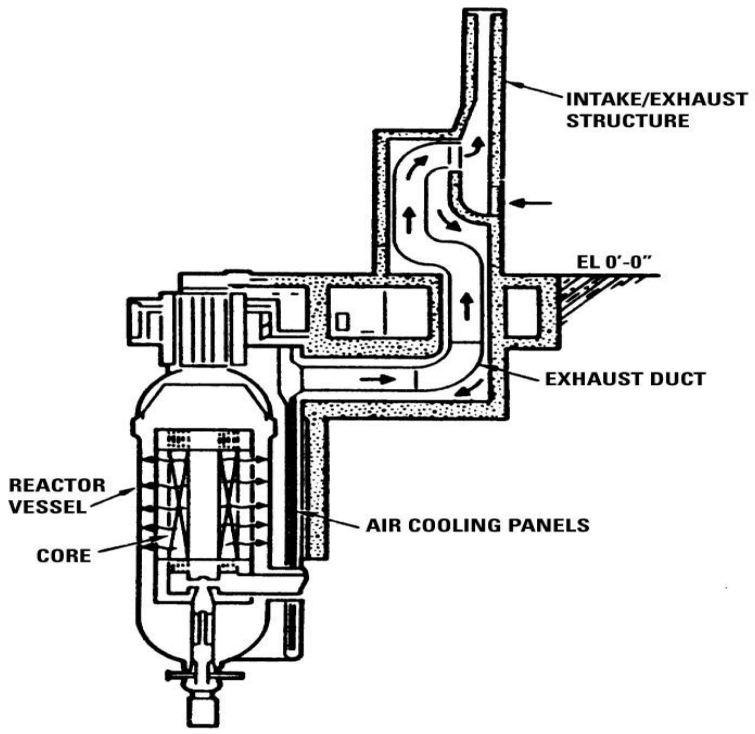

Figure 4-1: Schematic of the RCCS showing the air circulation (Jun, 2012).

Atmospheric air enters through the chimney and flows downwards into the downcomer duct which is located in the reactor cavity. The cold air flows to the lower plenum from where it is directed into 220 cooling tube panels or “risers” which are situated around the inner wall of the containment building. This can be seen in Figure 4-2. The geometry of the riser and downcomer section can be visualised as a simple U-tube.

In the riser, the cold air absorbs heat radiated from the RPV wall. The air temperature increases and the density decreases. Since the density is higher in the downcomer than in the riser, the warmer molecules driven by buoyancy begin to move upwards and are replaced by the colder molecules. The colder molecules in turn heat up and flow upwards initiating a natural circulation effect. The hotter air collects in a hot plenum which connects the risers to the chimney, before flowing in the inner ducts within the chimney to be released into the atmosphere. For design purposes, the hot air is released at an elevation higher than the cold air to prevent mixing of the different temperature streams.

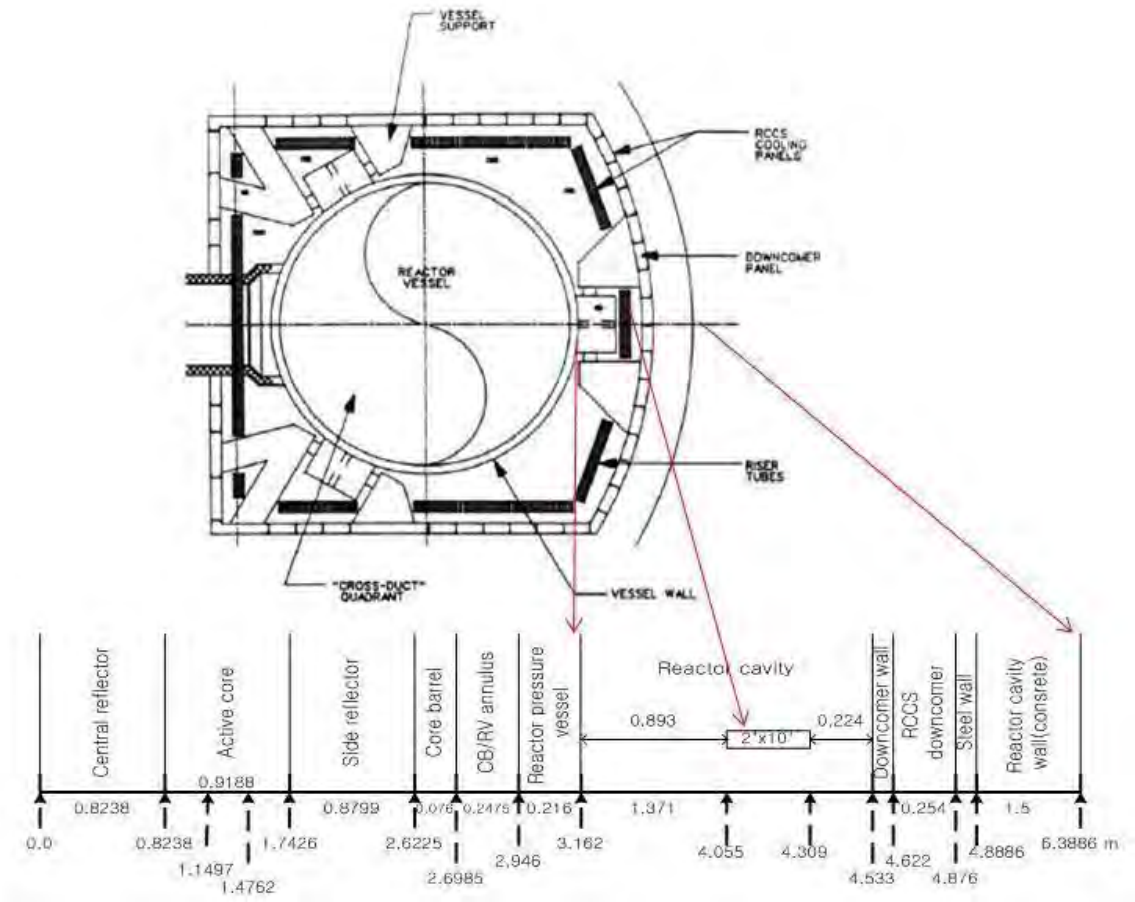

Figure 4-2: Radial location of reactor vessel and the air-cooled RCCS (Jun, 2012).

In Figure 4-2, the cross-sectional top view of the inner reactor cavity is shown. It can be seen that the reactor cavity assumes an almost square cross-section with the downcomer panel forming the wall of the cavity. The risers (***indicated in black***) surround the RPV and are located a few meters from the RPV wall depending on where they are placed. The distance between each riser tube is approximately one riser width. This is to ensure that enough surface area is available to absorb heat from the RPV. This space, however allows heat to penetrate the downcomer. It is for this reason that the downcomer wall is lined with a reflective insulating surface to minimize heat transfer to the downcomer since this cold air is used to remove heat. Furthermore, the heat that is reflected from the downcomer wall is absorbed by the sides and back of the risers. This is important to distribute the heat around the riser wall.

4.2 RCCS unit cell

To simplify the study, a two-dimensional axially symmetric cell was developed and is shown in Figure 4-3. The unit cell consists of the vessel wall, cavity wall, and a riser tube. The assumption here is that the risers surround the reactor radially and not almost rectangular as shown in Figure 4-2 . The angle (1.64°) was obtained by dividing 360° between the 220 riser tubes. Two imaginary reflective walls are located half distance between the riser and its adjacent neighbour. There is no physical wall at the cell boundaries, but because symmetry is assumed about the cell's centre, the radiation from the adjacent cells makes these boundaries act as if there are walls located there reflecting radiation incident upon them. The radial dimensions are obtained from Figure 4-2.

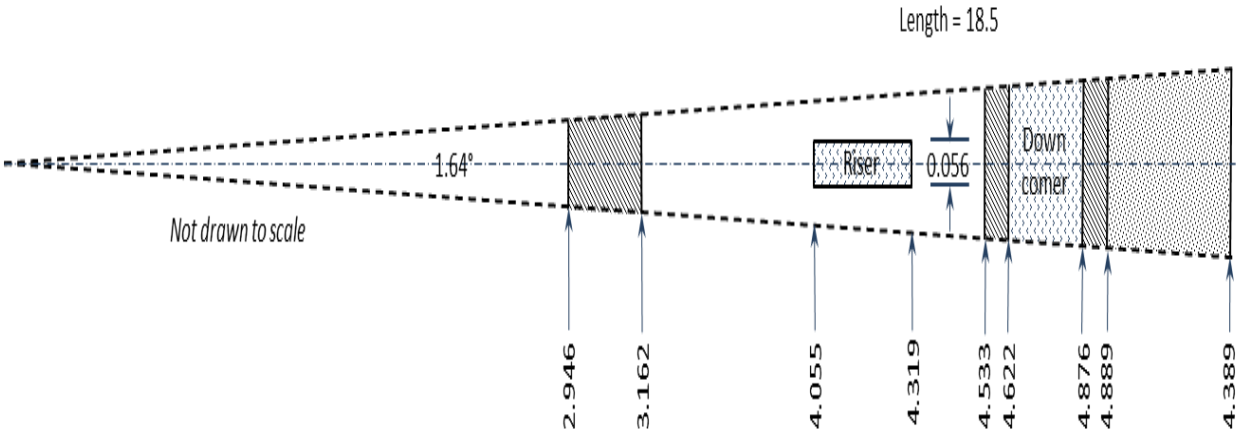

Figure 4-3: Two-dimensional axially symmetric reference frame.

The dimensions of the components in the Figure 4-3 are described in the next sections. The areas associated with the solid parts and the flow area of the fluid are required inputs into the Flownex® elements.

4.2.1 Riser description

The risers are rectangular ducts (2" x 10") inner dimensions with a thickness of 0.1875" (0.0047625 m) as shown in Figure 4-4. One riser height is approximately 18.5 m. The shortened side (2") faces the RPV wall and the risers are vertically supported by the bottom cold plenum and laterally supported by the downcomer through the lateral support plates. Table 4-1 gives the geometric details of the riser as provided by the KAERI. The hydraulic diameter is based on inner dimensions of the riser.

Table 4-1: Riser geometric details (provided by the KAERI).

Flow area	(220 × 2" ×10" ×0.0254^2) =2.838	m^2
Length	18.5	m
D_H	0.0846	m
Shape	Rectangular	

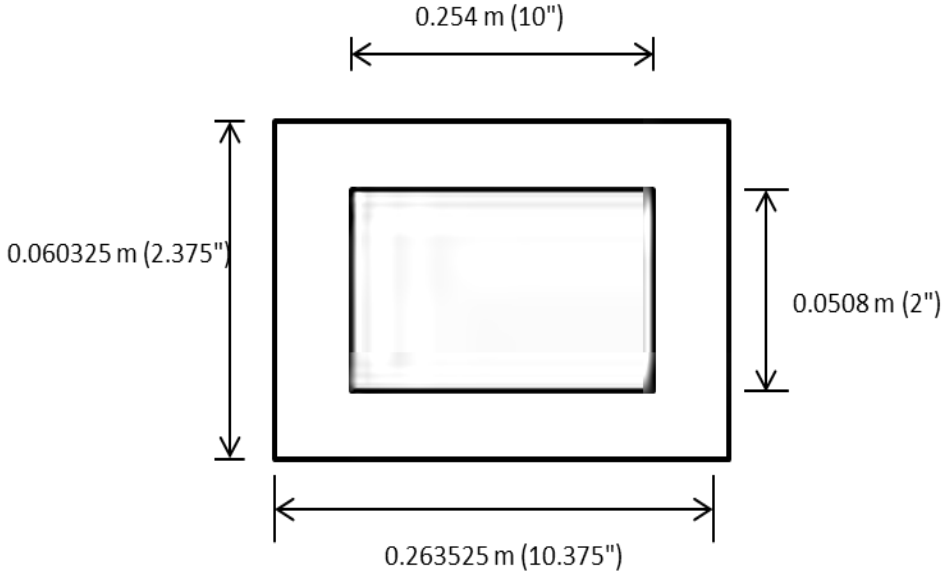

Figure 4-4: Geometric cross section of the riser.

The inside surface areas for a 1.85 m increment can be calculated as follows;

$$A_{front} = A_{back} = 0.0508 \times 1.85 \times 220 = 20.6756\,\mathrm{m}^2 \qquad \text{Equation 4-1}$$

$$A_{side} = 2 \times 0.254 \times 1.85 \times 220 = 206.756\,\mathrm{m}^2 \qquad \text{Equation 4-2}$$

The corresponding outer surface areas are;

$$A_{front\_out} = A_{back\_out} = 0.060325 \times 1.85 \times 220 = 24.55228\,\mathrm{m}^2 \qquad \text{Equation 4-3}$$

$$A_{side\_out} = 2 \times 0.263525 \times 1.85 \times 220 = 214.5094\,\mathrm{m}^2 \qquad \text{Equation 4-4}$$

The circumference/perimeter of the pipe element is also required as an input to the Flownex® model. This is based on the inner dimensions of the risers.

$$P_w = 2 \times \left(0.254 + 0.0508\right) \times 220 = 134.112\,\mathrm{m} \qquad \text{Equation 4-5}$$

The wetted perimeter (P_w) in Equation 4-5 is calculated above is for all 220 risers. Table 4-2 presents the calculated areas that will be used in this study for the different riser configurations. In this project, three models of the RCCS will be built in Flownex®; the single, double and quad loop. This will be explained in detail in **Chapter 6**.

Table 4-2: Flownex inputs for the riser pipe element.

	Units	Single Loop	Double loop	Quad loop
Flow area	m^2	2.839	1.419	0.710
Perimeter	M	134.112	67.056	33.528
Riser front area (outer)	m^2	24.553	12.276	6.138
Riser side area (outer)	m^2	214.509	107.255	53.627
Riser back area (outer)	m^2	24.553	12.276	6.138
Riser front area (inner)	m^2	20.6756	10.338	5.1689
Riser side area (inner)	m^2	206.756	103.378	51.689
Riser back area (inner)	m^2	20.6756	10.3378	5.1689

4.2.2 Downcomer description

Table 4-3 gives the geometric details of the downcomer as provided by the KAERI. In reality, the downcomer is an annulus through which the cold fluid flows. The walls of the downcomer consist of an inner and outer reflective surface. The inner surface (inside surface of the reactor cavity) is lined with an insulating layer while the outermost surface (outside surface of the reactor cavity) is connected to the concrete wall. The distance of the inner and outer wall from the RPV centre is approximately 4.622 m and 4.876 m respectively as in Figure 4-3.

Table 4-3: Downcomer geometrical details (provided by the KAERI).

Flow area	$\pi \times(4.875^2 - 4.622^2) = 7.57907$	m^2
Length	18.5	m
D_H	0.5080	m
Shape	Co-centric (annulus)	

The wetted perimeter can be calculated from the following expression;

$$P_w = \frac{4 \times A_{ff}}{D_H} \qquad \text{Equation 4-6}$$

where

A_{ff} - Flow area (m^2)

P_w - Wetted perimeter (m)

From Equation 4-6, the wetted perimeter is calculated to be 59.678 m which was used as an input to the pipe element representing the cold air in the downcomer increments. With reference to Figure 4-2, the areas of the walls lining the downcomer can be calculated. For the insulating surface, the following equation is used as an illustration;

$$A_{insulation} = \pi \times D_{insulation} \times H_{inc} = 52.6911 \mathrm{m}^2 \qquad \text{Equation 4-7}$$

where

$D_{insulation}$ - 4.533 m (Distance from RPV centre to the insulation wall)

H_{inc} - 1.85 m (Height of increment)

The areas of the walls lining the downcomer are given in Table 4-4 including the materials selected from the Flownex® library.

Table 4-4: Areas of downcomer walls.

	Material	Area	Units
Insulation	Micro-therm insulation	52.6911	m^2
Inner RS_{inner}	SS304	53.7259	m^2
Inner RS_{outer}	SS304	53.7259	m^2
Outer RS_{inner}	SS304	56.6781	m^2
Outer RS_{outer}	SS304	56.825	m^2
$Concrete_{Inner}$	Concrete/Stone	56.825	m^2
$Concrete_{outer}$	Concrete/Stone	74.2604	m^2

4.2.3 RPV description

The RPV is modelled as two nodes connected by a conduction element to represent the RPV wall. The dimensions (inside and outside radius) of the RPV wall are obtained from Figure 4-2 as 2.946 m and 3.162 m respectively. The circumference ($Circ_{in}$) can easily be calculated;

$$Circ_{in} = \pi D = \pi \times 2 \times 2.946 = 18.51\,\mathrm{m} \qquad \text{Equation 4-8}$$

$$A_{inner} = Circ_{in} \times H_{inc} = 18.51 \times 1.85 = 34.24\,\mathrm{m}^2 \qquad \text{Equation 4-9}$$

In Equation 4-8, A_{inner} is the area of the inside RPV wall. Similarly, the outer area was calculated to be 36.75 m^2. The RPV wall is 0.215 m thick as shown in Figure 4-2 and Figure 4-3.

4.2.4 Chimney descriptions

Although not shown in Figure 4-3, the chimney is a very important component that provides the driving force for natural circulation. In section 6.2 a simplified schematic of the chimney is given detailing the most important components. The information regarding the dimensions of the chimney ducts can be found in **Appendix F**.

4.3 Summary of the chapter

The purpose of this chapter was to breakdown the RCCS into its various components for modelling purposes. Further, to calculate, from these components, the input parameters as required by Flownex®. To this end, the basic information regarding the RCCS geometry was given. This included a description of the air flow and heat transfer in the RCCS. Thereafter, the simplified unit cell of the RCCS was developed and presented in section 4.2. Finally, from this unit cell and information provided by the KAERI, the areas and perimeters of the different surfaces were calculated.

Chapter 5

5 Separate effects modeling and verification

5.1 Introduction

Prior to attempting to simulate the RCCS on a larger scale, a series of tests were conducted, with the primary objective to develop a physical sense of the anticipated natural convection flow, with conduction and radiation heat transfer taking part. A Further objective was to verify that the Flownex® software has been set up correctly to model natural circulation systems such as the RCCS. To this end, Flownex® was tested against a numerical model developed by the candidate using EES on particular case studies relevant to the RCCS.

The same geometry was used for these benchmark tests in order to create a consistent basis for comparisons. The case studies are simulated in Flownex® and EES and the results are compared. This makes it easier to identify faults and inconsistencies between Flownex® and a more accessible and transparent mathematical model (EES). Furthermore, this exercise will create confidence in the results that will be obtained from the Flownex® regarding the RCCS.

As a first step, a steady state natural convection simulation was conducted in a simple U-tube with one of the walls heated (Constant heat flux boundary condition) but without any of the complex heat transfer network elements. Both ends of the U-tube are open to the atmosphere. This closely resembles the downcomer and riser configuration and the purpose is to isolate the flow rate calculation. Secondly, the same model was tested for different discretization's to evaluate how the results are affected by different numbers of pipe increments. Thirdly, a transient case was modelled where the heat input changes with time. This was done to test Flownex® software capability to model transient systems. The methodology that Flownex® uses is that which is described in section 3.6. These particular tests were conducted to verify the natural convection mass flow rate calculation in Flownex®.

Finally, a simple test was conducted both in EES and Flownex® where the heat transfer networks were included. The main aim was to verify that Flownex® was setup correctly to

perform calculations of heat transfer rates and surface temperatures with conduction, convection and radiation taking part. In this exercise, the mass flow rate was simply specified.

5.2 Natural circulation case studies

5.2.1 Case study 1A - Natural circulation in a simple U-tube (constant heat flux)

A simple U-tube node and element network was setup in Flownex® and is shown in Figure 5-1. A constant heat flux boundary condition of 0.05 kW was specified to each of the elements (pipe increments) on one side of the U-Tube. At each node an elevation was specified (i.e. the top most node is 6 m while the bottom node is 0 m to represent the ground level of the U-tube). The remainder of the nodes was given elevations corresponding to the height.

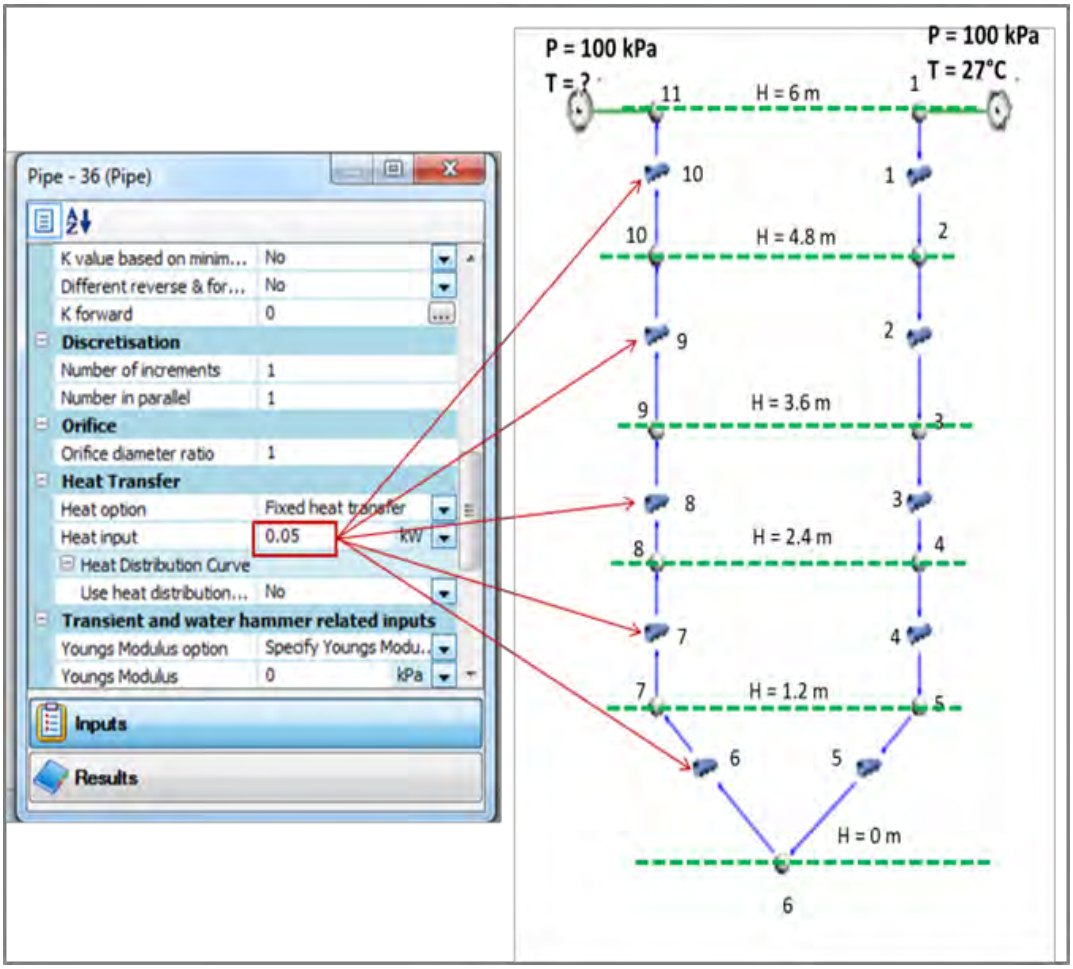

Figure 5-1: Single U-Tube Flownex® Canvas.

At node 1, the temperature and pressure were specified in the boundary condition element. At node 11 the outlet pressure was also specified as the atmospheric pressure. The temperature at this node was not specified and had to be calculated. The simple U-tube was discretized into 10 elements and 11 nodes connecting the elements. The use of increments is particularly important to properly track the change in temperature and the associated fluid properties, such as the density. Some factors required during the simulations may be non-linear; however by dividing the pipe into small increments allows the non-linear factors to be approximated by linear property increments. The result of each increment is consolidated into a final result for the total length of the pipe. More accurate results can be obtained with a larger number of increments but this increases the time to complete the simulation. A compromise had to be reached between accuracy and simulation completion time.

For this case study only a steady state simulation was done in both Flownex® and EES. Firstly, when a heat input of zero was added to the elements a mass flow rate of 2.31E-10 kg/s and 3.43E-10 kg/s were calculated in Flownex® and EES respectively. This is encouraging since it means that no mass flow will be experienced if no heat is added to the U-Tube and appropriately predicted by the software.

The results for when heat was added are shown in Table 5-1. It can be seen that there is very good comparison between the EES and Flownex® models. The EES model calculations are given in **Appendix B.** The main reason for the small differences between the Flownex® and EES results is that Flownex® and EES use slightly different fluid properties. These properties include density and viscosity. The fluid properties are given in Table 5-2 and have an obvious effect on mass flow rate, the heat transferred to the fluid and inter alia the temperature distribution at the different increments.

Table 5-1: Simple U-Tube model results (constant heat flux boundary condition).

Increment	Heat Input	Temperature		Pressure		Mass Flow	
	Kw	°C		kPa		kg/s	
		Flownex	EES	Flownex	EES	Flownex	EES
1	0.00	27.00	27.00	100.00	100.00	0.0079	0.0079
2	0.00	27.01	27.01	100.01	100.01	0.0079	0.0079
3	0.00	27.02	27.02	100.03	100.03	0.0079	0.0079
4	0.00	27.03	27.04	100.04	100.04	0.0079	0.0079
5	0.00	27.05	27.05	100.05	100.05	0.0079	0.0079
6	0.05	27.06	27.06	100.07	100.07	0.0079	0.0079
7	0.05	33.29	33.32	100.05	100.05	0.0079	0.0079
8	0.05	39.52	39.58	100.04	100.04	0.0079	0.0079
9	0.05	45.75	45.84	100.03	100.03	0.0079	0.0079
10	0.05	51.98	52.10	100.01	100.01	0.0079	0.0079
11		58.21	58.35	100.00	100.00		

Table 5-2: Calculated fluid properties in the U-tube (constant heat flux boundary condition).

Increment	density		viscosity		friction factor		Reynolds no	
	kg/m3		kg/m.s					
	Flownex	EES	Flownex	EES	Flownex	EES	Flownex	EES
1	1.1610	1.1610	1.85E-05	1.85E-05	0.03730	0.03734	5435.08	5435.03
2	1.1612	1.1612	1.85E-05	1.86E-05	0.03780	0.03734	5434.92	5434.86
3	1.1613	1.1613	1.85E-05	1.86E-05	0.03730	0.03734	5434.75	5434.70
4	1.1614	1.1614	1.85E-05	1.86E-05	0.03730	0.03734	5434.59	5434.53
5	1.1615	1.1615	1.85E-05	1.86E-05	0.03730	0.03734	5434.42	5434.37
6	1.1492	1.1495	1.87E-05	1.87E-05	0.03739	0.03743	5390.55	5390.54
7	1.1262	1.1261	1.90E-05	1.90E-05	0.03756	0.03760	5306.36	5305.70
8	1.1037	1.1036	1.93E-05	1.93E-05	0.03773	0.03778	5225.20	5224.20
9	1.0820	1.0820	1.96E-05	1.96E-05	0.03790	0.03794	5147.04	5145.84
10	1.0615	1.0613	1.99E-05	1.99E-05	0.03807	0.03811	5071.97	5070.45

5.2.2 Case study 1B - Different discretization calculations

In order to determine whether the 10 increments in the axial direction are sufficient, the U-tube was discretized into 20 increments instead of 10 in Flownex®. A heat input boundary condition of 0.025 kW was specified on each increment of the U-tube to maintain the overall heat flux. In Figure 5-2 and Figure 5-3, the total temperature and total pressure simulation results for the different increments are presented. It can be seen that there is good comparison between the 10 and 20 increments. The RCCS standpipes and downcomer have therefore been discretized into 10 increments which were deemed sufficient for the simulations.

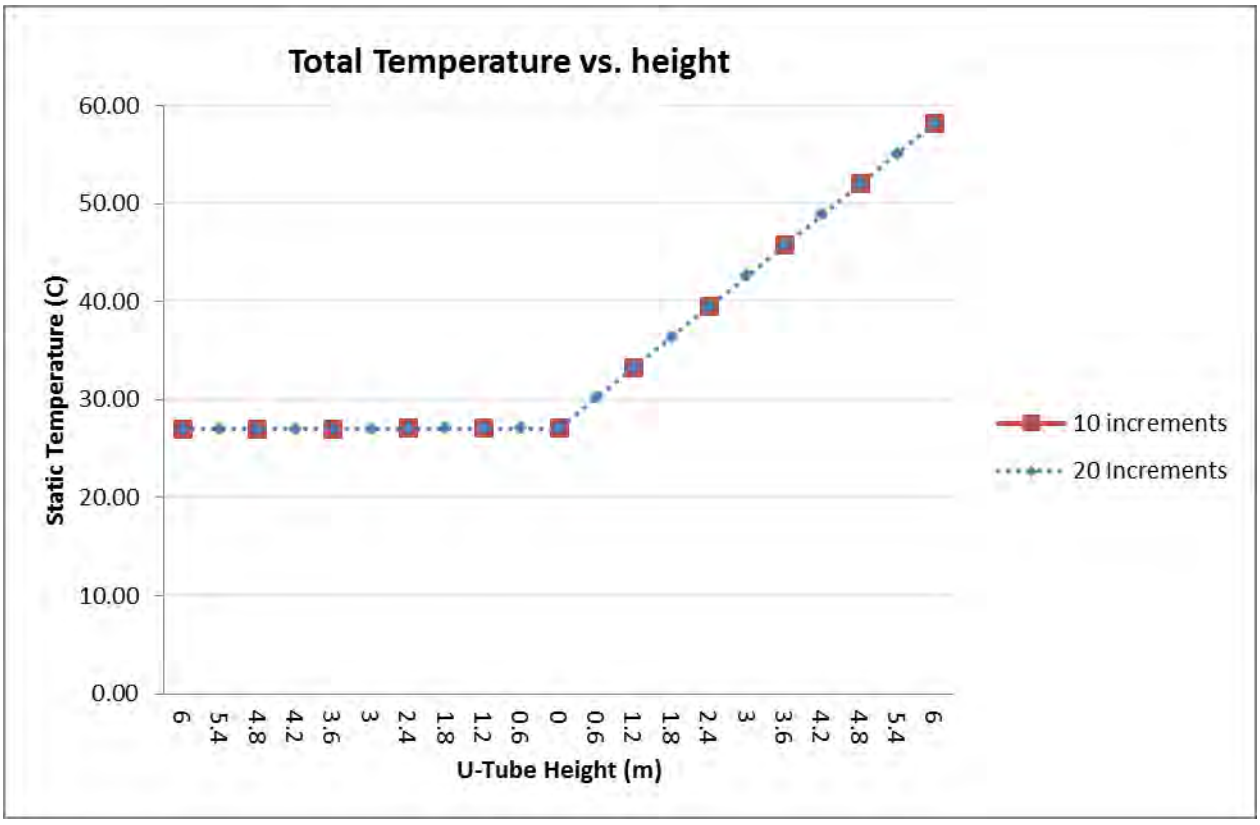

Figure 5-2: Total temperature (°C) for 10 vs. 20 increments.

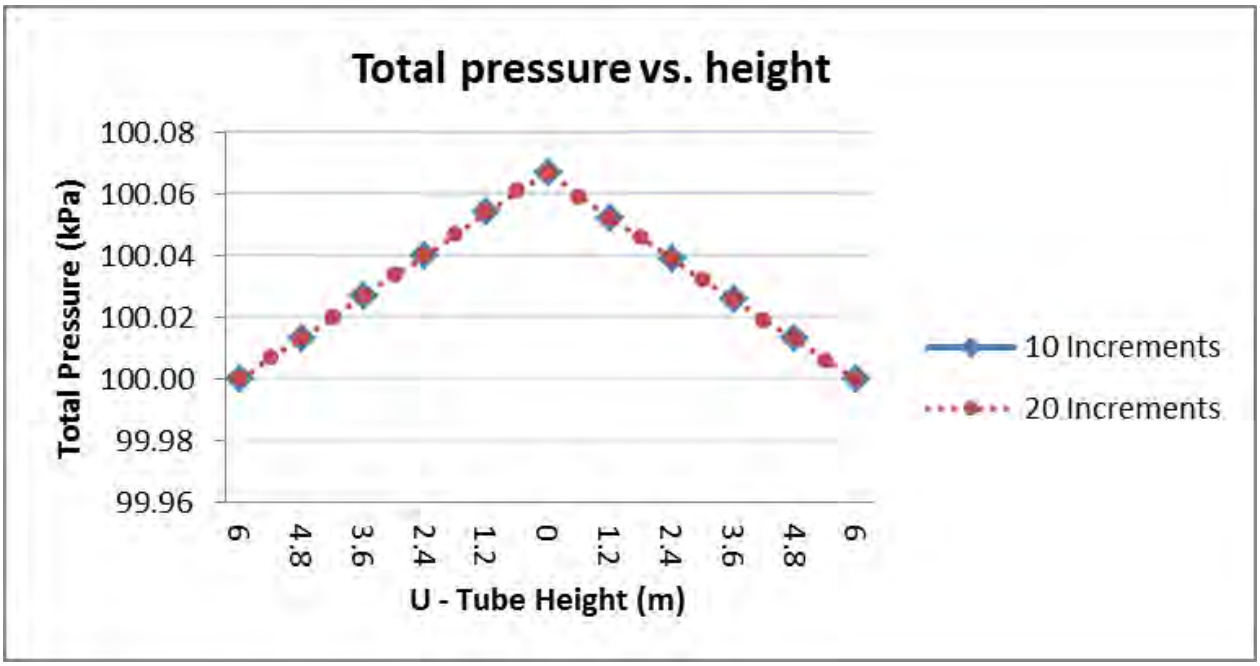

Figure 5-3: Total pressure (kPa) for 10 vs. 20 increments.

5.2.3 Case study 2 - Transient simulation of natural circulation in a simple U-Tube

The first case study was conducted for steady state conditions (i.e. no change in boundary values). However, part of this project is to demonstrate that the model of the RCCS can also be used to study various transient operational phenomena. It therefore becomes important to understand how representative the software is setup to model transient behaviours. The same U-Tube that was setup for case 1 was used except in this case the heat flux was varied over time. Both EES and Flownex® were used to solve Equation 3-29 through Equation 3-39.

In Flownex® the user can set up a transient scenario as described in **Appendix A**. The simulation started with a steady state heat flux of 0.05 kW at each of the five elements on the one side of the U-Tube. The heat flux was instantaneously increased to 0.5 kW for the remainder of the simulation.

The methodology to simulate transient scenarios was introduced in section 3.6. To simulate a transient scenario for the simple U-tube in EES, the following methodology was used and is summarized. The full methodology can be found in Rousseau and Van Eldik (2013:159-169):

In EES a parametric table is created which lists the known values of ρ^0, T^0, p^0, $h_0{}^0$, $p_0{}^0$, $S_c{}^0$, $S_e{}^0$, $\dot{m}^0$, $\bar{\rho}^0$ and $S_m{}^0$. The start time was set at zero. The row number was initialized to 1 (Row 1) by using the following expression;

$$Row = \frac{time}{\Delta t} + 1 \qquad \text{Equation 5-1}$$

In Equation 5-1, Row is the row number in the parametric table.

For each element the following were calculated:

$$\frac{\partial \bar{\rho}}{\partial t} = \frac{\bar{\rho} - \bar{\rho}^0}{\Delta t} \qquad \text{Equation 5-2}$$

$$\bar{\rho} = f(p, h) \qquad \text{Equation 5-3}$$

In Equation 5-3, h is the static enthalpy of the fluid. Equation 5-3 is evaluated using the built-in EES fluid property functions. The momentum source term S_m is equal to the RHS of Equation 3-32. The mass flow rate at the current time can be calculated by

$$\dot{m} = \dot{m}^0 + \frac{\partial \dot{m}}{\partial t}\Delta t \qquad \text{Equation 5-4}$$

The derivative in Equation 5-4 is calculated using Equation 3-38.

At each node the following were calculated:

$$\rho = \rho^0 + \frac{\partial \rho}{\partial t}\Delta t \qquad \text{Equation 5-5}$$

$$p = f(\rho, h) \qquad \text{Equation 5-6}$$

$$\frac{\partial p}{\partial t} = \frac{p - p^0}{\Delta t} \qquad \text{Equation 5-7}$$

$$h_0 = h_0^{\,0} + \frac{\partial h_0}{\partial t}\Delta t \qquad \text{Equation 5-8}$$

In Equation 5-8, h_0 is the total enthalpy in the node. The static enthalpy can be calculated from the definition of total enthalpy (Rousseau & Van Eldik, 2013):

$$h_0 = h + \frac{1}{2}V^2 \qquad \text{Equation 5-9}$$

V , is the fluid velocity in the node taken as the average velocity between the element before and after the node. Further, in the node the mass and energy flows entering the node equal the mass and energy flows within the element before the node. The mass and energy flows exiting the node are equal to the mass and energy flows within the elements connected to the outlet of the node.

The mass (S_c) and energy (S_e) source terms are calculated from Equation 3-29 and Equation 3-33.

To model a transient scenario, the heat input into the individual elements is increased. The time is increased with one time-step to run the simulation. The values calculated at this point become the previous values in the next time step. This is an iterative procedure which repeats until sufficient convergence is obtained for ρ , h_0 and pressure at each node and $\dot{m}$ at each element.

5.2.3.1 Timestep independence study

In order to determine the appropriate timestep to use in the transient analysis, a timestep independence study was conducted. For this study, the EES simulation was ran for different timesteps as shown in Figure 5-4. The lowest timestep that could be successfully implemented in EES was 0.045s, and further attempts to implement a lower timestep yielded error messages. It can be seen however, that the results remain fairly identical between timesteps 0.045s to 0.06s. For this reason therefore, a timestep of 0.05s was selected and used for this study.

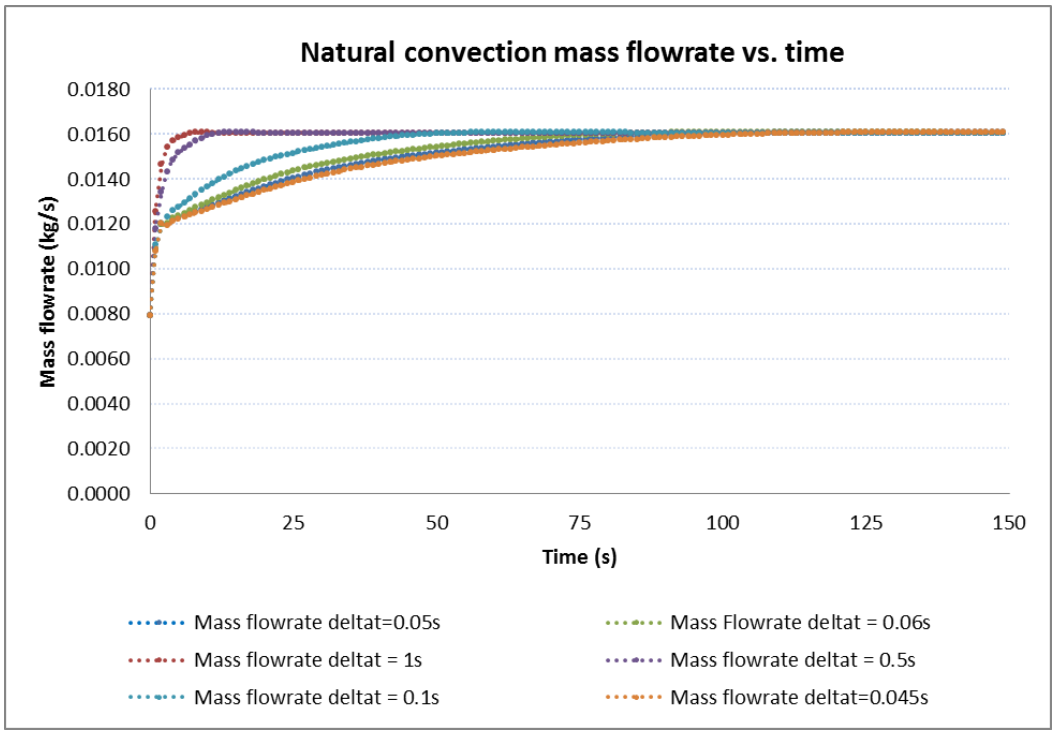

Figure 5-4: Timestep independence test.

To create a consistent basis of comparison between EES and Flownex®, a timestep of 0.05s was also used in the Flownex® model. The results are given in Figure 5-5. It can be seen that the mass flow rate increases steadily from 0.007913 kg/s at steady state to the new steady state value of 0.01606 kg/s when heat is added to the fluid, for both Flownex® and EES. The comparison of the results obtained from the two software packages is acceptable for the purposes of this study in which the focus is on the overall operational characteristics of the system, rather than on the detailed transient response for control purposes. The EES simulation is given in **Appendix C**.

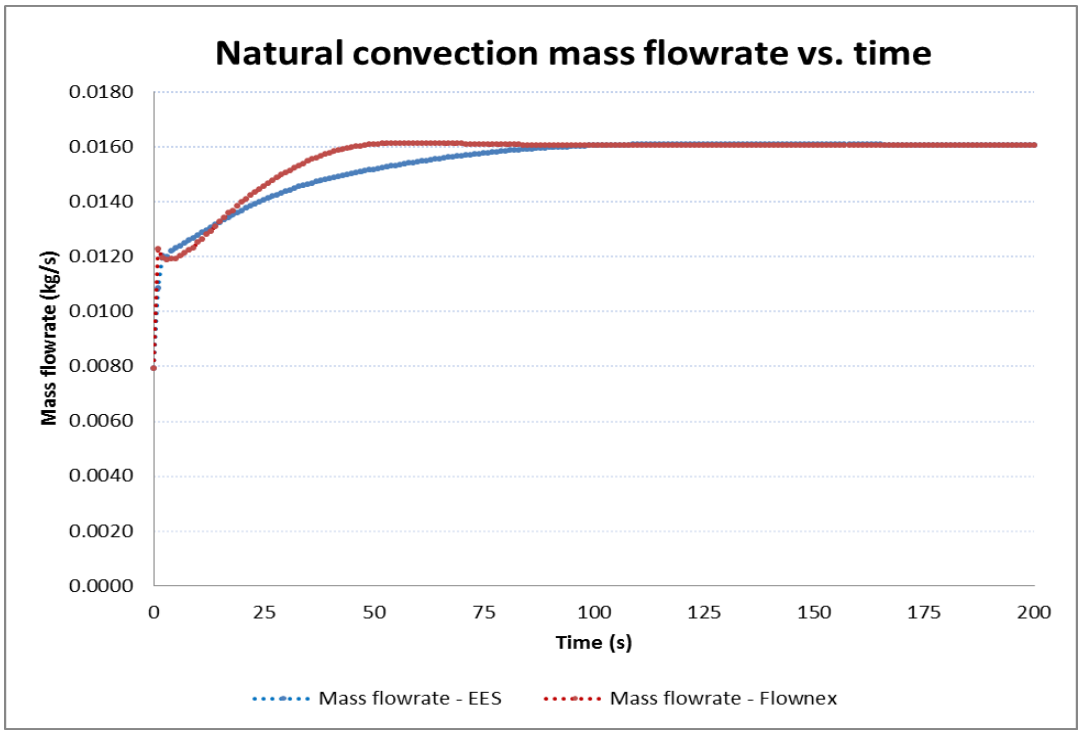

Figure 5-5: Transient simulation of the simple U-tube - Mass flow rate vs. time.

5.3 Heat transfer case studies

In the previous case studies, a constant heat flux was set as a boundary condition directly on the pipe element. It was shown that the mass flow rates predicted by the Flownex® model are in good agreement with a custom developed numerical model (EES). In the real RCCS model, a constant temperature boundary condition is set on the RPV inner wall. Further in the RCCS, there are different modes of heat transfer that work concurrently to effect the heat removal. To this end, a case study will be conducted to verify that Flownex® is also setup correctly to model

the heat transfer phenomena in such a system. This will be done once again by comparing a Flownex® model to a custom developed EES simulation of the same geometries.

In fact reverting back to Figure 4-3, the unit cell of the RCCS that will be used as a reference frame was presented. It is clear the following areas need to be considered:

- Radiation heat transfer from the RPV to the standpipe and cavity walls, and subsequent re-radiation. Convection in the cavity will also be considered.

- Conduction through the solid parts (i.e. RPV wall, riser tube walls, downcomer walls and ultimately the concrete wall)

- Removal of heat by the flowing air (downcomer and riser by natural convection and inside radiation.

Figure 5-7 presents a schematic illustration of the above mentioned heat transfer phenomena and interactions at the different surfaces. Two case studies will be considered; a so called single loop (Figure 5-7) and a double loop (Figure 5-8). Figure 5-6 provides a schematic illustration to highlight the differences between the single loop and the double loop configurations. It can be seen that for the single loop all 220 risers have been lumped into a single group while the double loop consist of two groups with 110 risers in each group. The double loop consists of two riser loops which are mirror symmetric images of the single riser loop. An explanation of how the single and double loops were constructed will be given in section 6.5 and 6.6. The only major difference between the models is the way in which the view factors are calculated for the different surfaces. The results for both analyses are presented at the end of this section.

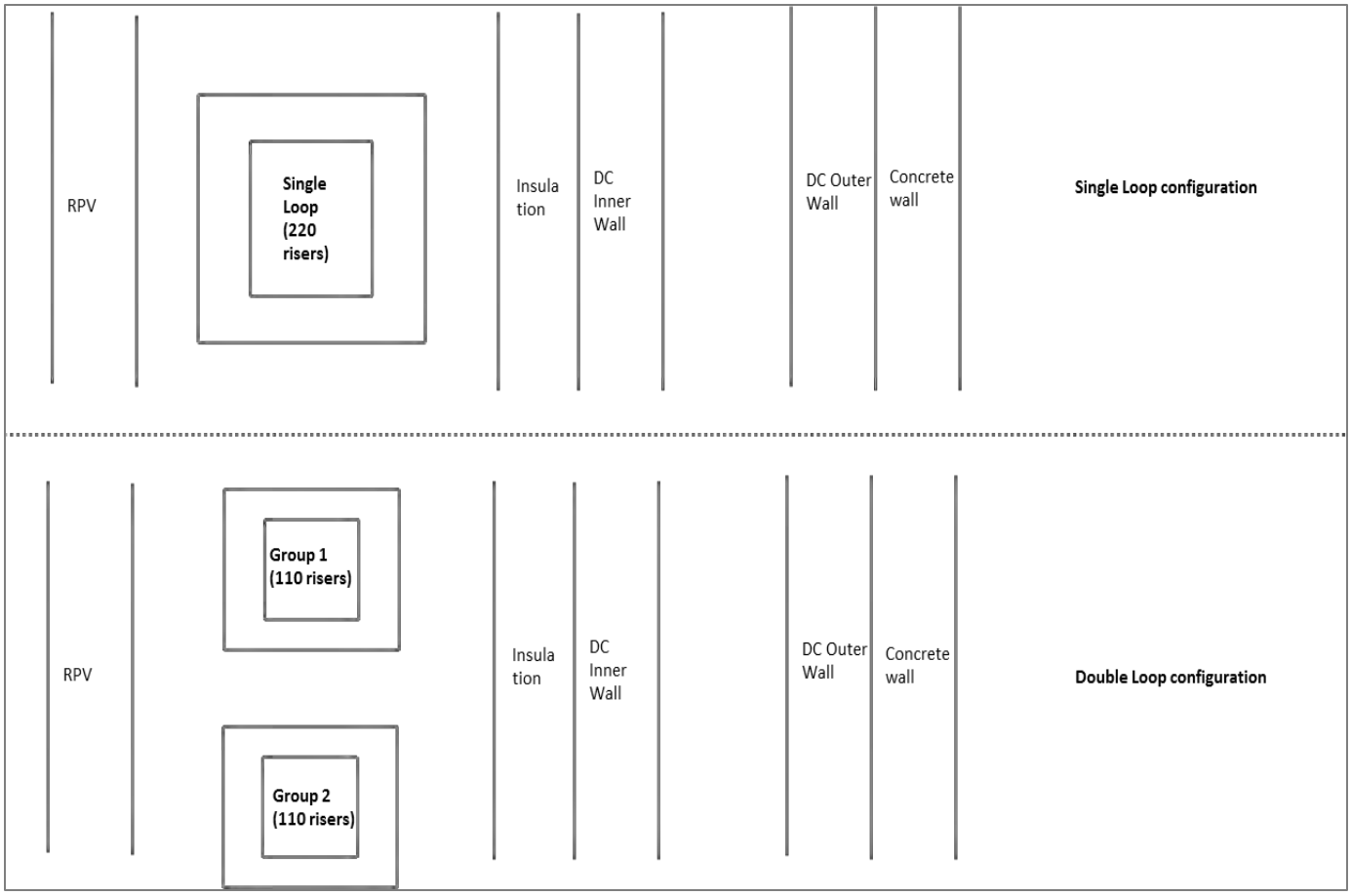

Figure 5-6: Differences between the single loop and the double loop RCCS systems.

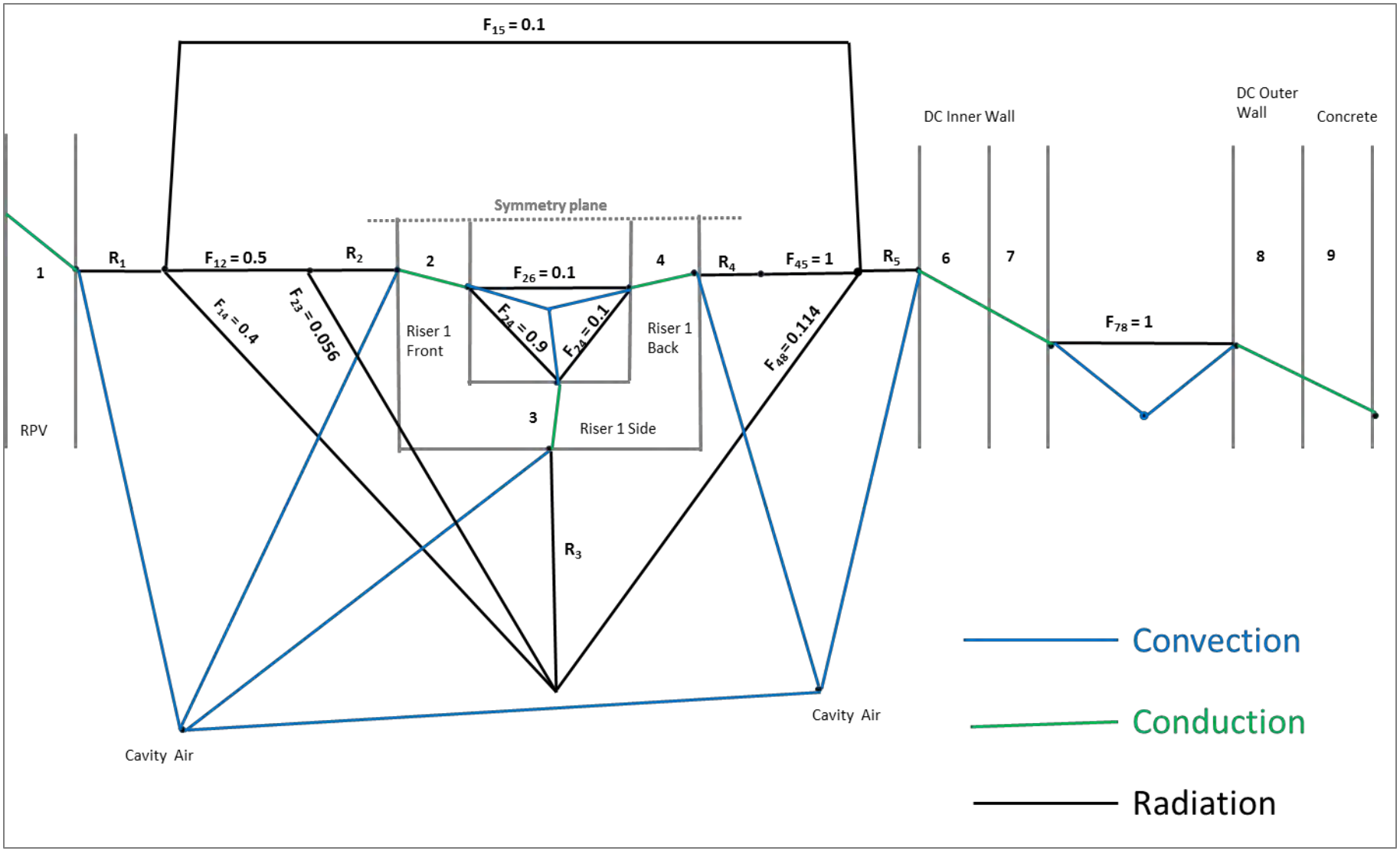

Figure 5-7: Simple heat transfer phenomena in the single loop RCCS.

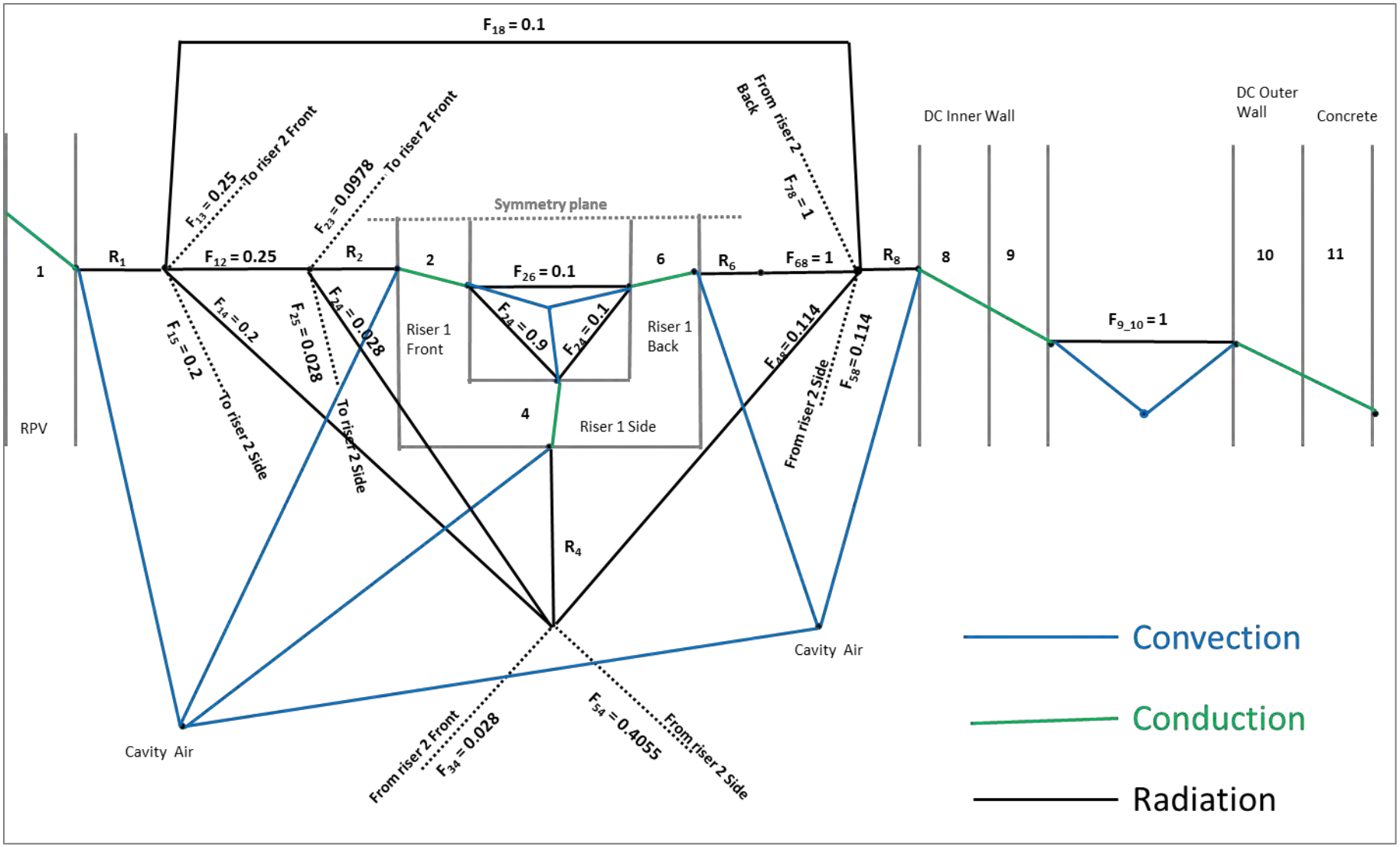

Figure 5-8: Simple heat transfer phenomena in the double loop RCCS.

Firstly, in Figure 5-8, the dashed lines indicate interactions with the second group of risers (***not shown in figure***). The solid black lines represent the radiation heat transfer interactions between the different surfaces. For instance in Figure 5-7, it can be seen that surface 1 (RPV) only interacts with one group of risers and the downcomer. In Figure 5-8, surface 1 interacts with both groups of risers and the downcomer. Also shown in Figure 5-8 are interactions between the second groups of risers with the first group, the RPV and the downcomer. The symbols F_{ij} represent the view factors between the difference surfaces. The manner in which the view factors have been obtained is explained in section 6.5 and 6.6. In both Figure 5-7 and Figure 5-8, the symbols R_1 through R_8 represent the surface resistances at the different walls. Further, riser 1 and riser 2 represent one loop and double loop riser groups respectively.

A table describing the different surfaces as numbered in Figure 5-7 and Figure 5-8 is presented in Table 5-3.

Table 5-3: Description of the surface numbers.

Surface number	Single loop	Double loop
	Name	Name
1	Reactor Pressure Vessel	Reactor Pressure Vessel
2	Riser 1 front	Riser 1 front
3	Riser 1 side	
4	Riser 1 back	Riser 1 side
5		
6	Insulation	Riser 1 back
7	Downcomer inner wall	Riser 2 back
8	Downcomer outer wall	Insulation
9	Concrete wall	Downcomer inner wall
10		Downcomer outer wall
11		Concrete wall

Figure 5-9 presents an idea of the simple Flownex® model that was used in this case study. This was constructed directly from the simple network shown in Figure 5-7. In fact, Figure 5-9 is the bottom-most increment on the RCCS. The walls of the riser tube and the downcomer are represented as nodes connected by conduction elements. These were constructed with particular reference to Figure 4-2 and Figure 4-3. The width of each wall was specified in the conduction elements. A temperature boundary condition was specified for the RPV inside wall using the boundary condition element. Convection elements were selected from the Flownex® library to represent heat transfer between all solid and fluid parts (i.e. in the cavity and in the RCCS). The air in the cavity was represented through a pipe element at atmospheric pressure. The reason for this is that Flownex® does not model a fluid as a node. The boundary conditions for the fluid elements are the same as those employed in section 5.2.1.

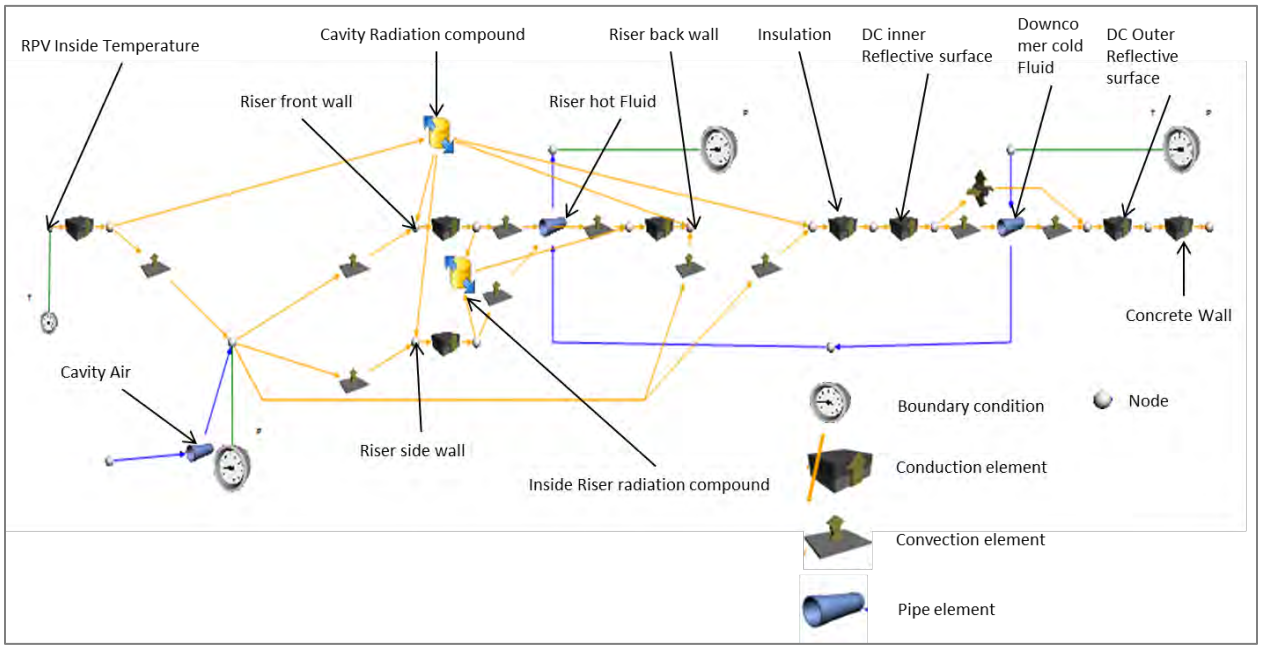

Figure 5-9: One increment of the single loop Flownex® RCCS model.

The cavity and inside riser radiation are represented as so called “compounds” which will be discussed in section 6.5. In this particular case study, the view factors given in Table 6-2 and Figure 6-9 were used for the cavity and inside riser radiation.

Before the results of this case study are presented, consider the following case study with two standpipe loops (riser hot fluid in Figure 5-9) modelled instead of one loop.

5.3.1 Case Study 3B – double loop analysis

In Case Study 3A, a single pipe element was used to represent the fluid element. In the RCCS, this is analogous to grouping all 220 risers into a single or one riser loop, much like the work done by Lomperski et al. (2011). However, it is also the objective of this study to show that the model of the RCCS developed can be used to also model certain transient operational phenomena in the RCCS such as blockages or pipe breaks. To group the risers into one loop would mean the user is restricted to modelling for example a blockage in all the pipes at once. The likely scenario in the RCCS is that one or two of the 220 pipes could be blocked and not necessarily all of them. In this study, three RCCS models were developed, a so called single, double and quad loop model. The double loop RCCS consists of two groups of risers and the volume of both the groups is equal to the volume of the single riser loop. Similarly, the quad loop has four riser groups with a volume equal to the single loop. A single downcomer is modelled for all cases. The fluid is distributed from the single downcomer to the group of risers in the double and quad loop RCCS.

The aim of this case study was to investigate how the results compare when two pipe elements are used instead of one. The expectation is that the heat transferred to both loops should be equal and the total equalling the single loop heat transfer. The reason for this was given in section 2.7.2 that the heat load on the two or quad loops is mirror symmetric to the single loop.

A simple Flownex® model of the double loop configuration was constructed and is shown in Figure 5-10. The Flownex® model presented in Figure 5-10 was constructed directly from the simple network given in Figure 5-8. Both riser groups are indicated. The interactions between the risers in the different loops have also been shown through the compound element. The red, green and blue dashed lines indicate that the compound element has been extended to include interactions with the second riser group. The point **A** indicates the common cold plenum that branches into the respective riser loops. **B** is the air cavity indicating that both riser groups are located within the same reactor cavity. In Flownex®, a node can be copied and replicated to another location using the “paste view” capability of the software. This eliminates the need to repeat the process particularly where a lot of increments are considered. The boundary values are the same as in the single loop increment except that the compound was set up differently. An explanation of the compound element is given in section 6.6. The view factors given in Figure 6-5 have been used for this illustration.

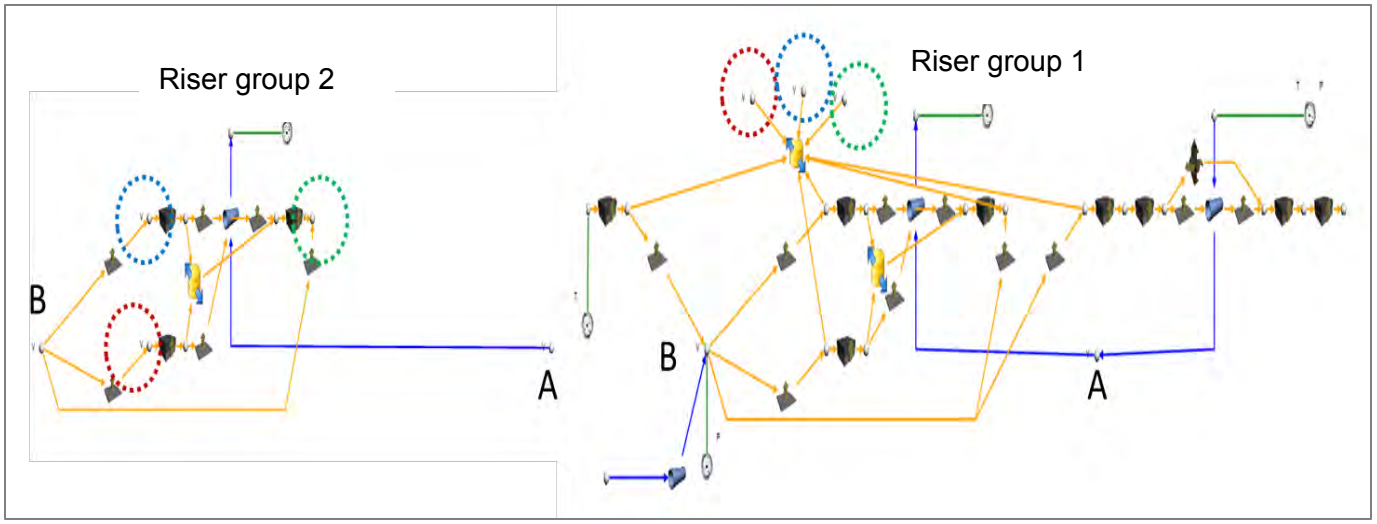

Figure 5-10: One increment of the double loop Flownex® RCCS model.

5.3.2 Case Study 3A & B – results and discussion

The EES and Flownex® results for case study 3A and 3B are presented below in Table 5-4. Firstly, the models presented in Figure 5-9 and Figure 5-10 was implemented in Flownex®. Secondly, since the particular interest of this exercise is the radiation network and heat transfer, the momentum equation was not solved in the EES model and the mass flow rate and the pressures obtained from the Flownex® simulations were used as inputs to the EES model. The mass flow rate calculations were dealt with in section 5.2. The EES model was simulated to the same specifications and geometry as the Flownex® models in Figure 5-9 and Figure 5-10. The EES simulation is given in **Appendix D** (single loop) and **Appendix E** (double loop)**.**

The other boundary conditions that were used in the EES models as obtained from the Flownex® simulations are:

Concrete wall temperature: - 49.7 °C

Cavity temperature : - 189.7 °C

Inlet and outlet Pressure : - 100 kPa

Inlet temperature : - 40 °C

Mass flow rate : - 2.95 kg/s

The concrete wall and cavity temperatures are specified as boundary conditions in the EES simulations. These values were obtained from the Flownex® simulations. The particular interest of this exercise was to verify that the radiation network and heat transfer calculations have been set up correctly in Flownex®, by comparing with an EES model of the same geometry. It was not the aim of this exercise at this point to calculate the concrete wall and cavity temperature.

It can be seen from Table 5-4 that the results from the Flownex® models are the same for the single and double loop configuration, even with the interactions between the risers included in the view factor setup. Secondly, it can be seen that there is very good agreement between the EES and Flownex® model of the single increment of the RCCS. The small differences can be attributed to reasons given in section 5.2.

This is encouraging because it means that the results obtained for the full scale RCCS should be reliable and the model using the Flownex® software has been set up correctly to perform heat transfer calculations in the RCCS and not natural circulation calculations since in this exercise, the mass flow rate was held constant

Table 5-4: EES and Flownex® RCCS single increment results.

		Single Loop				Double Loop						
		EES	Flownex			EES			Flownex®			
				% Error		Riser 1	Riser 2	Total	Riser 1	Riser 2	Total	% Error
T_{RPV}	°C	328.29	328.53	-0.07%	T_{RPV}			328.26			328.53	-0.08%
T_{Riser_Front}	°C	225.75	228.24	-1.09%	T_{Riser_Front}	225.55	225.55	225.55	225.75	225.75	228.24	-1.18%
T_{Riser_Side}	°C	162.79	166.43	-2.19%	T_{Riser_Side}	162.36	162.36	162.36	162.79	162.79	166.43	-2.45%
T_{Riser_Back}	°C	163.43	166.92	-2.09%	T_{Riser_Back}	162.48	162.48	162.48	163.43	163.43	166.92	-2.66%
$T_{Downcomer}$	°C	178.86	180.04	-0.66%	$T_{Downcomer}$			178.87			180.04	-0.65%
$T_{\_exit}$	°C	88.77	87.25	1.74%	$T_{\_exit}$			88.57			87.25	1.51%
$Q_{\_pipe}$	kW	143.67	139.12	3.27%	$Q_{\_pipe}$	71.83	71.83	143.66	69.56	69.56	139.12	3.26%
$Q_{\_downcomer}$	kW	2.11	2.13	-0.94%	$Q_{\_downcomer}$			2.11			2.13	-0.94%
$Qrad_{RPV}$	kW	127.5	125.93	1.25%	$Qrad_{RPV}$			127.5			125.93	1.25%
$Qrad_{Riser\ Front}$	kW	-44.92	-44.18	1.67%	$Qrad_{Riser\ Front}$	-22.46	-22.46	-44.92	-22.09	-22.09	-44.17	1.70%
$Qrad_{Riser\ Side}$	kW	-74.8	-73.91	1.20%	$Qrad_{Riser\ Side}$	-37.4	-37.4	-74.8	-36.95	-36.95	-73.91	1.20%
$Qrad_{Riser\ Back}$	kW	-7.38	-7.25	1.79%	$Qrad_{Riser\ Back}$	-3.69	-3.69	-7.38	-3.62	-3.62	-7.24	1.93%
$Qcond_{insulation}$	kW	2.11	2.13	-0.94%	$Qcond_{insulation}$			2.11			2.13	-0.94%
$Qcond_{RPV}$	kW	142.78	141.24	1.09%	$Qcond_{RPV}$			142.78			141.24	1.09%
$Qrad_{RF\_in}$	kW	23.63	23.66	-0.13%	$Qrad_{RF\_in}$	11.82	11.82	23.63	11.83	11.83	23.66	-0.13%
$Qrad_{RS\_in}$	kW	-21.51	-21.51	0.00%	$Qrad_{RS\_in}$	-10.75	-10.75	-21.51	-10.75	-10.75	-21.49	0.09%
$Qrad_{RB\_in}$	kW	-2.12	-2.17	-2.30%	$Qrad_{RB\_in}$	-1.06	-1.06	-2.12	-1.08	-1.08	-2.17	-2.30%

5.4 Summary of the verification chapter

In this chapter, the main objective was to verify that the Flownex® models have been set up accurately to model natural circulation flows, and further with convection, conduction .and convection taking part. Steady state and transient simulations were conducted on selected case studies using Flownex® and comparing with EES models specifically developed by the candidate for this purpose. The case studies were divided into two parts; constant heat flux for the mass flow rate calculation and constant heat temperature boundary condition, more relevant to the RCCS system that will be studied.

Regarding the mass flow rate calculation, the following were established:

- The EES and Flownex® simulations are in good agreement. The small differences in the results are due to the different methods used by the codes to calculate the fluid properties and resultant friction factors.

- A good agreement was observed between the EES and Flownex® models in the transient modelling of the U-tube. Particularly, the new steady state value of the mass flow rate.

The second part of this chapter was to test and verify Flownex® ability to model flows with radiation, convection and conduction taking part. The following was established:

- The results from Flownex® model of a single and double riser loop are in good agreement. This is a valuable finding, since it infers that the view factors have been accurately extracted from the single to the double loop. Moreover, this finding shows that the double loop is accurately setup as a mirror symmetric image of the single loop. Therefore, to setup a quad loop model will be merely to extend from the double loop.

- There was a good comparison between the EES and Flownex® models of the one increment of the RCCS.

This creates confidence in the software capabilities and the models can be expanded to full RCCS models.

Chapter 6

6 Integrated RCCS model development

6.1 Introduction

Extending from the findings in ***Chapter 5,*** the simulation model for the natural circulation in the RCCS is given with the basic description of the components. This is followed by the method of the simulation model set up in Flownex® and the different assumptions that were made in modelling the different simulation areas. Finally, the integrated model of the RCCS is presented.

6.2 RCCS nodalization

The system modelling for the natural circulation analysis in the air-cooled RCCS is shown in Figure 6-1. The solid parts consist of the RPV, the riser tubes, the downcomer and the concrete wall. The fluid part consists of the reactor cavity (air gap) and a single flow path of the RCCS which comes through the RCCS inlet pipes from the atmosphere, inlet manifold, inlet header, inlet lower duct, inlet connector to downcomer, downcomer annulus, lower plenum, riser tube, outlet connector to hot plenum, outlet lower duct, outlet header, outlet manifold and finally through the RCCS outlet pipes to the atmosphere (***indicated in grey***). The dimensions and specifications of all the chimney components are given in **Appendix F*.*** The basic geometries of the relevant sections were also described in section 4.2

In the realistic design, the air-cooled RCCS shall have multiple air inlets and outlets in order to ensure cooling even if the flow path is partially blocked. A single flow path has been assumed for this benchmark calculation. In Figure 6-1, the symbols RS refers to the reflective surface that forms the downcomer inner and outer walls through which the cold air flows. The model of the RCCS developed in Flownex® closely resembles Figure 6-1.

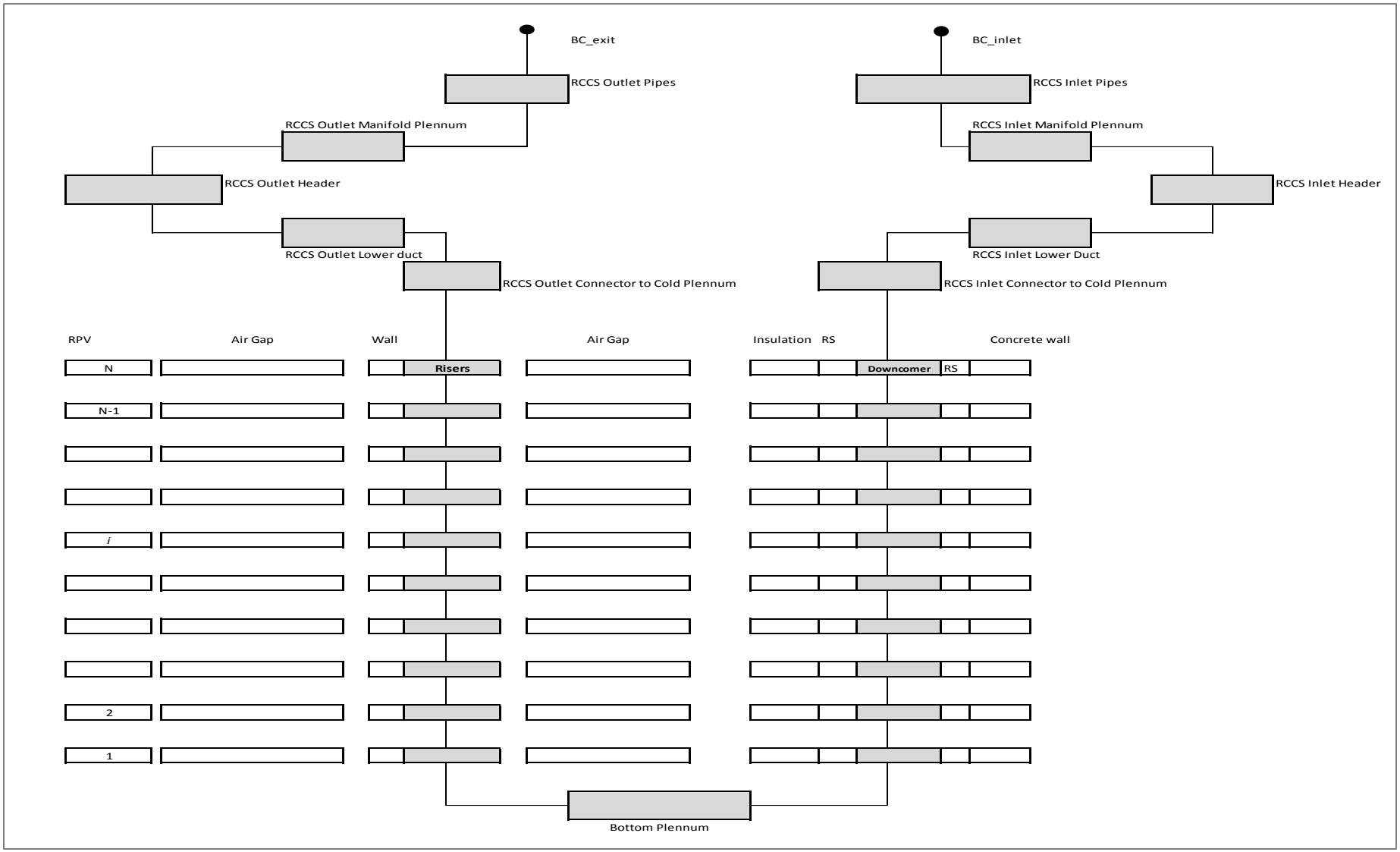

Figure 6-1: System modeling for the natural circulation analysis in the air-cooled RCCS.

6.3 RCCS model inputs and boundary conditions

In developing the numerical model, a number of boundary conditions were imposed and are given in Table 6-1. Further, this table gives a summary of where certain parameters were sourced as required by the model or specified if a value was required. Finally, the types of heat transfer modes are mentioned regarding where they are modelled.

Table 6-1: Inputs to the Flownex® model.

Temperature at the RPV wall	250 or 350	˚C
Wall emissivity (all walls)	0.8	
Wall emissivity (insulation)	0.1	
Air inlet temperature	40	˚C
Air inlet pressure	100	kPa
Air outlet pressure	100	kPa
Outer concrete boundary	adiabatic	
Heat transfer coefficient (cavity)	3	kW/m^2K
Heat transfer coefficient (riser and downcomer)	Dittus-Boelter	
Conduction in riser and downcomer walls	Yes	
Radiation in cavity	Yes	
Inside riser radiation	Yes	
Convection inside riser and downcomer	Yes	
Radiation in downcomer	Yes	
Flow secondary loss coefficient (increment 1)	2 forward/1.5 reverse	
Chimney pipes	(**Appendix F**)	
downcomer and riser height	18.5	m
Height per increment	1.85	per increment

The Nusselt number for laminar flow in the downcomer duct can be obtained from (Incropera & DeWitt, 2002:496) as:

$$Nu_{riser} = 5.60 \qquad \text{Equation 6-1}$$

The Nusselt numbers for the inner annular and outer annular walls for laminar flows in the downcomer were obtained from (Incropera & DeWitt, 2002:501) as:

$$Nu_i = 7.37 \qquad \text{Equation 6-2}$$

$$Nu_o = 4.23 \qquad \text{Equation 6-3}$$

The calculation must be able to determine the following;

1 Total heat removal rate from RPV.

2 Natural convection mass flow rate through the RCCS.

3 RCCS air outlet temperature.

4 Maximum temperature of the concrete wall.

6.4 Assumptions and model simplifications

The following assumptions were made in developing the RCCS models;

- The RPV, riser and downcomer were discretized into 10 equal increments. The total height of the RPV, riser and downcomer is 18.5 m.
- Radiation heat transfer takes place between surfaces on the same level. (Radiation view factors provided by the KAERI).
- One-dimensional radial heat transfer through solid structures (axial conduction between increments neglected).
- Constant heat transfer coefficient assumed for convective heat transfer in the cavity.
- One-dimensional flow assumed in the riser and downcomer.
- Inside riser radiation will be taken into account as well as radiation between the inner and outer annular surfaces on each level of the downcomer.
- The riser side walls can be modelled as one surface with an area equal to the sum of the two areas. This is because the unit cell used is symmetric about its centre.
- Convection in the cavity occurs between the RPV wall and the air in the air gap as well as between the air and the different surfaces exposed to the air in the reactor cavity.

- The air in the cavity is assumed to be at the same temperature and pressure at all increments.

- The air in the cavity, riser and downcomer is assumed to be non-participating for all radiation.

- The concrete outer wall temperature is assumed to be uniform along the axial direction.

- The bottom plenum was modelled as a node with a volume of 18.5 m^3.

As a point of departure, the radiation in the cavity is discussed in the next section.

6.5 Radiation view factors in the reactor cavity (single loop)

Reverting back to the unit cell presented in Figure 4-3, it can be seen that the reactor cavity is enclosed by six surfaces namely;

1. Vessel wall (RPV).

2. Riser front wall.

3. Riser side wall.

4. Riser side wall.

5. Riser back wall.

6. Downcomer inside cavity wall.

The method used in the enclosure radiation calculation is the so-called Net-Radiation Method that was described in section 3.2.3. The view factor and surface emissivity are key parameters in the equations associated with this method. In this study, the view factors for the enclosure have been provided by the KAERI as shown in Figure 6-2.

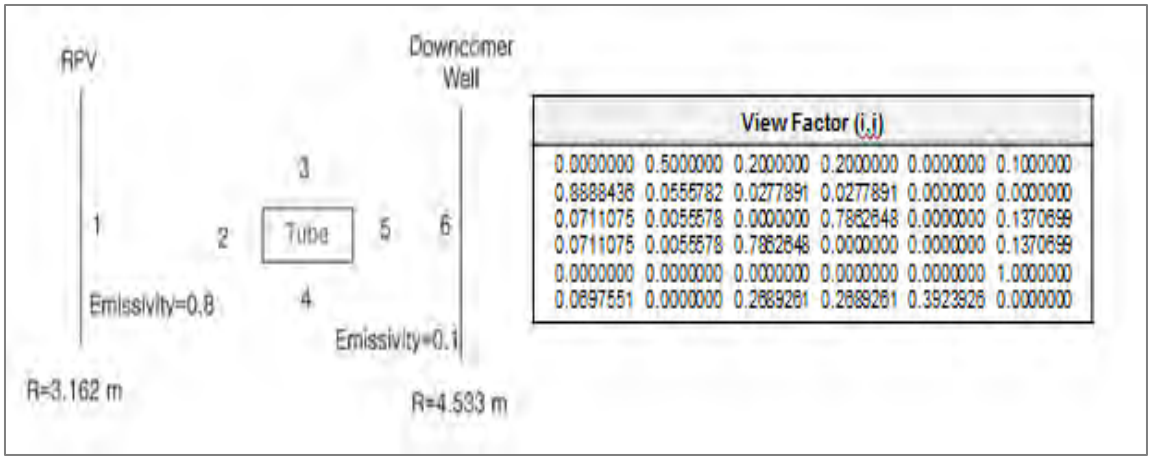

Figure 6-2: The KAERI reactor cavity view factors.

Due to the symmetry in the unit cell (Figure 4-3) about its centre it is only necessary to model one side surface. In fact, a single side surface is modelled with an area equal to the sum of the two side surfaces. This reduces the number of surfaces in the enclosure to five as can be seen in Figure 6-3 and therefore the view factors have to be recalculated to account for this. Firstly, it can be seen from Figure 6-2 that the view factor from the RPV to one side surface is 0.2 (i.e. $F_{1\to3} = F_{1\to4} = 0.2$). If one side wall is to be modelled, it would infer that the view factor from the RPV to this new surface is 0.4. This means that 40% of the radiation from the RPV is incident upon the side surface and 50% of the radiation from the RPV is incident on the front wall of the riser. 10% of the radiation from the RPV penetrates through the gap between adjacent risers to the downcomer wall.

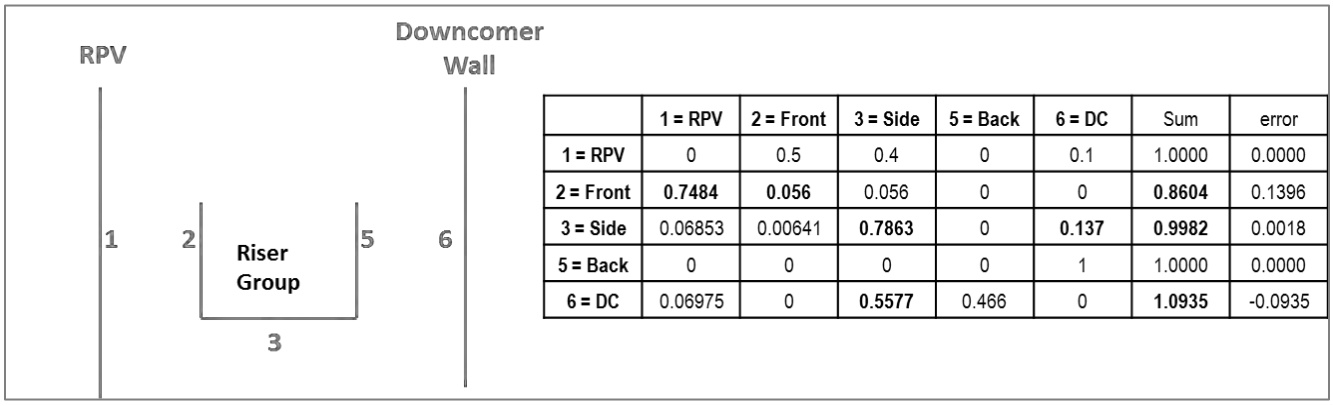

	1 = RPV	2 = Front	3 = Side	5 = Back	6 = DC	Sum	error
1 = RPV	0	0.5	0.4	0	0.1	1.0000	0.0000
2 = Front	**0.7484**	**0.056**	0.056	0	0	**0.8604**	0.1396
3 = Side	0.06853	0.00641	**0.7863**	0	**0.137**	**0.9982**	0.0018
5 = Back	0	0	0	0	1	1.0000	0.0000
6 = DC	0.06975	0	**0.5577**	0.466	0	**1.0935**	-0.0935

Figure 6-3: Calculated view factors for a single loop riser configuration.

The new view factors are shown in Figure 6-3; firstly, it can be seen that Equation 3-16, the summation rule, is not preserved. The reason for this was found upon evaluating Equation 3-15, the reciprocity rule, that there are discrepancies between the KAERI view factors (Figure 6-2) and the re-calculated view factors (Figure 6-3) as shown in bold. Since no radiation can escape the enclosure, the summation rule must be preserved at all times. Therefore, Table 6-2 presents the updated view factors. It was decided to focus on the view factors between the front and side surfaces. For example, in Figure 6-3, it was calculated that 5.6% of the radiation from the front of the riser is incident upon the front of one other riser due to the concave arrangement of the risers. This was increased to 19.6% in Table 6-2 to conserve the summation rule. Therefore the view factors in Table 6-2 are derived from those in Figure 6-3 to conserve both the summation and reciprocity rule.

Table 6-2: Updated view factor for the single loop RCCS

	1 = RPV	**2 = Front**	**3 = Side**	**5 = Back**	**6 = DC**	Sum	error
1 = RPV	*0*	**0.5**	**0.4**	*0*	**0.1**	**1.0000**	0.0000
2 = Front	**0.7484**	**0.1956**	**0.056**	*0*	0	**1.0000**	0.0000
3 = Side	0.06853	0.00641	**0.81106**	*0*	**0.114**	**1.0000**	0.0000
5 = Back	*0*	*0*	*0*	*0*	1	**1.0000**	0.0000
6 = DC	0.06975	*0*	**0.46425**	0.466	*0*	**1.0000**	0.0000

As an illustration consider the view factor given in Figure 6-2 between the RPV and the front of the riser (i.e. $F_{1\to 2} = 0.5$). The view factor for the re-radiation from the front wall to the RPV (i.e. $F_{2\to 1}$) can be calculated using Equation 3-15 and the associated areas calculated in Section 4.2 as follows;

$$F_{2\to 1} = \frac{A_1 F_{1\to 2}}{A_2} = \frac{36.75 \times 0.5}{2.4.55228} = \mathbf{0.7484} \qquad \text{Equation 6-4}$$

As can be seen the value obtained in Equation 6-4 is different to that given in Figure 6-2 of 0.888436. Further, if Equation 3-16 is used; the sum of all the view factors from surface 2 (front wall) to all the other surface is less than one (**0.8604**) in Figure 6-3. This finding clearly underestimates the total radiation heat transfer in the enclosure. It also appears that the view factors calculated by the KAERI are based on the inner riser dimensions. To correct this, the

view factor between the front (surface 2) and itself (i.e. $F_{2\to 2}$) is changed from 5.6% to 19.56% in Table 6-2 so that the summation rule is conserved.

The view factor from side 5 to the downcomer ($F_{5\to 6}$) is one because heat only radiates outward due to the concave arrangement of the geometry. The view factor from side wall to itself ($F_{3\to 3}$) is approximately 81%. This means that one side wall sees 81% of the adjacent side wall and 11.4% of the downcomer. This is realistic since the side walls are virtually adjacent to each other.

From Table 6-2, the radiation network for the cavity radiation can be constructed in Flownex® using the techniques described in section 3.2.3 and **Appendix A.** This is shown in Figure 6-4 and is a so called "*compound element*" that will be used whenever radiation is modelled in the cavity to eliminate the need for repetition. The symbols R_1 through R_5 represent the surface resistances at the different surfaces while $F_{i\to j}$ represents the view factors between interacting surfaces.

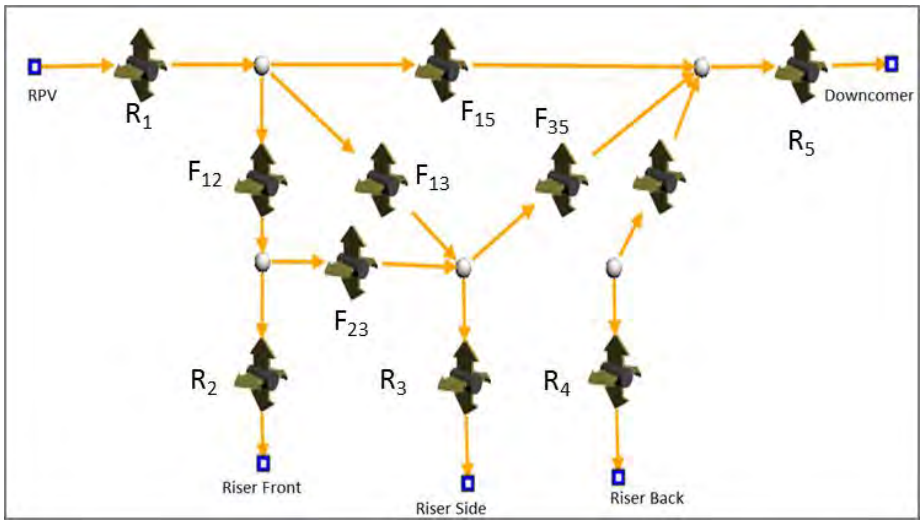

Figure 6-4: Flownex® Compound Setup Single loop RCCS.

6.6 Radiation view factors in the reactor cavity (double and quad loops)

The only major difference between the single and multi-loop riser configurations is the manner in which the view factors and heat transfer networks for the cavity radiation are computed. For the two loop model, firstly, it can be seen from Figure 6-5 that introducing another riser loop

increases the surfaces in the enclosure to eight. In the single loop model that was discussed in the previous section, it was seen from Table 6-2 that 50% of all radiation from the RPV is incident upon the front of the riser. For the double riser loop this will mean that 25% of the radiation from the RPV is incident upon each of the riser loops and 12.5% in the case of the quad loop.

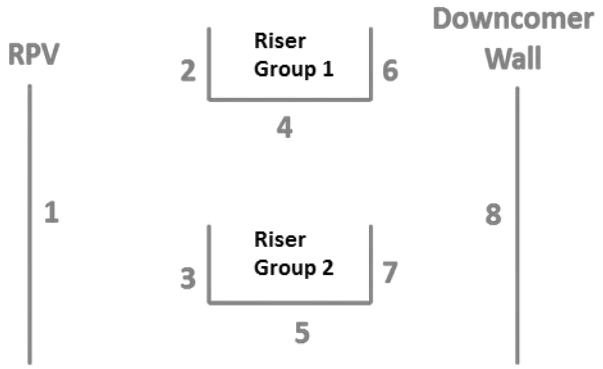

	1=RPV	2 = F1	3 = F2	4= S1	5 = S2	6 = B1	7 = B2	8=DC	Sum	error
1=RPV	0	0.25	0.25	0.2	0.2	0	0	0.1	1.0000	0.0000
2 = F1	0.7484	0.0978	0.0978	0.028	0.028	0	0	0	1.0000	0.0000
3 = F2	0.7484	0.0978	0.0978	0.028	0.028	0	0	0	1.0000	0.0000
4= S1	0.0685	0.003205	0.003205	0.4055	0.4056	0	0	0.114	1.0000	0.0000
5 = S2	0.0685	0.003205	0.003205	0.4055	0.4056	0	0	0.114	1.0000	0.0000
6 = B1	0	0	0	0	0	0	0	1	1.0000	0.0000
7 = B2	0	0	0	0	0	0	0	1	1.0000	0.0000
8=DC	0.06975	0	0	0.2321	0.2321	0.233	0.233	0	1.0000	0.0000

Figure 6-5: Calculated view factors for a double loop riser configuration.

As an illustration of how the view factors for the double loop were calculated; consider the view factor from the front to the front ($F_{2\to 2} = 0.196$) in Table 6-2. For the double and quad loop this value is 0.0978 (Figure 6-5) and 0.0489 (Figure 6-6) because one front wall can view itself (a riser in its loop) or another riser (a riser in another loop). This reasoning was used to compute the view factors in Figure 6-5 for the double loop and Figure 6-6 for the quad loop configuration.

The compounds that will be used in the double and quad loop models are given in Figure 6-7 and Figure 6-8. For example, one can see that the back walls (**B**) are only connected to the downcomer (**DC**) because the view factor is unity. In Flownex® only view factors in one direction need to be specified. The re-radiation or reciprocity is computed internally within the

software. As an illustration, a connection is made between the RPV and DC (i.e. $F_{1\to 8} = 0.1$), the subsequent re-radiation (i.e. $F_{8\to 1} = 0.06975$), is computed internally using the reciprocity rule.

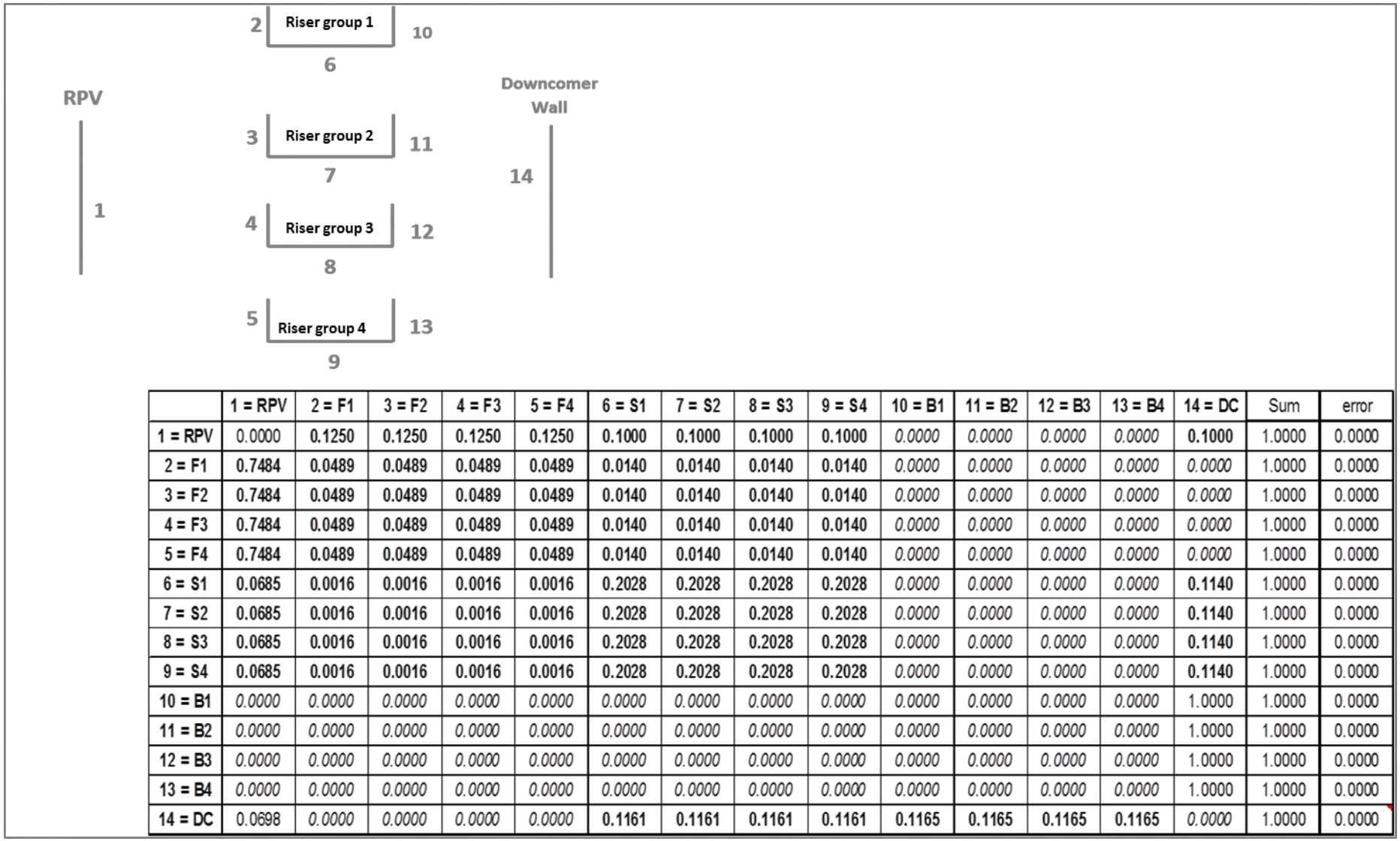

	1 = RPV	2 = F1	3 = F2	4 = F3	5 = F4	6 = S1	7 = S2	8 = S3	9 = S4	10 = B1	11 = B2	12 = B3	13 = B4	14 = DC	Sum	error
1 = RPV	0.0000	0.1250	0.1250	0.1250	0.1250	0.1000	0.1000	0.1000	0.1000	0.0000	0.0000	0.0000	0.0000	0.1000	1.0000	0.0000
2 = F1	0.7484	0.0489	0.0489	0.0489	0.0489	0.0140	0.0140	0.0140	0.0140	0.0000	0.0000	0.0000	0.0000	0.0000	1.0000	0.0000
3 = F2	0.7484	0.0489	0.0489	0.0489	0.0489	0.0140	0.0140	0.0140	0.0140	0.0000	0.0000	0.0000	0.0000	0.0000	1.0000	0.0000
4 = F3	0.7484	0.0489	0.0489	0.0489	0.0489	0.0140	0.0140	0.0140	0.0140	0.0000	0.0000	0.0000	0.0000	0.0000	1.0000	0.0000
5 = F4	0.7484	0.0489	0.0489	0.0489	0.0489	0.0140	0.0140	0.0140	0.0140	0.0000	0.0000	0.0000	0.0000	0.0000	1.0000	0.0000
6 = S1	0.0685	0.0016	0.0016	0.0016	0.0016	0.2028	0.2028	0.2028	0.2028	0.0000	0.0000	0.0000	0.0000	0.1140	1.0000	0.0000
7 = S2	0.0685	0.0016	0.0016	0.0016	0.0016	0.2028	0.2028	0.2028	0.2028	0.0000	0.0000	0.0000	0.0000	0.1140	1.0000	0.0000
8 = S3	0.0685	0.0016	0.0016	0.0016	0.0016	0.2028	0.2028	0.2028	0.2028	0.0000	0.0000	0.0000	0.0000	0.1140	1.0000	0.0000
9 = S4	0.0685	0.0016	0.0016	0.0016	0.0016	0.2028	0.2028	0.2028	0.2028	0.0000	0.0000	0.0000	0.0000	0.1140	1.0000	0.0000
10 = B1	0.0000	0.0000	0.0000	0.0000	0.0000	0.0000	0.0000	0.0000	0.0000	0.0000	0.0000	0.0000	0.0000	1.0000	1.0000	0.0000
11 = B2	0.0000	0.0000	0.0000	0.0000	0.0000	0.0000	0.0000	0.0000	0.0000	0.0000	0.0000	0.0000	0.0000	1.0000	1.0000	0.0000
12 = B3	0.0000	0.0000	0.0000	0.0000	0.0000	0.0000	0.0000	0.0000	0.0000	0.0000	0.0000	0.0000	0.0000	1.0000	1.0000	0.0000
13 = B4	0.0000	0.0000	0.0000	0.0000	0.0000	0.0000	0.0000	0.0000	0.0000	0.0000	0.0000	0.0000	0.0000	1.0000	1.0000	0.0000
14 = DC	0.0698	0.0000	0.0000	0.0000	0.0000	0.1161	0.1161	0.1161	0.1161	0.1165	0.1165	0.1165	0.1165	0.0000	1.0000	0.0000

Figure 6-6: Calculated view factors for a quad loop riser configuration.

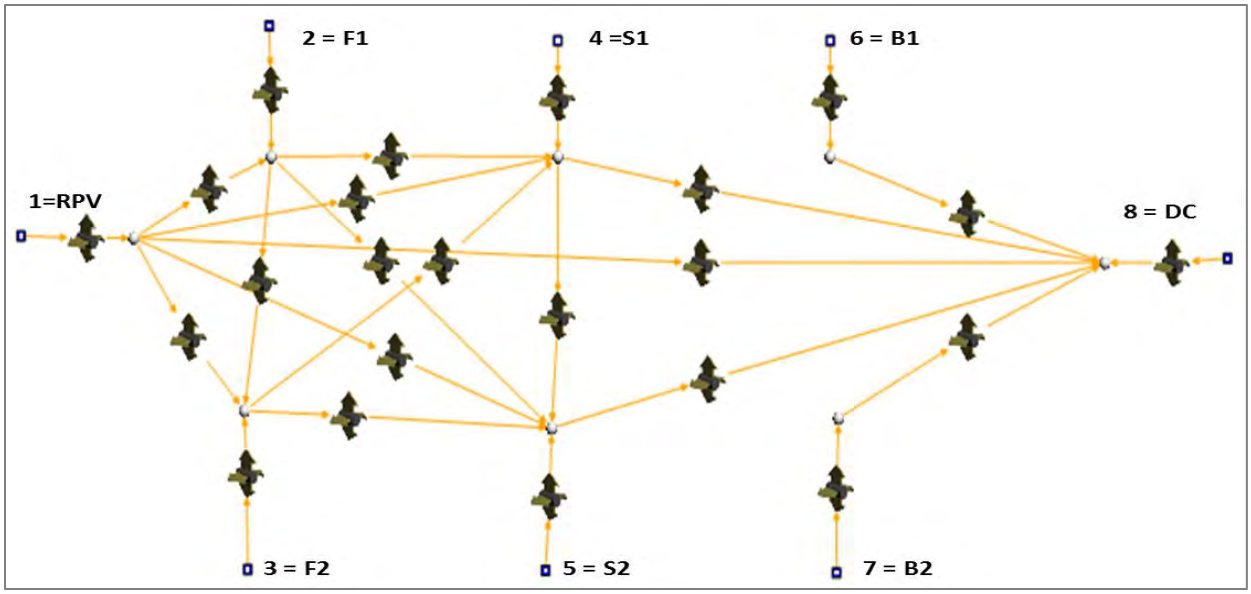

Figure 6-7: Flownex® compound setup double loop RCCS.

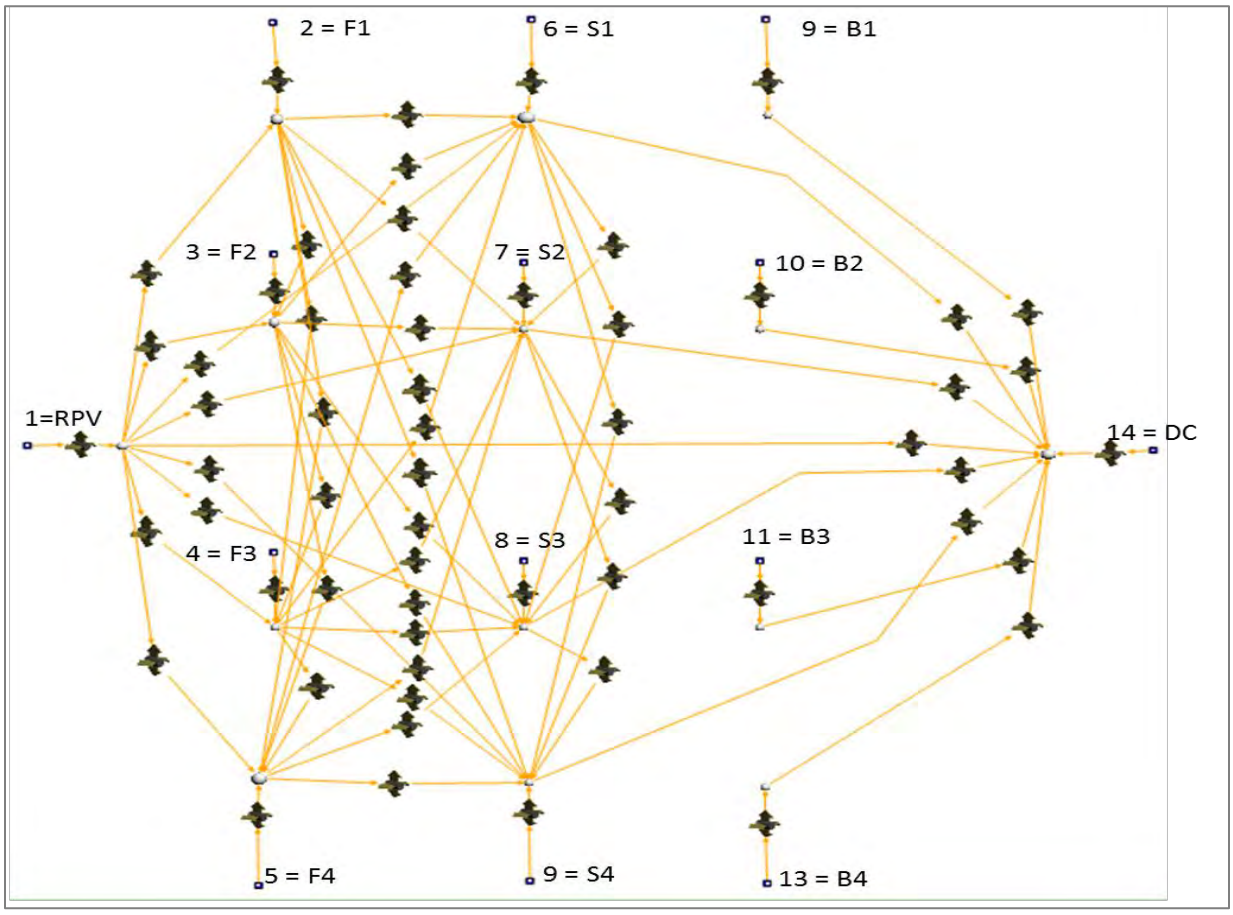

Figure 6-8: Flownex® compound setup quad loop RCCS.

6.7 Radiation inside the riser tubes and in the downcomer

Inside the risers and the downcomer, radiation heat transfer takes place between the different sides which are at different temperatures. The view factors for the inside riser radiation are given in Figure 6-9 and that of the downcomer are given in Figure 6-10. The compound that was set up for the intra-riser radiation network is given in Figure 6-11.

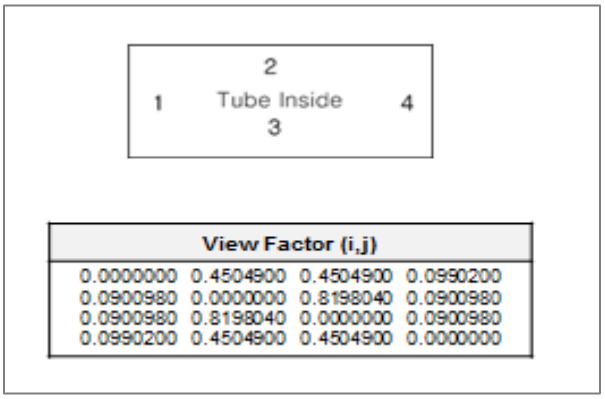

Figure 6-9: Inside riser view factors.

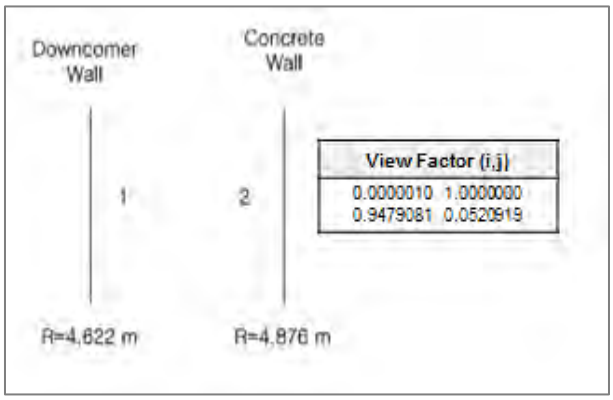

Figure 6-10: Downcomer inner and outer wall view factors.

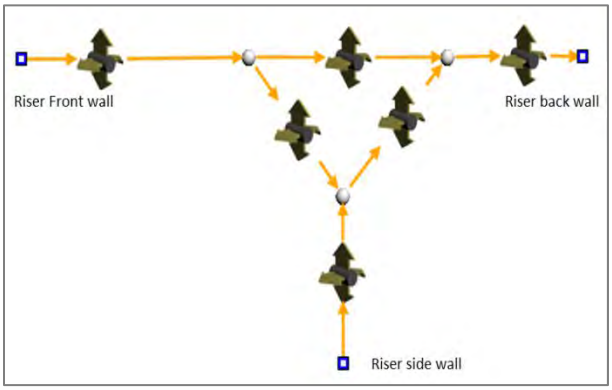

Figure 6-11: Flownex® compound setup for inside riser radiation.

It can be deducted from Figure 6-9 that 90% of the radiation from the inside front wall is incident upon the side walls and 10% to the back walls. From Figure 6-10 it can be seen that the view factor from the inner wall of the downcomer to the outer wall is one. This is true due to the concave nature of the geometry. From the inside wall, heat can only radiate outwards, such as described for the riser back wall.

6.8 Convective heat transfer in the cavity

The convective heat transfer from the reactor vessel to the riser array can also be considered as convection in an enclosure. The parameter of interest is the heat transfer coefficient between the walls and the air in the cavity. While natural convection in an enclosure has been studied extensively both experimentally and numerically, it was not the scope of this study to calculate this parameter for the different surfaces and location.

For this benchmark study a constant heat transfer coefficient of 3 $W/m^2.K$ was used in Equation 3-1 as an input to the Flownex® convection element. This value was chosen as a first approximation to create a basis for further comparisons. This value is not the actual heat transfer coefficient in the cavity. It is investigated in section 7.4 how the results of the theoretical model are affected by different values and if at all in a real design, the actual values of the heat transfer coefficient at the different surfaces need to be calculated.

6.9 Full RCCS Flownex® models

The single loop RCCS model is composed of 10 increments of Figure 5-9 stacked at different elevations. The height difference between the increments is specified at the nodes connecting the increments, much similar to the manner in which the simple U-tube was set up in Figure 5-1. The risers and the downcomer network are connected to a common node at the inlet and outlet of the chimney respectively. These are labelled **A** and **B** in Figure 6-12. The chimney is modelled as a series of pipes with resemblance to the systematic modelling given in Figure 6-1 and the dimensions of each pipe are given in **Appendix F**. Point **C** is the common cold plenum which connects the downcomer to the risers. This is modelled as a node with a volume of 18.75 m^3. The geometry of the bottom plenum was not known at the time of this simulation since the actual RCCS design is still in the development phase.

The double and quad loop RCCS models are shown in Figure 6-13 and Figure 6-14 respectively. It can be seen that from point **C**, the common downcomer branches into the two or quad loops of risers. The top-most pipe elements of the risers are connected to a single

common hot plenum (**Point B**). From point **B**, the hot fluid flows into the chimney to be ultimately released to the atmosphere. Point **D** is the cavity air; at each level in the RCCS the same virtual node is used to represent the cavity air since it was assumed that the temperature and pressure in the cavity is the same at the different locations.

In the RCCS models that were developed, the concrete wall was specified as a common node at the different heights. It was assumed for this study that the concrete temperature is the same at the different elevations due to the large mass of the concrete.

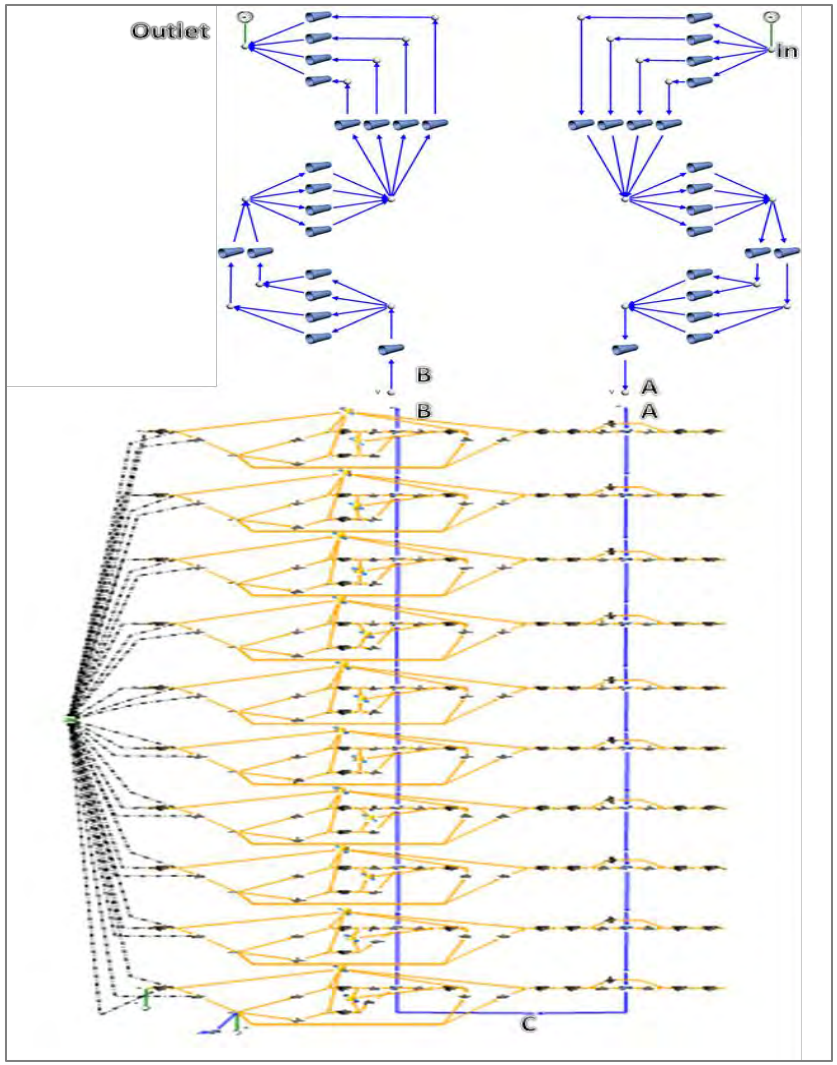

Figure 6-12: Full RCCS single loop Flownex® model.

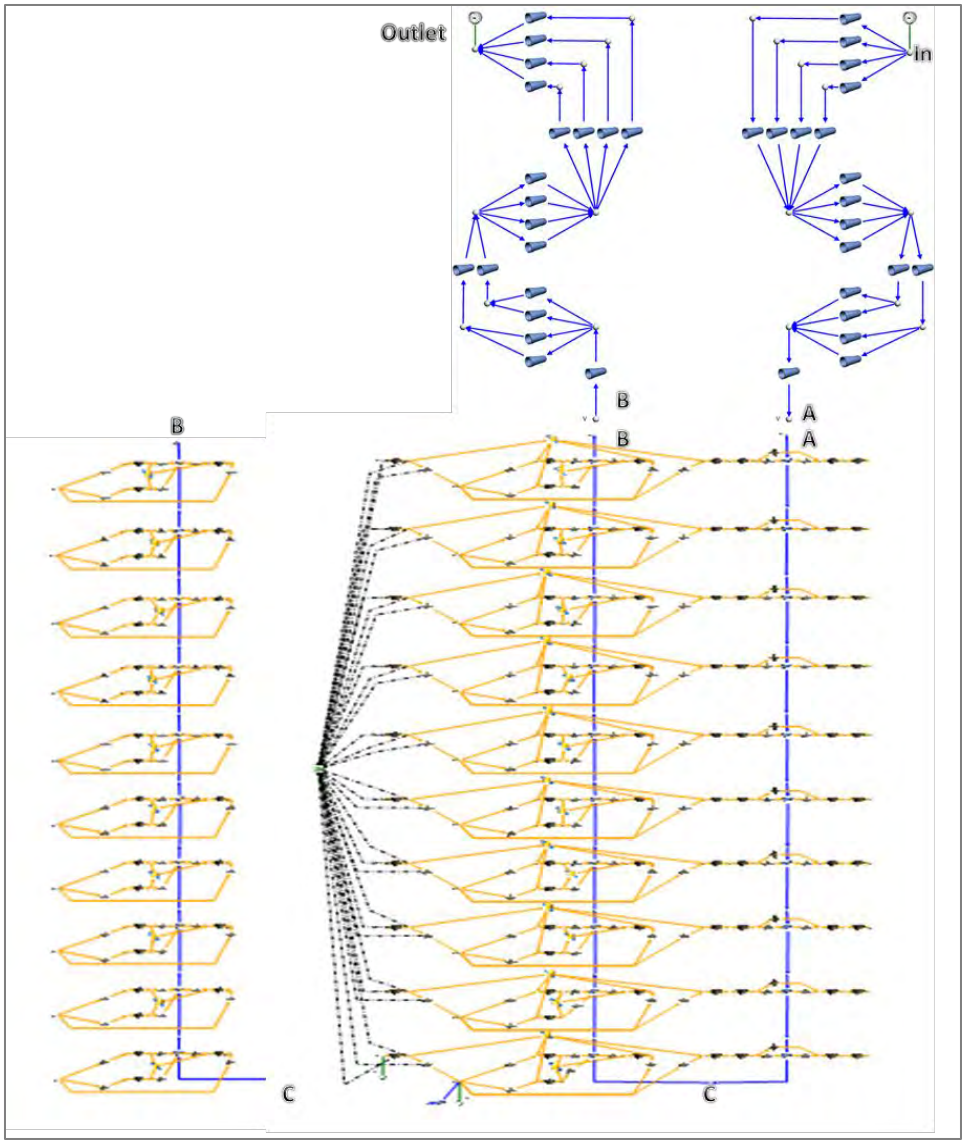

Figure 6-13: Full RCCS double loop Flownex® model.

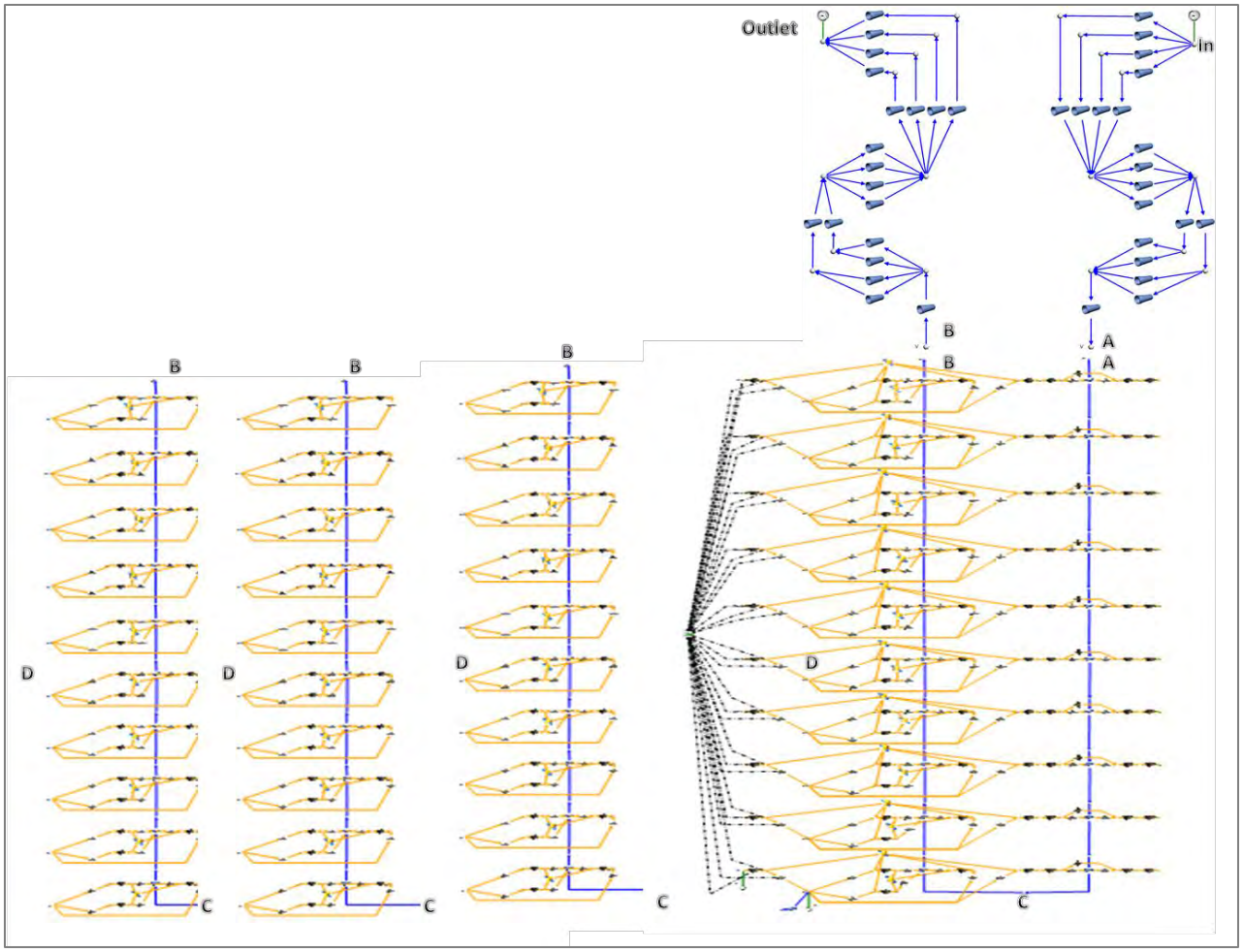

Figure 6-14: Full RCCS quad loop Flownex® model.

6.10 Summary of the model development chapter

In this chapter, the RCCS nodalization or system modelling of the natural circulation in the air-cooled RCCS was developed and presented. Table 6-1 was developed to identify and generate suitable input data for the Flownex® model. The simplifying assumptions were then presented for modelling purposes.

The main objective of this chapter was to develop a full model of the RCCS in Flownex®. However, before this could be done, it was important to characterise certain physical phenomena that must be considered. The view factors for the single, double and quad loop riser configurations were developed for the unit cell geometry in Figure 4-3.

Finally, a full RCCS model of the single, double and quad loop configurations were established that captures all of the important physical phenomena. The models are merely extensions of the one increment case studies presented in section 5.3

Chapter 7

7 Flownex® RCCS model results and discussions

7.1 Introduction

This chapter presents and discusses the results obtained from the integrated RCCS models that were developed in ***Chapter 6***. The models are applied to selected steady state scenarios in order to illustrate the operational characteristics of the system. As can be seen in Table 6-1, two temperature boundary conditions were applied on the RPV inner wall; the boundary condition of 250°C is taken as the most probable temperature of the RPV inside wall during normal operations while 350°C is regarded for this purpose as the worst case temperature during an accident condition. For this Flownex® simulation of the RCCS, the main results are the total heat removed from the RPV surface and the maximum temperature of the concrete wall which should be maintained below 65°C.

The heat transfer coefficient in the cavity was needed to construct the Flownex® model of the RCCS. In this chapter, a parametric study is discussed that was conducted with the aim of determining the sensitivity of the results to different values of the heat transfer coefficient, and if further work should be invested in calculating the actual values, especially in the design of a real RCCS.

Finally, the view factors used in the reactor cavity were obtained from the KAERI and modified for this project. In this chapter, the view factors for the cavity are calculated independently using Star-CCM+ and compared to those obtained from the KAERI.

7.2 RCCS performance at VHTR conditions

The steady state results of the RCCS simulations are given in Table 7-1 and Table 7-2 for the two different boundary conditions imposed at the RPV inner wall (250°C or 350°C). Firstly, it can be seen that the results for the single, double and quad loop RCCS are virtually identical. This was expected since the double and quad loop Flownex® models were built as mirror symmetric images of the single loop RCCS model. Secondly, it was found that the dominant heat transfer mode in the reactor cavity is radiation heat transfer which accounts for 84% of the total heat

transfer for the 250°C case and 89% for the 350°C case. These results are in line with the findings from the literature study. The increase in the portion of radiation heat transfer can be attributed to the T^4 dependency of the radiation heat transfer on the temperatures of the interacting surfaces.

7.2.1 RCCS performance at T_RVP = 250°C (nominal condition)

The results of the Flownex® models for the nominal case are shown in Table 7-1.

Table 7-1: Steady State RCCS results (T_{RPV_WALL} = 250°C).

Parameter	Units	Flownex®	Flownex®			Flownex®					
		Single Loop	Double Riser Group			Quad Loop					
		Riser 1	Riser 1	Riser 2	Total	Riser 1	Riser 2	Riser 3	Riser 4	Total	%error
		T_{RPV_WALL} = 250 °									
Total Heat Loss at RPV Surface	MW	0.82			0.82					0.82	0.00
Radiation Heat Transfer at RPV Surface	MW	0.69			0.69					0.69	0.00
Convection Heat Transfer at RPV Surface	MW	0.13			0.13					0.13	0.00
Chimney Air Flowrate in RCCS	kg/s	11.10	5.55	5.55	11.10	2.78	2.78	2.78	2.78	11.10	0.00
Chimney Exit Temperature	°C	112.95			112.94					112.96	0.01
Maximum Temperature of Riser Tube	°C	121.88	121.88	121.88	121.88	121.90	121.90	121.90	121.90	121.90	0.01
Maximum Temperature of Concrete Wall	°C	42.23			42.23					42.22	0.01
ΔP in Riser Tube	kPa	0.24			0.24					0.24	0.00
ΔT in Riser Tube	°C	71.73			71.72					71.74	0.01
RPV average outside temperature	°C	237.54			237.54					237.54	0.00

The analysis revealed that 0.82 MW of heat will be removed from the RPV wall by the RCCS. The air is heated from 40°C to 112.95°C during the nominal condition. The concrete temperature was calculated to be 42°C well below the benchmark condition of 65°C.

The buoyancy force driving the RCCS flow established an air flow rate of 11.10 kg/s during the nominal condition.

7.2.2 RCCS performance at T_RVP = 350°C (upset conditions)

The results of the Flownex® models for the upset conditions are presented in Table 7-2.

Table 7-2: Steady state RCCS results (T_{RPV_WALL} = 350°C).

Parameter	Units	Flownex® Single Loop	Flownex® Double Riser Group			Flownex® Quad Loop					
		Riser 1	Riser 1	Riser 2	Total	Riser 1	Riser 2	Riser 3	Riser 4	Total	%error
		T_{RPV_WALL} = 350 °									
Total Heat Loss at RPV Surface	MW	1.58			1.58					1.58	0.00
Radiation Heat Transfer at RPV Surface	MW	1.40			1.40					1.40	0.00
Convection Heat Transfer at RPV Surface	MW	0.18			0.18					0.18	0.00
Chimney Air Flowrate in RCCS	kg/s	13.08	6.54	6.54	13.08	3.27	3.27	3.27	3.27	13.08	0.00
Chimney Exit Temperature	°C	159.40			159.40					159.40	0.00
Maximum Temperature of Riser Tube	°C	220.67	220.68	220.68	220.68	220.68	220.68	220.68	220.68	220.68	0.00
Maximum Temperature of Concrete Wall	°C	42.90			42.90					42.89	0.01
ΔP in Riser Tube	kPa	0.26			0.26					0.26	0.00
ΔT in Riser Tube	°C	118.00			118.00					118.00	0.00
RPV average outside temperature	°C	325.98			325.98					325.97	0.01

It is encouraging that even after a 100°C increase in the RPV wall temperature (from nominal to upset conditions), the concrete wall temperature only increases by 1°C and is still maintained well below the benchmark condition of 65°C. For the upset case (i.e. 350°C), this is particularly important since after the reactor is shutdown, fission reactions from the delayed neutrons cause the temperatures in the fuel to increase particularly in the first hour. Since at this point, there is no forced cooling, it is expected that the RPV wall will heat up and as a consequence the temperature in the cavity will increase. These results are encouraging because it means the concrete temperature responds rather slowly to changes in the RPV temperature. Therefore, the dangerous fission products and heat are well contained within the reactor building because the integrity of the concrete is retained. Also, during nominal operating conditions (i.e. 250°C), the integrity of the concrete is retained as the wall temperature is below 65°C.

Therefore, it can be deduced that the RCCS maintains its functionality during nominal and upset conditions imposed.

7.3 Heat transfer and fluid flow Analysis in the RCCS (T_RPV = 350°C)

The upset condition will be used to evaluate the heat transfer and fluid flow in the riser tubes. The air and tube wall temperature distribution in the heated section are given in Figure 7-1. The air temperature varies from 42°C to 156°C while the maximum temperature of the riser is 221°C due to the heat received from the RPV and cavity wall. The front wall temperature is highest

because it is the most exposed surface to the RPV. Even though a much larger portion of heat RPV is absorbed by the side walls owing to the larger temperature difference between the RPV and the side walls, the side walls have a larger combined area and therefore, a lower temperature than the front walls. It can also be seen from Figure 7-1, that the wall and fluid temperatures increase along the heated section. The increase in temperature changes the fluid properties as shown in Table 7-3. Firstly, it can be seen that there is a 37% decrease in density, 19% increase in the viscosity and 23% increase in the fluid conductivity from the entrance to the exit of the riser tube. These changes in fluid properties affect the Reynolds number, the Nusselt number (and therefore the heat transfer coefficient), as well as the friction factor.

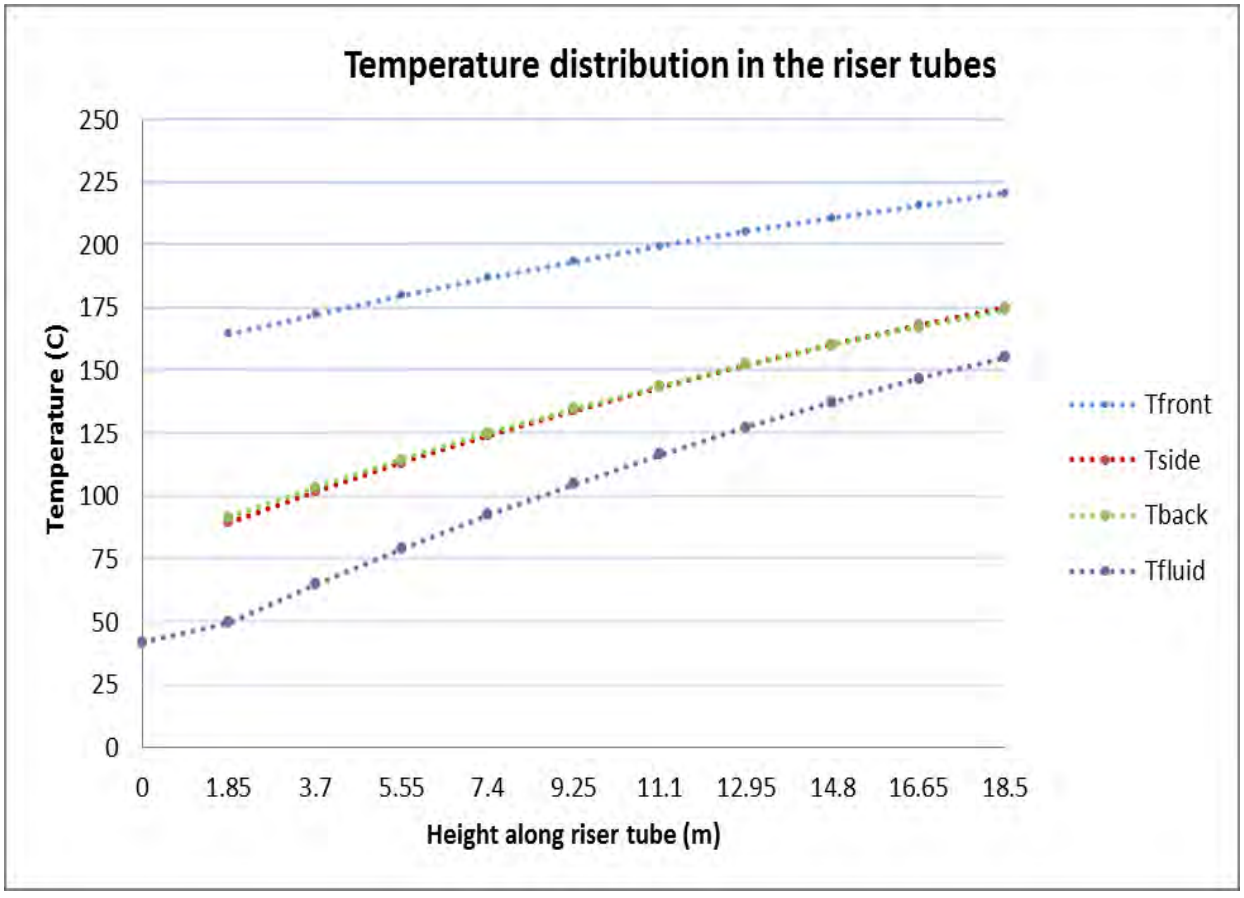

Figure 7-1: Temperature along the heated tube length (T_RPV=350°C).

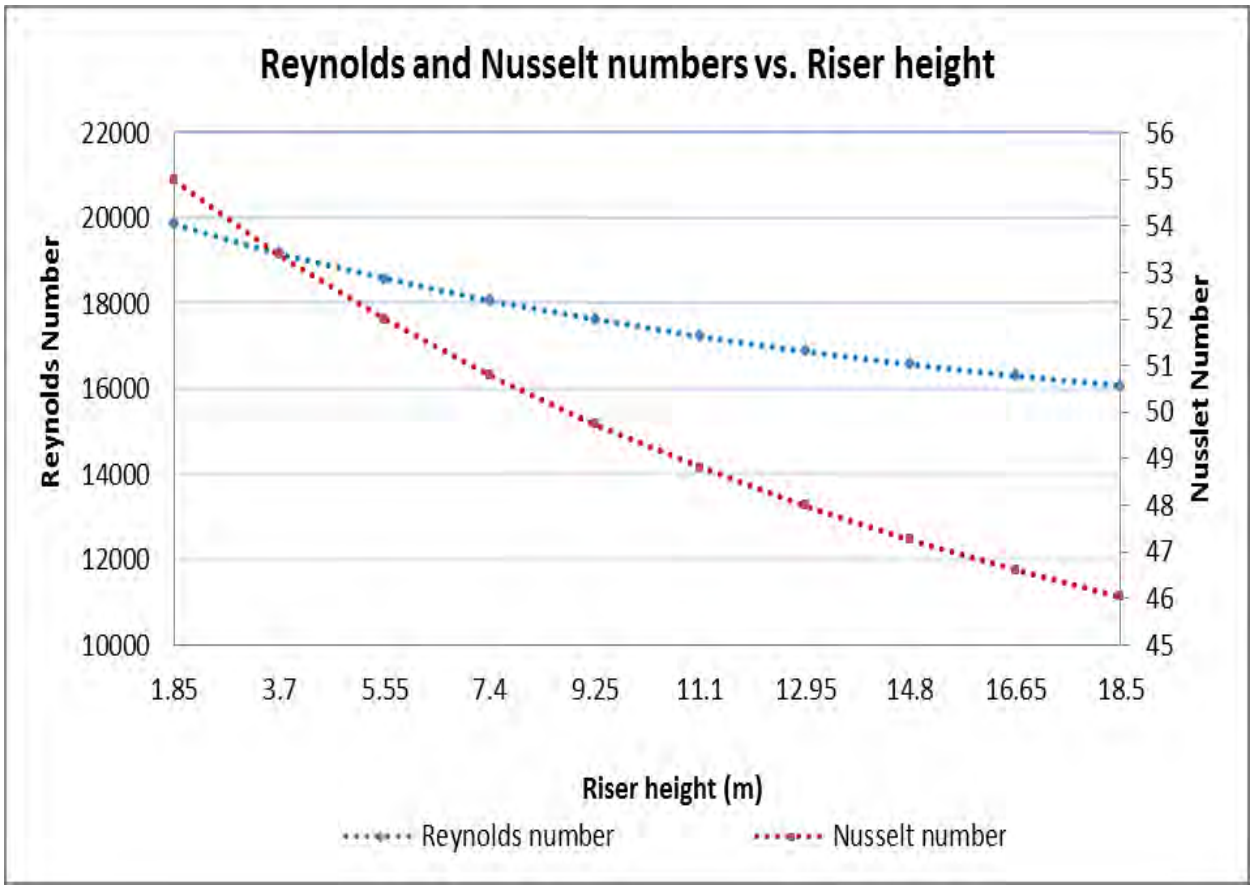

Figure 7-2: Reynolds and Nusselt number vs. height (T_RPV=350°C).

Table 7-3: Calculated fluid properties along the height of the riser tube (T_RPV=350°C).

Height (m)	velocity m/s	density $kg.m^3$	Conductivity W/m-K	viscosity kg/s-m
0	4.145	1.112	0.027	1.962E-05
1.85	4.251	1.084	0.028	2.033E-05
3.7	4.453	1.035	0.029	2.098E-05
5.55	4.643	0.992	0.030	2.157E-05
7.4	4.820	0.956	0.031	2.157E-05
9.25	4.985	0.924	0.032	2.212E-05
11.1	5.140	0.896	0.033	2.262E-05
12.95	5.284	0.872	0.033	2.308E-05
14.8	5.418	0.850	0.034	2.351E-05
16.65	5.542	0.831	0.035	2.390E-05
18.5	5.658	0.814	0.035	2.425E-05
% Change	**26.738%**	**-36.575%**	**22.86%**	**19.091%**

It can be seen in Figure 7-2, that the Reynolds number decreases along the height of the riser tube from 20,000 to 16,000 at the exit of the riser. As the air is heated up, its viscosity increases and the Reynolds number is consequently reduced despite the increase in velocity. As a consequence of the decreasing Reynolds number, the Nusselt number decreases because they are linked via the Dittus-Boelter correlation. According to Equation 3-25, the heat transfer coefficient is proportional to the Nusselt number; however, it can be seen from Figure 7-3 that the heat transfer coefficient increases along the height of the riser tube. This is somewhat contradictory and can be explained via the thermal fluid conductivity trends in Table 7-4. The thermal conductivity increases more than the Nusselt number decreases (23% vs. -18.47%), therefore, the heat transfer coefficient increases.

Table 7-4: Fluid conductivity and Nusselt number along the heated height (T_RPV=350°C).

Height (m)	Conductivity W/m-K	Nusselt number
0	0.027	
1.85	0.028	55.05
3.7	0.029	53.51
5.55	0.03	52.19
7.4	0.031	51.03
9.25	0.032	50.02
11.1	0.033	49.13
12.95	0.033	48.34
14.8	0.034	47.64
16.65	0.035	47.02
18.5	0.035	46.46
% Change	**22.86%**	**-18.47%**

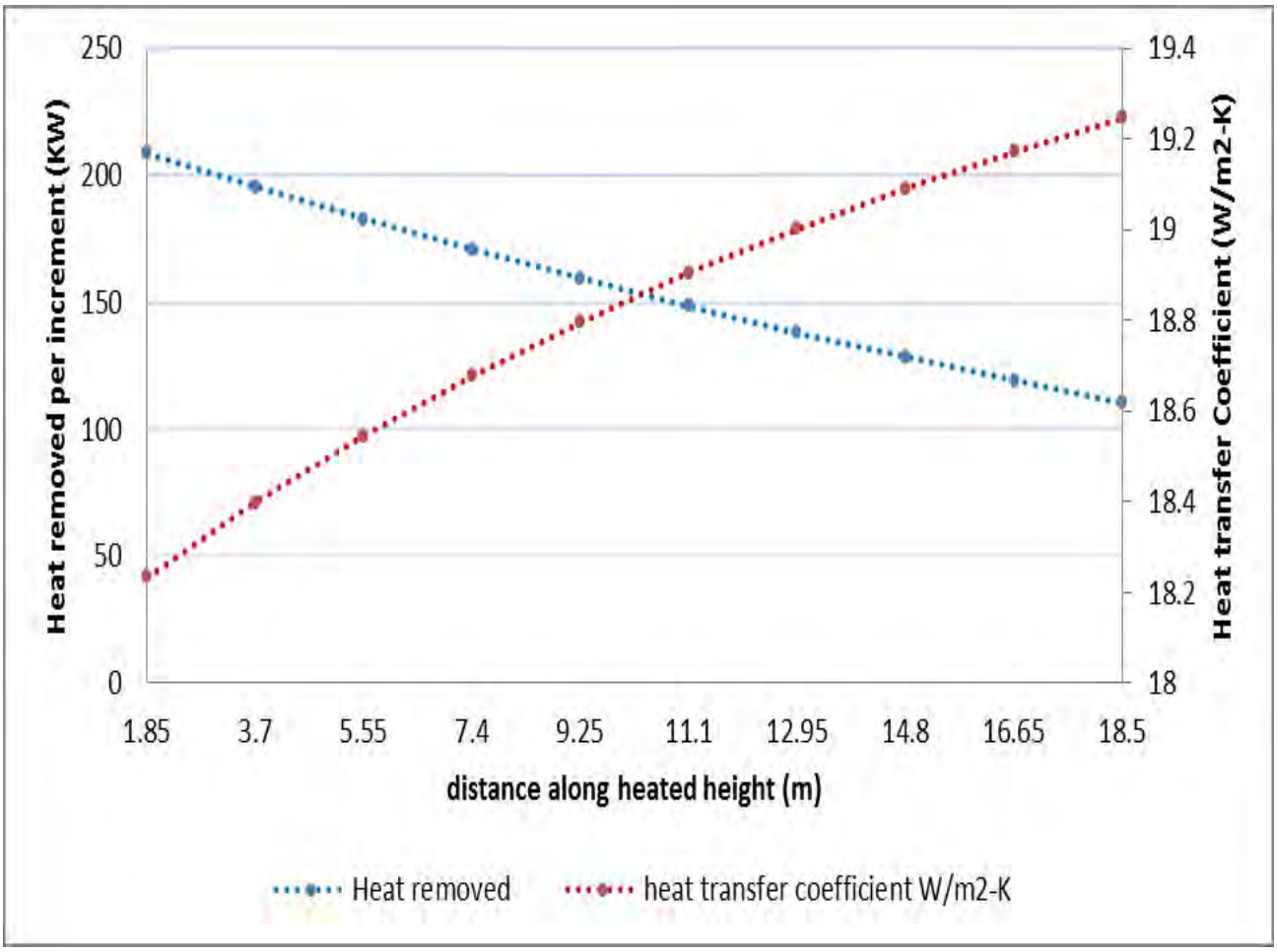

Figure 7-3: Heat transfer coefficient and heat removed vs. height (T_RPV=350°C).

The amount of heat removed per increment decreases along the height of the tubes, despite the increase in heat transfer coefficient. This can be seen in Figure 7-3. It can be seen from Table 7-5 that the decrease in **ΔT** along the heated height is greater than the increase in the heat transfer coefficient along the heated height (5% vs. -76%). Therefore, the driving force for heat transfer is the temperature difference between the fluid and the tube walls. Since the temperature difference decreases along the height so will the amount of heat removed.

Table 7-5: Heat transfer coefficient and ΔT (T_{wall} - T_{fluid}) along the heated height (T_RPV=350°C).

Increment	heat transfer coefficient	ΔT
	W/m^2-K	°C
1.85	18.235	114.9558
3.7	18.3978	107.5316
5.55	18.5443	100.6649
7.4	18.6765	94.3135
9.25	18.7961	88.4418
11.1	18.9041	83.015
12.95	19.0023	78.0035
14.8	19.0917	73.3755
16.65	19.1725	69.1055
18.5	19.2462	65.167
	5.25%	-76.40%

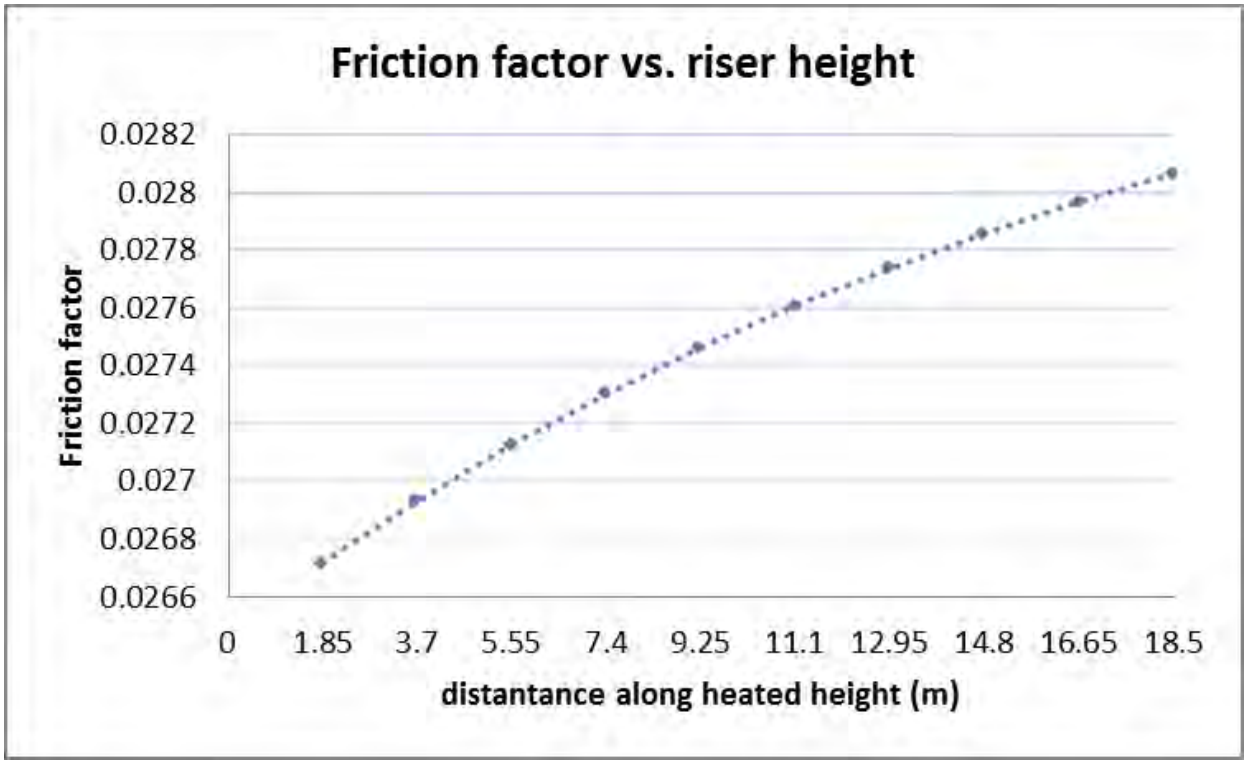

Figure 7-4: Friction factor vs. height (T_RPV=350°C).

Finally, it can be seen from Figure 7-4 that friction factor increases along the height of the tube. The friction factor is a function of the Reynolds number via the Darcy-Weisbach correlation and

since the Reynolds number decreases the friction factor increases. The friction factor is important factor in determining the mass flow rate through the pipe. The mass flow rate is calculated due to the balance between the buoyancy driving force and frictional losses.

7.4 Cavity heat transfer coefficient

It has been mentioned in section 6.8 that a heat transfer coefficient of 3 W/m^2-K was used for the cavity convection for all the different surfaces since the actual heat transfer coefficient in the cavity was not known at the outset. To test how different values of the heat transfer coefficient affect the simulation results, the model was implemented for different values as shown in Table 7-6. A constant value was used at all the different locations in the cavity.

Table 7-6: Results of the heat transfer coefficient parametric study (T_RPV=350°C).

Heat transfer coefficient	% Heat transfer by Radiation	Cavity Temperature	Maximum Temperature Concrete Wall	Heat Removed
W/m^2-K		°C	°C	MW
1	96.00	156.824	42.73	1.50
3	88.61	163.069	42.90	1.58
5	82.53	168.302	43.02	1.66
7	77.91	172.919	43.10	1.72
9	73.18	177.083	43.18	1.79
10	70.88	179.029	43.21	1.82
12	67.55	182.677	43.28	1.88
13	65.79	184.391	43.31	1.90
15	62.76	187.632	43.36	1.96
18	58.62	192.089	43.43	2.03
20	56.25	194.82	43.48	2.08

It can be seen that as the heat transfer coefficient in the cavity is increased, the contribution of radiation to the overall heat transfer rate decreases. Increased convection will bring the entire riser surface temperatures closer together, towards the cavity air temperature. The temperature difference between the surfaces is reduced and therefore the radiation heat transfer is reduced.

A higher heat transfer coefficient reduces the overall resistance to heat transfer through the cavity and therefore, there is more heat transfer overall. The results reveal that the mass flow rate increases, however not as significantly as the heat removal rate. The parameter of interest is the concrete wall temperature. It can be seen from Table 7-6 that increasing the heat transfer coefficient from 1 W/m^2–K to 20 W/m^2–K increases the temperature of the concrete by only 0.75 °C.

A heat transfer coefficient of 3 W/m^2-K was used for calculation purposes and is not the actual heat transfer coefficient in the cavity. For real-life design purposes the heat transfer coefficient at the different surfaces should be determined as accurately as possible and incorporated into the RCCS Flownex® models that are developed. One possible way of doing this is to use heat transfer correlations, such as those used by (Tadaka *et al.*, 1997) to calculate the heat transfer coefficients at all the different locations.

7.5 Reactor cavity view factors

It was mentioned that the view factors used to characterize the radiation heat transfer in the cavity were provided by the KAERI. These were modified and corrected to suit this particular study in section 6.5 and 6.6 to arrive at the results in Figure 7-1 and Figure 7-2. In this section, the Star-CCM+ CFD software was used to calculate the view factors based on the unit cell geometry described in section 4.2. This was done to determine the sensitivity of the model results to different view factors and to verify the validity of the values provided by the KAERI. It must be mentioned at this point that the view factors calculated here are not the real view factors in the cavity but are based on the unit cell geometry. Therefore, a different assumption of the geometry may arrive at different view factors. However, the results presented here should closely resemble the actual values.

A description of the Star-CCM+ radiation heat transfer capabilities can be found in **Appendix G**. A test example was also conducted to illustrate the candidate's ability to use the software, particularly the radiation calculations. The view factor results obtained from the Star-CCM+ calculations are presented in Table 7-7. The values are compared with the updated view factors in Table 7-8 (provided again for easy comparison). It can be seen that there are differences between the two sets of view factors in Table 7-9. However, these differences are due to the small values involved. In-terms of the overall picture, there is a good agreement between the two sets of view factors; particularly the view factors between the RPV and the other surfaces in the cavity. One notable omission from the KAERI view factors is that the downcomer doesn't view itself (i.e. $F_{5\to5}=0$). This is not necessarily true as the downcomer arrangement is concave in the cavity and will have self-views. It has been calculated using Star-CCM+ that $F_{5\to5}=0.05$ or 5% of the radiation from the downcomer is incident upon itself. The calculated view factors will be implemented into the RCCS models to evaluate if these differences will result in significant influences to the results obtained thus far.

Table 7-7: RCCS view factors calculated in STAR-CCM+.

	1 = RPV	2 = Front	3 = Side	5 = Back	6 = DC	Sum	error
1 = RPV	0	0.545	0.383	0	0.0723	1.0000	0.0000
2 = Front	0.782	0.124	0.094	0	0	1.0000	0.0000
3 = Side	0.07	0.0113	0.821	0	0.102	1.0000	0.0000
5 = Back	0	0	0	0	1	1.0000	0.0000
6 = DC	0.051	0	0.41	0.488	0.048	1.0000	0.0000

Table 7-8: The KAERI view factors

	1 = RPV	2 = Front	3 = Side	5 = Back	6 = DC	Sum	error
1 = RPV	*0*	**0.5**	**0.4**	*0*	**0.1**	**1.0000**	0.0000
2 = Front	0.7484	**0.1956**	**0.056**	*0*	0	**1.0000**	0.0000
3 = Side	0.06853	0.00641	**0.81106**	*0*	**0.114**	**1.0000**	0.0000
5 = Back	*0*	*0*	*0*	*0*	1	**1.0000**	0.0000
6 = DC	0.06975	*0*	**0.46425**	0.466	*0*	**1.0000**	0.0000

Table 7-9: Comparing KAERI and Star-CCM+ view factors.

	RPV	Front	Side	Back	Downcomer
RPV	*0.00%*	*8.19%*	*-4.43%*	*0.00%*	*-38.19%*
Front	*4.32%*	*36.62%*	*-67.53%*	*0.00%*	*0.00%*
Side	*-3.87%*	*-75.52%*	*-1.24%*	*0.00%*	*10.86%*
Back	*0.00%*	*0.00%*	*0.00%*	*0.00%*	*0.00%*
Downcomer	*-37.53%*	*0.00%*	*-12.28%*	*4.45%*	*100.00%*

The results of the Flownex® models using the two sets of view factors are given in Table 7-10. It can be seen that there is no significant differences between the results for the two sets of view factors. Therefore, it appears that as long as the view factors are computed appropriately, the result tend to be robust. The view factors provided by the KAERI will be used for further assessment so as to create a consistent basis for future comparisons.

Table 7-10: The KAERI and Star-CCM+ view factor Flownex® results.

Parameter	Units	Flownex® KAERI View Factors	Flownex® STAR-CCM+ View Factors
Total Heat Loss at RPV Surface	**MW**	1.58	1.56
Radiation Heat Transfer at RPV Surface	**MW**	1.40	1.38
Convection Heat Transfer at RPV Surface	**MW**	0.18	0.18
Chimney Air Flow rate in RCCS	**kg/s**	13.08	13.04
Chimney Exit Temperature	**°C**	159.40	158.20
Maximum Temperature of Riser Tube	**°C**	221.00	222.00
Maximum Temperature of Concrete Wall	**°C**	42.90	42.85
ΔP in Riser Tube	**kPa**	0.26	0.26
ΔT in Riser Tube	**°C**	118.00	117.00
RPV average outside temperature	**°C**	325.98	326.28

7.6 Summary of the chapter

In this chapter the Flownex® models developed in ***Chapter 6*** were applied to two steady state conditions; the first was with a temperature boundary condition of 250°C and secondly 350°C. The following were established:

- The RCCS is able to remove 0.82 MW and 1.58 MW of heat from the RPV wall for the 250°C and 350°C cases.
- The air was heated from 40°C to 112.5°C and 159.4°C for the boundary conditions imposed (250°C and 350°C).
- The concrete temperature for both conditions remained well below 65°C.

The second part of this chapter was to determine the sensitivity of the results to selected parameters. The heat removal capacity and the concrete wall temperature were tested for different values of the heat transfer coefficient in the cavity. In the design of a real RCCS, it will be worthwhile to calculate the heat transfer coefficients at the different surfaces and locations in the cavity since it can have a significant influence on the calculated total heat removal rate. It

was found however that the concrete wall temperature only increased by 0.75°C and remained well below the benchmark condition of 65°C for all tests. A heat transfer of 3 W/m^2-K was used for the analysis as a typical value used in heat transfer in buildings.

Finally, the view factors are calculated in Star-CCM+ using the developed unit cell geometry. These view factors are used in the single RCCS Flownex® model and compared with those from the KAERI. There was no significant effects on the model developed using the KAERI view factors.

Chapter 8

8 Modeling selected operational phenomena

8.1 Introduction

There are some operational phenomena that are likely to be encountered during the operation of the RCCS which are necessary to investigate. It was the objective of this study to show that the Flownex® model of the RCCS can be used to model these scenarios and the results can be used as guidelines for design purposes.

The upset condition of 350°C (inside RPV wall boundary condition) will be used for these analyses. Three operational phenomena were selected for this purpose and are explained.

8.2 Flow reversal in the RCCS

In a real RCCS, a situation may arise that the air flow changes direction (i.e. flow from the hot leg to the cold leg). The practical situation could be that there is a higher static pressure at the outlet of the chimney than at the inlet due to changes in atmospheric conditions. Although in practice the design should be such that the potential of this occurring is minimized, the effect of such an event should still be considered. A Flownex® model was set up to model such a scenario.

A slight pressure increase is imposed on the outlet boundary condition element of the RCCS model using the conditions specified in Table 8-1. For the first 50 seconds, the pressure remains at 100 kPa and from there increases linearly for the next 50 seconds until 100.14 kPa and remains at this value for the next 150 seconds. After 150 seconds the pressure decreases linearly to 100 kPa at 300 seconds and will remain at this value for the duration of the simulation.

This particular scenario was also selected to model a transient scenario in the RCCS.

Table 8-1: Pressure pulse scenario setup.

Time (s)	Pressure (kPa)
0	100
50-100	100 + 0.0028*t
100-250	100.14
250 – 300	100.14 - 0.0028*t
300	100

A snapshot of the Flownex® scenario setup is shown in Figure 8-1and Figure 8-2.

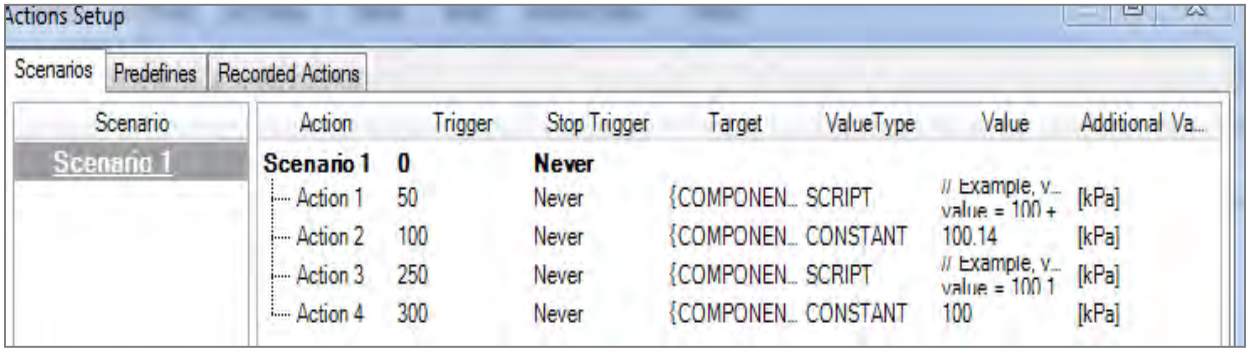

Figure 8-1: Flownex® pressure pulse scenario configuration.

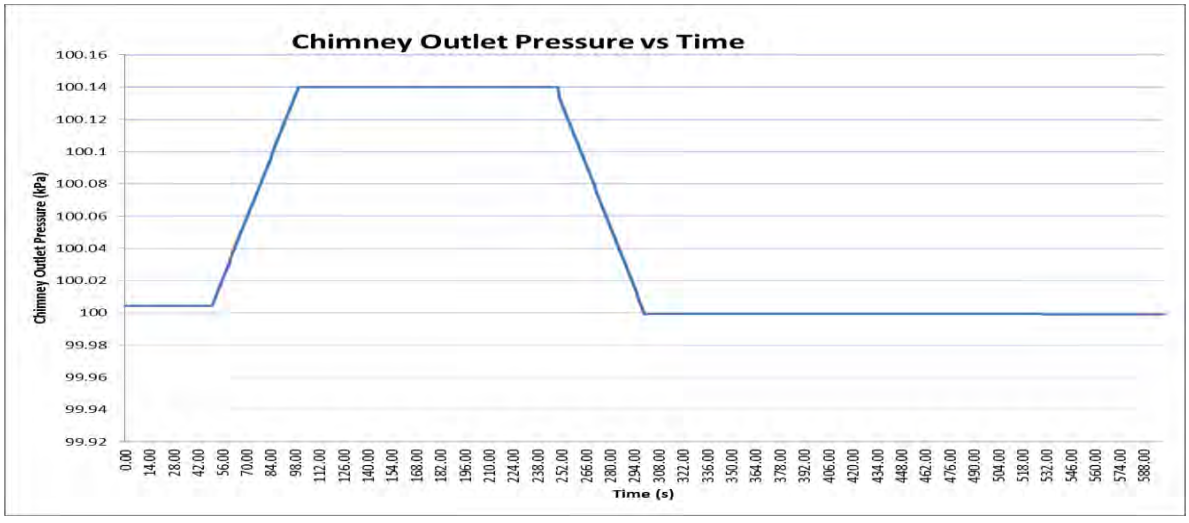

Figure 8-2: Chimney outlet pressure transient setup.

8.2.1.1 Results and discussion

The pressure pulse simulation was done for the single, double and quad loop RCCS Flownex® models. The air flow rate is given in Figure 8-3. Figure 8-4 gives the cold and hot plenum temperatures respectively. Finally, Figure 8-5 shows the concrete wall temperature. Firstly, it can be seen that there is good agreement in the results of the different RCCS riser configurations, further verifying that the double and quad loop RCCS models have been accurately extracted from the single loop model.

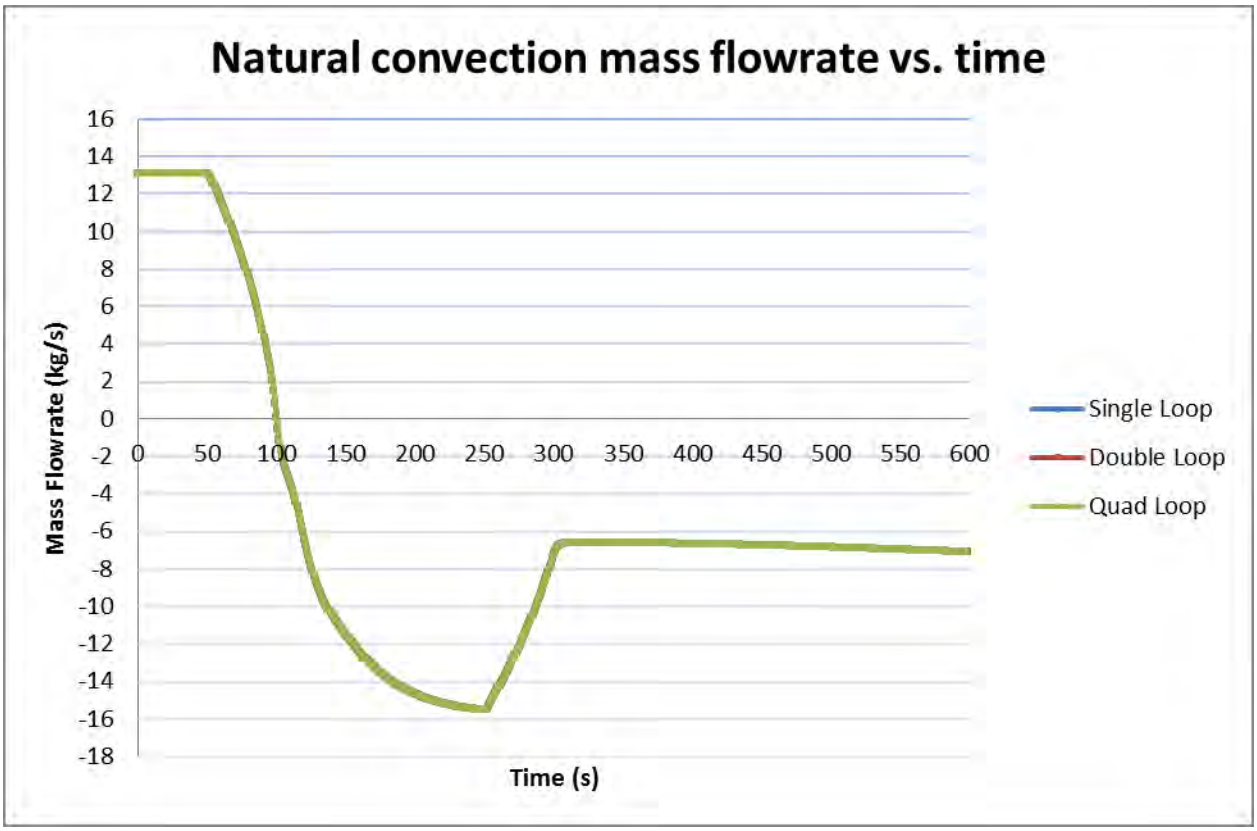

Figure 8-3: Mass flow rate vs. time during pressure pulse transient.

It can be seen from Figure 8-3 that after 50 seconds the air flow rate begins to decrease due to the pressure being increased at the outlet. When the outlet pressure has reached 100.14 kPa, the flow rate is zero and becomes negative from there onwards. The negative flow rate infers that the flow has changed direction and the air is moving from the outlet of the chimney to the inlet. After 250 seconds, the flow rate begins to decrease as the outlet pressure is reduced. This occurs until 300 seconds when the outlet and inlet pressure are again equal and the flow rate settles at a new value of 6.5 kg/s. It is interesting to note that the flow rate continues to increase

in the negative direction reaching -11.8 kg/s after 15.5 hours continuing to heat the concrete wall.

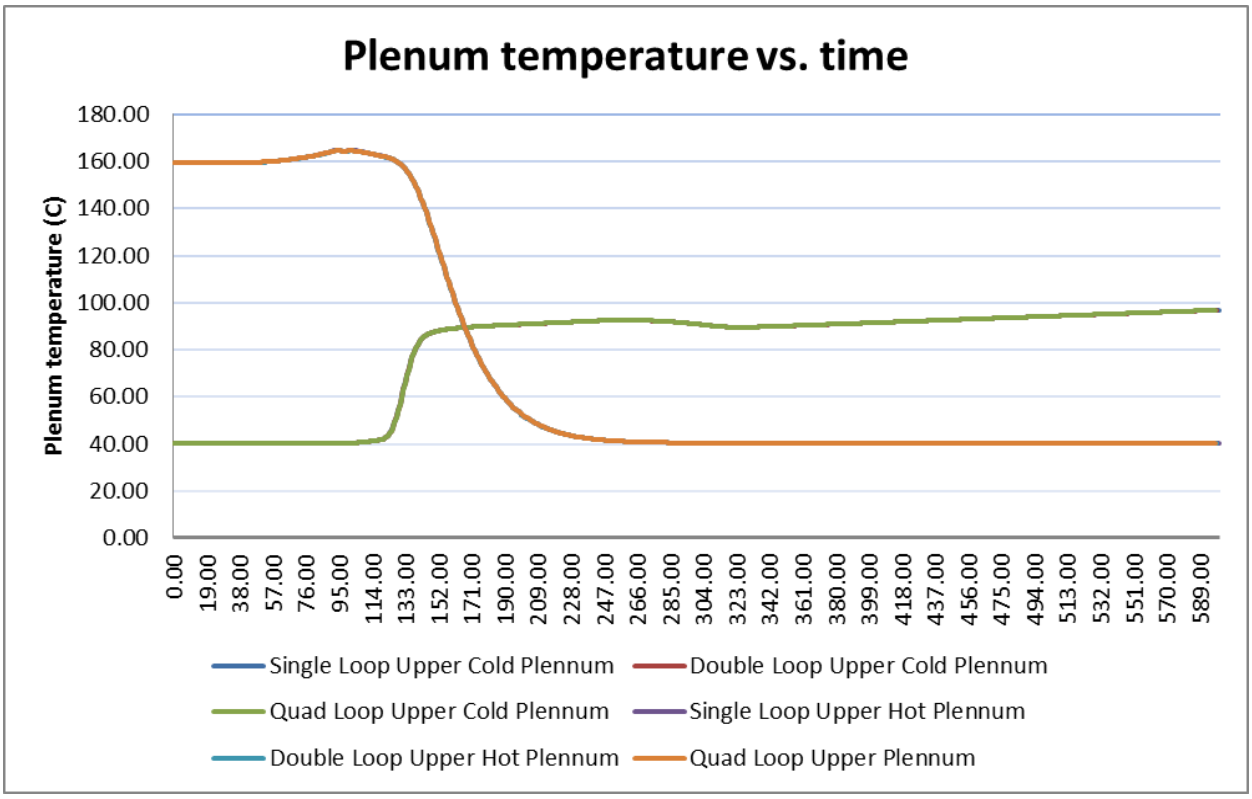

Figure 8-4: Cold and hot plenum temperatures during pressure pulse transient.

In Figure 8-4, the changes in the top and bottom plenum temperatures for a transient scenario are shown. It can be seen that around 110 seconds, the temperature in the bottom plenum begins to rise as a result of the hotter air which has changed direction around 100 seconds. Similarly, the temperature of the hot plenum decreases to indicate that colder air is being drawn in from ambient. The hot plenum cools down to 40°C which is the ambient temperature. The temperature of the cold plenum continues to increase throughout the simulation due to heat received from the reactor cavity.

The outer walls of the downcomer walls are lined with a layer of concrete. Therefore, the temperature of the concrete will increase through conduction heat transfer. This is an undesirable event for the RCCS performance since concrete becomes brittle at temperatures above 65°C, increasing the likelihood of fission product release to the environment. The concrete temperature during the transient is shown in Figure 8-5.

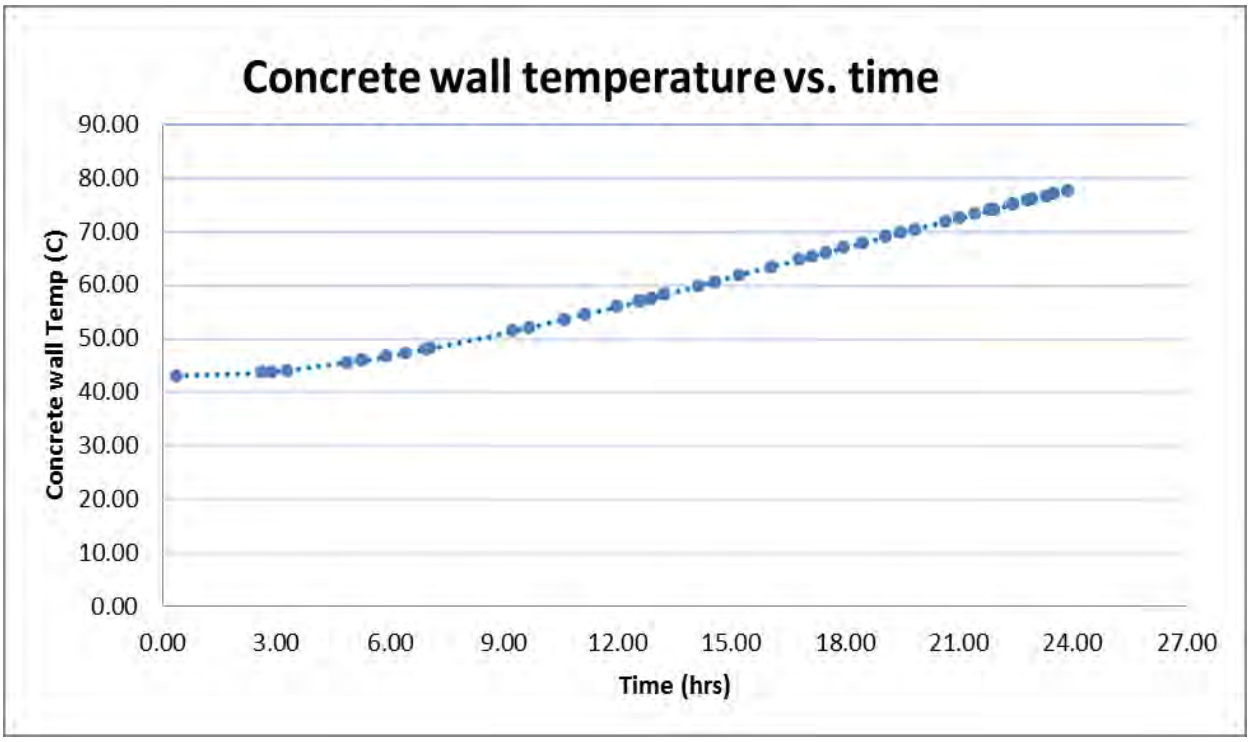

Figure 8-5: Concrete wall temperature during pressure pulse transient.

It can be seen in Figure 8-5 that the temperature of the concrete wall increases with time as the fluid heats the wall. However, due to the large thermal storage capacity of the concrete wall, it takes approximately 17 hours for the temperature to reach 65°C. The temperature of the concrete wall continues to increase as more heat is transferred to the downcomer wall due to increased mass flow rate in the negative direction (i.e. flows from the outlet to the inlet of the chimney).

In this case study it was shown that the model of the RCCS developed in Flownex® can model a scenario with a pressure pulse at the outlet.

8.3 Pipe Breaks

A second scenario that was considered is an event where there is a break in one of the pipes. For this purpose a break in the chimney pipe was selected. The practical situation where this might occur is an event that there is an earthquake and one of the inner ducts containing hot fluid breaks causing a leak of the hot fluid into the cold fluid. This will result in the mixing of the fluids. Shown in Figure 8-6 is a Flownex® canvas of how the pipe break is modelled. Only the

chimney section is indicated here, the remainder of the RCCS Flownex® canvas remains unchanged as shown in Figure 6-12.

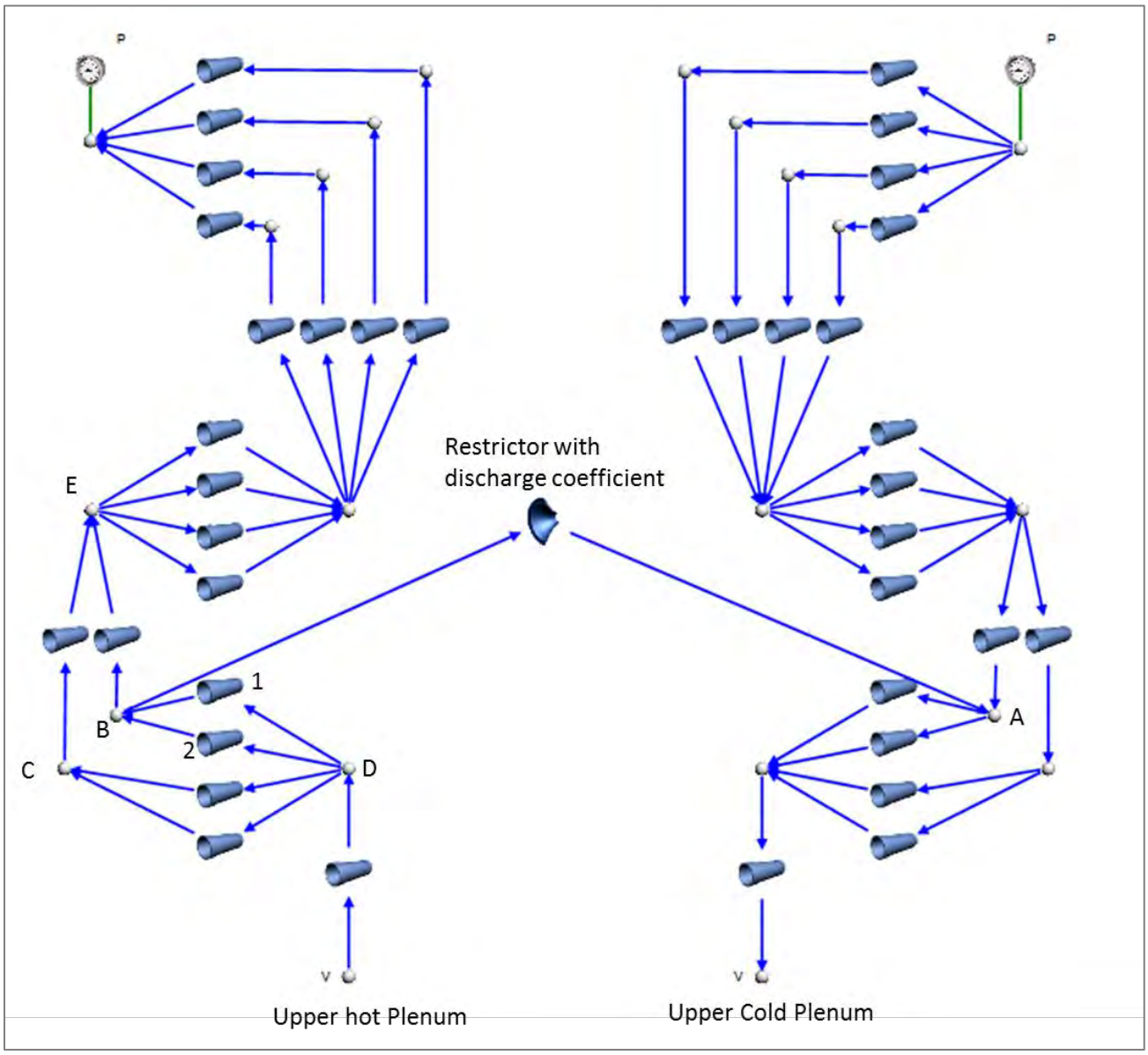

Figure 8-6: Chimney pipe break simulation canvas.

In Flownex® an element (restrictor with a discharge coefficient) was selected. The reason for this selection was that with this element, the user has the choice to choose the fraction that the resistor will be open. This represents the different breaking or opening fractions of the pipe. The inputs to the element are shown in **Appendix A**. For this case study, a full break of the hot fluid pipe (opening fraction is 1) was modelled after 50 seconds at the point **B** indicated in Figure 8-6.

A snapshot of how the transient was modelled is shown in Figure 8-7.

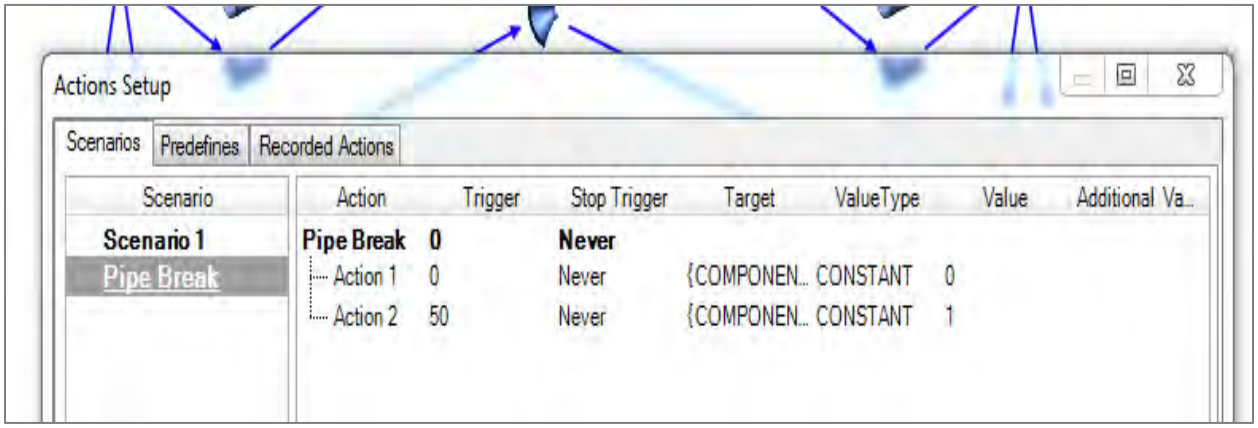

Figure 8-7: Flownex® pipe break scenario configuration.

The results for this simulation are presented below.

8.3.1 Results and discussions

Firstly, it was found that the total mass flow rate through the chimney increases. This is due to the fact that restrictor is added parallel to the RCCS. This decreases the overall resistance and hence an increase in the total mass flow rate. Secondly, at the instant the transient scenario was initiated, the mass flow rate in the riser ducts decreased and immediately there was a flow rate through the restrictor element. The mass flow rate through the restrictor element is negative as can be seen in Figure 8-8. This is an important finding because it means that in the event of a pipe break, the chimney provides enough driving force (due to differences in pressure) to push the cold fluid into the hot fluid. Therefore, the cold air flow is split between the RCCS and the restrictor such that the RCCS operates at a lower mass flow rate.

The negative mass flow rate through the restrictor means that cold air now flows into the pipes containing hot fluid. Therefore, the temperature a point **B** in Figure 8-6 decreases, even to a point of being equal to the temperature at Point **A**. At point **B,** it was noted that a portion of the flow pushes downwards through pipe **B1D** and **B2D** and a portion is drawn upwards through pipe **BE**. The temperature at point **E** is higher than the fluid temperature in **BE**, therefore, the air in pipe **BE** is heated and begins to flow upwards initiating a natural circulation effect, much like in the RCCS riser ducts.

The air flowing downwards through **BD** is heated again at point **D** and flows upwards through **BC** to be ejected to the atmosphere. The buoyancy driven flow in the RCCS is sufficient to keep the flow in the positive direction (i.e. flows from the chimney inlet to the outlet). A simple mass flow rate diagram is shown in Figure 8-9 detailing the direction and magnitude of the flow during a pipe break.

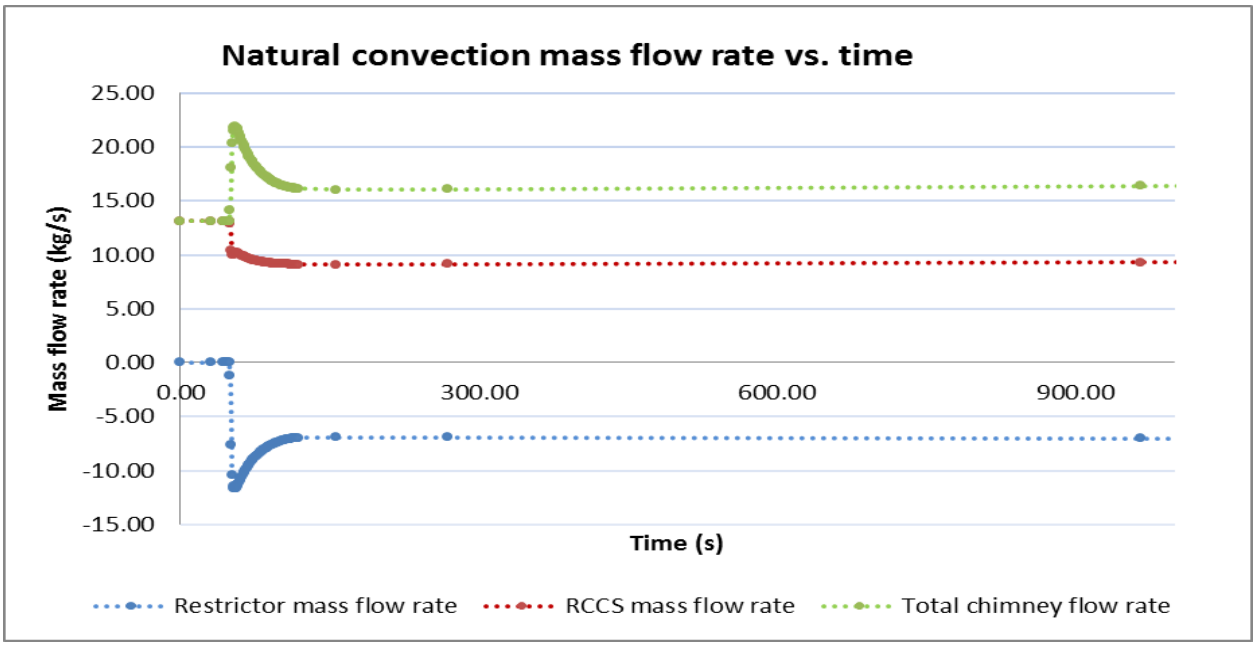

Figure 8-8: Mass flow rate vs. time for a pipe break event.

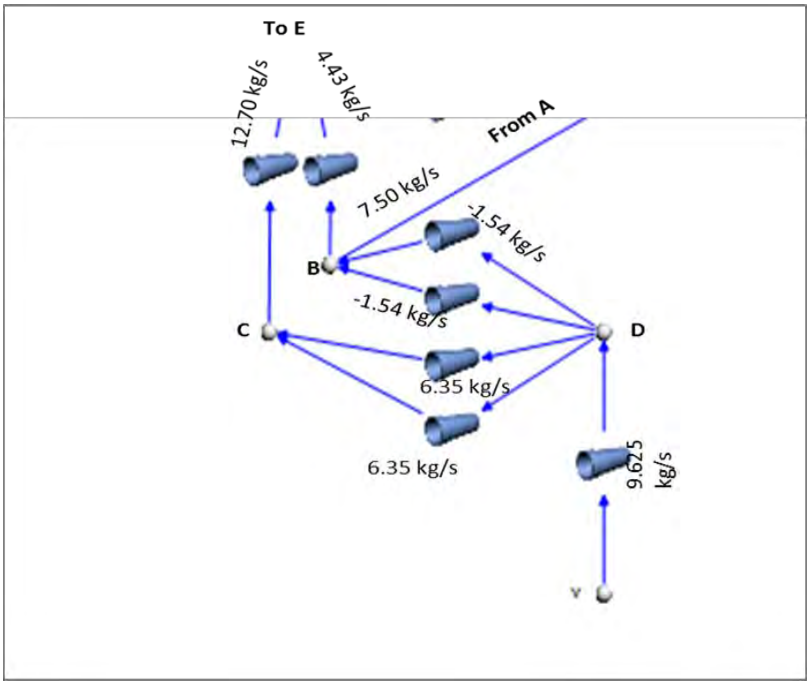

Figure 8-9: Simple mass flow around the position of the pipe break (steady state).

It can be seen from Table 8-2 that the Reynolds number is lower in the event of a pipe break than without owing to the decreased mass flow rate. The decrease in the Reynolds number in turn leads to a reduction in the heat transfer coefficient since Reynolds number is linked to the Nusselt number via the Dittus-Boelter correlation and the heat transfer coefficient is a function of the Nusselt number.

Due to the fact that the RCCS is operating at a lower mass flow rate, its performance is affected. Firstly, it was noted that the total heat removed from the RPV decreases as can be seen in Figure 8-10. This is directly attributable to the increase in the fluid temperature. As the fluid temperature increases due to the reduced mass flowrate, the temperature difference between the walls and the fluid decreases and less heat can thus be removed by the fluid. Furthermore, due to the decreased heat removal in the risers, the temperature of the surfaces in the cavity including the cavity itself increases. Therefore, the radiation and convection heat transfer components decreases due to the decreased temperature difference. Ultimately, this will result in a decrease in the overall heat removal rate from the RPV wall.

Table 8-2: Heat transfer coefficient, Reynolds number and fluid temperature with height during a pipe break.

Height	Heat transfer coefficient	Heat transfer coefficient	Reynolds number	Reynolds number	Fluid Temperature	Fluid Temperature
	Without break	with break	Without break	with break	Without break	with break
m	W/m^2-K	W/m^2-K			°C	°C
1.85	18.24	14.30	19866.10	14496.70	49.74	53.39
3.7	18.40	14.47	19178.00	13839.50	64.99	73.87
5.55	18.54	14.62	18585.20	13300.20	79.27	92.67
7.4	18.68	14.74	18073.00	12851.60	92.61	109.86
9.25	18.80	14.86	17626.20	12475.60	105.07	125.53
11.1	18.90	14.96	17234.40	12157.00	116.68	139.80
12.95	19.00	15.04	16889.40	11885.60	127.49	152.75
14.8	19.09	15.12	16584.60	11653.00	137.53	164.49
16.65	19.17	15.19	16314.10	11452.40	146.86	175.11
18.5	19.25	15.25	16073.30	11279.00	155.51	184.70

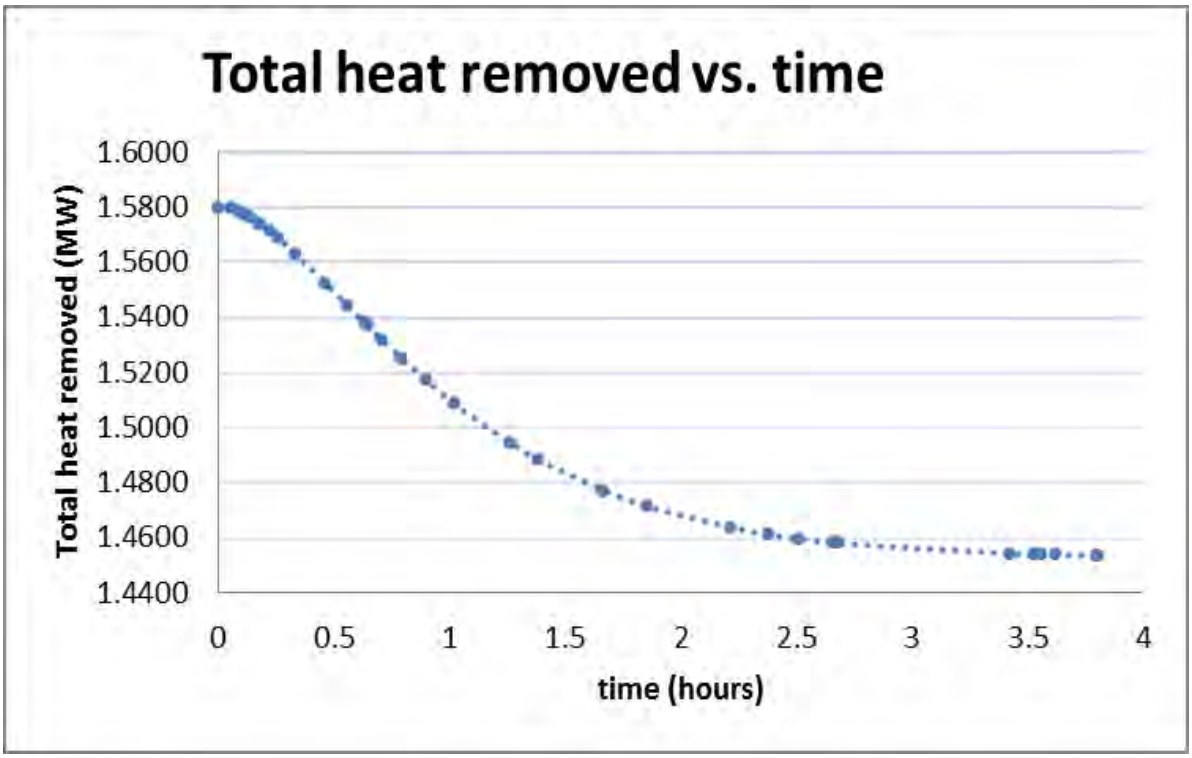

Figure 8-10: Total heat removed from the RPV wall during a pipe break.

The RCCS will be able to remove approximately 1.45 MW of heat from the RPV during this pipe break scenario. A final value of 44.48°C was reached after 5 days for the concrete wall

temperature. This is due to the large thermal storage of the concrete. It can thus be deduced that a break in one of the hot ducts in the chimney will not significantly affect the function of the RCCS, which is to ultimately protect the concrete citadel from overheating, by removing heat from the RPV wall.

8.4 Pipe blockages

Another operational phenomenon that has the potential of being encountered in a real RCCS is an event where there are blockages in the channels. There are many areas in the RCCS where this can occur and will be of interest in a real design. In this analysis, a blockage at the riser inlet was modelled as a reference case to illustrate the capability of the developed Flownex® models to represent such scenarios.

Flow resistance or blockage could potentially cause the RCCS to operate at a lower flow rate. This will result in less heat removal by the RCCS and consequently an increase in the concrete wall temperature. The current RCCS analysis has 220 riser tubes which have been grouped into one, two and quad loops. To model a blockage in Flownex®, an element (resistor with loss coefficient) was selected from the Flownex® library and placed at the inlet to the risers. The inputs to the element are shown in **Appendix A** as well as the relevant information regarding the resistor element. Figure 8-11 shows the Flownex® canvas and the position of the blockage as depicted by the resistor with a loss coefficient.

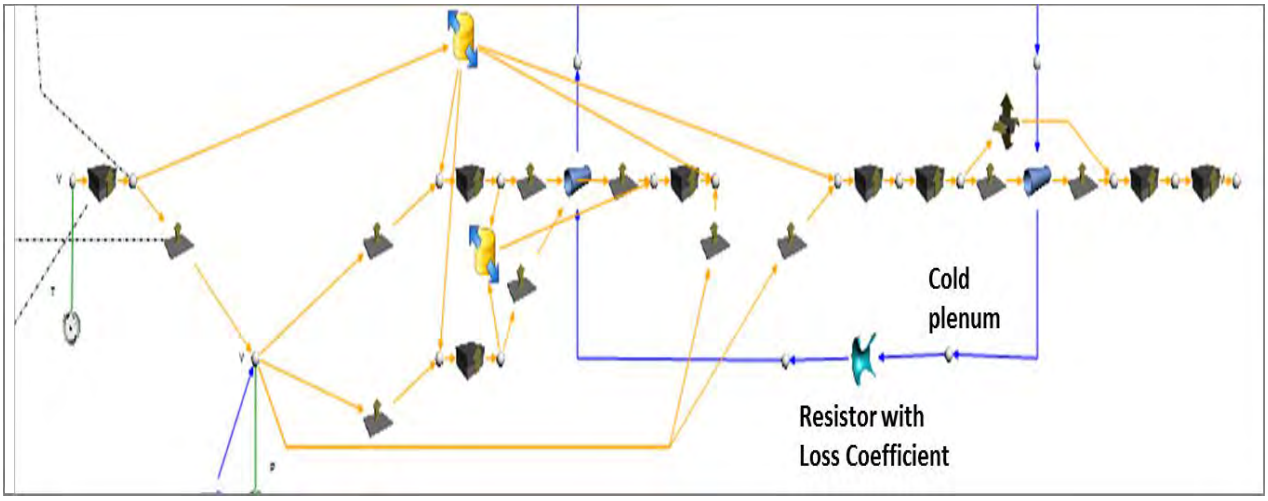

Figure 8-11: Riser blockage Flownex(R) canvas.

The values of C_l^* (loss coefficient) to be used in the Flownex® model are shown in Table 8-3. The blockage fractions that will be modelled are also shown.

Table 8-3: Pseudo Loss Coefficient values for different blockage fractions.

% Blocakge	0.00	0.10	0.20	0.30	0.40	0.50	0.60	0.65	0.70	0.75	0.80	0.85	0.90	0.91	0.92	0.93	0.94	0.95	0.96	0.97	0.98	0.99
Blockage Fraction	0.00	0.10	0.20	0.30	0.40	0.50	0.60	0.65	0.70	0.75	0.80	0.85	0.90	0.91	0.92	0.93	0.94	0.95	0.96	0.97	0.98	0.99
Cc	1.00	0.90	0.80	0.70	0.60	0.50	0.40	0.35	0.30	0.25	0.20	0.15	0.10	0.09	0.08	0.07	0.06	0.05	0.04	0.03	0.02	0.01
C_k	0.06	0.08	0.10	0.13	0.17	0.25	0.39	0.51	0.69	0.99	1.55	2.76	6.21	7.66	9.70	12.67	17.24	24.83	38.80	68.98	155.20	620.79
C_L^*	0.01	1.23	1.56	2.04	2.78	4.00	6.25	8.16	11.11	16.00	25.00	44.44	100.00	123.46	156.25	204.08	277.78	400.00	625.00	1111.11	2279.00	10000.00

The methodology that was adopted to calculate the C_l^* values is detailed in **Appendix A**. Some equations are repeated here for clarity. As an illustration, consider a blockage fraction of 0.7 (70% blockage). The C_c value is the contraction coefficient, defined by;

$$C_c = \frac{100 - \%_{blockage}}{100} = 0.3 \qquad \text{Equation 8-1}$$

Using Equation A–5 the effective area A' can be calculated

$$A' = C_c \times A = 0.85\,\mathrm{m}^2 \qquad \text{Equation 8-2}$$

where

A - Physical area of the throat (2.838 m^2)

The C_k value is calculated directly from Equation A–6

$$C_k = \frac{C_l}{2A'^2} = 0.69 \qquad \text{Equation 8-3}$$

Finally, the value of pseudo-loss coefficient can be C_l^* calculated for a sharp edged orifice from Equation A–7. This is the value that was used as an input to represent a 70% blockage at the

inlet of the riser pipes. Similarly, the C_l^* values calculated in Table 8-3 represent their corresponding blockage fractions in Flownex®.

$$C_l^* = 2A^2C_k = 16 \qquad \text{Equation 8-4}$$

The blockage scenarios were modelled for the following riser configurations: 25%, 50%, 75% and 100% of the risers. When the RCCS models were developed, they were configured into single, double and quad loop groups. To model a situation where all the risers (100%) are blocked at the same time, the single loop was used. To model a blockage in half the risers (50%), a single loop was blocked in the double loop and two loops in the quad loop. It follows that a single loop was blocked in the quad loop for 25% riser blockage and three loops were blocked in the quad loop to indicate a blockage in 75% (three quarters) of the risers.

The results are discussed in the following section, only steady state simulations were conducted for this scenario to indicate the ultimate effect of a blockage on the overall RCCS performance.

8.4.1 Steady state results and discussions

The air flow rates were calculated for the pseudo loss coefficients given in Table 8-3. Firstly, it must be mentioned that the graphs are given for a percentage of risers blocked (i.e. 25, 50, 75 and 100%). In each loop a certain blockage fraction was modelled. Therefore for the 25% blockage (i.e. quarter of risers blocked), a blockage fraction from zero (no blockage) to 99% (25% of the risers are blocked 99%) was modelled. It can be seen that the air flow rate in the RCCS decreases with an increase percentage blocked (number of risers) and blockage fraction. When all risers (100%) are 99% blocked (0.99 blockage fraction), the mass flow rate reduces from 13 kg/s to approximately1 kg/s. In terms of the study this will obviously have an effect on the RCCS performance.

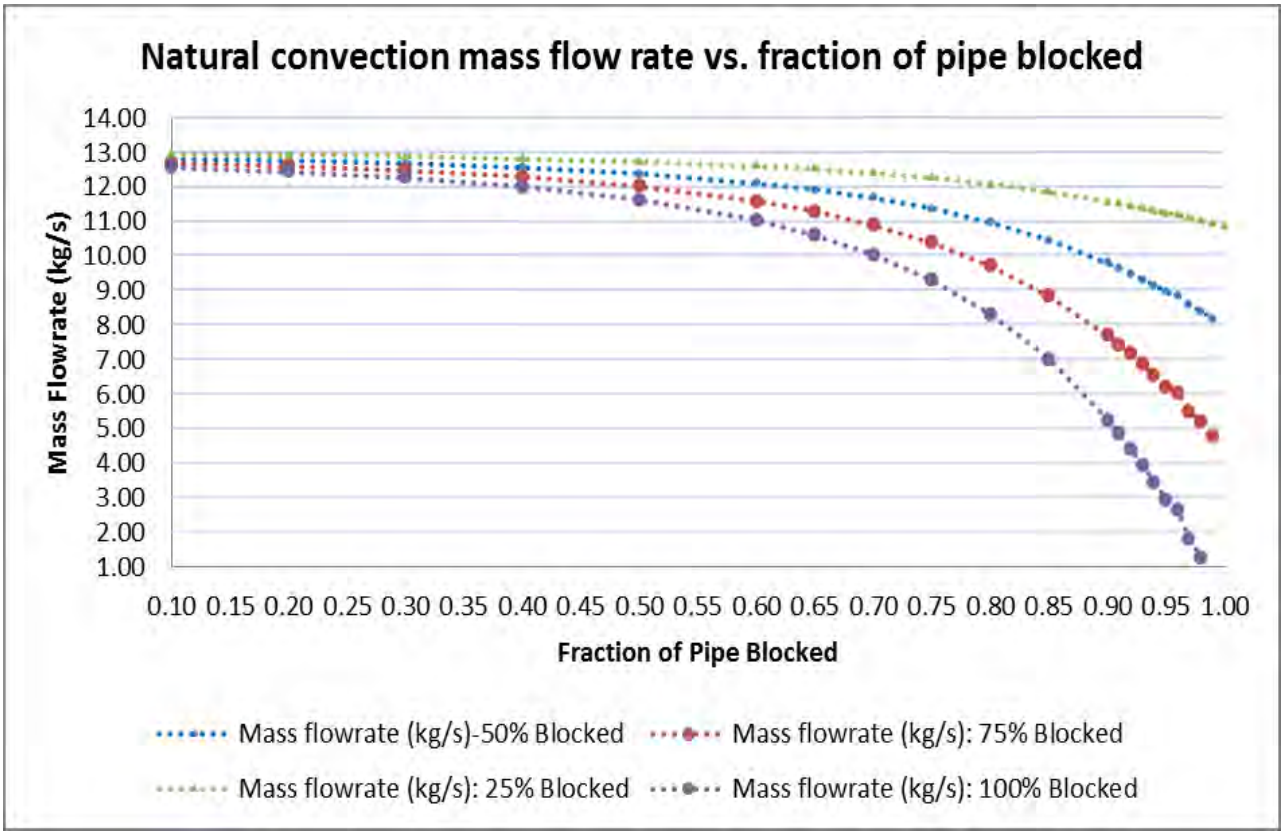

Figure 8-12: Mass flow rate results for pipe blockages.

The total heat removed is given in Figure 8-13 for the conditions imposed on the model. It can be seen that for the case where 99% of all risers (100%) are blocked the heat removal is reduced from 1.56 MW to 0.37 MW. At the same conditions, when half the risers (50%) are blocked, the heat removal only decreases to 1.29 MW, a decrease in heat removal capacity of only 17% compared to 76% if all risers are 99% blocked. It appears Figure 8-13 that significant decreases in heat transfer is achieved when the riser configurations are blocked from 65% onwards due to increased resistance to flow. For the case where 25% (quarter) of the risers are blocked, there was virtually no significant decrease in heat removal capacity to note.

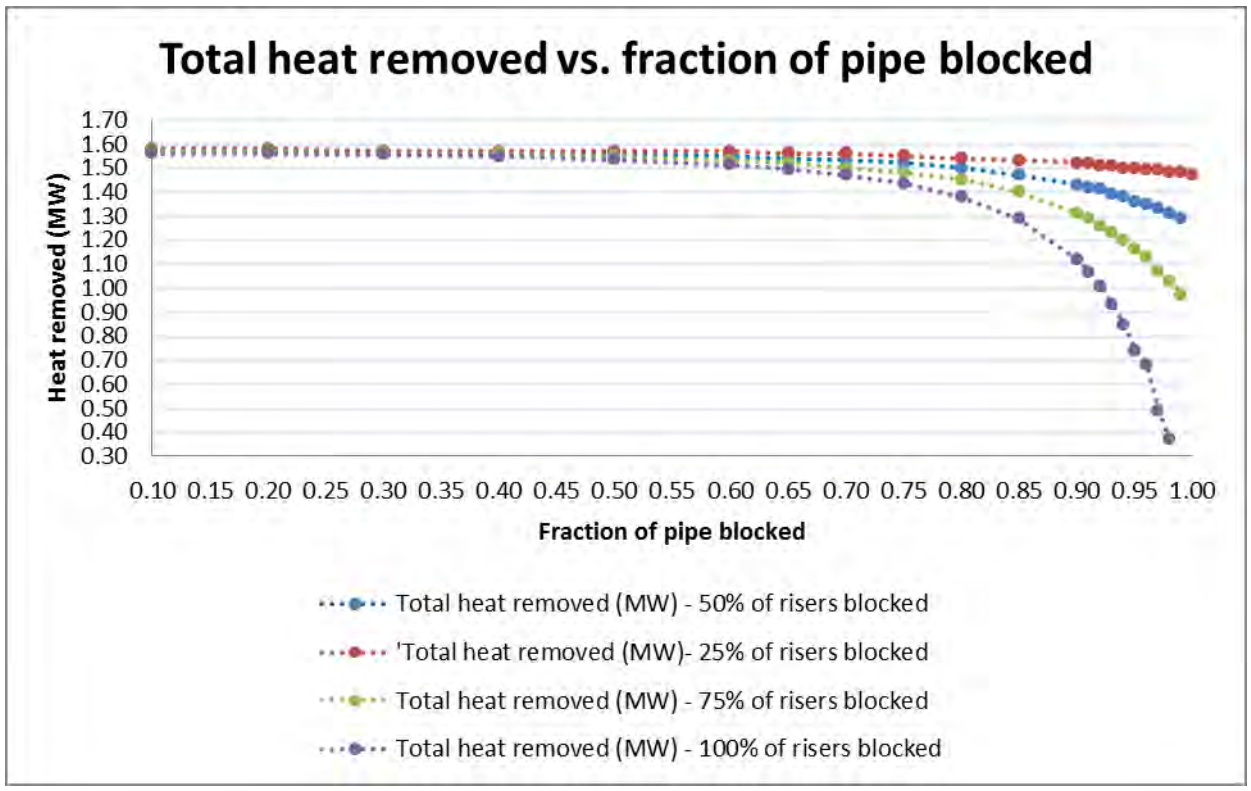

Figure 8-13: Total heat removed vs. fraction of pipe blockage.

A decreased heat removal capacity of the RCCS has a direct influence on the concrete wall temperature. First it can be seen from Figure 8-14 that for the cases (25 – 75%) of the risers blocked, the temperature of the concrete wall is below 65°C. Furthermore, it can be seen that virtually all risers (100%) must have a blockage fraction of 95% or above for the temperature of the concrete to reach 65°C. It can be seen from Figure 8-15, however, that it takes approximately five days for the temperature to reach 60°C. While the likelihood that all 220 risers can be blocked at the same time is low, it can be concluded that even with 75% (three quarters) of the risers blocked, the RCCS maintains its functionality.

Lastly, it was shown that the Flownex® model of the RCCS can be used to analyse situations with pipe blockages. For design purposes this same reasoning can be extended to other parts of the RCCS as the designer sees fit.

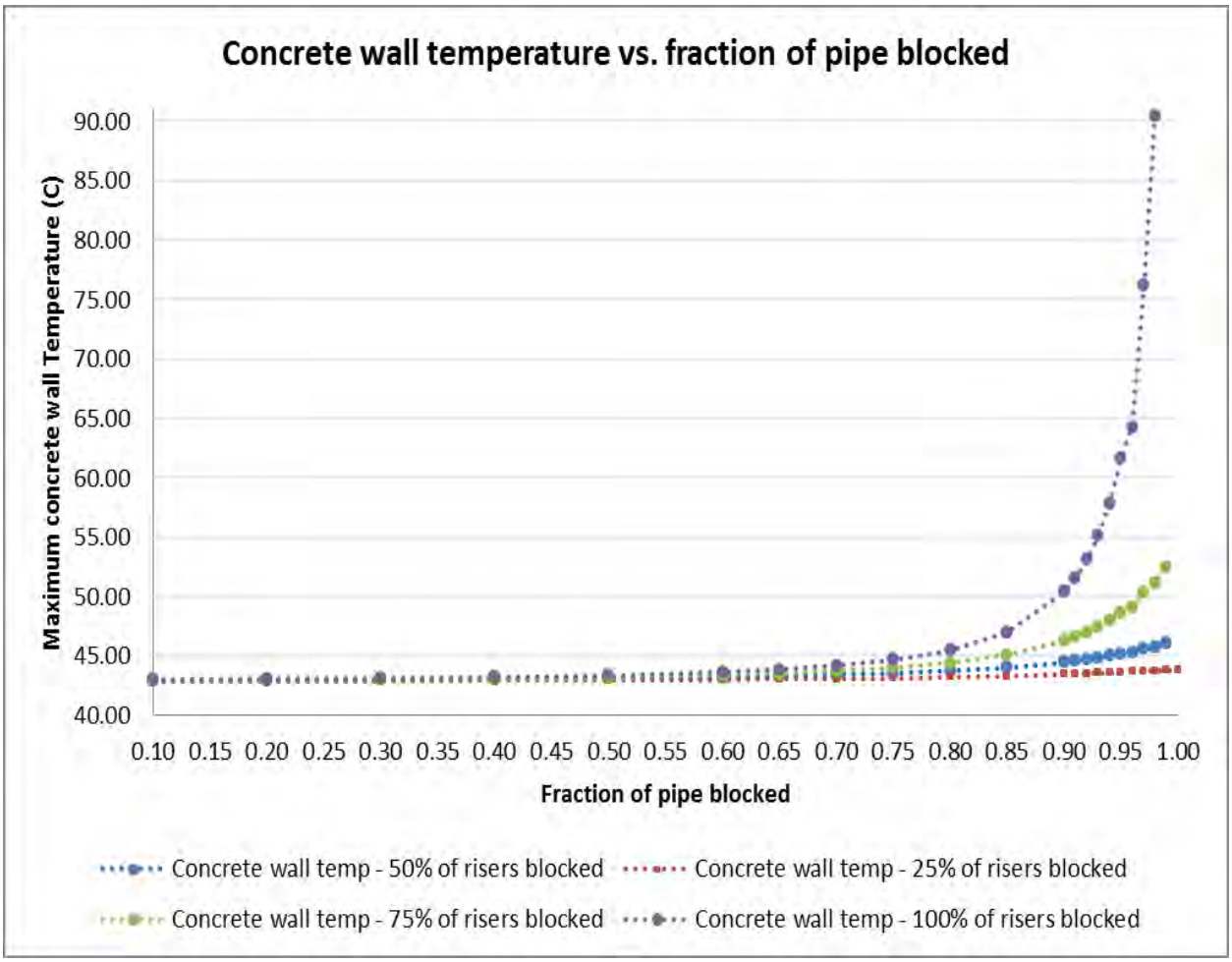

Figure 8-14: Maximum concrete wall temperature vs. fraction of pipe blocked.

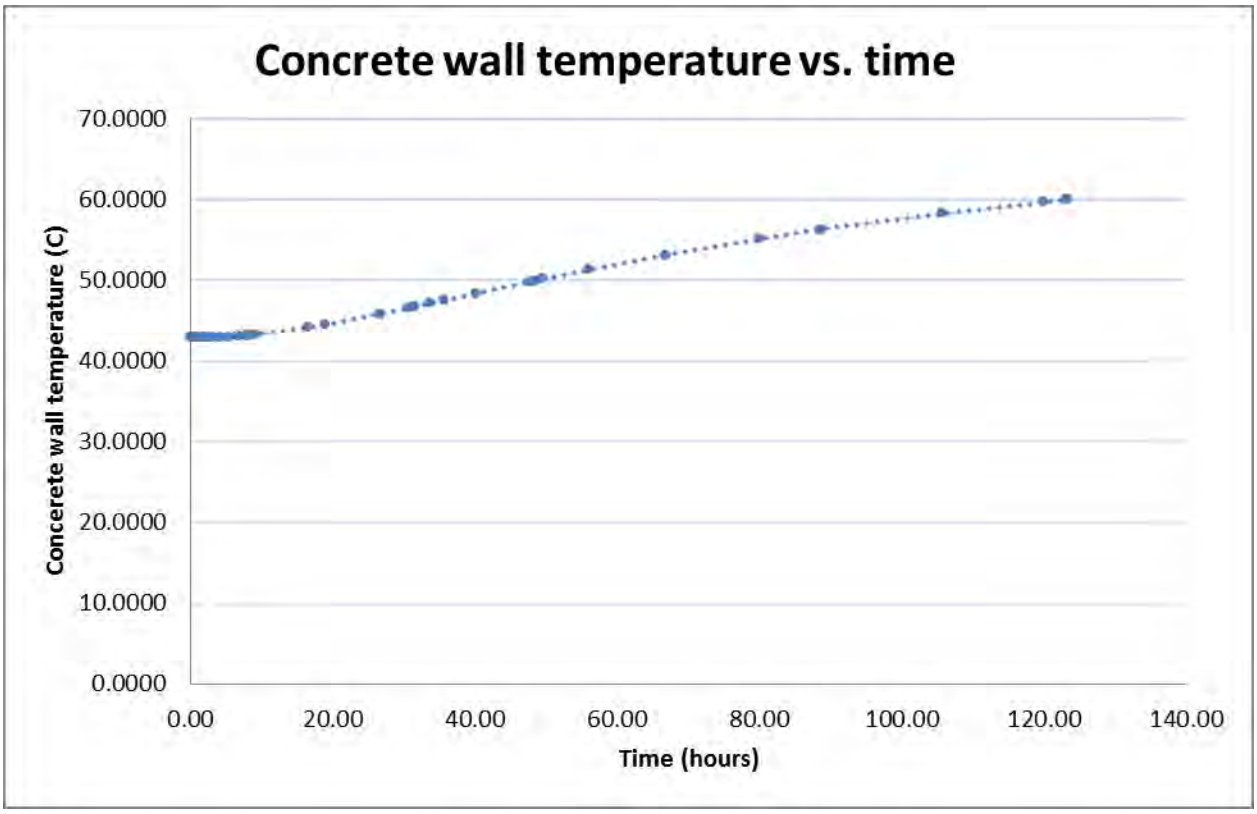

Figure 8-15: Concrete wall temperature during pipe blockage scenario.

8.5 Summary of the chapter

The main aim of this chapter was to apply the models developed in ***Chapter 6*** to three selected transient and steady state scenarios to illustrate the operational characteristics of the RCCS system. The following emanated from this chapter:

- Flownex® models of the RCCS that represent a pipe break, pressure pulse at the outlet and pipe blockage scenarios were developed. The qualitative results are available and can be used for future comparative studies.

- Due to the large thermal storage capacity of the concrete, it takes a long time for the concrete wall temperature to reach 65°C. Therefore, even if the flow reverses, there is no immediate danger in as far as overheating of the concrete wall is concerned.

- Even in the event of a break in the hot chimney duct, the RCCS retains most of its ability to remove the heat, even at a reduced mass flow rate.

- Finally, it was found that virtually all the RCCS pipes have to be blocked to above 95% for the concrete wall temperature to exceed 65°C.

Chapter 9

9 Summary and conclusions

The VHTR is a leading candidate for the Next Generation Nuclear Plant (NGNP). A major discussion regarding deployment of these reactors is centred on improving the safety aspects, by designing reactor concepts that utilize passive cooling systems as opposed to active cooling systems.

The design of the RCCS requires attention, both from an experimental and analytical point of view in order to build confidence in the models that will be used to characterise its performance, and to aid in the design of a real life RCCS. In this study, the software package Flownex® was used to evaluate its ability to simulate the important phenomena associated with the air-cooled RCCS concept. This involves proper characterization of the heat transfer in the reactor cavity and fluid flow in the RCCS itself.

The main objective of this study was to establish a methodology to create a system level process model of a typical air cooled RCCS in Flownex®. Secondly, to illustrate its ability to simulate different scenarios that will illustrate the operational characteristics of such a system. To achieve these objectives a number of enabling goals were deduced.

The first goal was to conduct a literature review on the concepts and techniques used to create a model of the RCCS. This was the particular focus of **Chapter 2.** It was found that currently there are two RCCS modes under consideration; a water-cooled RCCS and air-cooled RCCS, or a combination of both. An overview of theoretical work relating to RCCSs of the most recent designs was given. It emerged that investigations have successfully demonstrated the heat removal capabilities of the RCCS experimentally and theoretically using CFD and system codes. The major finding from the literature study was that forced convection correlation values for the heat transfer coefficient and friction factor can be applied to model heat transfer and fluid flow in the RCCS downcomer and riser tubes.

The second goal was to identify the major physical phenomena that need to be taken into account in the model in order to simulate the operational characteristics. The literature review revealed the following that must be accounted for:

- Radiation and convection heat transfer in the cavity.
- Conduction heat transfer through all solid parts.
- Convection and radiation heat transfer inside the riser standpipes and the down comer.
- Flow of air in the chimney.

The third goal was to develop a Flownex® model of the existing RCCS concept design that captures the major physical phenomena. The envisioned PMR200 RCCS was used for this purpose. A basic simulation model of a simple U-tube was constructed to verify that the Flownex® software is accurately setup to perform natural circulation calculations. The model was compared with the results of an EES model for the same simplified case study. Good agreement was found between the models regarding the mass flow rate calculation. Secondly, Flownex® was tested to perform heat transfer calculations with radiation, conduction and convection taking part. For this case the mass flow rate was held constant. A single increment of the RCCS was modelled both in EES and Flownex® and there was good agreement between the results of the models, even when the pipe elements were divided into two loops as opposed to a single loop.

The fourth goal was to identify, obtain or generate suitable input data for the Flownex® model. This is shown in Table 6-1. Three models were constructed, a single loop model and a double and quad loop RCCS models which are mirror symmetric images of the single loop. Using these models, steady state simulations as well as selected transient simulations were done. The steady state simulations were used to determine the heat removal capacity of the RCCS and the maximum temperature of the concrete wall under certain boundary conditions. Transient simulations were done to demonstrate the ability of the Flownex® models to represent certain operational phenomena that can be encountered in a real life RCCS.

Finally, the last goal was to evaluate the results of the simulations and put forward insights gained that may be useful in the future design of a real-life air cooled RCCS. In **Chapter 7**, the

results of the steady state simulations are given while **Chapter 8** focussed on the modelling the operational phenomena that can be encountered.

The following are the major conclusions that can be drawn from the study:

- The RCCS carries with it enough heat to the ambient such that the concrete wall temperature is maintained below the benchmark value of 65°C.

- In the design of a real RCCS it will be necessary to calculate appropriate values for the heat transfer coefficients at the different surfaces and locations in the cavity.

- There was no significant effects on the model developed using the KAERI view factors versus that with the calculated view factors. It is however important to have a good representative set of view factors since the calculated radiation heat transfer rate is directly dependent on it.

- In the event of a pressure pulse, the flow can change direction in the RCCS and the concrete wall can heat up reaching temperatures above the benchmark value of 65°C. However, due to the large thermal storage capacity of the concrete, this takes a long time, approximately 17 hours. It may therefore be possible to mitigate this risk via appropriate operational procedures and measures.

- In the event of a break in one of the pipes carrying the hot fluid in the chimney, the RCCS still retains its functionality, even though it is operating at a lower mass flow rate. It was also noted that the temperature of the concrete wall does not exceed the benchmark condition of 65°C.

- Finally, it was established that all the riser pipes must be blocked from 95% onwards for the temperature of the concrete wall to reach 65°. In a real life RCCS, it may be impossible to clean out individual risers due to the manner in which the RCCS will be constructed. Therefore, it is encouraging that even with 75% (three quarters) of the riser tubes blocked; the RCCS still maintains its functionality.

Based on the findings elaborated above, the objectives of this study have been achieved. The qualitative results are valuable since they can be used to compare with the KAERI results as part of the collaboration study between the KAERI and the NWU. The newly developed models

are conceptually simple and computationally efficient solving within a few seconds for steady state solutions. The RCCS models developed will provide a solid background for other researchers in this field or as a guideline during the design phase.

Chapter 10

10 Contributions and recommendations

10.1 Contributions

The following were identified as the major contributions of this study:

- This study contributes to the development of numerical codes that can be used in the design and analysis of the RCCS.
- To promote the South African software Flownex® in the field on nuclear engineering in order to create more confidence in the software.
- The literature review has looked into various RCCS options currently being investigated, and therefore can serve as a starting basis for future and current researchers in this field.
- The major contribution of this study is that an integrated Flownex® model of the RCCS was developed. The impact of selected steady state and transient phenomena on the overall performance of the RCCS are also shown which can be a useful guideline during the scoping and design phase of a real RCCS.
- The results obtained can be used for inter code comparisons between the NWU and the KAERI as part of a collaboration study between the two institutions.

10.2 Recommendations

The following are some of the suggestions emanating from this study:

- The heat transfer coefficient must be calculated for the different surfaces or regions in the cavity.

- After obtaining applicable power profiles or decay heat profiles, the RCCS performance can be investigated for a PLOFC or DPLOFC scenarios.

- Once the geometries of the bottom and hot plenum are known; they should be incorporated into the model.

- Include an additional chimney to model an RCCS with multiple inlets and outlets. This will enable future studies to investigate for instance, the mixing of fluids in the upper collectors of the chimneys.

- The models were developed under the assumption that the riser tubes surround the RPV radially. The models should be converted to an almost square cross-section and therefore, the new view factors have to be calculated.

- Consider radiation heat transfer between different elevations.

- If a temperature boundary condition is used, accurate temperature profiles on the inside RPV wall must be sourced and can easily be applied in the model.

- The concrete temperature was assumed to be constant at the different heights as a first approximation. The temperatures at the different heights can be calculated by including cross conduction elements and using independent nodes at the different elevations along the wall in the Flownex® models.

- The temperatures in the cavity were assumed to be constant at the different regions and elevations. For future studies, the temperatures at the different regions can be calculated using a CFD code and used in the Flownex® models.

11 Works Cited

Anon. 2013. Flownex Library Manual. Potchefstroom: M-Tech Industrial.

Anon. 2013. Flownex Version 8.0 User manual. Potchefstroom: M-Tech Industrial.

Bae, Y.Y., Hong, S.D. & Kim, Y.W. 2012. Scaling analysis of reactor cavity cooling system for PMR200. (*In* Proceedings of the HTR 2012. Tokyo: Available from: http://www.sciencedirect.com/science/article/pii/S0029549313007073. [20 May 2014].)

Brey, H.L. 2000. Current status and future development of modular high temperature gas cooled reactor technology. Vienna: IAEA.: Available from: http://www-pub.iaea.org/MTCD/Publications/PDF/te_1198_prn.pdf. [3 March 2014]. (IAEA-TECDOC-1198).

Capone, L., Hassan, Y.A. & Vaghetto, R. 2011. Reactor Cavity Cooling System (RCCS) experimental characterization. *Nuclear Engineering and Design*, 241(12):4775-4782.

Cegnel, A.Y., Turner, R.H. & Cimbala, J.M. 2008. Fundamentals of Thermal-Fluid Sciences. 3rd ed. New York: McGraw-Hill. (877-919).

Chang, H.OH., Cliff, Davis., Larry, Siefken., Richard, Moore., Hee, C.No., Jong, Kim., Goon C. Park, John,C.Lee. & William, R.Martin. 2006. Development of Safety Analysis Codes and Experimental Validation for a Very High Temperature Gas-Cooled Reactor. Idaho National Laboratory: Available from: http://www.inl.gov/technicalpublications/documents/3028244.pdf. [21 February 2014]. (INL/EXT-06-01362).

Cheng, X., Erbacher, F.J. & Neitzel, H.J. 2000. Passive containment cooling by natural air convection and thermal radiation after severe accidents. *Nuclear Engineering and Design*, 202:219-229.

Cheng, X. & Muller, U. 1998. Turbulent natural convection coupled with thermal radiation in large vertical channels with assymetric heating. *Internation Journal of Heat and Mass transfer*, 41(12):1681 - 1692.

Coulson, J.M. & Richardson, J.F. 1999. Fluid flow, Heat transfer and Mass transfer. Sixth ed. 1 vols. Oxford: Butterworth-Heinemann. (447-455).

CRP. 2000. Heat Transport and Afterheat Removal for Gas Cooled Reactors Under Accident. VIENNA: Available from: http://www-pub.iaea.org/MTCD/publications/PDF/te_1163_prn.pdf. [24 April 2014]. (IAEA-TECDOC-1163).

Dilling, D.A., Ghose, S.K. & Berkoe, J.M. 1982. Passive Decay and Residual Heat Removal in the MHTGR. (*In* IAEA-TECDOC-757. Vienna: IAEA. p. 75-82.)

DOE. 2014. Passive Heat Removal System Testing Supporting the Modular HTGR Safety Basis. IAEA technical meeting, Idaho National Laboratory: Available from: http://www.iaea.org/NuclearPower/Downloadable/Meetings/2014/2014-04-08-04-11-TM-NPTDS/16_Kinsey01.pdf. [5 September 2014].

Fedorov, A.G. & Viskanta, R. 1997. Turbulent natural convection heat transfer in an asymmetrically heated, vertical parallel-plate channel. *Internationa Journal of Heat Mass Transfer.*, 40(16):3849-3860.

Frisani, Angelo. 2010. Analysis of the Reactor Cavity Cooling System for Very High Temperature Gas-Cooled Reactors Using Computational Fluid Dynamic Tools. Texas: Texas A&M University. (Master of Science Thesis).

Frisani, A., Hassan, Y.A. & UGAZ, V.M. 2011. Computational Fluid Dynamics Analysis of Very High Temperature Gas-Cooled Reactor Cavity Cooling System. *Nuclear Technology*:238-259.

Galanis, Nicolas. & Behzadmehr, Amin. 2008. Mixed Convection in Vertical Ducts. (*In* 6th IASME/WSEAS International Conference on Fluid Mechanics and Aerodynamics. Rhodes. p. 35-43.)

Gang, Fu. 1991. Experimental and Analytic Evaluation of Gas-Cooled Reactor Cavity Cooling System Performance. Boston: Massachusetts Institute of Technology.: Available from: http://dspace.mit.edu/handle/1721.1/13290. [16 August 2013]. (PhD Thesis).

Gao, Z., Shuyan, H.E. & Zhang, M. 1992. Afterheat removal for HTR-10 Test Module inder accident condition. (*In* IAEA-TECDOC-757. Vienna: IAEA. p. 63-72.)

GIF. 2002. A Technology Roadmap for Generation IV Nuclear Energy Systems. Available from: https://www.gen-4.org/gif/upload/docs/application/pdf/2013-09/genivroadmap2002.pdf. [16 July 2013]: U.S. DOE Nuclear Energy Research Advisory Committee and the Generation IV International Forum.

Golovo, V.F., Kiryushin, A.I. & Kuzzavkov, N.G. 1992. Flow Schemes and design features of HTGR residual heat removal systems. (*In* IAEA-TECDOC-757. Vienna: IAEA. p. 72-75.)

Gougar, Hans. D. & Schultz, Richard. 2010. Next Generation Nuclear Plant Methods Technical Program Plan. Idaho Falls: Idaho National Laboratory.: Available from: https://www.google.co.za/?gws_rd=ssl#q=Next+Generation+Nuclear+Plant+Methods+Technical+Program+Plan+INL%2FEXT-06-11804. [13 September 2013]. (INL/EXT-06-11804).

Greyvenstein, G.P. 2001. An implicit method for the analysis of transient flows in pipe networks. *International Journal for Numerical Methods in Engineering*:1127-1143.

Hicks, Thomas. E. 2011. Next Generation Nuclear Plant Project: Modular HTGR Safety Basis and Approach. Idaho: Idaho National Laboratory: Available from: https://www.google.co.za/?gws_rd=ssl#q=Next+Generation+Nuclear+Plant+Project:+Modular+HTGR+Safety+Basis+and+Approach. [3 November 2013]. (INUEXT-11-22708).

Ibrahim, Ummi. Kalthum. & Mohd, Salleh. Ruzitah. 2012. Application of Network Representation Model for radiation analysis. *International Journal of Chemical Engineering and Applications*, 3(3):195-200.

Ibrahim, U. K., Mohd, Salleh. R. & W.b, Zhou. 2012. Radiation Heat Transfer Analysis in High Emissivity Baking Oven Using Network Representation Method. *APCBEE Procedia*, 3:11-16. 5-6 May.

Incropera, Frank. P. & DeWitt, David. P. 2002. Fundamentals of Heat and Mass Transfer. Fifth ed. New Jersey: John Wiley & Sons. (1-34;789-811).

Jackson, J.D., Cotton, M.A. & Axcell, B.P. 1989. Studies of mixed convection in vertical tubes. *Int. J. Heat and Fluid Flow*, 10(1):1-15.

Jun, J. 2012. Nuclear Hydrogen Project Calculation Note. Calculation Note. Potchefstroom: distributed to the University of North-West on 5 February 2014.

Kim, S., Park, R.Y. & Sim, Y.S. 2006. Analysis on the heat transfer characteristics in an air cooled Rccs of a HTGR. (*In* In NTHAS5: Fifth Korea-Japan Symposium on Nuclear Thermal Hydraulics and Safety. Jeju. p. 1-7.)

Kugeler, K. 1992. Principles of decay heat removal in reactor technology - present status and future prospects. (*In* IAEA-TECDOC-757. Vienna: IAEA. p. 15-29.)

Kumar, P.P., Khardekar, A. & Iyer, K.N. 2012. Experimental and Numerical Investigation on a Two-Phase Natural Circulation Test Facility. *Heat Transfer Engineeing*, 33(9):775-85.

Lee, Jeongik. 2005. The Flow Structure under Mixed Convection in a Uniformly Heated Vertical Pipe. Boston: Massachusetts Institute of Technology.: Available from: http://dspace.mit.edu/bitstream/handle/1721.1/34449/70691594.pdf?sequence=1. [16 March 2014]. (Msc Thesis).

Lisowski, D.D., Haskin, T.C., Tokuhiro, A. & Anderson, M.H. 2013. Study on the behaviour of an assymetrically heated reactor cavity cooling system with water in single phase. *Nuclear Technology*, 183:75-87.

Lommers, Lew. 2010. HTGR Technology Course for the Nuclear Regulatory Commision. Module 10d: Available from: https://inlportal.inl.gov/portal/server.pt?open=space&name=Dir&id=cached&psname=Dir&psid=1&in_hi_userid=2&cached=true&control=DirRepost&rangeFrom=21&rangeTo=30&subfolderID=2683&DirMode=1. [10 February 2014].

Lomperski, S., W.D, Pointer., Tzanos, C.P., Wei, T.Y.C. & Krauss, A.R. 2011. Generation IV Nuclear Energy System Initiative. Air-Cooled Option RCCS Studies and NSTF Preparation. Argonne National Laboratory: Available from: http://www.ipd.anl.gov/anlpubs/2012/11/71292.pdf> [9 August 2013].

Mears, L.D. & GoodJohn, L.J. 1989. The status of high-temperature gas-cooled reactor development and design. (*In* IAEA Bulletin, 3. p. 36-39.)

Park, G.C., Cho, H.K. & Cho, H.K. 2006. Assessment of a new design for a Reactor Cavity Cooling System in a High Temperature Gas-Cooled Reactor. *Nuclear Engineering and Technology*, 38(1):45-60.

Rousseau, PG. & Van Eldik, M. 2013. Thermal-Fluid systems modelling 1 - Lecture Notes. Potchefstroom: North West University.

Sim, Y.S., Park, R.Y. & Kim, S. 2007. Development of a new decay heat removal system for a high temperature gas-cooled reactor. *Annals of Nuclear Energy*, 34:803-812.

Tadaka, Shoji., Suzuki, Kunihiko., Ingagaki, Yoshiyuki. & Sudo, Yukio. 1997. Design and Evaluation Methods for a Water Cooling Panel System for Decay Heat Removal from a High-Temperature Gas-Cooled Reactor. *Heat Transfer - Japanese Research*:159 - 175.

Tak, NamIL., Kim, MinHwan., Lim, Hong. Sik. & Jae, Man. 2011. A Practical Method for Whole-core Thermal Analysis of a Prismatic Gas-cooled Reactor. *Nuclear Technology*, 177:352-365.

Terekhov, V.I. & Ekaid, A.L. 2012. Turbulent free convection between vertical isothermal plates with asymetrical heating. *Thermodynamics and Aerodynamics*, 20(2):151-162.

Theron, William. 2013. Flownex Traing Course-Lecture Notes, M-Tech Industrial. Potchefstroom: M-Tech Industrial.

Tzanos, C.P. 2005. CFD Analysis for the Applicability of the Natural Convection Shutdown Heat Removal Test Facility (NSTF) for the Simulation of the VHTR RCCS. Argonne National

Laboratory: Available from: http://www.ipd.anl.gov/anlpubs/2007/05/59274.pdf. [6 November 2013].

USER-GUIDE. 2012. STAR-CCM+. Version 7.06 vols. CD-ADAPCO.

Verwey, Aldo. 2010. Modelling of a passive Reactor Cavity Cooling System (RCCS) for a nuclear reactor core subject to environmental changes and the optimisation of theRCCS radiation heat shield. Stellenbosch: University of Stellenbosch. (Msc Thesis).

Vilim, R.B., Feldman, E.E., Pointer, W.D. & Wei, T.Y.C. 2004. INITIAL VHTR ACCIDENT SCENARIO CLASSIFICATION: MODELS AND DATA. Argonne National Laboratory: Nuclear Engineering Division.: Available from: http://nuclear.inl.gov/deliverables/docs/screening_1.pdf. [3 April 2014]. (Status Report).

Wei, T.Y.C. 2012. Ex-Vessel Heat Removal (Reactor Cavity Cooling System) Update. Argonne National Laboratory: Available from: https://secure.inl.gov/vhtrrdtr12/pres/MethodsExp/05_Wei_ExCoreHeat.pdf. [17 June 2014].

Yilmaz, T. & Frazer, S.M. 2007. Turbulent natural convection in a vertical parallel-plate channel with asymmetric heating. *International Journal of Heat and Mass Transfer*, 50:2612-2623.

You, Jongwoo., Yoo, Jung. Y. & Choi, Haecheon. 2002. Direct numerical simulation of heated veritcal air flows in fully developed turbulent mixed convection. *Internation Journal of Heat and Mass Transfer*, 46:1613-1627.

Zhen, N. 2008. Prismatic Modular Reactor Analysis with MELCOR. Texas: Texas A&M University.: Available from: http://repository.tamu.edu/bitstream/handle/1969.1/ETD-TAMU-2402/ZHEN-THESIS.pdf?sequence=1&isAllowed=y. [20 November 2013]. (Msc Thesis).

Appendices

Contents of the appendices:

Appendix A gives a description of Flownex® and all the elements that were used in this study.

Appendix B presents the simulation and analysis study that was done on the U-tube in EES. Steady state simulations are given here.

Appendix C presents the dynamic calculations on the U-tube in EES

Appendix D presents the *a*nalysis on the heat transfer calculation in EES for a single riser loop increment.

Appendix E presents the *a*nalysis on the heat transfer calculation in EES for a double riser loop increment.

Appendix F gives the dimensions of the chimney geometry as well as a typical Flownex® canvas of the chimney.

Appendix G presents the view factor calculation in Star-CCM+.

Appendix A: Flownex®

For this project, the software Flownex® was used to set up a simulation of natural circulation in an air-cooled RCCS.

Flownex® software research started in 1986 and was initially developed to solve air distribution networks for aero belt conveyor systems. Over the years, the software was expanded by M-Tech industrial (South Africa) to perform studies on the Pebble Bed Modular Reactor (PBMR). In 2007, the National Nuclear Regulator (NNR) reviewed the Flownex® software Verification and Validation (V&V) status and found it to be acceptable to be used to support the design and safety cases in the PBMR (Anon., 2013).

In 2008, Flownex was once again expanded and integrated into the Engineering Simulation Environment (Flownex® SE) to form part of a comprehensive plant simulation, analysis and optimization (Anon., 2013). This software helps the user to perform detailed analysis and design of complex thermal-fluid simulations and structures such as power plants and thermal-fluid networks (Anon., 2013). In Flownex®, the system is divided into conceptual volumes much like the conventional CFD code. However, Flownex® does not solve the three-dimensional Navier-Stokes equations like normal CFD software. A number of basic one-dimensional momentum equations are applied into the three-dimensional spatial control volumes.

Flownex® is based on an Implicit Pressure Correction Method (IPCM) that solves the momentum equation in each element and the continuity and energy equation at each node in large structured networks for both steady-state and dynamic situations (Anon., 2013). This gives the software a pseudo-CFD capability and allows Flownex® to analyze complex scenarios such as temperature and pressure gradient through pipes and buoyancy effects (Anon., 2013).

Flownex® is capable of calculating the steady state and dynamic simulation of systems that consist of any combination of the following (Anon., 2013):

- Liquid systems.
- Mixtures of gasses.
- Two phase systems with phase change.
- Incondensable mixtures of two phase fluids with gasses.
- Gas systems.
- Heat transfer between systems.
- Combustion.
- Control systems.
- Electric systems.

In Flownex®, the model builder helps the user to build any advanced model by using complex components or sub-systems such as nuclear reactors and heat exchangers. The standard components include a pipe model, orifice model, a reservoir model, turbine model, valves, PID (proportional integral derivative) controller, heat exchanger models, and two reactor models.

Heat transfer in Flownex®

The following effects can be taken into account in Flownex® when heat transfer simulations are done (Theron, 2013).

- The effects of cooling and heating of fluids on pipes and component walls.
- Determination of the total heat loss to the atmosphere through walls and pipes.
- During dynamic simulation the thermal inertia and heat capacitance of materials and fluids can be determined.
- The total heat loss or gain when there is a change to the atmospheric temperatures.
- The determination of the heat transfer of the fluids through the wall and plate in heat exchangers.
- The optimal calculation of the insulation of pipes, components and housings.

Flownex® uses a heat transfer element to convey the effect of the heat transferred to other elements. The calculation of the heat transfer element is done using the same principles that were explained in section 3.2. This heat transfer element allows the user to choose convection, conduction or radiation or any combination (Theron, 2013). This enables the user to determine the total heat transfer.

Flownex® library and nodalization

The Flownex® library contains a variety of elements that can be used to develop different simulation models. Figure A–2 shows some of the elements that can be used for a model simulation.

An element in Figure A–2 can be dragged from the library to design a model according to the user's specifications. The different elements can be linked to one another via a node to

calculate the flow and heat transfer through the model. The most common elements that were used in this study were the pipe and heat transfer elements, node and the boundary condition node. Figure A–1 shows an example of how the different elements can be linked on the Flownex® canvas. The canvas in Figure A–1 may represent a fluid flowing through a heated pipe; both ends open to the atmosphere. Each element is identifiable by a subscript. The user has the choice to input a heat source directly at the pipe element or use a heat transfer element from the Flownex® library. The conservation equations of mass, momentum and energy are solved using the SCFD approach described section 3.5.2 where properties such as pressure, density and temperature are stored at the nodes and velocity at the elements.

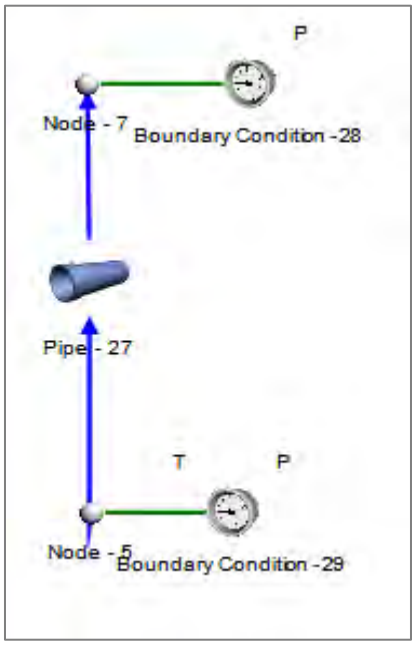

Figure A–1: Flownex® canvas.

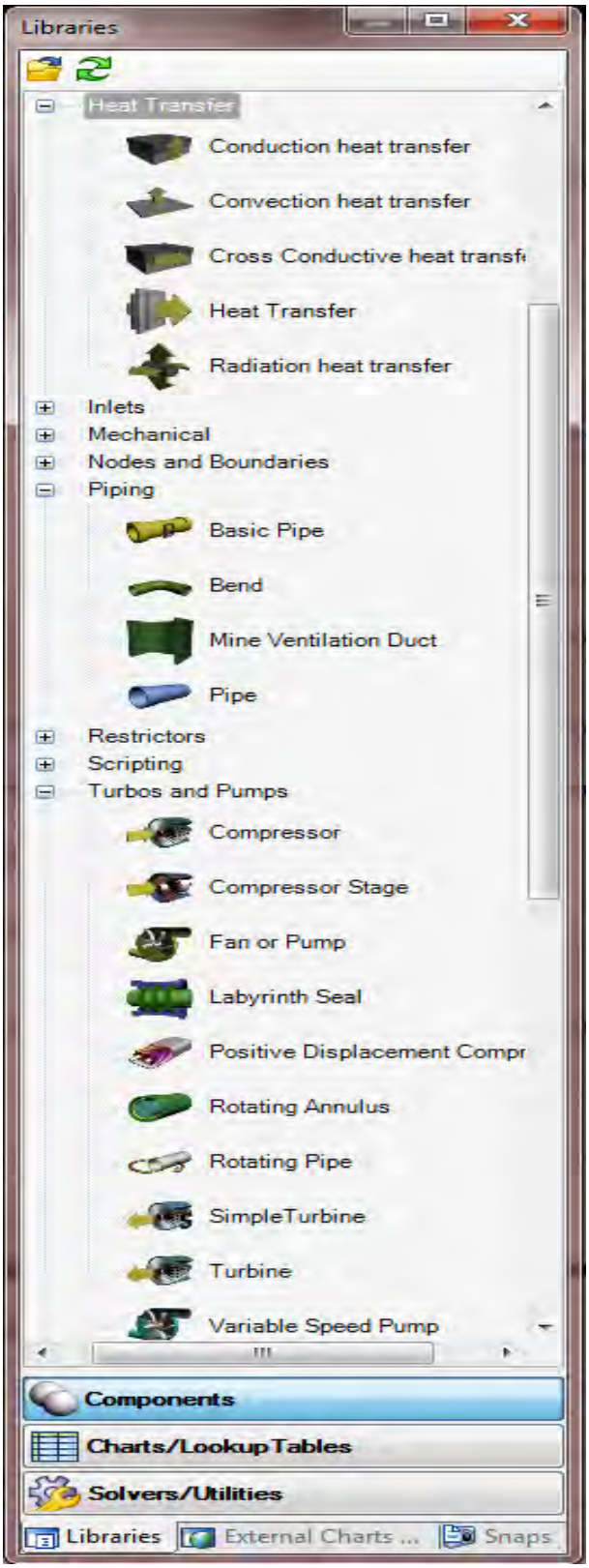

Figure A–2: Flownex® library.

The discussion which follows describes the different elements that were used in the study.

Pipe element

A pipe element was used to represent the flow of air through the RCCS. The fluid material can be specified in the element. In Flownex®, one has a choice between a specifying the diameter of the pipe or the flow area and circumference in the cross sectional option. The RCCS standpipes are rectangular in geometry and for this study the flow area and circumference options were chosen. The flow length of the pipe increment was specified as the total length of the riser tube divided by the number of increments. The inputs to the pipe element are shown in Figure A–3.

As mentioned before, in any flow channel, there will be a pressure drop caused by the friction forces on the surface, secondary losses due to fittings, bends, etc., and by gravity.

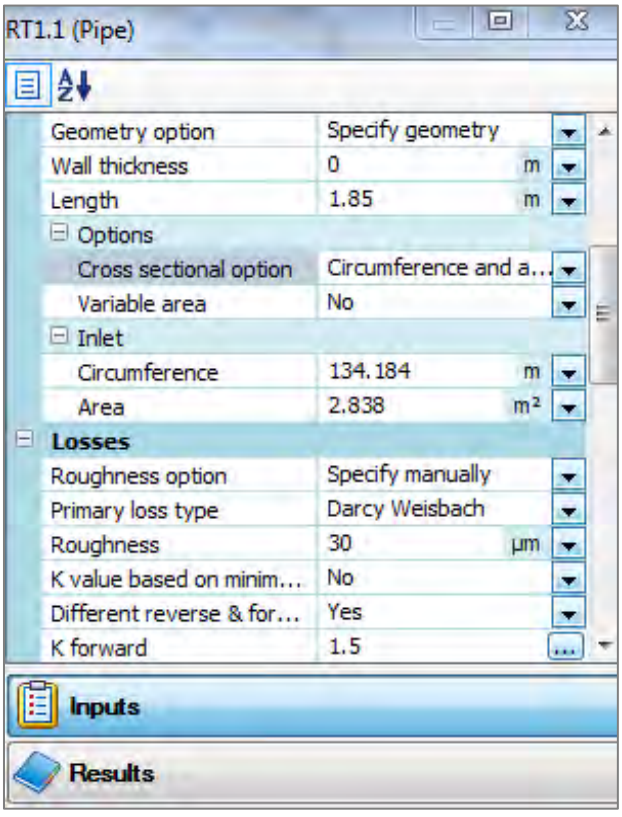

Figure A–3: Pipe element inputs.

Node

Nodes are used in Flownex® to link elements to one another as well as to specify certain boundary conditions such as a heat source.

The RCCS pipe network is divided into increments and the nodes are used to connect the pipe elements. In the node, the user can specify the elevation to represent the height difference in the RCCS structure. For example, a height of (0 m) can be specified for the ground level and (18.5 m) can be specified to represent the top most increment of the RCCS stand pipes. Furthermore, a node can be used to represent a connection between a wall and a heat transfer element.

Boundary condition element

The boundary condition element was used to specify the boundary conditions in the RCCS. In this project cold air is drawn into the RCCS from the atmosphere and hot air leaves the RCCS directly to the atmosphere. To this end, the boundary condition element is connected to a node to specify the inlet and outlet boundary conditions as shown in Figure A–1.

As was discussed in ***Chapter 6****,* a constant temperature boundary condition was specified on all the nodes which represent the inner surface of the RPV wall.

Heat transfer elements

Convection heat transfer elements

Figure A–5 shows how a heat transfer element was linked to the pipe network. The heat transfer element must be connected to an upstream (inlet) and downstream (outlet) node or elements. In the case of convection heat transfer, the heat transfer element is connected on one end to a node signifying a surface and to an element signifying a fluid. The inputs for the convection heat transfer element are given in Figure A–4. The heat transfer area refers to the area of the solid (node). The user can specify a constant heat transfer coefficient or select the Dittus-Boelter correlation to calculate the turbulent Nusselt number. For laminar flows the Nusselt number is specified and the heat transfer coefficient calculated using Equation 3-26.

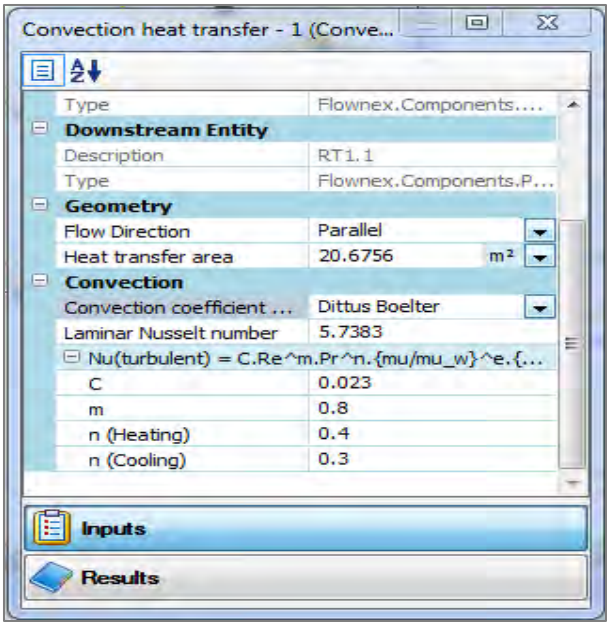

Figure A–4: Convection heat transfer element inputs.

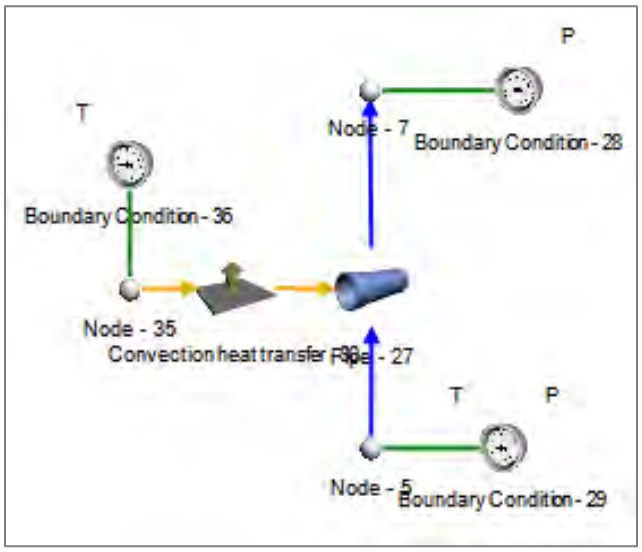

Figure A–5: Flownex® canvas with a heat transfer element.

Conduction heat transfer element

A heat transfer element can dragged from the Flownex® library and connects two nodes as shown in Figure A–7. The nodes represent the two ends of the wall at different temperatures. The heat transfer element has a function where certain material can be selected. Stainless steel was selected for the RPV wall and the riser standpipes while concrete was selected for the building wall. The areas of the two layers or surfaces must be specified in the heat transfer

element, including the thickness of the material. The heat transfer through the wall is evaluated using Equation 3-2. In the event that the areas of the walls are different, an average area is used.

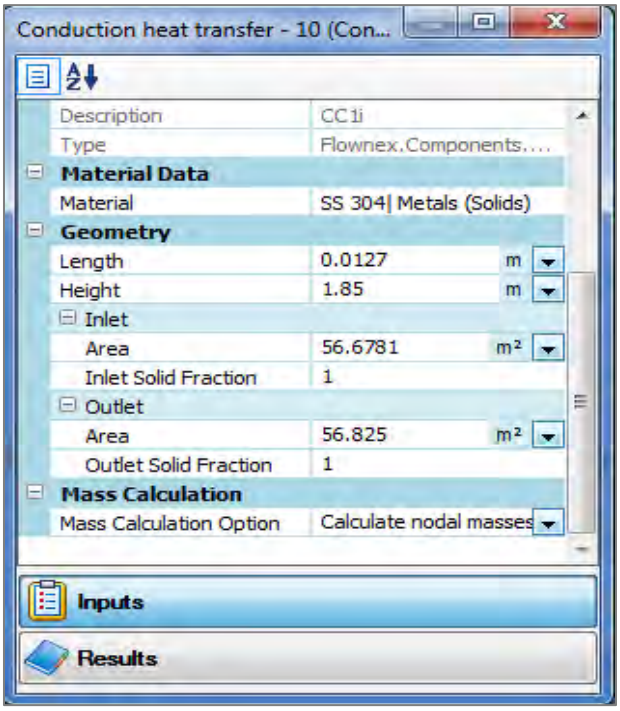

Figure A–6: Conduction heat transfer element input.

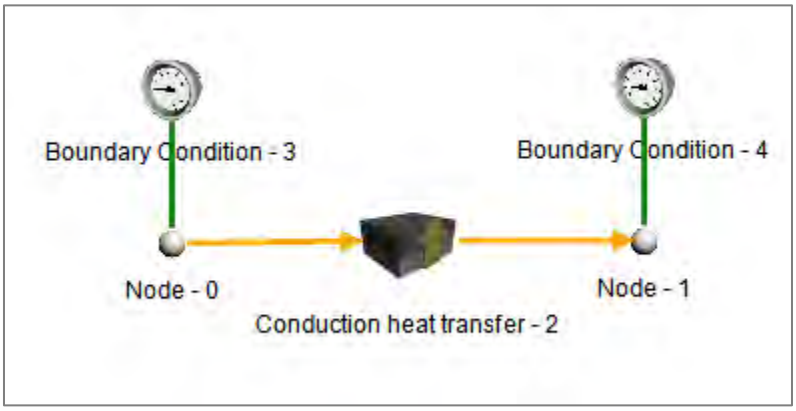

Figure A–7: Flownex® conduction canvas.

Radiation heat transfer elements

In Flownex® the user has a choice between a two-surface radiation element and a surface and space resistance depending on the nature of the problem. In the RCCS, a two surface radiation

element will be used for the radiation between the downcomer walls. The view factor between the surfaces, the areas as well as emissivity of the interacting walls must be specified. A simple Flownex® canvas is shown in Figure A–9. The radiation network of this two surface enclosure consists of two surface resistances and one space resistance. The input to the two surface enclosures is shown in Figure A–8.

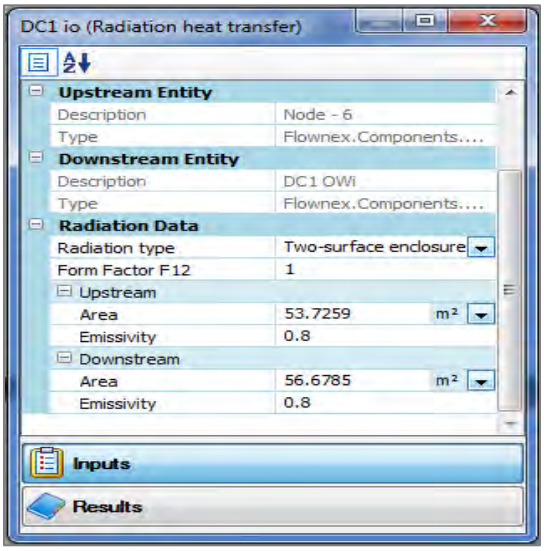

Figure A–8: Two surface radiation inputs.

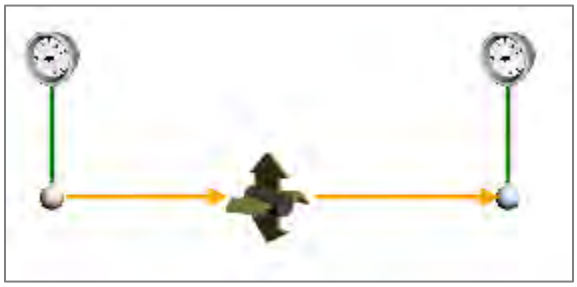

Figure A–9: Two surface Flownex® radiation canvas.

The net rate of radiation heat transfer is calculated using the methods described in section 3.2.3 internally within Flownex® as follows;

$$Q_{12} = \frac{E_{b1} - E_{b2}}{R_1 + R_{12} + R_2} \qquad \text{Equation A–1}$$

Or

$$Q_{12} = \frac{\sigma\left(T_1^4 - T_2^4\right)}{\frac{1-\varepsilon_1}{A_1\varepsilon_1} + \frac{1}{A_1 F_{1\to 2}} + \frac{1-\varepsilon_2}{A_1\varepsilon_2}}$$

Equation A–2

A network of surface and space resistance elements can be built for net interactions between surfaces in an enclosure. The area and emissivity must be specified for the surface resistances while the view factor and the area of the associated surface must be specified. The inputs for the surface and space resistances are shown in Figure A–10. A Flownex® model of the network discussed in section 3.2.3 is presented in Figure A–11 as an illustration of how the surface resistances and space resistances are connected in a Flownex® canvas.

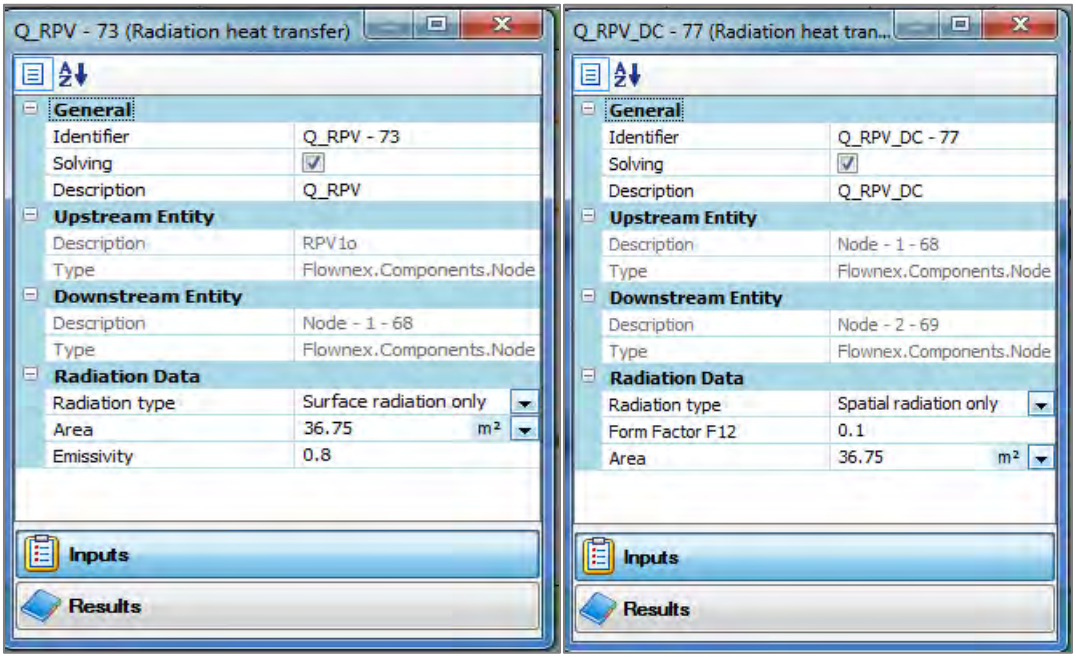

Figure A–10: inputs for the Flownex® surface and space resistance elements.

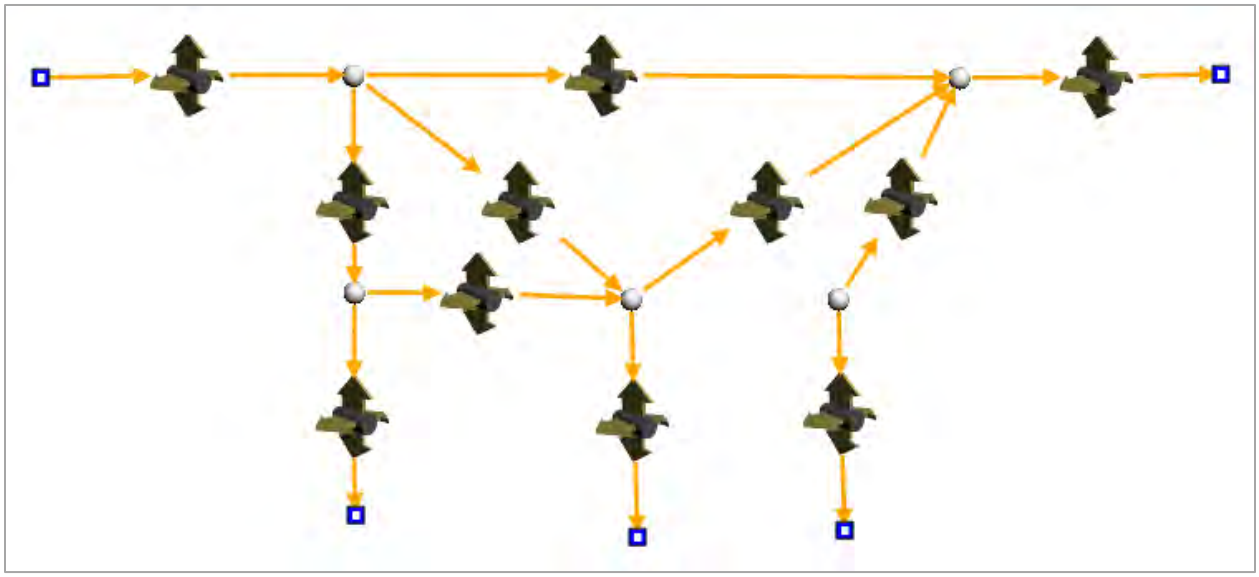

Figure A–11: Surface and space resistance radiation canvas.

Transient setup in Flownex®

In Flownex® the user can set up a transient scenario as shown in Figure A–12. This is done in the Flownex® configuration tab. The trigger option is the time a certain action is to take place. This is specified by the user as well as the time to stop the trigger. The target is the component used to represent the transient. In this study, the transient could be a heat input to a pipe, restrictor with loss coefficient or opening fraction in the restrictor with discharge coefficient. After the property or boundary condition that changes has been selected, a value can be specified, either to a constant value or a correlation depending on the change.

In this illustration, the simulation will start with a steady state heat flux of 0.05 kW at each of the five elements on the one side of the U-Tube. Instantaneously the heat flux is increased to 0.5 kW for the remainder of the simulation.

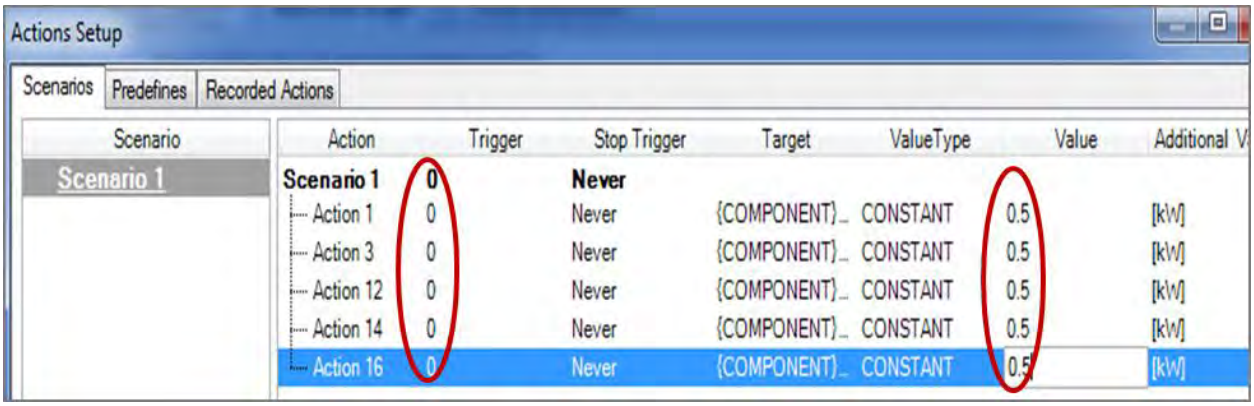

Figure A–12: Transient scenario setup in Flownex®.

Restrictor with loss coefficient

To model a blockage in Flownex® and element was selected for this purpose. In the Flownex® library a restrictor with a loss coefficient was selected and placed at the inlet to the risers. The inputs to the element are shown in Figure A– 13. The cross sectional area is the flow area and only one restrictor is placed in parallel.

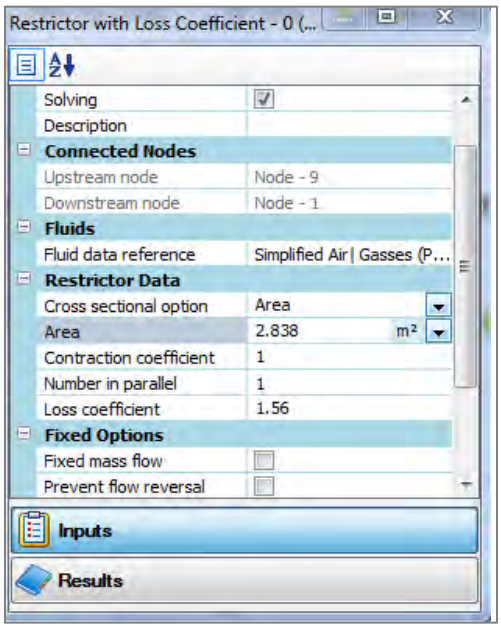

Figure A– 13: Resistor with loss coefficient element Flownex® input sheet.

The value of the loss coefficient can be calculated from the equation of the pressure drop across a Resistor with Loss Coefficient which is given as follows (Anon., 2013);

$$\Delta P_{0L} = C_k \rho^{\beta} Q^{\alpha}$$ Equation A–3

where

ρ - Mean density of the fluid (kg/m^3)

Q - Volumetric flow rate based on ρ (m^3/s)

β and α - Pressure constants

Equation A–3 is valid for incompressible flow; however the Mach numbers in the current analysis are low enough that the compressible effects can be ignored and Equation A–3 is applicable. The value of C_k can be calculated from the following expression (Anon., 2013);

$$C_k = \frac{C_l}{2A'^2}$$ Equation A–4

Where

C_l - Loss coefficient

A' - Effective area of the throat

The effective area of the throat is the area of the restrictor through which the fluid is discharged. It is described by the following expression;

$$A' = C_c A$$ Equation A–5

In Equation A–5, C_c is the ratio between the orifice area and the area of the vena contracta, and A is the physical area of the throat or pipe. Substituting, Equation A–5 into Equation A–4 an expression for C_k can be written

$$C_k = \frac{C_l}{2C_c^{\,2}A^2}$$ Equation A–6

It was not known what type of restriction will be used since the purpose is not to design an RCCS. A sharp edged restriction is selected for which $C_l = 1$. In Flownex®, it is desirable to vary the loss coefficient to relate to a certain blockage fraction. This means that one would like to keep the contraction coefficient as one in the element input. To achieve this, a pseudo C_l^* is calculated for which $C_c = 1$. Equation A–6 can be arranged as

$$C_l^* = 2C_k A^2$$ Equation A–7

The value of C_k is calculated from Equation A–6, for $C_l = 1$ (sharp edged restrictor). The values of C_l^* to be used in the Flownex® model are shown in Table 8-3. The blockage fractions that will be modelled are also shown. A 50% blockage means that the area of the pipe has been reduced by 50%. This means that in Equation A–5 C_c is 0.5 and so forth.

Restrictor with a discharge coefficient

The theory regarding the restrictor was discussed in the previous section. The area is selected as the area of the area pipe at which the leak will be modelled. In Flownex®, an element (restrictor with a discharge coefficient) was selected. The reason for this selection was that with this element the user has the choice to choose the fraction that the restrictor will be open thus representing the different breaking fractions of the pipe. The inputs to the element are shown in Figure A–14. The cross sectional area is the flow area. The opening fraction shall for this purpose indicate the fraction of the pipe break, therefore an opening fraction of 0.5 means the flow area of the element is reduced by 50% and inter alia an opening fraction of 0 means the restrictor is closed.

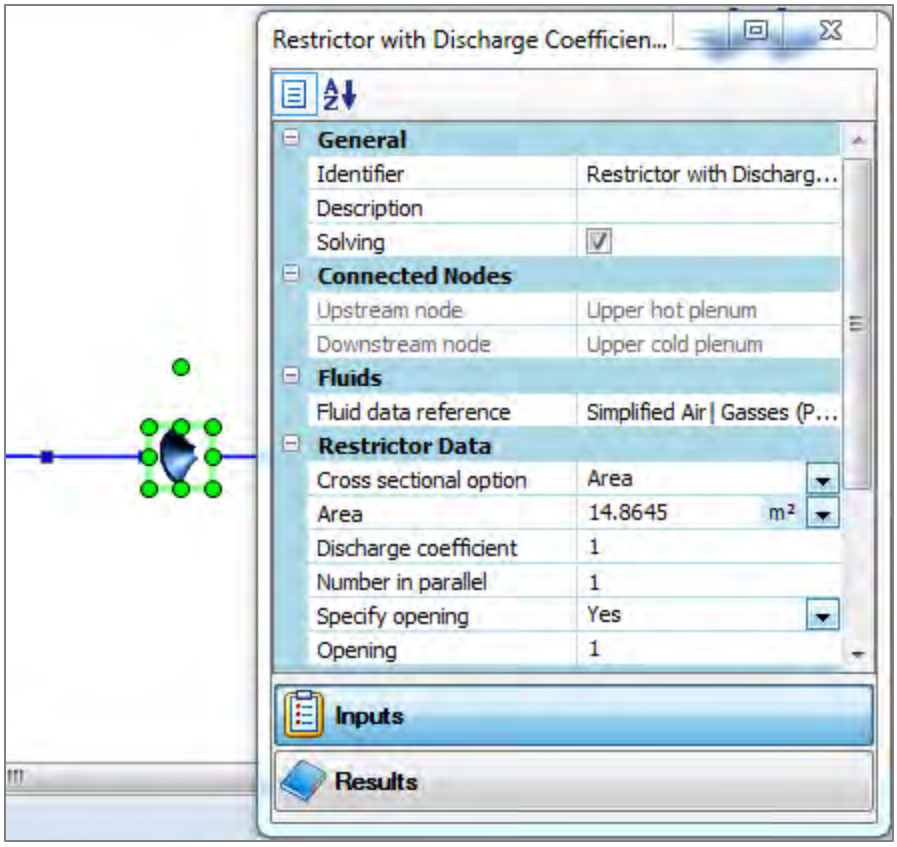

Figure A–14: Flownex® inputs to the resistor with discharge coefficient.

Appendix B: Steady state simulation of the simple U-tube (Constant heat flux)

This code was written for case study 1 in section 5.2.1. A steady state simulation of a simple U-tube was conducted to calculate the natural convection mass flow rate, with heat added to one side of the U-tube. The following can be found in the code:

- The general constants are given including the geometry of the simple U-tube.
- The boundary conditions, that is, the heat added and the atmospheric pressure and temperature at the inlet of the U-tube. The outlet pressure was also specified but the outlet temperature had to be calculated.
- For all elements the following were written;
  - Energy equation one the heated side since heat is added to the pipe (element).
  - Momentum conservation equation.
  - Average fluid properties.
- For all the nodes the following were written;
  - Continuity source term
  - Energy source term
  - The density is calculated through iteration for pressure and enthalpy in the nodes.
  - Node fluid properties.

For steady state all the terms in the conservation equations with time have been equated to zero. The simulation calculates all the fluid properties such that the inlet pressure equals the outlet pressure.

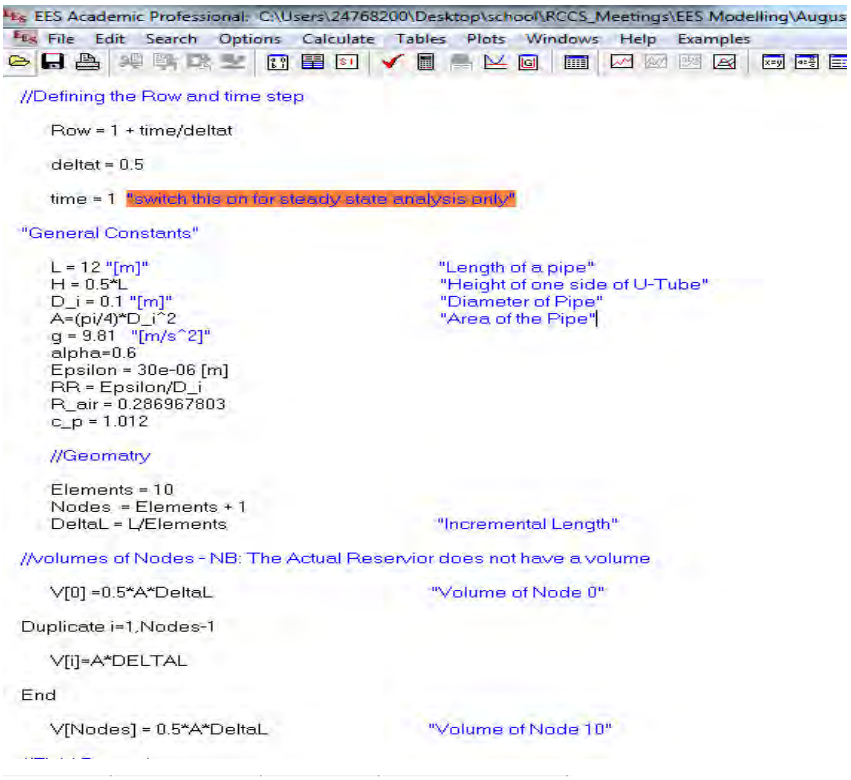


```
//Fluid Properties

    Fluid$ = 'air_ha'

//Defining the Increments

//Riser Increments

    z_e[0] = H

Duplicate i = 1, Elements/2

    z_i[i] = z_e[i-1]
    z_e[i] = z_i[i] - DeltaL

End

// Downcomer Increments

Duplicate i = Elements/2+1,Elements

    z_i[i]=z_e[i-1]
    z_e[i]=z_i[i]+DELTAL

End

//Boundary Values - Node 0

    Q = 1 [kW]

    P_atm = 100 "[kPa]"
    T_amb = 27 "[C]"
     h_0i = enthalpy(Fluid$,P=P_atm,T=T_amb)

    P_0[Nodes] =P_atm

//Initialize incremental loop - Imaginary Loop
```

```
P_0[1]    = P_atm
h_0[1]    = h_0i
T_0[1]    = T_amb

//SIMULATION METHODOLOGY FOR  ELEMENTS

Duplicate e = 1, Elements


    "Inlet Properties"

    P_0i[e] = P_0[e]
    h_0i[e] = if(m_dot[e],0,h_0e[e] +1E-03*g*(z_e[e]-z_i[e]) - Q_dot[e]/m_dot[e],h_0[e],h_0[e])


    "Outlet Properties"

    P_0e[e] = P_0[e+1]
    h_0e[e] = IF(m_dot[e],0,h_0[e+1],h_0i[e] + 1E-03*g*(z_i[e]-z_e[e]) + Q_dot[e]/m_dot[e]

    "Average Properties"

    P0_bar[e] = average(P_0i[e],P_0e[e])
    h0_bar[e] = average(h_0i[e],h_0e[e])
    T0_bar[e] = Temperature(Fluid$,h=h0_bar[e],P=P0_bar[e])
    P0_bar[e] = P_bar[e] + 1E-03*0.5*rho_bar[e]*v_bar[e]*abs(v_bar[e])
    h0_bar[e] = h_bar[e]+1E-03*0.5*v_bar[e]*abs(v_bar[e])
    T0_bar[e] = T_bar[e] + 0.5*1e-03*v_bar[e]*abs(v_bar[e])*(1/c_p)

    rho_bar[e] = P_bar[e]/(R_air*(T_bar[e]+273.15))
    v_bar[e] = m_dot[e]/(rho_bar[e]*A)

    mu_bar[e] =viscosity(Fluid$,T=T_bar[e],P=P_bar[e])
    Re_bar[e] = (rho_bar[e]*v_bar[e]*D_i)/mu_bar[e]



  "Momentum Equation"

  S_mom[e] = (A/DeltaL)*(P_0i[e] - P_0e[e]- DELTAp_0L[e] + 1e-03*rho_bar[e]*g*(z_i[e]-z_e[e]) + DeltaL*v_bar[e]*drho_bardt[e])


  "Component Characteristics"

  DELTAp_0L[e] =1E-03*0.5*((F[e]*abs(L/Elements)/D_i)+K[e])*m_dot[e]*abs(m_dot[e])/(rho_bar[e]*A^2)
  Q_dot[e] =  IF(e,Elements/2,0,0,Q/Elements/2)
  F[e] = IF(Re_bar[e],2000,64/Re_bar[e],64/Re_bar[e],moodychart(Re_bar[e],RR))
  K[e] = IF(e,Elements/2-1,0,1.5,IF(e,Elements/2+1,0,1.5,0))

  "Steady State"

  S_mom[e] = 0
  drho_bardt[e] = 0

End

//SIMULATION METHODOLOGY FOR  NODES

Duplicate n = 2, Nodes - 1

  "Node Properties"

  v_n[n] = 0.5*(v_bar[n-1]+v_bar[n])
  h[n] = h_0[n] - 0.5*1e-03*v_n[n]*abs(v_n[n])
  P[n] = Pressure(Fluid$,h=h[n],v=1/rho[n])
  T[n] = Temperature(Fluid$,P=P[n],h=h[n])
  rho[n] = P_0[n]/(R_air*(T_0[n]+273.15))
  T_0[n] = Temperature(Fluid$,h=h_0[n],P=P_0[n])

  "Continuity Source term"

  S_c[n]=(1/V[n])*(m_dot[n-1]-m_dot[n])

  "Energy Source term"

  Q_n[n] = 0
```

```
    Sume_in[n] = m_dot[n-1]*(h_0e[n-1]+1e-03*g*z_e[n-1])
    Sume_out[n] = m_dot[n]*(h_0i[n] + 1e-03*g*z_i[n])

    S_e[n] = (1/(rho[n]*V[n]))*(Sume_in[n] - Sume_out[n] + Q_n[n] + V[n]*(dpdt[n] - h_0[n]*drodt[n]))

    "Steady State"

    S_c[n] = 0
    S_e[n] = 0
    dpdt[n] = 0
    drodt[n] = 0

End

    h_0[Nodes] = h_0e[Nodes-1]
    T_0[Nodes] = Temperature(Fluid$,h=h_0[Nodes],P=P_0[Nodes])
```

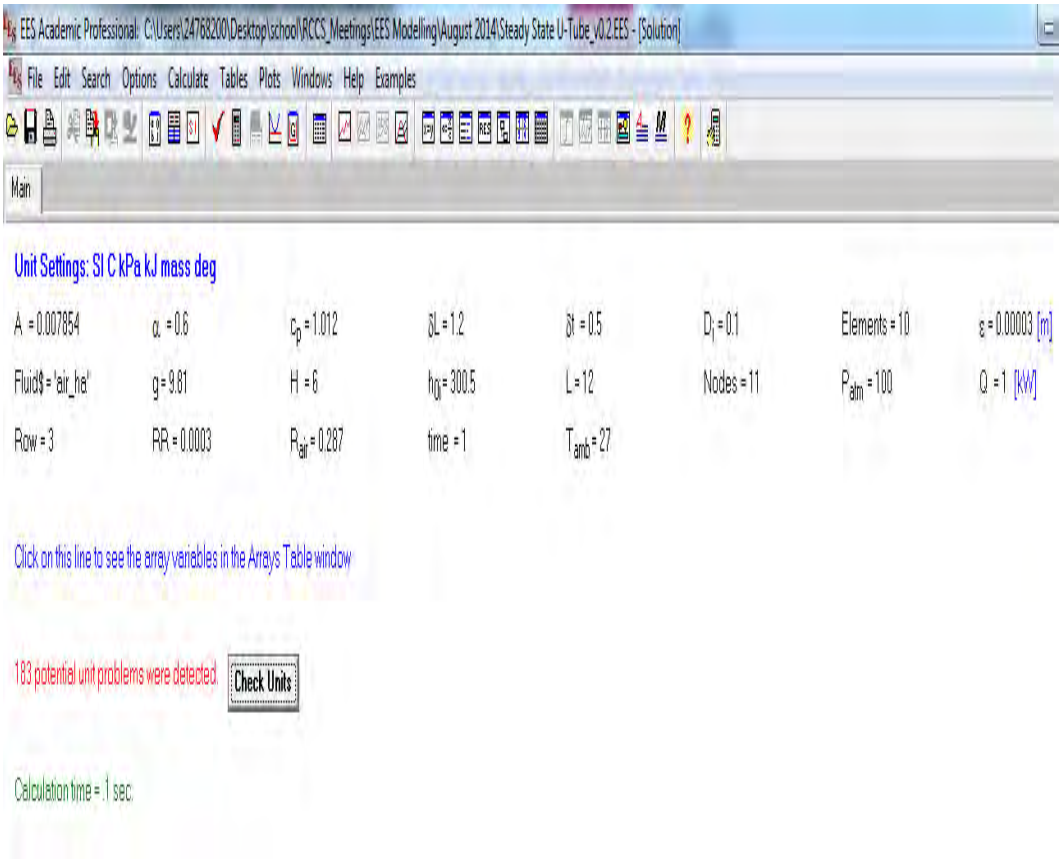

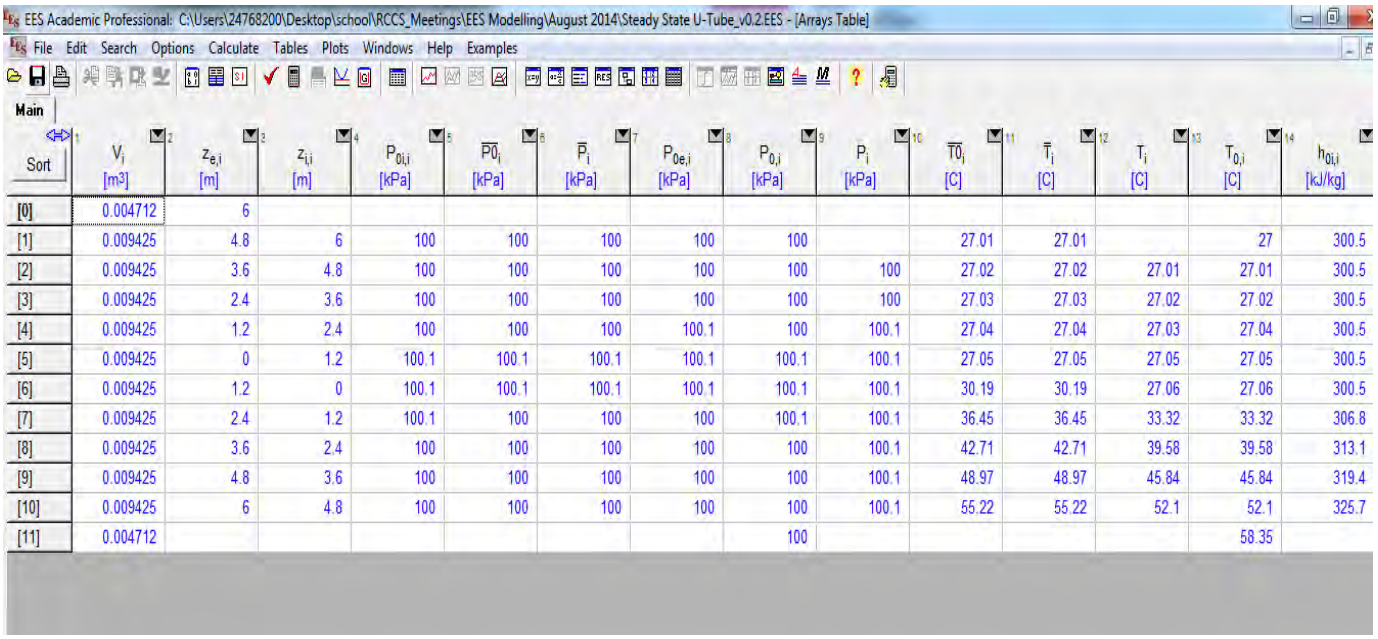

	V_i [m3]	$z_{e,i}$ [m]	$z_{i,i}$ [m]	$P_{0i,i}$ [kPa]	$\overline{P0}_i$ [kPa]	$\overline{P}_i$ [kPa]	$P_{0e,i}$ [kPa]	$P_{0,i}$ [kPa]	P_i [kPa]	$\overline{T0}_i$ [C]	$\overline{T}_i$ [C]	T_i [C]	$T_{0,i}$ [C]	$h_{0i,i}$ [kJ/kg]
[0]	0.004712	6												
[1]	0.009425	4.8	6	100	100	100	100	100		27.01	27.01		27	300.5
[2]	0.009425	3.6	4.8	100	100	100	100	100	100	27.02	27.02	27.01	27.01	300.5
[3]	0.009425	2.4	3.6	100	100	100	100	100	100	27.03	27.03	27.02	27.02	300.5
[4]	0.009425	1.2	2.4	100	100	100	100.1	100	100.1	27.04	27.04	27.03	27.04	300.5
[5]	0.009425	0	1.2	100.1	100.1	100.1	100.1	100.1	100.1	27.05	27.05	27.05	27.05	300.5
[6]	0.009425	1.2	0	100.1	100.1	100.1	100.1	100.1	100.1	30.19	30.19	27.06	27.06	300.5
[7]	0.009425	2.4	1.2	100.1	100	100	100	100.1	100.1	36.45	36.45	33.32	33.32	306.8
[8]	0.009425	3.6	2.4	100	100	100	100	100	100.1	42.71	42.71	39.58	39.58	313.1
[9]	0.009425	4.8	3.6	100	100	100	100	100	100.1	48.97	48.97	45.84	45.84	319.4
[10]	0.009425	6	4.8	100	100	100	100	100	100.1	55.22	55.22	52.1	52.1	325.7
[11]	0.004712							100					58.35	

Main

Sort

	$\overline{h}_i$ [kJ/kg]	$\overline{h0}_i$ [kJ/kg]	$h_{0e,i}$ [kJ/kg]	$h_{0,i}$ [kJ/kg]	h_i [kJ/kg]	$\dot{Q}_i$ [kW]	$Q_{n,i}$ [kW]	$\dot{m}_i$ [kg/s]	$\Delta p_{0L,i}$ [kPa]	ρ_i [kg/m3]	$\overline{\rho}_i$ [kg/m3]	$\overline{v}_i$ [m/s]	$v_{n,i}$ [m/s]	$\overline{Re}_i$
[0]														
[1]	300.5	300.5	300.5	300.5		0		0.007916	0.000196		1.161	0.8681		5435
[2]	300.5	300.5	300.5	300.5	300.5	0	0	0.007916	0.000196	1.161	1.161	0.868	0.8681	5435
[3]	300.5	300.5	300.5	300.5	300.5	0	0	0.007916	0.000196	1.161	1.161	0.868	0.868	5435
[4]	300.5	300.5	300.5	300.5	300.5	0	0	0.007916	0.0008521	1.161	1.161	0.8679	0.8679	5435
[5]	300.5	300.5	300.5	300.5	300.5	0	0	0.007916	0.000196	1.161	1.161	0.8678	0.8678	5435
[6]	303.7	303.7	306.8	300.5	300.5	0.05	0	0.007916	0.0008614	1.162	1.149	0.8769	0.8723	5391
[7]	310	310	313.1	306.8	306.8	0.05	0	0.007916	0.0002036	1.138	1.126	0.8951	0.886	5306
[8]	316.3	316.3	319.4	313.1	313.1	0.05	0	0.007916	0.0002086	1.115	1.104	0.9133	0.9042	5224
[9]	322.6	322.6	325.7	319.4	319.4	0.05	0	0.007916	0.0002138	1.093	1.082	0.9315	0.9224	5146
[10]	328.9	328.9	332	325.7	325.7	0.05	0	0.007916	0.0002189	1.072	1.061	0.9497	0.9406	5071
[11]				332										

Main

Sort

	$\overline{v}_i$ [m/s]	$v_{n,i}$ [m/s]	$\overline{Re}_i$	$\overline{\mu}_i$ [kg/m·s]	$S_{c,i}$	$S_{mom,i}$	$S_{e,i}$	$Sume_{in,i}$	$Sume_{out,i}$	$dpdt_i$	$drodt_i$	$drho_{bardt,i}$	F_i	K_i
[0]														
[1]	0.8681		5435	1.854E-05		0						0	0.03734	0
[2]	0.868	0.8681	5435	1.855E-05	0	0	0	2.379	2.379	0	0	0	0.03734	0
[3]	0.868	0.868	5435	1.855E-05	0	0	0	2.379	2.379	0	0	0	0.03734	0
[4]	0.8679	0.8679	5435	1.855E-05	0	0	0	2.379	2.379	0	0	0	0.03734	1.5
[5]	0.8678	0.8678	5435	1.855E-05	0	0	0	2.379	2.379	0	0	0	0.03734	0
[6]	0.8769	0.8723	5391	1.870E-05	0	0	0	2.379	2.379	0	0	0	0.03743	1.5
[7]	0.8951	0.886	5306	1.900E-05	0	0	0	2.429	2.429	0	0	0	0.0376	0
[8]	0.9133	0.9042	5224	1.929E-05	0	0	0	2.479	2.479	0	0	0	0.03778	0
[9]	0.9315	0.9224	5146	1.959E-05	0	0	0	2.529	2.529	0	0	0	0.03794	0
[10]	0.9497	0.9406	5071	1.988E-05	0	0	0	2.579	2.579	0	0	0	0.03811	0
[11]														

Appendix C: Transient simulation of the simple U-tube (Mass flow rate calculation)

This is an EES code of the transient simulation of the simple U-tube. This was written to compare to a Flownex® model and the discussion was given in section 5.2.3. This code is similar to that in **Appendix B** except that time terms have been included.

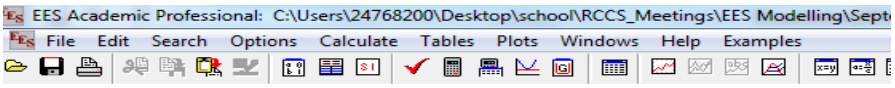


```
//Defining the Row and time step

    Row = 1 + time/deltat

    deltat = 0.05

    {time = 1} "switch this on for steady state analysis only"

"General Constants"

    g = 9.81  "[m/s^2]"
    R_air = 0.287
    c_p = 1.012

    //Geomatry

    L = 2*H "[m]"                          "Length of a pipe"
    H = 6                                  "Height of one side of U-Tube"
    D_i = 0.1 "[m]"                        "Diameter of Pipe"
    Epsilon = 30e-06 [m]
    RR = Epsilon/D_i


    Elements = 10
    Nodes  = Elements + 1

    Vol_e[0] =0                            "Volume of Element 0"

Duplicate i=1,Elements

    Vol_e[i]=A[i]*DELTAL[i]
    DeltaL[i] = L/Elements                  "Incremental Length"
    A[i]=(pi/4)*D_i^2                      "Area of the Pipe"

End

    Vol_e[11] = 0                          "Volume of Element 11"

//Fluid Properties
```

```
//Fluid Properties

    Fluid$ = 'air_ha'

//Defining the Increments

    "Riser Increments"

    z_e[0] = H

Duplicate i = 1, Elements/2

    z_i[i] = z_e[i-1]
    z_e[i] = z_i[i] - DeltaL[i]

End

    "Downcomer Increments"

Duplicate i = Elements/2+1,Elements

    z_i[i]=z_e[i-1]
    z_e[i]=z_i[i]+DELTAL[i]

End

Duplicate n = 1, Nodes

    Vol[n] = 0.5*Vol_e[n-1] + 0.5*Vol_e[n]

End

// Time-wise integration

    alpha = 0.7
    alpha_c = alpha
    alpha_m = alpha
    alpha_e = alpha



// Boundary values

    P_atm = 100 "[kPa]"
    T_amb = 27 "[C]"

//Initialize incremental loop

    P_0[1]    = P_atm
    T_0[1]    = T_amb
    P_0[Nodes] =P_atm
    v_n[1] = v_bar[1]
    T_0[1] = T[1] + 0.5*1e-03*v_n[1]*abs(v_n[1])*(1/c_p)
    rho[1] = density(Fluid$,P=P[1],h=h[1])
    P[1] = P_0[1] - 1e-03*0.5*rho[1]*v_n[1]*abs(v_n[1])
    h[1] = h_0[1] - 0.5*1e-03*v_n[1]*abs(v_n[1])
    T[1] = Temperature(Fluid$,h=h[1],P=P[1])

//SIMULATION METHODOLOGY FOR  ELEMENTS

    "Assign values at the inlet and outlet"

Duplicate e = 1, Elements


    "Inlet Properties"

    P_0i[e] = P_0[e]
    h_0i[e] = if(m_dot[e],0,h_0e[e] +1E-03*g*(z_e[e]-z_i[e]) - Q_dot[e]/m_dot[e],h_0[e],h_0[e])

    "Outlet Properties"

    P_0e[e] = P_0[e+1]
    h_0e[e] = IF(m_dot[e],0,h_0[e+1],h_0[e+1],h_0i[e] + 1E-03*g*(z_i[e]-z_e[e]) + Q_dot[e]/m_dot[e])


    "Average Properties"

    P0_bar[e] = average(P_0i[e],P_0e[e])
    h0_bar[e] = average(h_0i[e],h_0e[e])
```

```
    h0_bar[e] = average(h_0i[e],h_0e[e])
    T0_bar[e] = Temperature(Fluid$,h=h0_bar[e],P=P0_bar[e])
    P0_bar[e] = P_bar[e] + 1E-03*0.5*rho_bar[e]*v_bar[e]*abs(v_bar[e])
    h0_bar[e] = h_bar[e]+1E-03*0.5*v_bar[e]*abs(v_bar[e])
    T0_bar[e] = T_bar[e] + 0.5*1e-03*v_bar[e]*abs(v_bar[e])*(1/c_p)

    rho_bar[e] = density(Fluid$,h=h_bar[e],p=P_bar[e])
    v_bar[e] = m_dot[e]/(rho_bar[e]*A[e])

    mu_bar[e] =viscosity(Fluid$,T=T_bar[e],P=P_bar[e])
    Re_bar[e] = (rho_bar[e]*v_bar[e]*D_i)/mu_bar[e]

    "Momentum source term"
    S_mom[e] = (A[e]/DeltaL[e])*(1000*(P_0i[e] - P_0e[e])- DELTAp_0L[e] + rho_bar[e]*g*(z_i[e]-z_e[e]) + DeltaL[e]*v_bar[e]*drho_bardt[e])

    "Steady State"

{   S_mom[e] = 0
    drho_bardt[e] = 0}

    "Transient"

    drho_bardt[e] =(1/deltat)*(rho_bar[e] - tablevalue(Row-1,40+e))
    dmdt[e] = alpha*S_mom[e] + (1-alpha)*tablevalue(Row-1,20+e)
    m_dot[e] = tablevalue(Row-1,30+e) + dmdt[e]*deltat

    "Component Characteristics"

    DELTAp_0L[e] =0.5*((F[e]*abs(L/Elements)/D_i)+K[e])*m_dot[e]*abs(m_dot[e])/(rho_bar[e]*A[e]^2)
    Q_dot[e] = IF(e,Elements/2,0,0,Q/(Elements/2))
    F[e] =moodychart(Re_bar[e],RR)
    K[e] = IF(e,Elements/2-1,0,1.5,IF(e,Elements/2+1,0,1.5,0))

End

    Q = 0.25*10 [kW]

//SIMULATION METHODOLOGY FOR NODES
```

```
//SIMULATION METHODOLOGY FOR  NODES

Duplicate n = 2, Nodes - 1

    "Calculate node parameters"

    v_n[n] = 0.5*(v_bar[n-1]+v_bar[n])
    h[n] = h_0[n] - 0.5*1e-03*v_n[n]*abs(v_n[n])
    P[n] = P_0[n] - 1e-03*0.5*rho[n]*v_n[n]*abs(v_n[n])
    rho[n] = density(Fluid$,P=P[n],h=h[n])
    T[n] = Temperature(Fluid$,P=P[n],h=h[n])
    T_0[n]  = T[n] + 0.5*1e-03*v_n[n]*abs(v_n[n])*(1/c_p)

    "Continuity Source term"

    S_c[n]=(1/Vol[n])*(m_dot[n-1]-m_dot[n])

    "Energy Source term"

    Q_n[n] = 0

    Sume_in[n] = m_dot[n-1]*(h_0e[n-1]+1e-03*g*z_e[n-1])
    Sume_out[n] = m_dot[n]*(h_0i[n] + 1e-03*g*z_i[n])

    S_e[n] = (1/(rho[n]*Vol[n]))*(Sume_in[n] - Sume_out[n] + Q_n[n] + Vol[n]*(dpdt[n] - h_0[n]*drodt[n]))

    "Steady State"

{   S_c[n] = 0
    S_e[n] = 0
    dpdt[n] = 0
    drodt[n] = 0}

    "Transient"

    drodt[n] = alpha*S_c[n] + (1-alpha)*tablevalue(Row-1,1+n)
    rho[n] = tablevalue(Row-1,49+n) + drodt[n]*deltat
    dpdt[n] = (1/deltat)*(P[n] - tablevalue(Row-1,70+n))
    dhdt[n] = alpha*S_e[n] + (1-alpha)*tablevalue(Row-1,10+n)


    h_0[n] = tablevalue(Row-1,92+n) + dhdt[n]*deltat

    "End of Transient"

End

    h_0[Nodes] = h_0e[Nodes-1]
    v_n[Nodes] = v_bar[Nodes-1]
    h[Nodes] = h_0[Nodes] - 0.5*1e-03*v_n[Nodes]*abs(v_n[Nodes])
    P[Nodes] = P_0[Nodes] - 1e-03*0.5*rho[Nodes]*v_n[Nodes]*abs(v_n[Nodes])
    rho[Nodes] = density(Fluid$,P=P[Nodes],h=h[Nodes])
    T[Nodes] = Temperature(Fluid$,h=h[Nodes],P=P[Nodes])
    T_0[Nodes] = T[Nodes] + 0.5*1e-03*v_n[Nodes]*abs(v_n[Nodes])*(1/c_p)
```

EES Academic Professional: C:\Users\24768200\Desktop\school\RCCS_Meetings\EES Modelling\September 2014\Transient U-Tube_v0.0_Final.EES - [Parametric Table]

File Edit Search Options Calculate Tables Plots Windows Help Examples

Table 1

2..500	30 $S_{mom,10}$	31 $\dot{m}_1$ [kg/s]	32 $\dot{m}_2$ [kg/s]	33 $\dot{m}_3$ [kg/s]	34 $\dot{m}_4$ [kg/s]	35 $\dot{m}_5$ [kg/s]	36 $\dot{m}_6$ [kg/s]	37 $\dot{m}_7$ [kg/s]	38 $\dot{m}_8$ [kg/s]	39 $\dot{m}_9$ [kg/s]	40 $\dot{m}_{10}$ [kg/s]
Run 1	0	0.007922	0.007922	0.007922	0.007922	0.007922	0.007922	0.007922	0.007922	0.007922	0.007922
Run 2	0.08327	0.006832	0.006823	0.006804	0.006776	0.006737	0.006689	0.007758	0.008808	0.009831	0.01084
Run 3	-0.002268	0.006341	0.006353	0.006377	0.006413	0.006463	0.006528	0.007952	0.00937	0.01072	0.01201
Run 4	-0.0001092	0.006695	0.006695	0.006692	0.006688	0.006679	0.006664	0.008	0.009369	0.01069	0.01197
Run 5	0.006213	0.006842	0.00684	0.006836	0.006831	0.006827	0.006826	0.008145	0.009539	0.01089	0.01218
Run 6	0.000387	0.007011	0.007013	0.007017	0.007023	0.00703	0.007035	0.008299	0.009674	0.01101	0.01229
Run 7	0.002139	0.007235	0.007234	0.007232	0.00723	0.007227	0.007224	0.008423	0.009776	0.0111	0.01237
Run 8	0.002127	0.007424	0.007424	0.007425	0.007425	0.007427	0.007428	0.008571	0.009905	0.01121	0.01248
Run 9	0.001806	0.007629	0.007629	0.007629	0.007629	0.00763	0.00763	0.008713	0.01002	0.01132	0.01257
Run 10	0.001961	0.007834	0.007834	0.007834	0.007834	0.007834	0.007834	0.008858	0.01014	0.01143	0.01267
Run 11	0.001941	0.008039	0.008039	0.008039	0.008039	0.00804	0.00804	0.009007	0.01026	0.01153	0.01277
Run 12	0.001892	0.008246	0.008246	0.008246	0.008246	0.008247	0.008247	0.009156	0.01039	0.01164	0.01286
Run 13	0.001904	0.008454	0.008454	0.008454	0.008454	0.008455	0.008455	0.009307	0.01051	0.01175	0.01296
Run 14	0.001872	0.008663	0.008663	0.008663	0.008663	0.008663	0.008663	0.00946	0.01063	0.01185	0.01305
Run 15	0.001848	0.008872	0.008872	0.008872	0.008872	0.008872	0.008872	0.009614	0.01075	0.01196	0.01314
Run 16	0.001822	0.009081	0.009081	0.009081	0.009081	0.009081	0.009082	0.00977	0.01087	0.01206	0.01323
Run 17	0.00179	0.00929	0.00929	0.00929	0.00929	0.00929	0.009291	0.009926	0.01099	0.01216	0.01332
Run 18	0.001756	0.009499	0.009499	0.009499	0.009499	0.009499	0.009499	0.01008	0.01111	0.01226	0.01341
Run 19	0.001719	0.009707	0.009707	0.009707	0.009707	0.009707	0.009707	0.01024	0.01123	0.01236	0.0135
Run 20	0.00168	0.009914	0.009914	0.009914	0.009914	0.009914	0.009915	0.0104	0.01135	0.01246	0.01358
Run 21	0.001638	0.01012	0.01012	0.01012	0.01012	0.01012	0.01012	0.01056	0.01147	0.01255	0.01367
Run 22	0.001594	0.01032	0.01032	0.01032	0.01032	0.01033	0.01033	0.01072	0.01159	0.01265	0.01375
Run 23	0.001549	0.01053	0.01053	0.01053	0.01053	0.01053	0.01053	0.01088	0.01171	0.01274	0.01382
Run 24	0.001502	0.01073	0.01073	0.01073	0.01073	0.01073	0.01073	0.01104	0.01182	0.01283	0.0139
Run 25	0.001455	0.01093	0.01093	0.01093	0.01093	0.01093	0.01093	0.0112	0.01194	0.01292	0.01397
Run 26	0.001407	0.01112	0.01112	0.01112	0.01112	0.01113	0.01113	0.01136	0.01206	0.01301	0.01405

2..500	30 $S_{mom,10}$	31 $\dot{m}_1$ [kg/s]	32 $\dot{m}_2$ [kg/s]	33 $\dot{m}_3$ [kg/s]	34 $\dot{m}_4$ [kg/s]	35 $\dot{m}_5$ [kg/s]	36 $\dot{m}_6$ [kg/s]	37 $\dot{m}_7$ [kg/s]	38 $\dot{m}_8$ [kg/s]	39 $\dot{m}_9$ [kg/s]
Run 27	0.001358	0.01132	0.01132	0.01132	0.01132	0.01132	0.01132	0.01152	0.01218	0.0131
Run 28	0.001309	0.01151	0.01151	0.01151	0.01151	0.01151	0.01151	0.01168	0.01229	0.01318
Run 29	0.001261	0.0117	0.0117	0.0117	0.0117	0.0117	0.0117	0.01184	0.01241	0.01327
Run 30	0.001213	0.01188	0.01188	0.01188	0.01188	0.01188	0.01189	0.01199	0.01252	0.01335
Run 31	0.001166	0.01207	0.01207	0.01207	0.01207	0.01207	0.01207	0.01215	0.01264	0.01343
Run 32	0.00112	0.01225	0.01225	0.01225	0.01225	0.01225	0.01225	0.0123	0.01275	0.01351
Run 33	0.001075	0.01242	0.01242	0.01242	0.01242	0.01242	0.01242	0.01245	0.01286	0.01359
Run 34	0.001032	0.01259	0.01259	0.01259	0.01259	0.01259	0.01259	0.0126	0.01297	0.01366
Run 35	0.0009898	0.01276	0.01276	0.01276	0.01276	0.01276	0.01276	0.01275	0.01308	0.01374
Run 36	0.0009498	0.01292	0.01292	0.01292	0.01292	0.01292	0.01292	0.0129	0.01319	0.01381
Run 37	0.0009116	0.01308	0.01308	0.01308	0.01308	0.01308	0.01308	0.01304	0.0133	0.01388
Run 38	0.0008754	0.01324	0.01324	0.01324	0.01324	0.01324	0.01324	0.01318	0.01341	0.01396
Run 39	0.0008413	0.01339	0.01339	0.01339	0.01339	0.01339	0.01339	0.01332	0.01351	0.01403
Run 40	0.0008092	0.01353	0.01353	0.01353	0.01353	0.01353	0.01353	0.01345	0.01362	0.01409
Run 41	0.0007792	0.01368	0.01368	0.01368	0.01368	0.01368	0.01368	0.01358	0.01372	0.01416
Run 42	0.0007513	0.01381	0.01381	0.01381	0.01381	0.01381	0.01381	0.01371	0.01382	0.01423
Run 43	0.0007254	0.01395	0.01395	0.01395	0.01395	0.01395	0.01395	0.01384	0.01392	0.0143
Run 44	0.0007015	0.01407	0.01407	0.01407	0.01407	0.01407	0.01407	0.01396	0.01402	0.01436
Run 45	0.0006794	0.0142	0.0142	0.0142	0.0142	0.0142	0.0142	0.01408	0.01411	0.01443
Run 46	0.0006593	0.01432	0.01432	0.01432	0.01432	0.01432	0.01432	0.01419	0.01421	0.01449
Run 47	0.0006408	0.01443	0.01443	0.01443	0.01443	0.01443	0.01443	0.0143	0.0143	0.01455
Run 48	0.0006239	0.01454	0.01454	0.01454	0.01454	0.01454	0.01454	0.01441	0.01439	0.01461
Run 49	0.0006085	0.01465	0.01465	0.01465	0.01465	0.01465	0.01465	0.01451	0.01448	0.01467
Run 50	0.0005945	0.01475	0.01475	0.01475	0.01475	0.01475	0.01475	0.01461	0.01456	0.01473
Run 51	0.0005816	0.01485	0.01485	0.01485	0.01485	0.01485	0.01485	0.01471	0.01464	0.01479
Run 52	0.0005699	0.01494	0.01494	0.01494	0.01494	0.01494	0.01494	0.0148	0.01472	0.01484

Run 53	0.000559	0.01503	0.01503	0.01503	0.01503	0.01503	0.01503	0.01489	0.0148	0.0149	0.01523
Run 54	0.000549	0.01511	0.01511	0.01511	0.01511	0.01511	0.01511	0.01498	0.01488	0.01495	0.01525
Run 55	0.0005397	0.01519	0.01519	0.01519	0.01519	0.01519	0.01519	0.01506	0.01495	0.01501	0.01528
Run 56	0.0005309	0.01527	0.01527	0.01527	0.01527	0.01527	0.01527	0.01514	0.01502	0.01506	0.01531
Run 57	0.0005226	0.01534	0.01534	0.01534	0.01534	0.01534	0.01534	0.01521	0.01509	0.01511	0.01533
Run 58	0.0005146	0.01541	0.01541	0.01541	0.01541	0.01541	0.01541	0.01528	0.01516	0.01516	0.01536
Run 59	0.0005068	0.01547	0.01547	0.01547	0.01547	0.01547	0.01547	0.01535	0.01522	0.01521	0.01539
Run 60	0.0004992	0.01553	0.01553	0.01553	0.01553	0.01553	0.01553	0.01541	0.01528	0.01525	0.01541
Run 61	0.0004916	0.01559	0.01559	0.01559	0.01559	0.01559	0.01559	0.01547	0.01534	0.0153	0.01544
Run 62	0.0004841	0.01564	0.01564	0.01565	0.01565	0.01565	0.01565	0.01553	0.01539	0.01534	0.01546
Run 63	0.0004764	0.0157	0.0157	0.0157	0.0157	0.0157	0.0157	0.01559	0.01545	0.01539	0.01548
Run 64	0.0004686	0.01574	0.01574	0.01574	0.01574	0.01574	0.01574	0.01564	0.0155	0.01543	0.01551
Run 65	0.0004606	0.01579	0.01579	0.01579	0.01579	0.01579	0.01579	0.01569	0.01554	0.01547	0.01553
Run 66	0.0004525	0.01583	0.01583	0.01583	0.01583	0.01583	0.01583	0.01573	0.01559	0.01551	0.01555
Run 67	0.000444	0.01587	0.01587	0.01587	0.01587	0.01587	0.01587	0.01577	0.01563	0.01554	0.01558
Run 68	0.0004354	0.0159	0.0159	0.0159	0.0159	0.0159	0.0159	0.01581	0.01568	0.01558	0.0156
Run 69	0.0004264	0.01594	0.01594	0.01594	0.01594	0.01594	0.01594	0.01585	0.01571	0.01561	0.01562
Run 70	0.0004172	0.01597	0.01597	0.01597	0.01597	0.01597	0.01597	0.01588	0.01575	0.01565	0.01564
Run 71	0.0004077	0.016	0.016	0.016	0.016	0.016	0.016	0.01592	0.01579	0.01568	0.01566
Run 72	0.000398	0.01602	0.01602	0.01602	0.01602	0.01602	0.01602	0.01595	0.01582	0.01571	0.01568
Run 73	0.000388	0.01605	0.01605	0.01605	0.01605	0.01605	0.01605	0.01597	0.01585	0.01574	0.0157
Run 74	0.0003778	0.01607	0.01607	0.01607	0.01607	0.01607	0.01607	0.016	0.01588	0.01576	0.01572
Run 75	0.0003673	0.01609	0.01609	0.01609	0.01609	0.01609	0.01609	0.01602	0.0159	0.01579	0.01574
Run 76	0.0003567	0.01611	0.01611	0.01611	0.01611	0.01611	0.01611	0.01604	0.01593	0.01581	0.01576
Run 77	0.0003459	0.01612	0.01612	0.01612	0.01612	0.01612	0.01612	0.01606	0.01595	0.01584	0.01577
Run 78	0.000335	0.01614	0.01614	0.01614	0.01614	0.01614	0.01614	0.01608	0.01597	0.01586	0.01579

Run 79	0.0003239	0.01615	0.01615	0.01615	0.01615	0.01615	0.01615	0.0161	0.016	0.01588	0.01581
Run 80	0.0003128	0.01616	0.01616	0.01616	0.01616	0.01616	0.01616	0.01611	0.01601	0.0159	0.01582
Run 81	0.0003016	0.01617	0.01617	0.01617	0.01617	0.01617	0.01617	0.01613	0.01603	0.01592	0.01584
Run 82	0.0002904	0.01618	0.01618	0.01618	0.01618	0.01618	0.01618	0.01614	0.01605	0.01594	0.01585
Run 83	0.0002792	0.01619	0.01619	0.01619	0.01619	0.01619	0.01619	0.01615	0.01606	0.01595	0.01587
Run 84	0.0002681	0.0162	0.0162	0.0162	0.0162	0.0162	0.0162	0.01616	0.01607	0.01597	0.01588
Run 85	0.000257	0.0162	0.0162	0.0162	0.0162	0.0162	0.0162	0.01617	0.01609	0.01598	0.01589
Run 86	0.0002459	0.01621	0.01621	0.01621	0.01621	0.01621	0.01621	0.01617	0.0161	0.016	0.01591
Run 87	0.000235	0.01621	0.01621	0.01621	0.01621	0.01621	0.01621	0.01618	0.01611	0.01601	0.01592
Run 88	0.0002243	0.01621	0.01621	0.01621	0.01621	0.01621	0.01621	0.01618	0.01611	0.01602	0.01593
Run 89	0.0002137	0.01621	0.01621	0.01621	0.01621	0.01621	0.01621	0.01619	0.01612	0.01603	0.01594
Run 90	0.0002033	0.01622	0.01622	0.01622	0.01622	0.01622	0.01622	0.01619	0.01613	0.01604	0.01595
Run 91	0.000193	0.01622	0.01622	0.01622	0.01622	0.01622	0.01622	0.01619	0.01614	0.01605	0.01596
Run 92	0.000183	0.01622	0.01622	0.01622	0.01622	0.01622	0.01622	0.0162	0.01614	0.01606	0.01597
Run 93	0.0001732	0.01622	0.01622	0.01622	0.01622	0.01622	0.01622	0.0162	0.01614	0.01606	0.01598
Run 94	0.0001637	0.01622	0.01622	0.01622	0.01622	0.01622	0.01622	0.0162	0.01615	0.01607	0.01599
Run 95	0.0001544	0.01621	0.01621	0.01621	0.01621	0.01621	0.01621	0.0162	0.01615	0.01608	0.01599
Run 96	0.0001454	0.01621	0.01621	0.01621	0.01621	0.01621	0.01621	0.0162	0.01615	0.01608	0.016
Run 97	0.0001367	0.01621	0.01621	0.01621	0.01621	0.01621	0.01621	0.0162	0.01616	0.01609	0.01601
Run 98	0.0001282	0.01621	0.01621	0.01621	0.01621	0.01621	0.01621	0.0162	0.01616	0.01609	0.01601
Run 99	0.00012	0.01621	0.01621	0.01621	0.01621	0.01621	0.01621	0.01619	0.01616	0.0161	0.01602
Run 100	0.0001122	0.0162	0.0162	0.0162	0.0162	0.0162	0.0162	0.01619	0.01616	0.0161	0.01603
Run 101	0.0001046	0.0162	0.0162	0.0162	0.0162	0.0162	0.0162	0.01619	0.01616	0.0161	0.01603
Run 102	0.00009729	0.0162	0.0162	0.0162	0.0162	0.0162	0.0162	0.01619	0.01616	0.01611	0.01604
Run 103	0.0000903	0.01619	0.01619	0.01619	0.01619	0.01619	0.01619	0.01619	0.01616	0.01611	0.01604
Run 104	0.00008361	0.01619	0.01619	0.01619	0.01619	0.01619	0.01619	0.01618	0.01616	0.01611	0.01605

Run 105	0.00007721	0.01618	0.01618	0.01618	0.01618	0.01618	0.01618	0.01618	0.01616	0.01611	0.01605
Run 106	0.0000711	0.01618	0.01618	0.01618	0.01618	0.01618	0.01618	0.01618	0.01616	0.01611	0.01605
Run 107	0.00006527	0.01618	0.01618	0.01618	0.01618	0.01618	0.01618	0.01617	0.01615	0.01611	0.01606
Run 108	0.00005973	0.01617	0.01617	0.01617	0.01617	0.01617	0.01617	0.01617	0.01615	0.01612	0.01606
Run 109	0.00005447	0.01617	0.01617	0.01617	0.01617	0.01617	0.01617	0.01617	0.01615	0.01612	0.01606
Run 110	0.00004948	0.01616	0.01616	0.01616	0.01616	0.01616	0.01616	0.01616	0.01615	0.01612	0.01607
Run 111	0.00004476	0.01616	0.01616	0.01616	0.01616	0.01616	0.01616	0.01616	0.01615	0.01612	0.01607
Run 112	0.0000403	0.01616	0.01616	0.01616	0.01616	0.01616	0.01616	0.01616	0.01614	0.01612	0.01607
Run 113	0.00003609	0.01615	0.01615	0.01615	0.01615	0.01615	0.01615	0.01615	0.01614	0.01612	0.01607
Run 114	0.00003212	0.01615	0.01615	0.01615	0.01615	0.01615	0.01615	0.01615	0.01614	0.01611	0.01607
Run 115	0.0000284	0.01614	0.01614	0.01614	0.01614	0.01614	0.01614	0.01615	0.01614	0.01611	0.01607
Run 116	0.0000249	0.01614	0.01614	0.01614	0.01614	0.01614	0.01614	0.01614	0.01613	0.01611	0.01608
Run 117	0.00002163	0.01614	0.01614	0.01614	0.01614	0.01614	0.01614	0.01614	0.01613	0.01611	0.01608
Run 118	0.00001857	0.01613	0.01613	0.01613	0.01613	0.01613	0.01613	0.01613	0.01613	0.01611	0.01608
Run 119	0.00001572	0.01613	0.01613	0.01613	0.01613	0.01613	0.01613	0.01613	0.01613	0.01611	0.01608
Run 120	0.00001307	0.01613	0.01613	0.01613	0.01613	0.01613	0.01613	0.01613	0.01612	0.01611	0.01608
Run 121	0.00001061	0.01612	0.01612	0.01612	0.01612	0.01612	0.01612	0.01612	0.01612	0.01611	0.01608
Run 122	0.000008326	0.01612	0.01612	0.01612	0.01612	0.01612	0.01612	0.01612	0.01612	0.01611	0.01608
Run 123	0.000006218	0.01612	0.01612	0.01612	0.01612	0.01612	0.01612	0.01612	0.01612	0.01611	0.01608
Run 124	0.000004276	0.01611	0.01611	0.01611	0.01611	0.01611	0.01611	0.01612	0.01611	0.0161	0.01608
Run 125	0.000002492	0.01611	0.01611	0.01611	0.01611	0.01611	0.01611	0.01611	0.01611	0.0161	0.01608
Run 126	8.584E-07	0.01611	0.01611	0.01611	0.01611	0.01611	0.01611	0.01611	0.01611	0.0161	0.01608
Run 127	-6.331E-07	0.0161	0.0161	0.0161	0.0161	0.0161	0.0161	0.01611	0.01611	0.0161	0.01608
Run 128	-0.00000199	0.0161	0.0161	0.0161	0.0161	0.0161	0.0161	0.0161	0.0161	0.0161	0.01608
Run 129	-0.000003218	0.0161	0.0161	0.0161	0.0161	0.0161	0.0161	0.0161	0.0161	0.0161	0.01608
Run 130	-0.000004326	0.0161	0.0161	0.0161	0.0161	0.0161	0.0161	0.0161	0.0161	0.0161	0.01608

Run 131	-0.000005321	0.01609	0.01609	0.01609	0.01609	0.01609	0.01609	0.0161	0.0161	0.01609	0.01608
Run 132	-0.000006208	0.01609	0.01609	0.01609	0.01609	0.01609	0.01609	0.01609	0.0161	0.01609	0.01608
Run 133	-0.000006995	0.01609	0.01609	0.01609	0.01609	0.01609	0.01609	0.01609	0.01609	0.01609	0.01608
Run 134	-0.000007687	0.01609	0.01609	0.01609	0.01609	0.01609	0.01609	0.01609	0.01609	0.01609	0.01608
Run 135	-0.000008291	0.01609	0.01609	0.01609	0.01609	0.01609	0.01609	0.01609	0.01609	0.01609	0.01608
Run 136	-0.000008812	0.01608	0.01608	0.01608	0.01608	0.01608	0.01608	0.01609	0.01609	0.01609	0.01608
Run 137	-0.000009256	0.01608	0.01608	0.01608	0.01608	0.01608	0.01608	0.01608	0.01609	0.01609	0.01608
Run 138	-0.000009629	0.01608	0.01608	0.01608	0.01608	0.01608	0.01608	0.01608	0.01609	0.01608	0.01608
Run 139	-0.000009935	0.01608	0.01608	0.01608	0.01608	0.01608	0.01608	0.01608	0.01608	0.01608	0.01608
Run 140	-0.00001018	0.01608	0.01608	0.01608	0.01608	0.01608	0.01608	0.01608	0.01608	0.01608	0.01608
Run 141	-0.00001037	0.01608	0.01608	0.01608	0.01608	0.01608	0.01608	0.01608	0.01608	0.01608	0.01608
Run 142	-0.0000105	0.01607	0.01607	0.01607	0.01607	0.01607	0.01607	0.01608	0.01608	0.01608	0.01608
Run 143	-0.00001059	0.01607	0.01607	0.01607	0.01607	0.01607	0.01607	0.01607	0.01608	0.01608	0.01608
Run 144	-0.00001063	0.01607	0.01607	0.01607	0.01607	0.01607	0.01607	0.01607	0.01608	0.01608	0.01608
Run 145	-0.00001063	0.01607	0.01607	0.01607	0.01607	0.01607	0.01607	0.01607	0.01608	0.01608	0.01607
Run 146	-0.0000106	0.01607	0.01607	0.01607	0.01607	0.01607	0.01607	0.01607	0.01607	0.01608	0.01607
Run 147	-0.00001053	0.01607	0.01607	0.01607	0.01607	0.01607	0.01607	0.01607	0.01607	0.01607	0.01607
Run 148	-0.00001043	0.01607	0.01607	0.01607	0.01607	0.01607	0.01607	0.01607	0.01607	0.01607	0.01607
Run 149	-0.0000103	0.01607	0.01607	0.01607	0.01607	0.01607	0.01607	0.01607	0.01607	0.01607	0.01607
Run 150	-0.00001015	0.01607	0.01607	0.01607	0.01607	0.01607	0.01607	0.01607	0.01607	0.01607	0.01607
Run 151	-0.000009981	0.01606	0.01606	0.01606	0.01606	0.01606	0.01606	0.01607	0.01607	0.01607	0.01607
Run 152	-0.00000979	0.01606	0.01606	0.01606	0.01606	0.01606	0.01606	0.01607	0.01607	0.01607	0.01607
Run 153	-0.000009582	0.01606	0.01606	0.01606	0.01606	0.01606	0.01606	0.01606	0.01607	0.01607	0.01607
Run 154	-0.00000936	0.01606	0.01606	0.01606	0.01606	0.01606	0.01606	0.01606	0.01607	0.01607	0.01607
Run 155	-0.000009125	0.01606	0.01606	0.01606	0.01606	0.01606	0.01606	0.01606	0.01607	0.01607	0.01607
Run 156	-0.00000888	0.01606	0.01606	0.01606	0.01606	0.01606	0.01606	0.01606	0.01607	0.01607	0.01607

Run 157	-0.000008626	0.01606	0.01606	0.01606	0.01606	0.01606	0.01606	0.01606	0.01606	0.01607	0.01607
Run 158	-0.000008365	0.01606	0.01606	0.01606	0.01606	0.01606	0.01606	0.01606	0.01606	0.01607	0.01607
Run 159	-0.000008099	0.01606	0.01606	0.01606	0.01606	0.01606	0.01606	0.01606	0.01606	0.01607	0.01607
Run 160	-0.000007829	0.01606	0.01606	0.01606	0.01606	0.01606	0.01606	0.01606	0.01606	0.01607	0.01607
Run 161	-0.000007555	0.01606	0.01606	0.01606	0.01606	0.01606	0.01606	0.01606	0.01606	0.01607	0.01607
Run 162	-0.00000728	0.01606	0.01606	0.01606	0.01606	0.01606	0.01606	0.01606	0.01606	0.01606	0.01607
Run 163	-0.000007005	0.01606	0.01606	0.01606	0.01606	0.01606	0.01606	0.01606	0.01606	0.01606	0.01607
Run 164	-0.000006731	0.01606	0.01606	0.01606	0.01606	0.01606	0.01606	0.01606	0.01606	0.01606	0.01607
Run 165	-0.000006456	0.01606	0.01606	0.01606	0.01606	0.01606	0.01606	0.01606	0.01606	0.01606	0.01607
Run 166	-0.000006185	0.01606	0.01606	0.01606	0.01606	0.01606	0.01606	0.01606	0.01606	0.01606	0.01607
Run 167	-0.000005917	0.01606	0.01606	0.01606	0.01606	0.01606	0.01606	0.01606	0.01606	0.01606	0.01606
Run 168	-0.000005652	0.01606	0.01606	0.01606	0.01606	0.01606	0.01606	0.01606	0.01606	0.01606	0.01606
Run 169	-0.000005391	0.01606	0.01606	0.01606	0.01606	0.01606	0.01606	0.01606	0.01606	0.01606	0.01606
Run 170	-0.000005135	0.01606	0.01606	0.01606	0.01606	0.01606	0.01606	0.01606	0.01606	0.01606	0.01606
Run 171	-0.000004885	0.01606	0.01606	0.01606	0.01606	0.01606	0.01606	0.01606	0.01606	0.01606	0.01606
Run 172	-0.000004639	0.01606	0.01606	0.01606	0.01606	0.01606	0.01606	0.01606	0.01606	0.01606	0.01606
Run 173	-0.0000044	0.01606	0.01606	0.01606	0.01606	0.01606	0.01606	0.01606	0.01606	0.01606	0.01606
Run 174	-0.000004167	0.01606	0.01606	0.01606	0.01606	0.01606	0.01606	0.01606	0.01606	0.01606	0.01606
Run 175	-0.000003941	0.01606	0.01606	0.01606	0.01606	0.01606	0.01606	0.01606	0.01606	0.01606	0.01606
Run 176	-0.000003721	0.01606	0.01606	0.01606	0.01606	0.01606	0.01606	0.01606	0.01606	0.01606	0.01606
Run 177	-0.000003508	0.01606	0.01606	0.01606	0.01606	0.01606	0.01606	0.01606	0.01606	0.01606	0.01606
Run 178	-0.000003302	0.01606	0.01606	0.01606	0.01606	0.01606	0.01606	0.01606	0.01606	0.01606	0.01606
Run 179	-0.000003103	0.01606	0.01606	0.01606	0.01606	0.01606	0.01606	0.01606	0.01606	0.01606	0.01606
Run 180	-0.000002911	0.01606	0.01606	0.01606	0.01606	0.01606	0.01606	0.01606	0.01606	0.01606	0.01606
Run 181	-0.000002726	0.01606	0.01606	0.01606	0.01606	0.01606	0.01606	0.01606	0.01606	0.01606	0.01606
Run 182	-0.000002548	0.01606	0.01606	0.01606	0.01606	0.01606	0.01606	0.01606	0.01606	0.01606	0.01606

Run 182	-0.000002548	0.01606	0.01606	0.01606	0.01606	0.01606	0.01606	0.01606	0.01606	0.01606	0.01606
Run 183	-0.000002378	0.01606	0.01606	0.01606	0.01606	0.01606	0.01606	0.01606	0.01606	0.01606	0.01606
Run 184	-0.000002215	0.01606	0.01606	0.01606	0.01606	0.01606	0.01606	0.01606	0.01606	0.01606	0.01606
Run 185	-0.000002058	0.01606	0.01606	0.01606	0.01606	0.01606	0.01606	0.01606	0.01606	0.01606	0.01606
Run 186	-0.000001908	0.01606	0.01606	0.01606	0.01606	0.01606	0.01606	0.01606	0.01606	0.01606	0.01606
Run 187	-0.000001766	0.01606	0.01606	0.01606	0.01606	0.01606	0.01606	0.01606	0.01606	0.01606	0.01606
Run 188	-0.000001629	0.01606	0.01606	0.01606	0.01606	0.01606	0.01606	0.01606	0.01606	0.01606	0.01606
Run 189	-0.0000015	0.01606	0.01606	0.01606	0.01606	0.01606	0.01606	0.01606	0.01606	0.01606	0.01606
Run 190	-0.000001376	0.01606	0.01606	0.01606	0.01606	0.01606	0.01606	0.01606	0.01606	0.01606	0.01606
Run 191	-0.000001259	0.01606	0.01606	0.01606	0.01606	0.01606	0.01606	0.01606	0.01606	0.01606	0.01606
Run 192	-0.000001149	0.01606	0.01606	0.01606	0.01606	0.01606	0.01606	0.01606	0.01606	0.01606	0.01606
Run 193	-0.000001044	0.01606	0.01606	0.01606	0.01606	0.01606	0.01606	0.01606	0.01606	0.01606	0.01606
Run 194	-9.451E-07	0.01606	0.01606	0.01606	0.01606	0.01606	0.01606	0.01606	0.01606	0.01606	0.01606
Run 195	-8.515E-07	0.01606	0.01606	0.01606	0.01606	0.01606	0.01606	0.01606	0.01606	0.01606	0.01606
Run 196	-7.635E-07	0.01606	0.01606	0.01606	0.01606	0.01606	0.01606	0.01606	0.01606	0.01606	0.01606
Run 197	-6.807E-07	0.01606	0.01606	0.01606	0.01606	0.01606	0.01606	0.01606	0.01606	0.01606	0.01606
Run 198	-6.032E-07	0.01606	0.01606	0.01606	0.01606	0.01606	0.01606	0.01606	0.01606	0.01606	0.01606
Run 199	-5.298E-07	0.01606	0.01606	0.01606	0.01606	0.01606	0.01606	0.01606	0.01606	0.01606	0.01606
Run 200	-4.622E-07	0.01606	0.01606	0.01606	0.01606	0.01606	0.01606	0.01606	0.01606	0.01606	0.01606
Run 201	-3.983E-07	0.01606	0.01606	0.01606	0.01606	0.01606	0.01606	0.01606	0.01606	0.01606	0.01606
Run 202	-3.390E-07	0.01606	0.01606	0.01606	0.01606	0.01606	0.01606	0.01606	0.01606	0.01606	0.01606
Run 203	-2.838E-07	0.01606	0.01606	0.01606	0.01606	0.01606	0.01606	0.01606	0.01606	0.01606	0.01606
Run 204	-2.326E-07	0.01606	0.01606	0.01606	0.01606	0.01606	0.01606	0.01606	0.01606	0.01606	0.01606
Run 205	-1.850E-07	0.01606	0.01606	0.01606	0.01606	0.01606	0.01606	0.01606	0.01606	0.01606	0.01606
Run 206	-1.416E-07	0.01606	0.01606	0.01606	0.01606	0.01606	0.01606	0.01606	0.01606	0.01606	0.01606
Run 207	-1.008E-07	0.01606	0.01606	0.01606	0.01606	0.01606	0.01606	0.01606	0.01606	0.01606	0.01606

Appendix D: Steady state simulation of one RCCS increment (single loop with constant temperature boundary condition)

A Flownex® model of a single increment of the RCCS was given in Figure 5-9. This code was written to calculate the heat transfer rates at the different surfaces to compare to the Flownex® model in section 0.

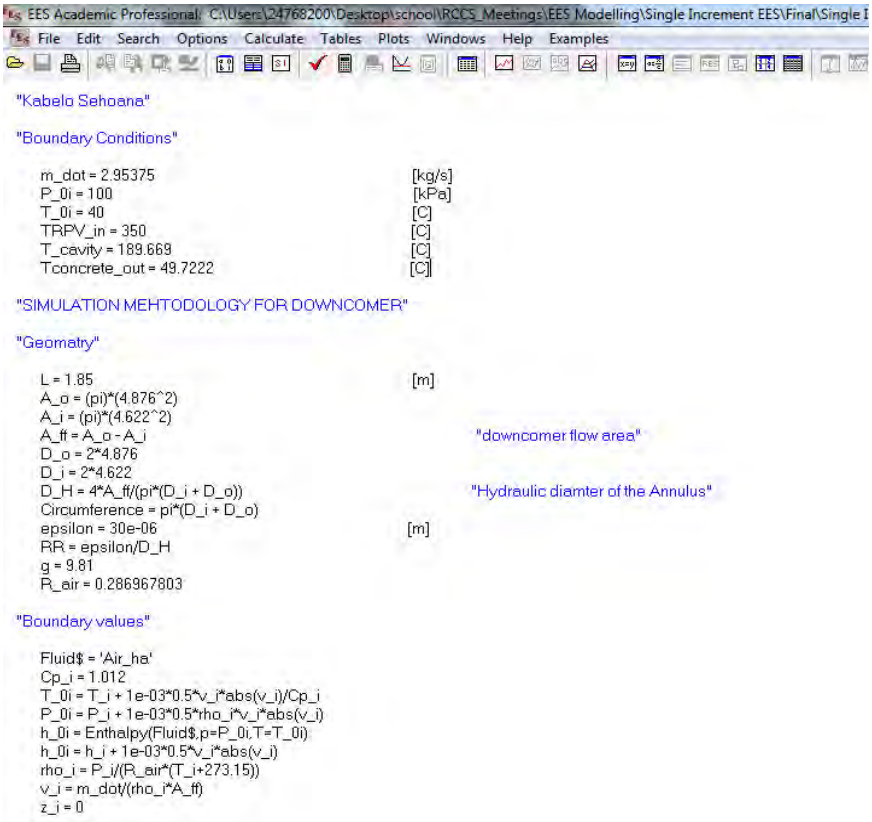

"Initialize incremental loop"

m_dot_e[0] = m_dot
P_0e[0] = P_0i
h_0e[0] = h_0i
T_0e[0] = T_0i
P_e[0] = P_i
h_e[0] = h_i
T_e[0] = T_i
rho_e[0] = rho_i
v_e[0] = v_i
Cp_e[0] = Cp_i
z_e[0] = z_i

"Pipe Incremental Loop"

dc = 1

DUPLICATE i = 1,dc

"Inlet Properties"

m_dot_i[i] = m_dot_e[i-1]
P_0i[i] = P_0e[i-1]
h_0i[i] = h_0e[i-1]
T_0i[i] = T_0e[i-1]
P_i[i] = P_e[i-1]
h_i[i] = h_e[i-1]
T_i[i] = T_e[i-1]
rho_i[i] = rho_e[i-1]
v_i[i] = v_e[i-1]
Cp_i[i] = Cp_e[i-1]
z_i[i] = z_e[i-1]

"Average Properties"

m_dot[i] = average(m_dot_i[i],m_dot_e[i])
P_0[i] = Average(P_0i[i],P_0e[i])
h_0[i] = Average(h_0i[i],h_0e[i])

h_0[i] = Average(h_0i[i],h_0e[i])
Cp[i] = 1.012
T_0[i] = T_Fluid[i] + 1e-03*0.5*v[i]*abs(v[i])/Cp[i]
h_0[i] = h[i] + 1e-03*0.5*v[i]*abs(v[i])
P_0[i] = P[i] + 1e-03*0.5*rho[i]*v[i]*abs(v[i])
T_Fluid[i] = Temperature(Fluid$,h=h[i],P=P[i])
rho[i] = P[i]/(R_air*(T_Fluid[i]+273.15))
v[i] = m_dot[i]/(rho[i]*A_ff)
z[i] = average(z_i[i],z_e[i])
mu[i] = viscosity(Fluid$,h=h[i],P=P[i])
Re[i]=rho[i]*v[i]*D_H/mu[i]
k[i] =1e-03*Conductivity(Fluid$,T=T_Fluid[i],P=P[i])
Pr[i] =0.71

"Outlet Properties"

m_dot_i[i] = m_dot_e[i]
P_0e[i] = 100.02 [kPa]
Q[i] = m_dot_e[i]*Cp_e[i]*T_0e[i] - m_dot_i[i]*Cp_i[i]*T_0i[i] + 1e-03*m_dot_e[i]*g*z_e[i] - 1e-03*m_dot_i[i]*g*z_i[i]
h_0e[i] = h_e[i] + 0.5*1e-03*v_e[i]*abs(v_e[i])
P_0e[i] = P_e[i] + 0.5*1e-03*rho_e[i]*v_e[i]*abs(v_e[i])
Cp_e[i] = 1.012
T_0e[i] = T_e[i] + 1e-03*0.5*v_e[i]*abs(v_e[i])/Cp_e[i]
T_e[i] = Temperature(Fluid$,h=h_e[i],P=P_e[i])
rho_e[i] = P_e[i]/(R_air*(T_e[i]+273.15))
v_e[i] = m_dot_e[i]/(rho_e[i]*A_ff)
z_e[i] = z_i[i] - L/dc

"Componenent Characteristics"

Q[i] = Qconv_dcout[i] + Qconv_dcin[i]

"Heat Transfer"

"Convection"

Nusselt_in[i] = IF(Re[i],2000,8.4549,84549,0.023*Re[i]^0.8*Pr[i]^0.4)
Nusselt_out[i] = IF(Re[i],2000,8.0311,8.0311,0.023*Re[i]^0.8*Pr[i]^0.4)

```
    Nusselt_in[i] = (h_in[i]*D_H)/k[i]
    Nusselt_out[i] = (h_o[i]*D_H)/k[i]

    Qconv_dcout[i] = Qconv_dcout
    Qconv_dcin[i] = Qconv_dcin

    Qconv_dcout[i] = h_o[i]*A_dcout*(T[10] - T_Fluid[i])
    Qconv_dcin[i] = h_in[i]*A_dcin*(T[9] - T_Fluid[i])

End

"SIMULATION METHODOLOGY FOR THE RISER"

" Riser Geomatry"

    A_ff_riser = 2.838                                  "downcomer flow area"
    D_H_riser = 0.08460                                 "Hydraulic diamter of the Riser"
    RR_riser = epsilon/D_H_riser

    R = 2

DUPLICATE e = dc+1,R

"Inlet Properties"

    m_dot_i[e] = m_dot_e[e-1]
    P_0i[e] = P_0e[e-1]
    h_0i[e] = h_0e[e-1]
    T_0i[e] = T_0e[e-1]
    P_i[e] = P_e[e-1]
    h_i[e] = h_e[e-1]
    T_i[e] = T_e[e-1]
    rho_i[e] = rho_e[e-1]
    v_i[e] = v_e[e-1]
    Cp_i[e] = Cp_e[e-1]
    z_i[e] = z_e[e-1]
```

"Average Properties"

m_dot[e] = average(m_dot_i[e],m_dot_e[e])
P_0[e] = Average(P_0i[e],P_0e[e])
T_0[e] = Average(T_0i[e],T_0e[e])
Cp[e] = 1.012
T_0[e] = T_Fluid[e] + 1e-03*0.5*v[e]*abs(v[e])/Cp[e]
P_0[e] = P[e] + 1e-03*0.5*rho[e]*v[e]*abs(v[e])
rho[e] = P[e]/(R_air*(T_Fluid[e]+273.15))
v[e] = m_dot[e]/(rho[e]*A_ff_riser)
z[e] = average(z_i[e],z_e[e])

mu[e] = viscosity(Fluid$,T=T_Fluid[e],P=P[e])
Re[e]=rho[e]*v[e]*D_H_riser/mu[e]
k[e] =1e-03*Conductivity(Fluid$,T=T_Fluid[e],P=P[e])
Pr[e] =0.71

"Outlet Properties"

m_dot_i[e] = m_dot_e[e]
P_0e[e] = 100 [kPa]
Q[e] = m_dot_e[e]*Cp_i*T_0e[e] - m_dot_i[e]*Cp_i*T_0i[e] + 1e-03*m_dot_e[e]*g*z_e[e] - 1e-03*m_dot_i[e]*g*z_i[e]
T_0e[e] = T_e[e] + 1e-03*0.5*v_e[e]*abs(v_e[e])/Cp_e[e]
P_0e[e] = P_e[e] + 0.5*1e-03*rho_e[e]*v_e[e]*abs(v_e[e])
rho_e[e] = P_e[e]/(R_air*(T_e[e]+273.15))
v_e[e] = m_dot_e[e]/(rho_e[e]*A_ff_riser)
Cp_e[e] = 1.012
z_e[e] = z_i[e] + L/dc

"Componenent Characteristics"

Q[e] = Qconv_RF[e] + Qconv_RS[e] + Qconv_RB[e]

"Heat Transfer"

"Convection"

Nusselt_in[e] = IF(Re[e],2000,5.7383,5.7383,0.023*Re[e]^0.8*Pr[e]^0.4)
Nusselt_in[e] = (h_in[e]*D_H_riser)/k[e]

Qconv_RF[e] = Qconv_RF
Qconv_RS[e] = Qconv_RS
Qconv_RB[e] = Qconv_RB

Qconv_RF[e] = h_in[e]*A[e+4]*(T[6] - T_Fluid[e])
Qconv_RS[e] = h_in[e]*A[e+6]*(T[8] - T_Fluid[e])
Qconv_RB[e] = h_in[e]*A[e+5]*(T[7] - T_Fluid[e])

End

"HEAT TRANSFER"

"NOTATION"

"1 = RPV
2 = RISER FRONT
3 = RISER SIDE
4 = RISER BACK
5 = DOWNCOMER"

"Emisivities"

e[1] = 0.8
e[2] = 0.8
e[3] = 0.8
e[4] = 0.8
e[5] = 0.1

"Surface Areas"

A[1] = 36.75 [m^2]
A[2] = 24.5523 [m^2]
A[3] = 214.5094 [m^2]
A[4] = 24.5523 [m^2]
A[5] = 52.6911 [m^2]

"1. RADIATION HEAT TRANSFER NETWORK"

n = 5

Duplicate i = 1,n

Eb[i] = sigma*(T[i] + 273.15)^4
c[i] = (1-e[i])/(A[i]*e[i])
Q_dot[i] = (Eb[i] - J[i])/c[i]

End

Q_dot[1] = A[1]*F[1,2]*(J[1] - J[2]) + A[1]*F[1,3]*(J[1]-J[3]) + A[1]*F[1,5]*(J[1]-J[5])
Q_dot[2] = A[1]*F[1,2]*(J[2]-J[1]) + A[2]*F[2,3]*(J[2]-J[3])
Q_dot[3] = A[1]*F[1,3]*(J[3]-J[1]) + A[2]*F[2,3]*(J[3]-J[2]) + A[3]*F[3,5]*(J[3]-J[5])
Q_dot[4] = A[4]*F[4,5]*(J[4]-J[5])
Q_dot[5] = A[1]*F[1,5]*(J[5]-J[1])+A[3]*F[3,5]*(J[5]-J[3])+A[4]*F[4,5]*(J[5]-J[4])

"2. HEAT TRANSFER THROUGH RPV WALL"

dx_wall = 0.215
k_wall = 1e-03*39.846
ARPV_in = 34.24 [m^2]
A_wall = 0.5*(ARPV_in + A[1])

Qcond_RPV = (k_wall*A_wall/dx_wall)*(TRPV_in - T[1])

"convection in the RPV wall with cavity"

h_cavity = 3e-03 [kW/m^2-K]
Qconv_RPV_cavity = h_cavity*A[1]*(T[1] - T_cavity)

"Energy Balance around the RPV wall - This is done to Release T[1]"

Qcond_RPV = Q_dot[1] + Qconv_RPV_cavity

"3. HEAT TRANSFER IN THE RISER FRONT WALL"

"convection"

"First Guesses"

{T[1] = 322.661}
{T[2] = 169.137}
{T[3] = 88.2814}
{T[4] = 84.3236}
{T[5] = 160.989}

"Known View Factors"

F[1,2] =0.5
F[1,3] = 0.4
F[1,5] = 0.1
F[2,3] = 0.056
F[3,5] = 0.114
F[4,5] = 1

"No Views - Surfaces do not see each other"

F[1,1] = 0;F[1,4] = 0;F[2,4] = 0;F[3,4] = 0
F[4,1] = 0;F[4,2] = 0; F[4,3] = 0; F[4,4] = 0; F[5,5] = 0;
F[5,2]=0;F[2,5]=0

"RECIPROCITY CHECKS"

A[1]*F[1,2] = B1;A[2]*F[2,1] = B2;B1 = B2
A[1]*F[1,3] = C1;A[3]*F[3,1] = C2;C1=C2
A[1]*F[1,5] = D1;A[5]*F[5,1] = D2;D2 = D1
A[2]*F[2,3] = E1;A[3]*F[3,2] = E2; E1=E2
A[3]*F[3,5] = F1;A[5]*F[5,3] = F2;F1 = F2
A[4]*F[4,5] = G1;A[5]*F[5,4] = G2; G1=G2

"Summation Rule"

F[2,1] + F[2,2] + F[2,3] + F[2,4] + F[2,5] = 1 "Calculate F[2,2]"
F[3,1] + F[3,2] + F[3,3] + F[3,4] + F[3,5] = 1 "Calculate F[3,3]"

sigma = 5.67e-11 [kW/m^2-K]

"Conduction through the RB wall"

dx_RS = 0.00473
A_RSin = 206.756
A_RSout = 214.5094
A_RS = 0.5*(A_RSin+A_RSout)
k_RS = 24.137e-03

Qcond_RS = ((k_RS*A_RS)/dx_RS)*(T[3] - TRS_in)

"6. RADIATION HEAT TRANSFER NETWORK INSIDE THE RISER"

"NOTATION"

"6 = RISER FRONT INSIDE
7 = RISER BACK INSIDE
8 = RISER SIDE INDISE"

b = 8

T[6] = TRF_in
T[7] = TRB_in
T[8] = TRS_in

e[6] = 0.8
e[7] = 0.8
e[8] = 0.8

A[6] = 20.6756
A[7] = 20.6756
A[8] = 206.756

RF_67 = 0.1
RF_68 = 0.9
RF_87 = 0.09

"energy balance"

ABS(Q_dot[2]) = Qcond_RF + abs(Qconv_RF_cavity)

"conduction through RF wall"

dx_RF = 0.004763 [m^2]
k_RF = 24.137e-03
A_RFin = 20.6756 [m^2]
A_RFout = 24.5523 [m^2]
A_RF = 0.5*(20.6756 + 24.5523)

Qcond_RF = (k_RF*A_RF/dx_RF)*(T[2] - TRF_in)

"4. HEAT TRANSFER IN THE RISER BACK WALL"

"Convection"

Qconv_RB_cavity = h_cavity*A[4]*(T_cavity - T[4])

"Energy balance"

abs(Q_dot[4]) + Qconv_RB_cavity = Qcond_RB

"Conduction through the RB wall"

Qcond_RB = (k_RP*A_RF/dx_RF)*(T[4] - TRB_in)

"5. HEAT TRANSFER IN THE RISER SIDE WALL"

"Convection"

Qconv_RS_cavity = h_cavity*A[3]*(T_cavity - T[3])

"Energy balance"

abs(Q_dot[3]) + Qconv_RS_cavity = Qcond_RS

"Conduction through the RB wall"

```
Duplicate i = 6,b

    Eb[i] = sigma*(T[i] + 273.15)^4
    c[i] = (1-e[i])/(A[i]*e[i])
    Q_dot[i] = (Eb[i]-J[i])/c[i]

End

    Q_dot[6] = A[6]*RF_67*(J[6] - J[7]) + A[6]*RF_68*(J[6] - J[8])
    Q_dot[7] = A[6]*RF_67*(J[7] - J[6]) + A[8]*RF_87*(J[7] - J[8])
    Q_dot[8] = A[6]*RF_68*(J[8] - J[6]) + A[8]*RF_87*(J[8] - J[7])

"7. ENERGY BALANCE INSIDE THE RISER"

    Qcond_RF - abs(Q_dot[6]) = Qconv_RF

    Qcond_RS + abs(Q_dot[8]) = Qconv_RS

    Qcond_RB + abs(Q_dot[7]) = Qconv_RB


"8. HEAT TRANSFER THROUGH THE INSULATION"

    k_insulation = 0.024e-03                                    [kW/m-K]
    dx_insulation = 0.0762                                      [m]
    Ains_in = 52.6911                                           [m^2]
    Ains_out = 53.7259                                          [m^2]
    A_insulation = 0.5*(Ains_in + Ains_out)

    Qcond_insulation = ((k_insulation  *A_insulation)/dx_insulation)*(T[5] - T_insulation)

    Qconv_DC_cav = h_cavity*A[5]*(T_cavity - T[5])

    Qconv_DC_cav  - Q_dot[5] = Qcond_insulation

"9. HEAT TRANSFER THROUGH THE DOWNCOMER STEEL"

    dx_DCin = 0.0127                                            [m^2]
    k_dcin = 24.137e-03                                         [kW/m-K]


    k_dcin = 24.137e-03                                         [kW/m-K]
    A_dcin = 53.7259                                            [m^2]

    Qcond_DCin = ((k_dcin *A_dcin )/dx_DCin)*(T_insulation - TDC_in)

Qcond_DCin = Qcond_insulation

"10. RADIATION HEAT TRANSFER NETWORK INSIDE THE DOWNCOMER"

    T[9] = TDC_in
    F_dcin_dcout = 1
    e_dcin = 0.8
    e_dcout = 0.8
    A_dcout = 56.6785                                           [m^2]

    Qrad_DCin_DCo = sigma*((T[9] + 273.15)^4 - (T[10]+273.15)^4)/((1-e_dcin)/(e_dcin*A_dcin)+(1/(A_dcin*F_dcin_dcout)) + ((1-e_dcout)/(e_dcout*A_dcout )))

"energy balance on the inside downcomer wall"

    Qcond_DCin = Qrad_DCin_DCo + Qconv_dcin


"energy balance on the outer downcomer wall"

    Qcond_DCout  + Qconv_dcout = Qrad_DCin_DCo

"11. HEAT TRANSFER IN THE OUTER DOWNCOMER STEEL WALL"

    dx_DCouter = 0.0127                                         [m]
    k_dcouter = 24.137e-03                                      [kW/m-K]


    Qcond_DCout = ((k_dcouter*A_dcout )/dx_DCouter)*(T[10] - Tconcrete_in)

    Qcond_DCout = Qcond_concrete


"12. HEAT TRANSFER THROUGH THE CONCRETE"

    dx_concrete = 1.5                                           [m]
    k_concrete = 1e-03*1.991                                    [kW/m-K]
    A_concrete = 56.6785                                        [m^2]

    Qcond_concrete = ((k_concrete*A_concrete)/dx_concrete)*(Tconcrete_in - Tconcrete_out)
```

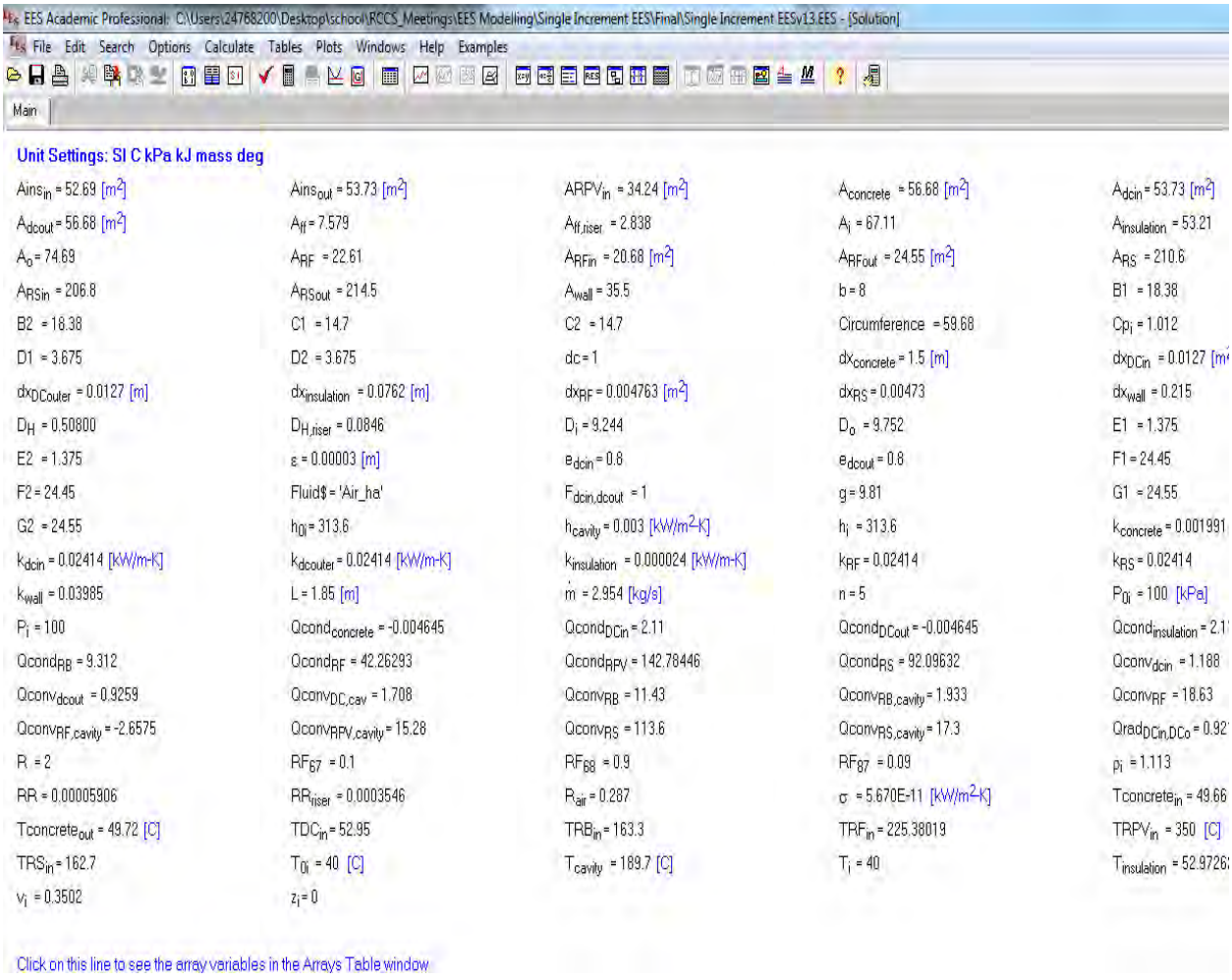
EES Academic Professional: C:\Users\24768200\Desktop\school\RCCS_Meetings\EES Modelling\Single Increment EES\Final\Single Increment EESv13.EES - [Solution]
File Edit Search Options Calculate Tables Plots Windows Help Examples
Main
Unit Settings: SI C kPa kJ mass deg
$A_{ins_{in}} = 52.69$ [m²]
$A_{ins_{out}} = 53.73$ [m²]
$A_{RPV_{in}} = 34.24$ [m²]
$A_{concrete} = 56.68$ [m²]
$A_{dcin} = 53.73$ [m²]
$A_{dcout} = 56.68$ [m²]
$A_{ff} = 7.579$
$A_{ff,riser} = 2.838$
$A_i = 67.11$
$A_{insulation} = 53.21$
$A_o = 74.69$
$A_{RF} = 22.61$
$A_{RFin} = 20.68$ [m²]
$A_{RFout} = 24.55$ [m²]
$A_{RS} = 210.6$
$A_{RSin} = 206.8$
$A_{RSout} = 214.5$
$A_{wall} = 35.5$
$b = 8$
B1 = 18.38
B2 = 18.38
C1 = 14.7
C2 = 14.7
Circumference = 59.68
$Cp_i = 1.012$
D1 = 3.675
D2 = 3.675
$dc = 1$
$dx_{concrete} = 1.5$ [m]
$dx_{DCin} = 0.0127$ [m
$dx_{DCouter} = 0.0127$ [m]
$dx_{insulation} = 0.0762$ [m]
$dx_{RF} = 0.004763$ [m²]
$dx_{RS} = 0.00473$
$dx_{wall} = 0.215$
$D_H = 0.50800$
$D_{H,riser} = 0.0846$
$D_i = 9.244$
$D_o = 9.752$
E1 = 1.375
E2 = 1.375
$\varepsilon = 0.00003$ [m]
$e_{dcin} = 0.8$
$e_{dcout} = 0.8$
F1 = 24.45
F2 = 24.45
Fluid$ = 'Air_ha'
$F_{dcin,dcout} = 1$
g = 9.81
G1 = 24.55
G2 = 24.55
$h_{0i} = 313.6$
$h_{cavity} = 0.003$ [kW/m²-K]
$h_i = 313.6$
$k_{concrete} = 0.001991$
$k_{dcin} = 0.02414$ [kW/m-K]
$k_{dcouter} = 0.02414$ [kW/m-K]
$k_{insulation} = 0.000024$ [kW/m-K]
$k_{RF} = 0.02414$
$k_{RS} = 0.02414$
$k_{wall} = 0.03985$
L = 1.85 [m]
$\dot{m} = 2.954$ [kg/s]
n = 5
$P_{0i} = 100$ [kPa]
$P_i = 100$
$Qcond_{concrete} = -0.004645$
$Qcond_{DCin} = 2.11$
$Qcond_{DCout} = -0.004645$
$Qcond_{insulation} = 2.1$
$Qcond_{RB} = 9.312$
$Qcond_{RF} = 42.26293$
$Qcond_{RPV} = 142.78446$
$Qcond_{RS} = 92.09632$
$Qconv_{dcin} = 1.188$
$Qconv_{dcout} = 0.9259$
$Qconv_{DC,cav} = 1.708$
$Qconv_{RB} = 11.43$
$Qconv_{RB,cavity} = 1.933$
$Qconv_{RF} = 18.63$
$Qconv_{RF,cavity} = -2.6575$
$Qconv_{RPV,cavity} = 15.28$
$Qconv_{RS} = 113.6$
$Qconv_{RS,cavity} = 17.3$
$Qrad_{DCin,DCo} = 0.92$
R = 2
$RF_{67} = 0.1$
$RF_{68} = 0.9$
$RF_{87} = 0.09$
$\rho_i = 1.113$
RR = 0.00005906
$RR_{riser} = 0.0003546$
$R_{air} = 0.287$
$\sigma = 5.670E-11$ [kW/m²-K]
$Tconcrete_{in} = 49.66$
$Tconcrete_{out} = 49.72$ [C]
$TDC_{in} = 52.95$
$TRB_{in} = 163.3$
$TRF_{in} = 225.38019$
$TRPV_{in} = 350$ [C]
$TRS_{in} = 162.7$
$T_{0i} = 40$ [C]
$T_{cavity} = 189.7$ [C]
$T_i = 40$
$T_{insulation} = 52.9726$
$v_i = 0.3502$
$z_i = 0$
Click on this line to see the array variables in the Arrays Table window

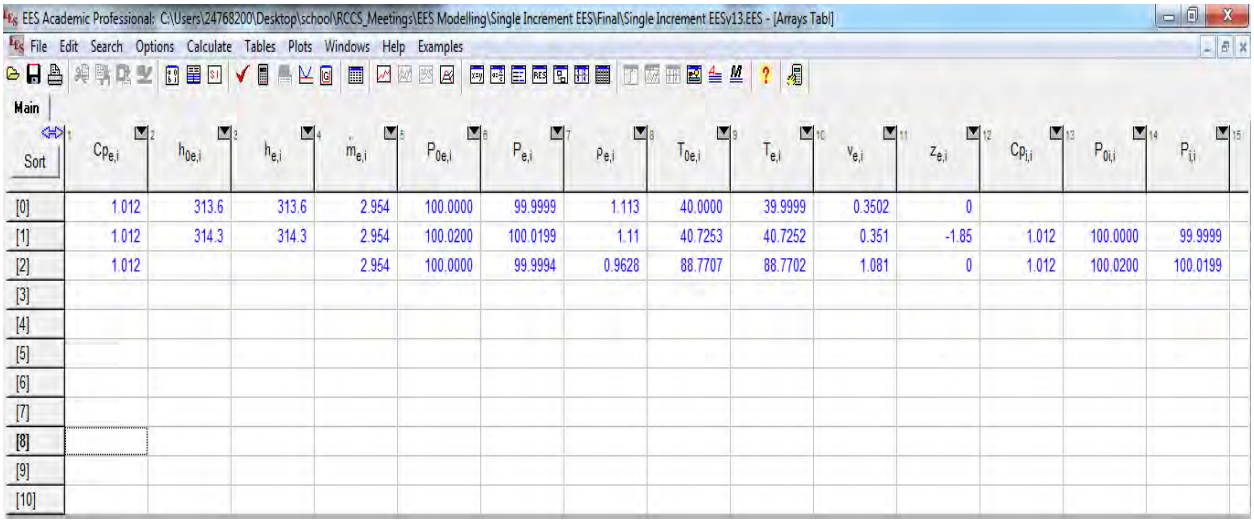
EES Academic Professional: C:\Users\24768200\Desktop\school\RCCS_Meetings\EES Modelling\Single Increment EES\Final\Single Increment EESv13.EES - [Arrays Tabl]
File Edit Search Options Calculate Tables Plots Windows Help Examples
Main
Sort
$Cp_{e,i}$ $h_{0e,i}$ $h_{e,i}$ $\dot{m}_{e,i}$ $P_{0e,i}$ $P_{e,i}$ $\rho_{e,i}$ $T_{0e,i}$ $T_{e,i}$ $v_{e,i}$ $z_{e,i}$ $Cp_{i,i}$ $P_{0i,i}$ $P_{i,i}$
[0] 1.012 313.6 313.6 2.954 100.0000 99.9999 1.113 40.0000 39.9999 0.3502 0 1.012 100.0000 99.9999
[1] 1.012 314.3 314.3 2.954 100.0200 100.0199 1.11 40.7253 40.7252 0.351 -1.85 1.012 100.0000 99.9999
[2] 1.012 2.954 100.0000 99.9994 0.9628 88.7707 88.7702 1.081 0 1.012 100.0200 100.0199
[3]
[4]
[5]
[6]
[7]
[8]
[9]
[10]

Main

Sort	$T_{i,i}$	$h_{0i,i}$	$h_{i,i}$	$\dot{m}_{i,i}$	$\rho_{i,i}$	$v_{i,i}$	$z_{i,i}$	Q_i	$\dot{m}_i$	Cp_i	P_i	$P_{0,i}$	Pr_i	Re_i
[0]														
[1]	39.9999	313.6	313.6	2.954	1.113	0.3502	0	2.114	2.954	1.012	100	100	0.71	10321
[2]	40.7252	314.3	314.3	2.954	1.11	0.351	-1.85	143.671	2.954	1.012	100	100	0.71	4334
[3]														
[4]														
[5]														
[6]														
[7]														
[8]														
[9]														
[10]														

Main

Sort	$T_{0,i}$	h_i	$h_{0,i}$	k_i	μ_i	ρ_i	v_i	z_i	$Nusselt_{in,i}$	$Nusselt_{out,i}$	$h_{in,i}$	$h_{o,i}$	$T_{Fluid,i}$	e_i
[0]														
[1]	40.3626	313.9	313.9	0.00002738	1.918E-05	1.112	0.3506	-0.925	32.59941	32.6	0.001757	0.001757	40.36	0.8
[2]	64.7480			0.00002914	2.032E-05	1.031	1.009	-0.925	16.28281		0.005609		64.75	0.8
[3]														0.8
[4]														0.8
[5]														0.1
[6]														0.8
[7]														0.8
[8]														0.8
[9]														
[10]														

Sort	A_i [m2]	c_i	Eb_i	J_i	$F_{i,1}$	$F_{i,2}$	$F_{i,3}$	$F_{i,4}$	$F_{i,5}$	$\dot{Q}_i$ [kW]	T_i [C]	$Qconv_{RB,i}$	$Qconv_{RF,i}$	$Qconv_{RS,i}$
[0]														
[1]	36.75	0.006803	7.419	6.552	0	0.5	0.4	0	0.1	127.5010	328.2946			
[2]	24.55	0.01018	3.513	3.97	0.7484	0.1956	0.056	0	0	-44.9205	225.7490	11.43	18.63	113.6
[3]	214.5	0.001165	2.048	2.135	0.06853	0.00641	0.8111	0	0.114	-74.8002	162.7920			
[4]	24.55	0.01018	2.06	2.135	0	0	0	0	1	-7.3788	163.4284			
[5]	52.69	0.1708	2.367	2.436	0.06975	0	0.4641	0.466	0	-0.4015	178.8623			
[6]	20.68	0.01209	3.502	3.216						23.6337	225.3802			
[7]	20.68	0.01209	2.058	2.084						-2.1234	163.3471			
[8]	206.8	0.001209	2.046	2.072						-21.5104	162.7064			
[9]											52.9520			
[10]											49.6604			

	$Qconv_{dcin,i}$	$Qconv_{dcout,i}$
	1.188	0.9259
.6		

Appendix E: Steady state simulation of one RCCS increment (double loop with constant temperature boundary condition)

A Flownex® model of a single increment of the RCCS was given in Figure 5-10. This code was written to calculate the heat transfer rates at the different surfaces to compare to the Flownex® model in section 5.3.1. The results are given section 5.3.2. This code is similar to the one written in **Appendix D** except that two loops are evaluated instead of one riser loop.

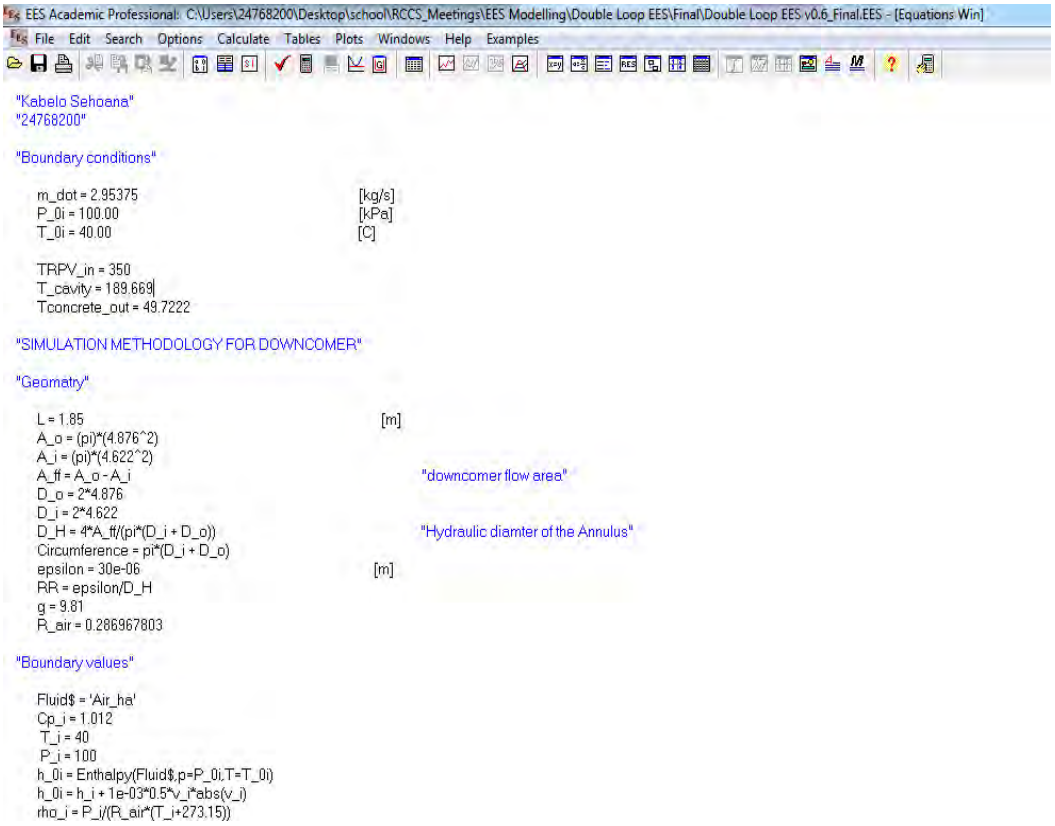

```
    v_i = m_dot/(rho_i*A_ff)
    z_i = 0

"Initialize incremental loop"

    m_dot_e[0] = m_dot
    P_0e[0] = P_0i
    h_0e[0] = h_0i
    T_0e[0] = T_0i
    P_e[0] = P_i
    h_e[0] = h_i
    T_e[0] = T_i
    rho_e[0] = rho_i
    v_e[0] = v_i
    z_e[0] = z_i

    n = 1

"Pipe Incremental Loop"

DUPLICATE i = 1,n

"Inlet Properties"

    m_dot_i[i] = m_dot_e[i-1]
    P_0i[i] = P_0e[i-1]
    h_0i[i] = h_0e[i-1]
    T_0i[i] = T_0e[i-1]
    P_i[i] = P_e[i-1]
    h_i[i] = h_e[i-1]
    T_i[i] = T_e[i-1]
    rho_i[i] = rho_e[i-1]
    v_i[i] = v_e[i-1]
    z_i[i] = z_e[i-1]

"Average Properties"

    m_dot[i] = average(m_dot_i[i],m_dot_e[i])
    P_0[i] = Average(P_0i[i],P_0e[i])



    T_fluid[i] = Temperature(Fluid$,h=h[i],P=P[i])
    rho[i] =  P[i]/(R_air*(T_Fluid[i]+273.15))
    v[i] = m_dot[i]/(rho[i]*A_ff)
    z[i] = average(z_i[i],z_e[i])

    mu[i] = viscosity(Fluid$,T=T_Fluid[i],P=P[i])
    Re[i]=rho[i]*v[i]*D_H/mu[i]
    k[i] =1e-03*Conductivity(Fluid$,T=T_fluid[i],P=P[i])
    Pr[i] =0.71

"Outlet Properties"

    m_dot_i[i] = m_dot_e[i]
    P_0e[i] = 100.02
    Q[i] = m_dot_e[i]*Cp_i*T_0e[i] - m_dot_i[i]*Cp_i*T_0i[i] + 1e-03*m_dot_e[i]*g*z_e[i] - 1e-03*m_dot_i[i]*g*z_i[i]
    h_0e[i] = h_e[i] + 0.5*1e-03*v_e[i]*abs(v_e[i])
    P_e[i] = 100.02
    Cp_e[i] = 1.012
    T_0e[i] = T_e[i] + 1e-03*0.5*v_e[i]*abs(v_e[i])/Cp_e[i]
    T_e[i] = Temperature(Fluid$,h=h_e[i],P=P_e[i])
    rho_e[i] = P_e[i]/(R_air*(T_e[i]+273.15))
    v_e[i] = m_dot_e[i]/(rho_e[i]*A_ff)
    z_e[i] = z_i[i] - L/n

"Componenent Characteristics"

    Q[i] =Qconv_dcin[i] + Qconv_dcout[i]

"Heat Transfer"

"Convection"

    Nusselt_in[i] = IF(Re[i],2000,8.4549,84549,0.023*Re[i]^0.8*Pr[i]^0.4)
    Nusselt_out[i] = IF(Re[i],2000,8.0311,8.0311,0.023*Re[i]^0.8*Pr[i]^0.4)

    Nusselt_in[i] = (h_in[i]*D_H)/k[i]
    Nusselt_out[i] = (h_o[i]*D_H)/k[i]

    Qconv_dcin[i] = Qconv_dcin
```

```
    Qconv_dcout[i] = Qconv_dcout

    Qconv_dcout[i] = h_o[i]*A_dcout*(T[17] - T_Fluid[i])
    Qconv_dcin[i] = h_in[i]*A_dcin*(T[16] - T_Fluid[i])

End


"SIMULATION METHODOLOGY FOR THE RISER"

" Riser Geomatry"

    A_ff_riser = 2.838/2                                    "downcomer flow area"
    D_H_riser = 0.08460                                     "Hydraulic diamter of the Riser"
    RR_riser = epsilon/D_H_riser

    m = 2

DUPLICATE e = n+1,m

"Inlet Properties"

    m_dot_i[e] = 0.5*m_dot_e[e-1]
    P_0i[e] = P_0e[e-1]
    h_0i[e] = h_0e[e-1]
    T_0i[e] = T_0e[e-1]
    P_i[e] = P_e[e-1]
    h_i[e] = h_e[e-1]
    T_i[e] = T_e[e-1]
    rho_i[e] = rho_e[e-1]
    v_i[e] = v_e[e-1]
    Cp_i[e] = Cp_e[e-1]
    z_i[e] = z_e[e-1]

"Average Properties"

    m_dot[e] = average(m_dot_i[e],m_dot_e[e])
    P_0[e] = Average(P_0i[e],P_0e[e])
    h_0[e] = Average(h_0i[e],h_0e[e])



    Cp[e] = 1.012
    T_0[e] = T_Fluid[e] + 1e-03*0.5*v[e]*abs(v[e])/Cp[e]
    h_0[e] = h[e] + 1e-03*0.5*v[e]*abs(v[e])
    P_0[e] = P[e] + 1e-03*0.5*rho[e]*v[e]*abs(v[e])
    T_fluid[e] = Temperature(Fluid$,h=h[e],P=P[e])
    rho[e] = P[e]/(R_air*(T_Fluid[e]+273.15))
    v[e] = m_dot[e]/(rho[e]*A_ff_riser)
    z[e] = average(z_i[e],z_e[e])

    mu[e] = viscosity(Fluid$,T=T_Fluid[e],P=P[e])
    Re[e]=rho[e]*v[e]*D_H_riser/mu[e]
    k[e] =1e-03*Conductivity(Fluid$,T=T_fluid[e],P=P[e])
    Pr[e] =0.71


"Outlet Properties"

    m_dot_i[e] = m_dot_e[e]
    P_0e[e] = 100
    Q[e] = m_dot_e[e]*Cp_i*T_0e[e] - m_dot_i[e]*Cp_i*T_0i[e] + 1e-03*m_dot_e[e]*g*z_e[e] - 1e-03*m_dot_i[e]*g*z_i[e]
    T_0e[e] = T_e[e] + 1e-03*0.5*v_e[e]*abs(v_e[e])/Cp_e[e]
    P_e[e] = 100
    h_0e[e] = h_e[e] + 0.5*1e-03*v_e[e]*abs(v_e[e])
    T_e[e] = Temperature(Fluid$,h=h_e[e],P=P_e[e])
     rho_e[e] = P_e[e]/(R_air*(T_e[e]+273.15))
    v_e[e] = m_dot_e[e]/(rho_e[e]*A_ff_riser)
    Cp_e[e] = 1.012
    z_e[e] = z_i[e] + L/n

"Componenent Characteristics"

    Q[e] = Qconv_RF1[e] + Qconv_RB1[e] + Qconv_RS1[e]

"Heat Transfer"

"Convection"

    Nusselt_in[e] = IF(Re[e],2000,5.7383,5.7383,0.023*Re[e]^0.8*Pr[e]^0.4)
    Nusselt_in[e] = (h_in[e]*D_H_riser)/k[e]
```

```
    Qconv_RF1[e] = Qconv_RF1
    Qconv_RB1[e] = Qconv_RB1
    Qconv_RS1[e] = Qconv_RS1

    Qconv_RF1[e] = h_in[e]*A[9]*(T[9]-T_Fluid[e])
    Qconv_RB1[e] = h_in[e]*A[10]*(T[10]-T_Fluid[e])
    Qconv_RS1[e] = h_in[e]*A[11]*(T[11]-T_Fluid[e])

End

    p = 3

DUPLICATE b = m+1,p

"Inlet Properties"

    m_dot_i[b] = 0.5*m_dot_e[b-2]
    P_0i[b] = P_0e[b-2]
    h_0i[b] = h_0e[b-2]
    T_0i[b] = T_0e[b-2]
    P_i[b] = P_e[b-2]
    h_i[b] = h_e[b-2]
    T_i[b] = T_e[b-2]
    rho_i[b] = rho_e[b-2]
    v_i[b] = v_e[b-2]
    Cp_i[b] = Cp_e[b-2]
    z_i[b] = z_e[b-2]

"Average Properties"

    m_dot[b] = average(m_dot_i[b],m_dot_e[b])
    P_0[b] = Average(P_0i[b],P_0e[b])
    h_0[b] = Average(h_0i[b],h_0e[b])
    Cp[b] = 1.012
    T_0[b] = T_fluid[b] + 1e-03*0.5*v[b]*abs(v[b])/Cp[b]
    h_0[b] = h[b] + 1e-03*0.5*v[b]*abs(v[b])
    P_0[b] = P[b] + 1e-03*0.5*rho[b]*v[b]*abs(v[b])
    T_fluid[b] = Temperature(Fluid$,h=h[b],P=P[b])
    rho[b] = P[b]/(R_air*(T_Fluid[b]+273.15))



    v[b] = m_dot[b]/(rho[b]*A_ff_riser)
    z[b] = average(z_i[b],z_e[b])

    mu[b] = viscosity(Fluid$,h=h[b],P=P[b])
    Re[b]=rho[b]*v[b]*D_H_riser/mu[b]
    k[b] =1e-03*Conductivity(Fluid$,T=T_fluid[b],P=P[b])
    Pr[b] =0.71

"Outlet Properties"

    m_dot_i[b] = m_dot_e[b]
    P_0e[b] = 100
    Q[b] = m_dot_e[b]*Cp_i*T_0e[b] - m_dot_i[b]*Cp_i*T_0i[b] + 1e-03*m_dot_e[b]*g*z_e[b] - 1e-03*m_dot_i[b]*g*z_i[b]
    T_0e[b] = T_e[b] + 1e-03*0.5*v_e[b]*abs(v_e[b])/Cp_e[b]
    P_e[b] = 100
    h_0e[b] = h_e[b] + 0.5*1e-03*v_e[b]*abs(v_e[b])
    T_e[b] = Temperature(Fluid$,h=h_e[b],P=P_e[b])
    rho_e[b] = P_e[b]/(R_air*(T_e[b]+273.15))
    v_e[b] = m_dot_e[b]/(rho_e[b]*A_ff_riser)
    Cp_e[b] = 1.012
    z_e[b] = z_i[b] + L/n

"Component Characteristics"

    Q[b] = Qconv_RF2[b]+Qconv_RB2[b]+Qconv_RS2[b]

"Heat Transfer"

"Convection"

    Nusselt_in[b] = IF(Re[b],2000,5.7383,5.7383,0.023*Re[b]^0.8*Pr[b]^0.4)
    Nusselt_in[b] = (h_in[b]*D_H_riser)/k[b]

    Qconv_RF2[b] = Qconv_RF2
    Qconv_RB2[b] = Qconv_RB2
    Qconv_RS2[b] = Qconv_RS2

    Qconv_RF2[b] = h_in[b]*A[12]*(T[12]-T_Fluid[b])
    Qconv_RB2[b] = h_in[b]*A[13]*(T[13]-T_Fluid[b])
```

```
    Qconv_RS2[b] = h_in[b]*A[14]*(T[14]-T_Fluid[b])

End

"Boltzmann - Constant"

sigma = 5.67e-08*1e-03                                  [kW/m^2-K]

"Emisivities"

    e[1] = 0.8
    e[2] = 0.8
    e[3] = 0.8
    e[4] = 0.8
    e[5] = 0.8
    e[6] = 0.8
    e[7] = 0.8
    e[8] = 0.1

"Surface Areas"

    A[1] = 36.75                                        [m^2]
    A[2] = 12.27614                                     [m^2]
    A[3] = 12.27614                                     [m^2]
    A[4] = 107.2547                                     [m^2]
    A[5] = 107.2547                                     [m^2]
    A[6] = 12.27614                                     [m^2]
    A[7] =12.27614                                      [m^2]
    A[8] = 26.3456*2                                    [m^2]

"First Guesses"

    {T[1] = 322.909}
    {T[2] = 172.64}
    {T[3] = 172.638}
    {T[4] = 91.4216}
    {T[5] = 91.4063}
    {T[6] = 87.5373}
    {T[7] = 87.5373}



    {T[8] = 163.649}

"known View Factors"

    F[1,2] = 0.25; F[1,3] = 0.25;  F[1,4] = 0.2; F[1,5] = 0.2; F[1,8] = 0.1     "From RPV"
    F[2,3] = 0.0978; F[2,4] = 0.028; F[2,5] = 0.028                             "From Front 1"
    F[3,4] = 0.028; F[3,5] = 0.028                                              "From Front 2"
    F[4,5] = 0.4055; F[4,8] = 0.114                                             "From Side 1"
    F[5,8] = 0.114                                                              "From Side 2"
    F[6,8] = 1                                                                  "From Back 1"
    F[7,8] = 1                                                                  "From Back 2"

"Zero View Factors"

    F[1,7]=0;F[1,6]=0;F[1,1]=0
    F[2,7]=0;F[2,6]=0;F[2,8]=0
    F[3,6]=0;F[3,7]=0;F[3,8]=0;
    F[4,6] = 0; F[4,7] = 0
    F[5,6]=0;F[5,7]=0


    F[8,2]=0;F[8,3]=0;F[8,8] = 0


f = 7

duplicate i = 1,f

    F[6,i] = 0
    F[7,i] = 0
end

"Self-Views"

    F[2,2] = 0.0978; F[3,3] = 0.0978; F[4,4] = 0.4055; F[5,5] = 0.4055

"Reciprocity Checks"

    A[1]*F[1,2] = A[2]*F[2,1]
```

```
A[1]*F[1,3] = A[3]*F[3,1]
A[1]*F[1,5] = A[5]*F[5,1]
A[1]*F[1,4] = A[4]*F[4,1]
A[1]*F[1,8] = A[8]*F[8,1]

A[2]*F[2,3] = A[3]*F[3,2]
A[2]*F[2,4] = A[4]*F[4,2]
A[2]*F[2,5] = A[5]*F[5,2]

A[3]*F[3,4] = A[4]*F[4,3]
A[3]*F[3,5] = A[5]*F[5,3]

A[4]*F[4,5] = A[5]*F[5,4]
A[4]*F[4,8] = A[8]*F[8,4]

A[5]*F[5,8] = A[8]*F[8,5]

A[6]*F[6,8] = A[8]*F[8,6]
A[7]*F[7,8] = A[8]*F[8,7]
```

"1. RADIATION HEAT TRANSFER NETWORK"

```
Rad = 8

Duplicate i = 1,Rad

    Eb[i] = sigma*(T[i] + 273.15)^4
    c[i] = (1-e[i])/(A[i]*e[i])
    Q_dot[i] = (Eb[i] - J[i])/c[i]

End

    Q_dot[1] = A[1]*F[1,2]*(J[1]-J[2]) + A[1]*F[1,3]*(J[1]-J[3]) +  A[1]*F[1,4]*(J[1]-J[4]) + A[1]*F[1,5]*(J[1]-J[5]) + A[1]*F[1,8]*(J[1]-J[8])
    Q_dot[2] = A[1]*F[1,2]*(J[2]-J[1]) + A[2]*F[2,3]*(J[2]-J[3]) + A[2]*F[2,4]*(J[2]-J[4]) + A[2]*F[2,5]*(J[2]-J[5])
    Q_dot[3] = A[1]*F[1,3]*(J[3]-J[1]) + A[2]*F[2,3]*(J[3]-J[2]) + A[3]*F[3,4]*(J[3]-J[4]) + A[3]*F[3,5]*(J[3]-J[5])
    Q_dot[4] = A[1]*F[1,4]*(J[4]-J[1]) + A[2]*F[2,4]*(J[4]-J[2]) + A[3]*F[3,4]*(J[4]-J[3]) + A[4]*F[4,5]*(J[4]-J[5]) + A[4]*F[4,8]*(J[4]-J[8])
    Q_dot[5] = A[1]*F[1,5]*(J[5]-J[1]) + A[2]*F[2,5]*(J[5]-J[2]) + A[3]*F[3,5]*(J[5]-J[3]) + A[4]*F[4,5]*(J[5]-J[4]) + A[5]*F[5,8]*(J[5]-J[8])
    Q_dot[6] = A[6]*F[6,8]*(J[6]-J[8])
    Q_dot[7] = A[7]*F[7,8]*(J[7]-J[8])
```

```
    Q_dot[8] = A[1]*F[1,8]*(J[8]-J[1]) + A[4]*F[4,8]*(J[8]-J[4]) +  A[5]*F[5,8]*(J[8]-J[5]) + A[6]*F[6,8]*(J[8]-J[6]) +  A[7]*F[7,8]*(J[8]-J[7])
```

"2. HEAT TRANSFER THROUGH RPV WALL"

```
    dx_wall = 0.215
    k_wall = 1e-03*39.846
    ARPV_in = 34.24                                                    [m^2]
    A_wall = 0.5*(ARPV_in + A[1])

    Qcond_RPV = (k_wall*A_wall/dx_wall)*(TRPV_in - T[1])
```

"convection in the RPV wall with cavity"

```
    h_cavity = 3e-03                                                   [kW/m^2-K]

    Qconv_RPV_cavity = h_cavity*A[1]*(T[1] - T_cavity)
```

"Energy Balance around the RPV wall - This is done to Release T[1]"

```
    Qcond_RPV = Q_dot[1] + Qconv_RPV_cavity
```

"3. HEAT TRANSFER IN THE RISER FRONT WALLS"

"convection"

```
    Qconv_RF1_cavity = h_cavity*A[2]*(T[2]-T_cavity)
    Qconv_RF2_cavity = h_cavity*A[3]*(T[3]-T_cavity)
```

"energy balance"

```
    abs(Q_dot[2]) = Qcond_RF1 + Qconv_RF1_cavity
    abs(Q_dot[3]) = Qcond_RF2 + Qconv_RF1_cavity
```

"conduction through RF wall"

```
    dx_RF = 0.004763                                                   [m^2]
    k_RF = 24.137e-03
    A_RFin = 20.6756/2                                                 [m^2]
    A_RFout = 24.55228/2                                               [m^2]
```

```
A_RF = 0.5*(A_RFin  + A_RFout )

Qcond_RF1 = (k_RF*A_RF/dx_RF)*(T[2] - TRF1_in)
Qcond_RF2 = (k_RF*A_RF/dx_RF)*(T[3] - TRF2_in)
```

"4. HEAT TRANSFER IN THE RISER BACK WALLS"

"Convection"

```
Qconv_RB1_cavity = h_cavity*A[7]*(T_cavity - T[7])
Qconv_RB2_cavity = h_cavity*A[6]*(T_cavity - T[6])
```

"Energy balance"

```
abs(Q_dot[7]) + Qconv_RB1_cavity = Qcond_RB1
abs(Q_dot[6]) + Qconv_RB2_cavity = Qcond_RB2
```

"Conduction through the RB wall"

```
Qcond_RB1 = (k_RF*A_RF/dx_RF)*(T[7] - TRB1_in)
Qcond_RB2 = (k_RF*A_RF/dx_RF)*(T[6] - TRB2_in)
```

"5. HEAT TRANSFER IN THE RISER SIDE WALLS"

"Convection"

```
Qconv_RS1_cavity = h_cavity*A[4]*(T_cavity - T[5])
Qconv_RS2_cavity = h_cavity*A[5]*(T_cavity - T[4])
```

"Energy balance"

```
abs(Q_dot[5]) + Qconv_RS1_cavity = Qcond_RS1
abs(Q_dot[4]) + Qconv_RS2_cavity = Qcond_RS2
```

"Conduction through the RS wall"

```
dx_RS = 0.00473
A_RSin = 206.756/2
A_RSout = 214.5094/2


A_RS = 0.5*(A_RSin+A_RSout)
k_RS = 24.137e-03

Qcond_RS1 = ((k_RS*A_RS)/dx_RS)*(T[5] - TRS1_in)
Qcond_RS1 = ((k_RS*A_RS)/dx_RS)*(T[4] - TRS2_in)
```

"6. RADIATION HEAT TRANSFER NETWORK INSIDE THE RISER 1"

```
b = 3

T[9] = TRF1_in
T[10] = TRB1_in
T[11] = TRS1_in

e[9] = 0.8
e[10] = 0.8
e[11] = 0.8

A[9] = 20.6756/2
A[10] = 20.6756/2
A[11] = 206.756/2

RF[9,10] = 0.1
RF[9,11] = 0.9
RF[11,10] = 0.09

Duplicate i = 1,b

        Eb[i+8] = sigma*(T[i+8] + 273.15)^4
        c[i+8] = (1-e[i+8])/(A[i+8]*e[i+8])
        Q_dot[i+8] = (Eb[i+8] - J[i+8])/c[i+8]

End

Q_dot[9] = A[9]*RF[9,10]*(J[9] - J[10]) + A[9]*RF[9,11]*(J[9] - J[11])
Q_dot[10] = A[9]*RF[9,10]*(J[10] - J[9]) + A[11]*RF[11,10]*(J[10] - J[11])
Q_dot[11] = A[9]*RF[9,11]*(J[11] - J[9]) + A[11]*RF[11,10]*(J[11] - J[10])
```

"7. RADIATION HEAT TRANSFER NETWORK INSIDE THE RISER 2"

```
d = 3

T[12] = TRF2_in
T[13] = TRB2_in
T[14] = TRS2_in

e[12] = 0.8
e[13] = 0.8
e[14] = 0.8

A[12] = 20.6756/2
A[13] = 20.6756/2
A[14] = 206.756/2

RF[12,13] = 0.1
RF[12,14] = 0.9
RF[14,13] = 0.09

Duplicate i = 1,d

Eb[i+11] = sigma*(T[i+11] + 273.15)^4
c[i+11] = (1-e[i+11])/(A[i+11]*e[i+11])
Q_dot[i+11] = (Eb[i+11] - J[i+11])/c[i+11]

End

Q_dot[12] = A[12]*RF[12,13]*(J[12] - J[13]) + A[12]*RF[12,14]*(J[12] - J[14])
Q_dot[13] = A[12]*RF[12,13]*(J[13] - J[12]) + A[14]*RF[14,13]*(J[13] - J[14])
Q_dot[14] = A[12]*RF[12,14]*(J[14] - J[12]) + A[14]*RF[14,13]*(J[14] - J[13])

"8. ENERGY BALANCE INSIDE THE RISER"

Qcond_RF1 - Q_dot[9] = Qconv_RF1
Qcond_RF2 - Q_dot[12] = Qconv_RF2

Qcond_RS1 + abs(Q_dot[11]) = Qconv_RS1
Qcond_RS2 + abs(Q_dot[14]) = Qconv_RS2

Qcond_RB1 + abs(Q_dot[10]) = Qconv_RB1
```

```
Qcond_RB2 + abs(Q_dot[13]) = Qconv_RB2

"9. HEAT TRANSFER THROUGH THE INSULATION"

k_insulation = 0.024e-03                                    [kW/m-K]
dx_insulation = 0.0762                                      [m]
Ains_in = 52.6911                                           [m^2]
Ains_out = 53.7259                                          [m^2]
A_insulation = 0.5*(Ains_in + Ains_out)

Qcond_insulation= ((k_insulation *A_insulation)/dx_insulation)*(T[8] - T_insulation)

Qconv_DC_cav = h_cavity*A[8]*(T_cavity - T[8])

Qconv_DC_cav - Q_dot[8] = Qcond_insulation

"10. HEAT TRANSFER THROUGH THE DOWNCOMER STEEL"

dx_DCin = 0.0127                                            [m^2]
k_dcin = 24.137e-03                                         [kW/m-K]
A_dcin = 53.7259                                            [m^2]

Qcond_DCin= ((k_dcin *A_dcin )/dx_DCin)*(T_insulation - TDC_in)

Qcond_DCin = Qcond_insulation

"11. RADIATION HEAT TRANSFER NETWORK INSIDE THE DOWNCOMER"

T[16] = TDC_in

F_dcin_dcout = 1
e_dcin = 0.8
e_dcout = 0.8
A_dcout = 56.6785                                           [m^2]

Qrad_DCin_DCo = sigma*((T[16] + 273.15)^4 - (T[17]+273.15)^4)/((1-e_dcin)/(e_dcin*A_dcin)+(1/(A_dcin*F_dcin_dcout)) + ((1-e_dcout)/(e_dcout*A_dcout )))

"energy balance on the inside downcomer wall"



Qcond_DCin = Qrad_DCin_DCo + Qconv_dcin

"energy balance on the outer downcomer wall"

Qcond_DCout  + Qconv_dcout = Qrad_DCin_DCo

"12. HEAT TRANSFER IN THE OUTER DOWNCOMER STEEL WALL"

dx_DCouter = 0.0127                                                 [m]
k_dcouter = 24.137e-03                                              [kW/m-K]

Qcond_DCout = ((k_dcouter*A_dcout )/dx_DCouter)*(T[17] - Tconcrete_in)

Qcond_DCout = Qcond_concrete

"13. HEAT TRANSFER THROUGH THE CONCRETE"

dx_concrete = 1.5                                                   [m]
k_concrete = 1e-03*1.991                                            [kW/m-K]
A_concrete = 56.6785                                                [m^2]

Qcond_concrete = ((k_concrete*A_concrete)/dx_concrete)*(Tconcrete_in - Tconcrete_out)
```

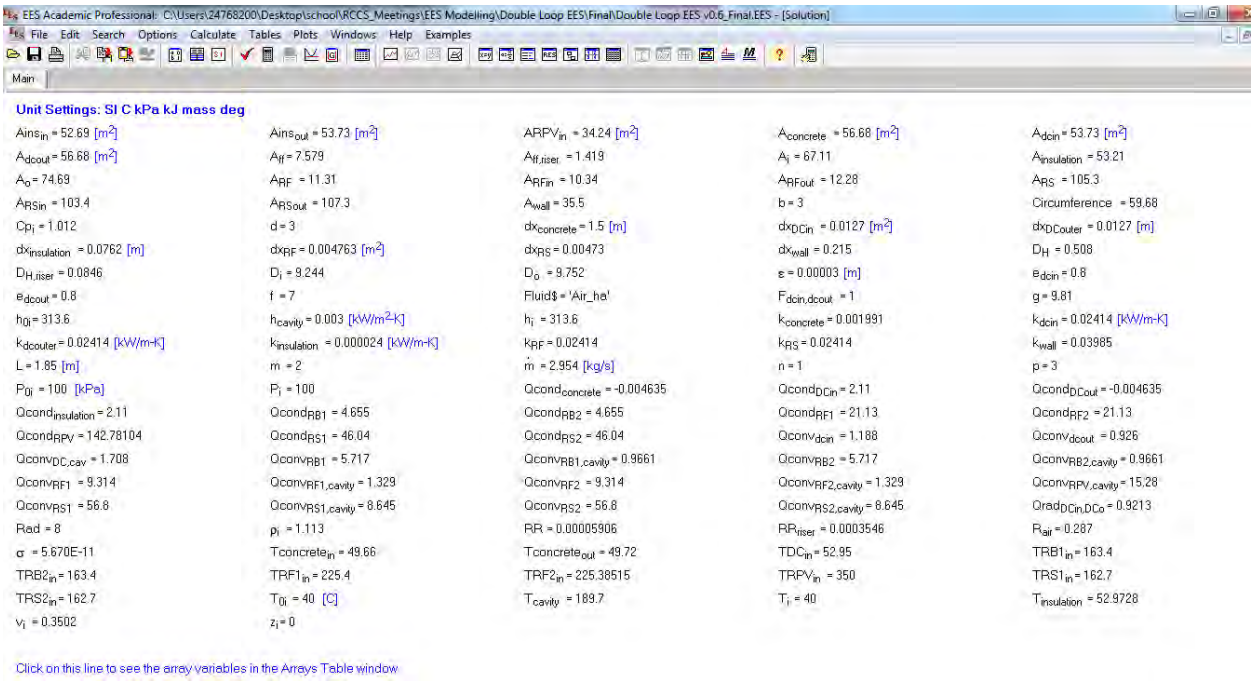
EES Academic Professional: C:\Users\24768200\Desktop\school\RCCS_Meetings\EES Modelling\Double Loop EES\Final\Double Loop EES v0.6_Final.EES - [Solution]
File Edit Search Options Calculate Tables Plots Windows Help Examples
Main
Unit Settings: SI C kPa kJ mass deg
Ains_in = 52.69 [m^2]
Ains_out = 53.73 [m^2]
ARPV_in = 34.24 [m^2]
A_concrete = 56.68 [m^2]
A_dcin = 53.73 [m^2]
A_dcout = 56.68 [m^2]
A_ff = 7.579
A_ff,riser = 1.419
A_i = 67.11
A_insulation = 53.21
A_o = 74.69
A_RF = 11.31
A_RFin = 10.34
A_RFout = 12.28
A_RS = 105.3
A_RSin = 103.4
A_RSout = 107.3
A_wall = 35.5
b = 3
Circumference = 59.68
Cp_i = 1.012
d = 3
dx_concrete = 1.5 [m]
dx_DCin = 0.0127 [m^2]
dx_DCouter = 0.0127 [m]
dx_insulation = 0.0762 [m]
dx_RF = 0.004763 [m^2]
dx_RS = 0.00473
dx_wall = 0.215
D_H = 0.508
D_H,riser = 0.0846
D_i = 9.244
D_o = 9.752
ε = 0.00003 [m]
e_dcin = 0.8
e_dcout = 0.8
f = 7
Fluid$ = 'Air_ha'
F_dcin,dcout = 1
g = 9.81
h_0i = 313.6
h_cavity = 0.003 [kW/m^2-K]
h_i = 313.6
k_concrete = 0.001991
k_dcin = 0.02414 [kW/m-K]
k_dcouter = 0.02414 [kW/m-K]
k_insulation = 0.000024 [kW/m-K]
k_RF = 0.02414
k_RS = 0.02414
k_wall = 0.03985
L = 1.85 [m]
m = 2
ṁ = 2.954 [kg/s]
n = 1
p = 3
P_0i = 100 [kPa]
P_i = 100
Qcond_concrete = -0.004635
Qcond_DCin = 2.11
Qcond_DCout = -0.004635
Qcond_insulation = 2.11
Qcond_RB1 = 4.655
Qcond_RB2 = 4.655
Qcond_RF1 = 21.13
Qcond_RF2 = 21.13
Qcond_RPV = 142.78104
Qcond_RS1 = 46.04
Qcond_RS2 = 46.04
Qconv_dcin = 1.188
Qconv_dcout = 0.926
Qconv_DC,cav = 1.708
Qconv_RB1 = 5.717
Qconv_RB1,cavity = 0.9661
Qconv_RB2 = 5.717
Qconv_RB2,cavity = 0.9661
Qconv_RF1 = 9.314
Qconv_RF1,cavity = 1.329
Qconv_RF2 = 9.314
Qconv_RF2,cavity = 1.329
Qconv_RPV,cavity = 15.28
Qconv_RS1 = 56.8
Qconv_RS1,cavity = 8.645
Qconv_RS2 = 56.8
Qconv_RS2,cavity = 8.645
Qrad_DCin,DCo = 0.9213
Rad = 8
ρ_i = 1.113
RR = 0.00005906
RR_riser = 0.0003546
R_air = 0.287
σ = 5.670E-11
Tconcrete_in = 49.66
Tconcrete_out = 49.72
TDC_in = 52.95
TRB1_in = 163.4
TRB2_in = 163.4
TRF1_in = 225.4
TRF2_in = 225.38515
TRPV_in = 350
TRS1_in = 162.7
TRS2_in = 162.7
T_0i = 40 [C]
T_cavity = 189.7
T_i = 40
T_insulation = 52.9728
v_i = 0.3502
z_i = 0
Click on this line to see the array variables in the Arrays Table window

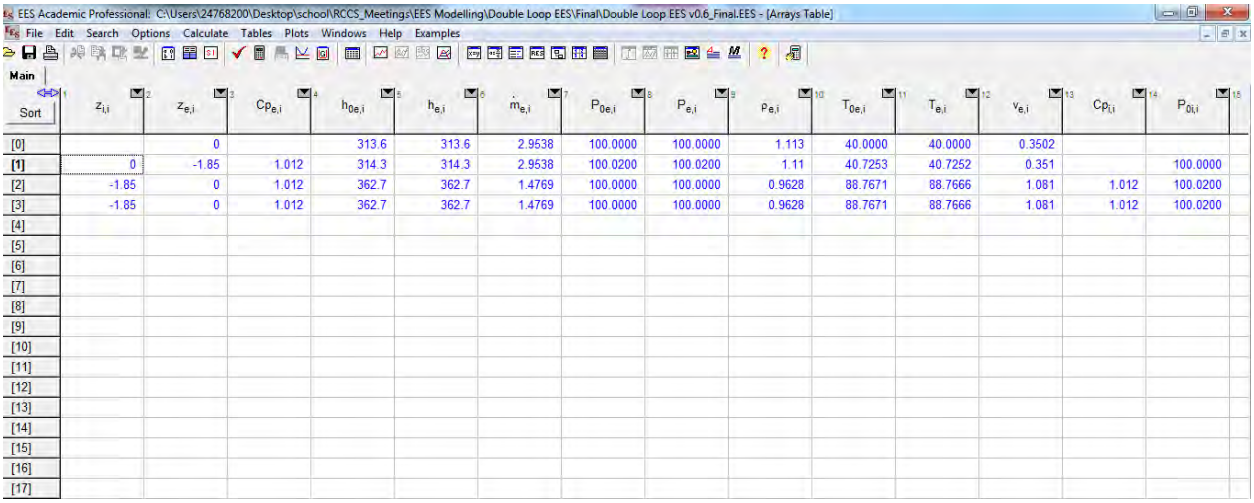
EES Academic Professional: C:\Users\24768200\Desktop\school\RCCS_Meetings\EES Modelling\Double Loop EES\Final\Double Loop EES v0.6_Final.EES - [Arrays Table]
File Edit Search Options Calculate Tables Plots Windows Help Examples
Main
Sort
z_i,i | z_e,i | Cp_e,i | h_0e,i | h_e,i | ṁ_e,i | P_0e,i | P_e,i | ρ_e,i | T_0e,i | T_e,i | v_e,i | Cp_i,i | P_0,i
[0] 0 313.6 313.6 2.9538 100.0000 100.0000 1.113 40.0000 40.0000 0.3502
[1] 0 -1.85 1.012 314.3 314.3 2.9538 100.0200 100.0200 1.11 40.7253 40.7252 0.351 100.0000
[2] -1.85 0 1.012 362.7 362.7 1.4769 100.0000 100.0000 0.9628 88.7671 88.7666 1.081 1.012 100.0200
[3] -1.85 0 1.012 362.7 362.7 1.4769 100.0000 100.0000 0.9628 88.7671 88.7666 1.081 1.012 100.0200
[4]
[5]
[6]
[7]
[8]
[9]
[10]
[11]
[12]
[13]
[14]
[15]
[16]
[17]

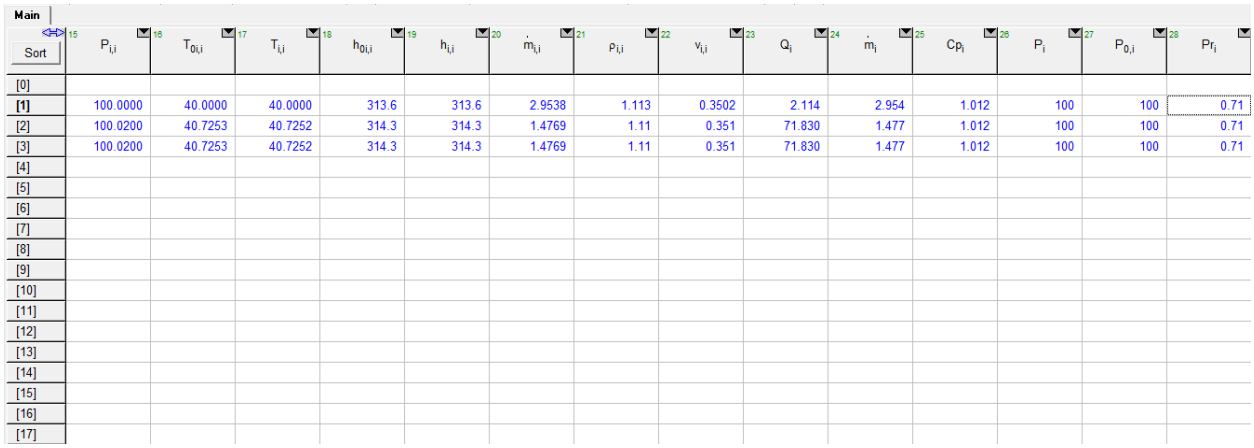
Main
Sort
P_i,i | T_0i,i | T_i,i | h_0i,i | h_i,i | ṁ_i,i | ρ_i,i | v_i,i | Q_i | ṁ_i | Cp_i | P_i | P_0,i | Pr_i
[0]
[1] 100.0000 40.0000 40.0000 313.6 313.6 2.9538 1.113 0.3502 2.114 2.954 1.012 100 100 0.71
[2] 100.0200 40.7253 40.7252 314.3 314.3 1.4769 1.11 0.351 71.830 1.477 1.012 100 100 0.71
[3] 100.0200 40.7253 40.7252 314.3 314.3 1.4769 1.11 0.351 71.830 1.477 1.012 100 100 0.71
[4]
[5]
[6]
[7]
[8]
[9]
[10]
[11]
[12]
[13]
[14]
[15]
[16]
[17]

Main

Sort

	29 Re_i	30 $T_{0,i}$	31 h_i	32 $h_{0,i}$	33 k_i	34 μ_i	35 ρ_i	36 v_i	37 z_i	38 $Nusselt_{in,i}$	39 $Nusselt_{out,i}$	40 $h_{in,i}$	41 $h_{o,i}$	42 $T_{fluid,i}$
[0]														
[1]	10321	40.3626	313.9	313.9	0.00002738	0.00001918	1.112	0.3506	-0.925	32.6	32.6	0.001757	0.001757	40.36
[2]	4334	64.7655	338.5	338.5	0.00002914	0.00002032	1.031	1.009	-0.925	16.28		0.005609		64.77
[3]	4334	64.7655	338.5	338.5	0.00002914	0.00002032	1.031	1.009	-0.925	16.28		0.005609		64.77
[4]														
[5]														
[6]														
[7]														
[8]														
[9]														
[10]														
[11]														
[12]														
[13]														
[14]														
[15]														
[16]														
[17]														

Main

Sort

	43 A_i [m2]	44 e_i	45 $F_{i,1}$	46 $F_{i,2}$	47 $F_{i,3}$	48 $F_{i,4}$	49 $F_{i,5}$	50 $F_{i,6}$	51 $F_{i,7}$	52 $F_{i,8}$	53 c_i	54 Eb_i	55 J_i	56 T_i
[0]														
[1]	36.75	0.8	0	0.25	0.25	0.2	0.2	0	0	0.1	0.006803	7.4194	6.552	328.2951
[2]	12.28	0.8	0.7484	0.0978	0.0978	0.028	0.028	0	0	0	0.02036	3.5128	3.97	225.7539
[3]	12.28	0.8	0.7484	0.0978	0.0978	0.028	0.028	0	0	0	0.02036	3.5128	3.97	225.7539
[4]	107.3	0.8	0.06853	0.003205	0.003205	0.4055	0.4055	0	0	0.114	0.002331	2.0480	2.135	162.8010
[5]	107.3	0.8	0.06853	0.003205	0.003205	0.4055	0.4055	0	0	0.114	0.002331	2.0480	2.135	162.8010
[6]	12.28	0.8	0	0	0	0	0	0	0	1	0.02036	2.0600	2.135	163.4370
[7]	12.28	0.8	0	0	0	0	0	0	0	1	0.02036	2.0600	2.135	163.4370
[8]	52.69	0.1	0.06975	0	0	0.2321	0.2321	0.233	0.233	0	0.1708	2.3670	2.436	178.8652
[9]	10.34	0.8									0.02418	3.5024	3.217	225.3851
[10]	10.34	0.8									0.02418	2.0585	2.084	163.3557
[11]	103.4	0.8									0.002418	2.0464	2.072	162.7154
[12]	10.34	0.8									0.02418	3.5024	3.217	225.3851
[13]	10.34	0.8									0.02418	2.0585	2.084	163.3557
[14]	103.4	0.8									0.002418	2.0464	2.072	162.7154
[15]														
[16]														52.9522
[17]														49.6606

Main

Sort

	56 T_i	57 $\dot{Q}_i$	58 $RF_{i,10}$	59 $RF_{i,11}$	60 $RF_{i,13}$	61 $RF_{i,14}$	62 $Qconv_{RB1,i}$	63 $Qconv_{RF1,i}$	64 $Qconv_{RS1,i}$	65 $Qconv_{RB2,i}$	66 $Qconv_{RF2,i}$	67 $Qconv_{RS2,i}$	68 $Qconv_{dcin,i}$	69 $Qconv_{dcout,i}$
[0]														
[1]	328.2951	127.4975											1.188	0.926
[2]	225.7539	-22.4596					5.717	9.314	56.8					
[3]	225.7539	-22.4596								5.717	9.314	56.8		
[4]	162.8010	-37.3990												
[5]	162.8010	-37.3990												
[6]	163.4370	-3.6892												
[7]	163.4370	-3.6892												
[8]	178.8652	-0.4020												
[9]	225.3851	11.8166	0.1	0.9										
[10]	163.3557	-1.0617												
[11]	162.7154	-10.7549	0.09											
[12]	225.3851	11.8166			0.1	0.9								
[13]	163.3557	-1.0617												
[14]	162.7154	-10.7549			0.09									
[15]														
[16]	52.9522													
[17]	49.6606													

Appendix F: Chimney layout and dimensions

Table F– 1 gives the chimney dimensions as provided by the KAERI. These were used to construct the chimney canvas in Flownex® using the methodologies detailed in **Appendix A**.

Table F– 1: Chimney dimensions provided by the KAERI.

Subsystem	Design Parameter	Value	Units
RCCS Inlets	Flow Area	4 x 4.62= 18.48	m^2
F1_RCCS_Inlets	Length	15.9	m
	Height difference	-15.9	m
	Hydraulic diameter	2.15	m
	k-forward	3.5	
	k-reverse	3.5	
	Circumference	8.60	m
RCCS Inlet Manifold Plenum	Flow Area	4 x 4.63= 18.52	m^2
F1_RCCS_Inlet Manifold	Length	19.6	m
	Height difference	0	m
	Hydraulic diameter	0.8965	m
	k-forward	4.2	
	k-reverse	4.2	
	Circumference	20.66	m
RCCS Inlet Header	Flow Area	2 x 4.63=9.26	m^2
	Length	26.7	m
	Height difference	-10.7	m
	Hydraulic diameter	0.8068	m
	k-forward	3.5	
	k-reverse	3.5	
	Circumference	22.95	m
RCCS Inlet Lower Duct	Flow Area	4 x 3.72=14.88	m^2
	Length	6.4	m
	Height difference	0	m
	Hydraulic diameter	1.0485	m
	k-forward	3.5	
	k-reverse	3.5	
	Circumference	14.19	m

RCCS Inlet Connector to Cold Plenum	Flow Area	14.8645	m^2
	Length	2.286	m
	Height difference	-2.286	m
	Hydraulic diameter	0.9754	m
	k-forward	3.3	
	k-reverse	3	
	Circumference	60.96	m
RCCS Outlet Connector to Hot Plenum	Flow Area	9.2903	m^2
	Length	3.2	m
	Height difference	2.286	m
	Hydraulic diameter	1.524	m
	k-forward	1.5	
	k-reverse	1.5	
	Circumference	24.38	m
RCCS Outlet Lower Duct	Flow Area	4 x 1.85806=7.4322	m^2
	Length	6.4	m
	Height difference	0	m
	Hydraulic diameter	1.86	m
	k-forward	2.1	
	k-reverse	2.1	
	Circumference	4.00	m
RCCS Outlet Header	Flow Area	2 x 3.71612=7.4322	m^2
	Length	26.7	m
	Height difference	10.7	m
	Hydraulic diameter	1.87	m
	k-forward	2.1	
	k-reverse	2.1	
	Circumference	7.95	m
RCCS Outlet Manifold Plenum	Flow Area	4 x 3.71612=14.8645	m^2
	Length	19.6	m
	Height difference	0	m
	Hydraulic diameter	1.87	m
	k-forward	2.1	
	k-reverse	2.1	
	Circumference	7.95	m

RCCS Outlets	Flow Area	4 x 2.31=9.24	m^2
	Length	15.9	m
	Height difference	15.9	m
	Hydraulic diameter	1.52	m
	k-forward	2.1	
	k-reverse	2.1	
	Circumference	6.08	m

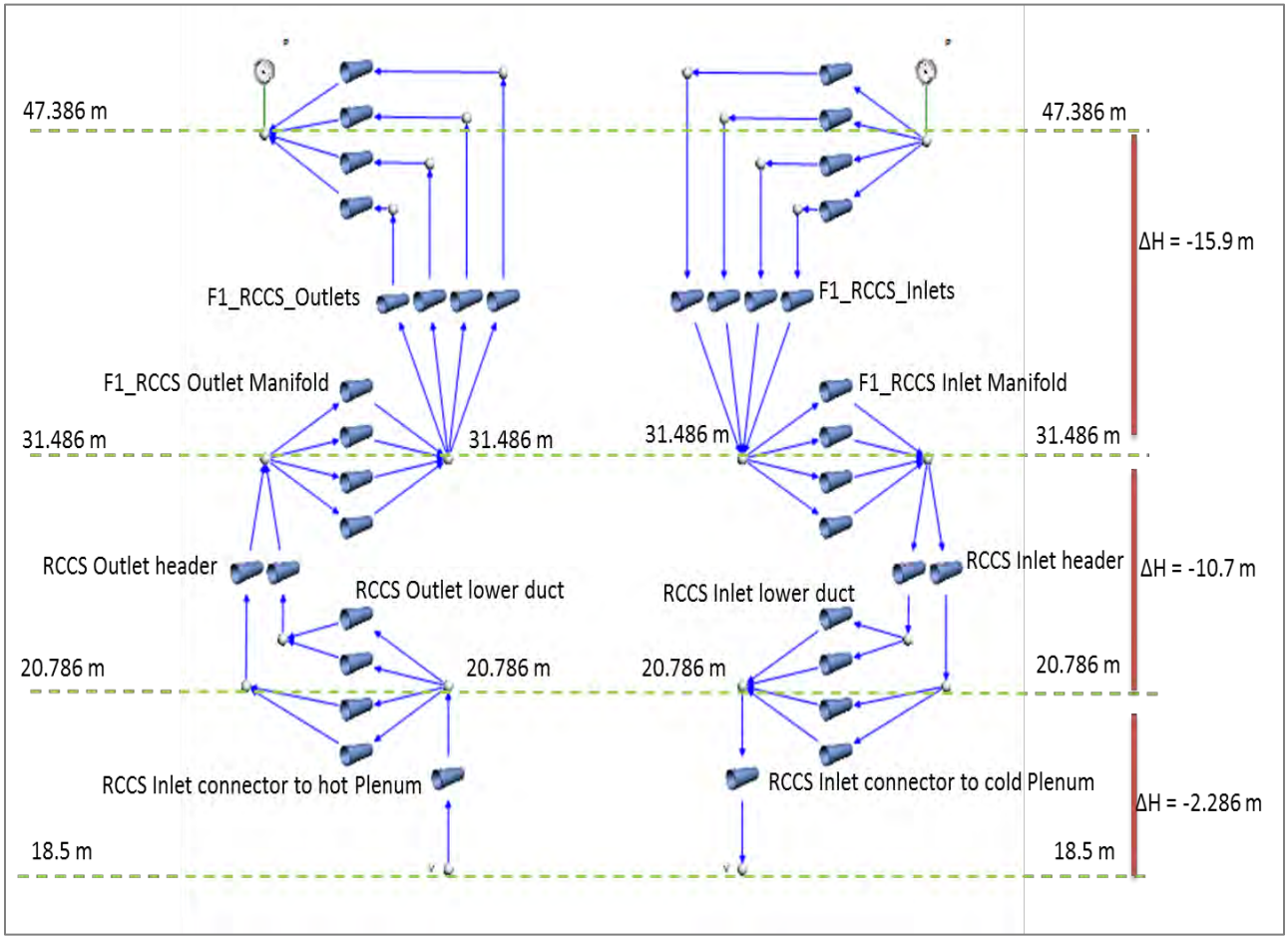

Figure F 1: Chimney Flownex® canvas.

Appendix G: View factors calculation in Star-CCM+

In Star-CCM+, a CFD software that has been validated considerably for this purpose, the surface to surface radiation model makes it possible to simulate thermal radiation exchange between diffuse surfaces forming a closed set. The medium that fills the space is non-participating and further the surface properties (emissivity, transmisivity and reflectivity) are not dependant on direction or wavelength. This is in line with the assumptions made in section 3.2.3. The S2S (surface-to-surface) model is operated in two steps;

1. Calculate the view factors using ray tracing technique.

2. Apply view factors to compute radiosity and irradiation fields on all surfaces.

In the view factor calculation step, deterministic ray tracing is applied to compute the view factors. Firstly, the surfaces are discretized spatially into patches. The double integral in Equation 3-14 is approximated using a ray tracing approach. A predetermined number of rays (1024 rays per patch) are traced through the computational domain randomly in all directions. A ray shot from one patch can do any of the following (USER-GUIDE, 2012)

    1. Hit an opaque patch.

    2. Pass through a semi-transparent patch if defined.

    3. Reflect from a reflective patch.

    4. Pass through a transparent boundary and can be dispersed to the environment.

After the beam tracking has finished, the array of view factors obtained satisfies conservation but not reciprocity, therefore a post-correction procedure is necessary to enforce reciprocity.

A unit cell was drawn in Star-CCM+ as shown in Figure G–1 with the top, bottom and reflective boundary of the layer specified as reflective boundaries within Star-CCM+. Therefore, a ray that hits these boundaries is reflected back into the domain, but in reality this refers to an interaction with an adjacent riser or a surface on a level below or above. The surfaces are defined internally in Star-CCM+ and the view factors are calculated.

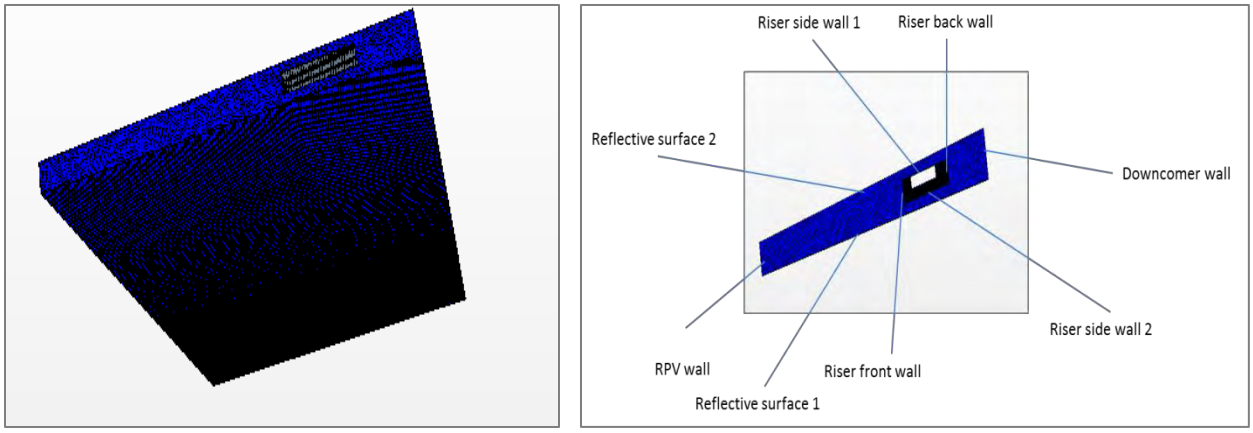

Figure G–1: RCCS unit cell modeled imported into STAR-CCM+.

Test problem for calculating view factors in STAR-CCM+

This problem was chosen from (Ibrahim & Mohd, 2012) who presented the development of a network representation method for calculating the radiation behaviour in an oven during the baking process.

A schematic of such a system is shown below in Figure G–2.

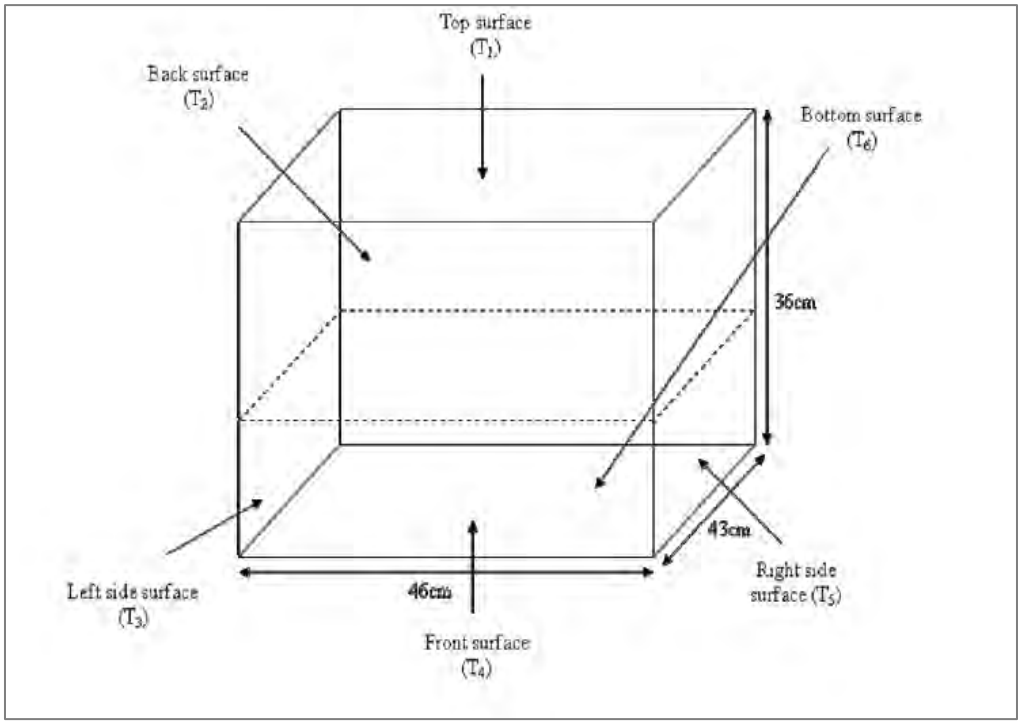

Figure G–2: Schematic representation of an oven (Ibrahim* et al.*, 2012).

The exercise will be to calculate the view factors from surface 1 (top surface) to all other surfaces in the oven. This configuration is shown in Figure G–3.

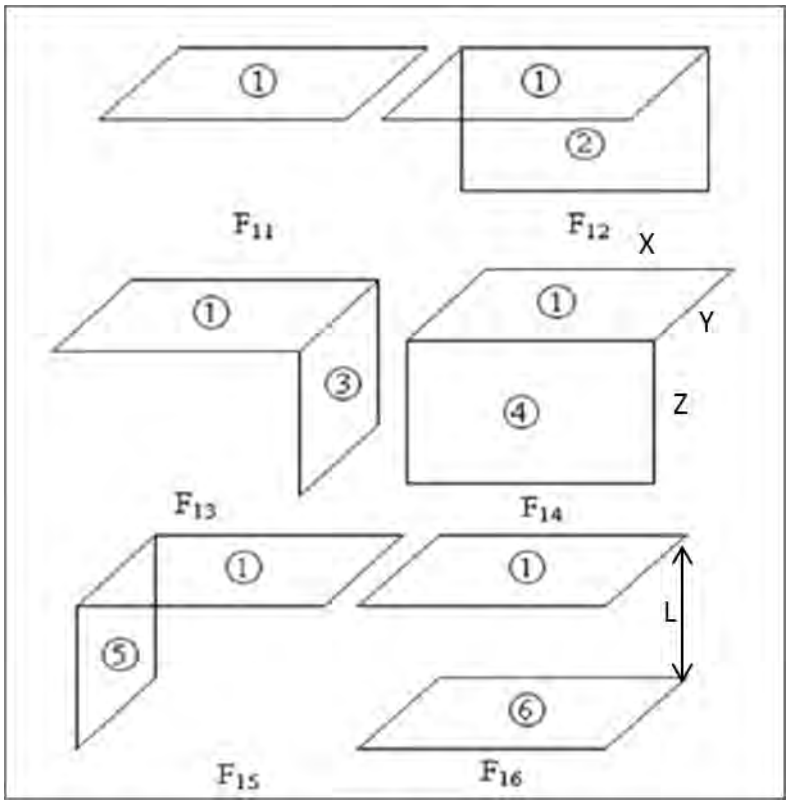

Figure G–3: Configuration layout for surface 1 with other surfaces inside the oven (Ibrahim & Mohd, 2012).

Ibrahim and Mohd (2012) used the following expressions to compute the view factors:

1. Aligned parallel

$$F_{i\to j}=\frac{2}{\pi \bar{X}\bar{Y}}\left\{\begin{array}{l} In\left[\frac{\left(1+\bar{X}^2\right)\left(1+\bar{Y}^2\right)}{1+\bar{X}^2+\bar{Y}^2}\right]^{1/2}+\bar{X}\left(1+\bar{Y}^2\right)^{1/2}\tan^{-1}\frac{\bar{X}}{\left(1+\bar{Y}^2\right)^{1/2}} \\ +\bar{Y}\left(1+\bar{X}^2\right)^{1/2}\tan^{-1}\frac{\bar{Y}}{\left(1+\bar{X}^2\right)^{1/2}}-\bar{X}\tan^{-1}\bar{X}-\bar{Y}\tan^{-1}\bar{Y} \end{array}\right\} \quad \text{Equation G–1}$$

$$H=\frac{Z}{X} \quad \text{Equation G–2}$$

$$\bar{Y} = \frac{Y}{L}$$

Equation G–3

2. Perpendicular rectangles with common edge

$$F_{i\to j} = \left(\begin{array}{l} \frac{1}{\pi W} W \tan^{-1} \frac{1}{W} + H \tan^{-1} \frac{1}{H} - \left(H^2 - W^2\right)^{1/2} \tan^{-1} \frac{1}{\left(H^2 + W^2\right)^{1/2}} \\ + \frac{1}{4} \ln \left\{ \frac{\left(1+W^2\right)\left(1+W^2\right)}{1+W^2+H^2} \left[\frac{W^2\left(1+W^2+H^2\right)}{\left(1+W^2\right)\left(W^2+H^2\right)} \right]^{W^2} \times \left[\frac{H^2\left(1+W^2+H^2\right)}{\left(1+H^2\right)\left(H^2+W^2\right)} \right]^{H^2} \right\} \end{array} \right)$$

Equation G–4

$$H = \frac{Z}{X}$$

Equation G–5

$$W = \frac{Y}{X}$$

Equation G–6

Equation G–1 and Equation G–4 can also be found in Coulson and Richardson (1999:451).

The problem in Figure G–3 was solved by incorporating the geometry in STAR-CCM+ and defining the different surfaces as shown in Figure G–4.

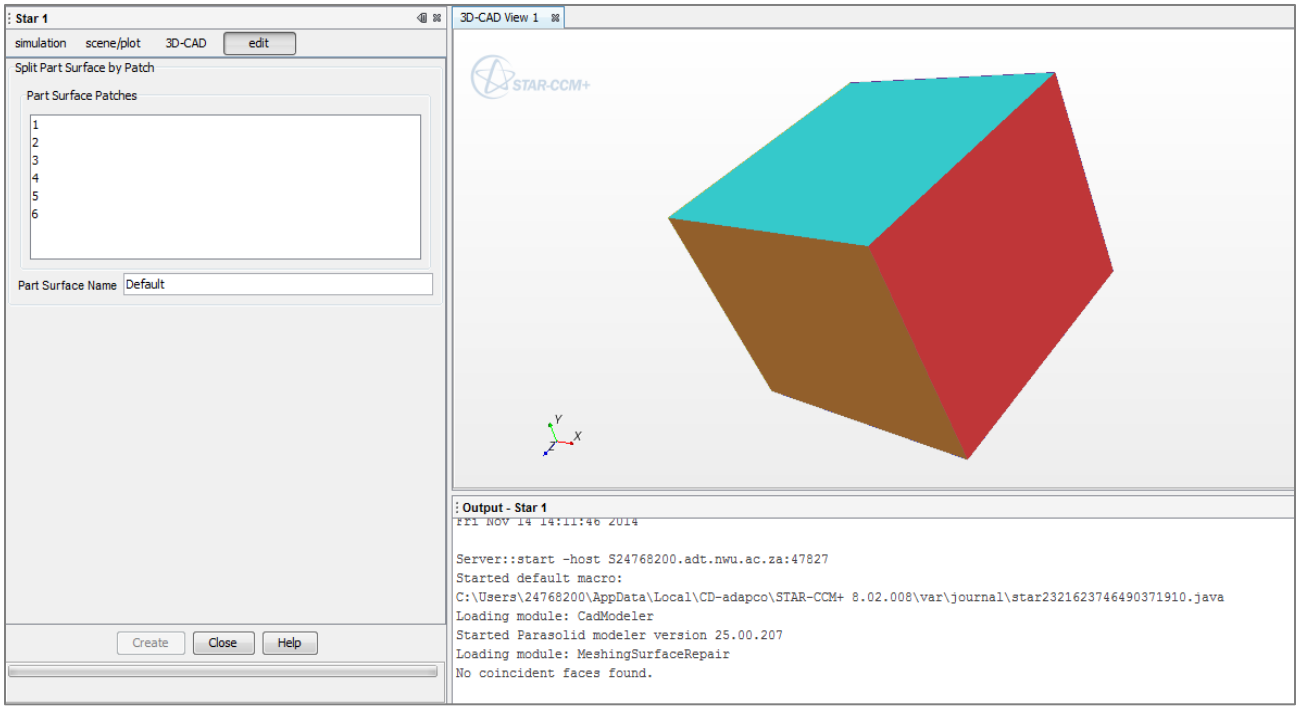

Figure G–4: Oven model constructed into STAR-CCM+.

The next step is to create a suitable mesh and to define the physics continuum for the problem. A polyhedral mesh was selected as appropriate for the problem. In fact, for view factor calculations, the mesh is not a requirement since the patches are defined internally within STAR-CCM+, but was necessary to run the simulation. The following were selected in STAR-CCM+ to calculate the view factors;

Table G–1: STAR-CCM+ radiation input table.

Space	3-Dimensional
Model	Radiation
Radiation	Surface to Surface
Radiation Spectrum	Gray thermal radiation

In the solvers tab, the radiation patches can be created, and the view factors calculated. The results can be summarized as shown in Table G–2 for the viewing of the top surface to all other surfaces in the oven.

Table G–2: Comparing STAR-CCM+ with numerically calculated view factors.

	STAR-CCM+	Numerical	% Error
$F_{top \to top}$	0	0	0
$F_{top \to bottom}$	0.264	0.259	2.2
$F_{top \to side1}$	0.177	0.179	-0.93
$F_{top \to side2}$	0.177	0.179	-0.93
$F_{top \to front1}$	0.190	0.192	-0.93
$F_{top \to front2}$	0.190	0.192	-0.93
Sum	0.998	1.001	

It can be seen that the agreement between the numerically calculated view factors by (Ibrahim & Mohd, 2012) and those from STAR-CCM+ is good. This shows that the candidate is competent to use STAR-CCM+ to calculate view factors.

For this study, the view factors were calculated for the surfaces in the reactor cavity using the unit cell model shown in Figure G–1. The results are shown in Table 7-7.